Gamma-Ray Bursts

Contents

1 Topics

- GRB classification: seven different families.
- GRB empirical correlations
- "Genuine short" GRBs: Possible identifications and selection effects
- A modified spectral energy distribution for highly energetic GRBs
- The observed spectra of the P-GRBs
- GRB prompt emission spectra below 5 keV: challenges for future missions
- Interpretation of the ultra high energy emission from GRBs observed by Fermi and AGILE
- Analysis of different families of progenitors for GRBs with different energetics
- GRBs at redshift $z > 6$
- GRBs originating from a multiple collapse
- Prompt emission: the clumpiness of CBM
- Microphysical description of the interaction between the fireshell and the CBM
- Theoretical interpretation of the "plateau" phase in the X-ray afterglow
- Emission from newly born neutron stars, or "neo neutron stars".
- Induced Gravitational Collapse process for GRBs associated with supernovae.
- Redshift estimators for GRBs with no measured redshift.

- Binary Driven Hypernovae (BdHNe) as progenitor of GRBs via Induced Gravitational Collapse.
- GRB light curves as composed of four different episodes.
- Different kinds of binary systems as GRB progenitors.
- "Cosmic Matrix" for GRBs.
- GRB X-Ray Flares and Gamma-Ray Flares.

2 Participants

2.1 ICRANet participants

- David Arnett
- Carlo Luciano Bianco
- Massimo Della Valle
- Marco Muccino
- Giovanni Battista Pisani
- Jorge Armando Rueda Hernandez
- Remo Ruffini
- Gregory Vereshchagin
- She-Sheng Xue

2.2 Past collaborators

- Andrey Baranov
- Maria Grazia Bernardini (OAB, Italy)
- Joao Braga (INPE, Brazil)
- Sabrina Casanova (MPIK, Germany)
- Letizia Caito
- Pascal Chardonnet (Université de Savoie, France)

- Guido Chincarini (Universit di Milano “Bicocca”, Italy)
- Demetrios Christodoulou (ETH Zurich, Switzerland)
- Alessandra Corsi (INAF-IASF Roma, Italy)
- Valeri Chechetkin
- Maria Giovanna Dainotti
- Thibault Damour (IHES, France)
- Walter Ferrara
- Federico Fraschetti (CEA Saclay, France)
- Roberto Guida
- Vahe Gurzadyan (Yerevan Physics Institute, Armenia)
- Wen-Biao Han
- Massimiliano Lattanzi (Oxford Astrophysics, UK)
- Vincenzo Liccardo
- Nino Panagia
- Barbara Patricelli (Pisa University, Italy)
- Elena Pian
- Giuliano Preparata (Università di Milano, Italy)
- Jay D. Salmonson (Livermore Lab, USA)
- Vineeth Valsan
- Jim Wilson (Livermore Lab, USA)

2.3 Ongoing collaborations

- Alexey Aksenov (ITEP, Russia)
- Lorenzo Amati (INAF-IASF Bologna, Italy)
- Ulisses Barres de Almeida (CBPF, Brazil)
- Riccardo Belvedere (ICRANet-Rio, Brazil)
- Sandip Kumar Chakrabarti (S.N. Bose National Centre and Indian Centre for Space Physics, India)
- Christian Cherubini (Universit Campus Biomedico, Italy)
- Alessandro Chieffi (INAF-IASF Roma, Italy)
- Stefano Covino (OAB, Italy)
- Gustavo de Barros (UFRJ, Brazil)
- Simonetta Filippi (Universit Campus Biomedico, Italy)
- Filippo Frontera (Universit di Ferrara, Italy)
- Chris Fryer (Los Alamos National Laboratories, USA).
- Dafne Guetta (OAR, Italy)
- Cristiano Guidorzi (OAB, Italy)
- Stanislav Kelner (MEPhI, Russia, and MPIK, Germany)
- Marco Limongi (OAR, Italy)
- Vanessa Mangano (INAF-IASF Palermo, Italy)
- Ana Virginia Penacchioni (INPE, Brazil)
- Luis Juracy Rangel Lemos (Fundao Universidade Federal do Tocantins, Brazil)
- Soroush Shakeri (Isfahan University of Technology, Iran)

- Ivan Siutsou (ICRANet-Rio, Brazil)
- Susanna Vergani (Dunsink Observatory, Ireland)
- Francesco Vissani (INFN, Italy)
- Elena Zaninoni (ICRANet-Rio, Brazil)

2.4 Students

- Yerlan Aimuratov (IRAP PhD, Kazakhstan)
- Laura Marcela Becerra Bayona (IRAP PhD, Colombia)
- Maxime Enderli (IRAP PhD, France)
- Mile Karlika (IRAP PhD, Croatia)
- Milos Kovacevic (IRAP PhD, Serbia)
- Hendrik Ludwig (IRAP PhD, Germany)
- J. David Melon Fuksman (IRAP PhD, Argentina)
- Rahim Moradi (IRAP PhD, Iran)
- Daria Primorac (IRAP PhD, Croatia)
- Jose Fernando Rodriguez Ruiz (IRAP PhD, Colombia)
- Yu Wang (IRAP PhD, China)

3 Brief summary of recent progresses

Major progresses have been accomplished this year in the following aspects:

- In identifying and analyzing two genuine Short GRBs (S-GRBs).
- In the comprehension of the early X-Ray flares of Driven Hypernovae (BdHNe), giving for the first time a complete theory of the phenomenon.
- In giving for the first time a full catalog of all the observed BdHNe, with their properties.

4 Selected publications before 2005

4.1 Refereed journals

1. D. Christodoulou, R. Ruffini; "Reversible Transformations of a Charged Black Hole"; Physical Review D, 4, 3552 (1971).

   A formula is derived for the mass of a black hole as a function of its "irreducible mass", its angular momentum, and its charge. It is shown that 50% of the mass of an extreme charged black hole can be converted into energy as contrasted with 29% for an extreme rotating black hole.

2. T. Damour, R. Ruffini; "Quantum electrodynamical effects in Kerr-Newman geometries"; Physical Review Letters, 35, 463 (1975).

   Following the classical approach of Sauter, of Heisenberg and Euler and of Schwinger the process of vacuum polarization in the field of a "bare" Kerr-Newman geometry is studied. The value of the critical strength of the electromagnetic fields is given together with an analysis of the feedback of the discharge on the geometry. The relevance of this analysis for current astrophysical observations is mentioned.

3. G. Preparata, R. Ruffini, S.-S. Xue; "The dyadosphere of black holes and gamma-ray bursts"; Astronomy & Astrophysics, 338, L87 (1999).

   The "dyadosphere" has been defined as the region outside the horizon of a black hole endowed with an electromagnetic field (abbreviated to EMBH for "electromagnetic black hole") where the electromagnetic field exceeds the critical value, predicted by Heisenberg & Euler for $e^{\pm}$ pair production. In a very short time ($\sim O(\hbar/mc^2)$) a very large number of pairs is created there. We here give limits on the EMBH parameters leading to a Dyadosphere for $10M_{\odot}$ and $10^5 M_{\odot}$ EMBH's, and give as well the pair densities as functions of the radial coordinate. We here assume that the pairs reach thermodynamic equilibrium

with a photon gas and estimate the average energy per pair as a function of the EMBH mass. These data give the initial conditions for the analysis of an enormous pair-electromagnetic-pulse or "P.E.M. pulse" which naturally leads to relativistic expansion. Basic energy requirements for gamma ray bursts (GRB), including GRB971214 recently observed at z=3.4, can be accounted for by processes occurring in the dyadosphere. In this letter we do not address the problem of forming either the EMBH or the dyadosphere: we establish some inequalities which must be satisfied during their formation process.

4. R. Ruffini, J.D. Salmonson, J.R. Wilson, S.-S. Xue; "On the pair electromagnetic pulse of a black hole with electromagnetic structure"; Astronomy & Astrophysics, 350, 334 (1999).

   We study the relativistically expanding electron-positron pair plasma formed by the process of vacuum polarization around an electromagnetic black hole (EMBH). Such processes can occur for EMBH's with mass all the way up to $6 \times 10^5 M_\odot$. Beginning with a idealized model of a Reissner-Nordstrom EMBH with charge to mass ratio $\xi = 0.1$, numerical hydrodynamic calculations are made to model the expansion of the pair-electromagnetic pulse (PEM pulse) to the point that the system is transparent to photons. Three idealized special relativistic models have been compared and contrasted with the results of the numerically integrated general relativistic hydrodynamic equations. One of the three models has been validated: a PEM pulse of constant thickness in the laboratory frame is shown to be in excellent agreement with results of the general relativistic hydrodynamic code. It is remarkable that this precise model, starting from the fundamental parameters of the EMBH, leads uniquely to the explicit evaluation of the parameters of the PEM pulse, including the energy spectrum and the astrophysically unprecedented large Lorentz factors (up to 6×10^3 for a $10^3 M_\odot$ EMBH). The observed photon energy at the peak of the photon spectrum at the moment of photon decoupling is shown to range from 0.1 MeV to 4 MeV as a function of the EMBH mass. Correspondingly the total energy in photons is in the range of 10^{52} to 10^{54} ergs, consistent with observed gamma-ray bursts. In these computations we neglect the presence of baryonic matter which will be the subject of forthcoming publications.

5. R. Ruffini, J.D. Salmonson, J.R. Wilson, S.-S. Xue; "On the pair-electro magnetic pulse from an electromagnetic black hole surrounded by a baryonic remnant"; Astronomy & Astrophysics, 359, 855 (2000).

   The interaction of an expanding Pair-Electromagnetic pulse (PEM pulse) with

a shell of baryonic matter surrounding a Black Hole with electromagnetic structure (EMBH) is analyzed for selected values of the baryonic mass at selected distances well outside the dyadosphere of an EMBH. The dyadosphere, the region in which a super critical field exists for the creation of e+e- pairs, is here considered in the special case of a Reissner-Nordstrom geometry. The interaction of the PEM pulse with the baryonic matter is described using a simplified model of a slab of constant thickness in the laboratory frame (constant-thickness approximation) as well as performing the integration of the general relativistic hydrodynamical equations. Te validation of the constant-thickness approximation, already presented in a previous paper Ruffini et al. (1999) for a PEM pulse in vacuum, is here generalized to the presence of baryonic matter. It is found that for a baryonic shell of mass-energy less than 1% of the total energy of the dyadosphere, the constant-thickness approximation is in excellent agreement with full general relativistic computations. The approximation breaks down for larger values of the baryonic shell mass, however such cases are of less interest for observed Gamma Ray Bursts (GRBs). On the basis of numerical computations of the slab model for PEM pulses, we describe (i) the properties of relativistic evolution of a PEM pulse colliding with a baryonic shell; (ii) the details of the expected emission energy and observed temperature of the associated GRBs for a given value of the EMBH mass; $10^3 M_\odot$, and for baryonic mass-energies in the range 10^{-8} to 10^{-2} the total energy of the dyadosphere.

6. C.L. Bianco, R. Ruffini, S.-S. Xue; "The elementary spike produced by a pure e+e- pair-electromagnetic pulse from a Black Hole: The PEM Pulse"; Astronomy & Astrophysics, 368, 377 (2001).

   In the framework of the model that uses black holes endowed with electromagnetic structure (EMBH) as the energy source, we study how an elementary spike appears to the detectors. We consider the simplest possible case of a pulse produced by a pure e^+e^- pair-electro-magnetic plasma, the PEM pulse, in the absence of any baryonic matter. The resulting time profiles show a *Fast-Rise-Exponential-Decay* shape, followed by a power-law tail. This is obtained without any special fitting procedure, but only by fixing the energetics of the process taking place in a given EMBH of selected mass, varying in the range from 10 to 10^3 $M_\odot$ and considering the relativistic effects to be expected in an electron-positron plasma gradually reaching transparency. Special attention is given to the contributions from all regimes with Lorentz γ factor varying from $\gamma = 1$ to $\gamma = 10^4$ in a few hundreds of the PEM pulse travel time. Although the

main goal of this paper is to obtain the elementary spike intensity as a function of the arrival time, and its observed duration, some qualitative considerations are also presented regarding the expected spectrum and on its departure from the thermal one. The results of this paper will be comparable, when data will become available, with a subfamily of particularly short GRBs not followed by any afterglow. They can also be propedeutical to the study of longer bursts in presence of baryonic matter currently observed in GRBs.

7. R. Ruffini, C.L. Bianco, P. Chardonnet, F. Fraschetti, S.-S. Xue; "Relative spacetime transformations in Gamma-Ray Bursts"; The Astrophysical Journal, 555, L107 (2001).

   The GRB 991216 and its relevant data acquired from the BATSE experiment and RXTE and Chandra satellites are used as a prototypical case to test the theory linking the origin of gamma ray bursts (GRBs) to the process of vacuum polarization occurring during the formation phase of a black hole endowed with electromagnetic structure (EMBH). The relative space-time transformation paradigm (RSTT paradigm) is presented. It relates the observed signals of GRBs to their past light cones, defining the events on the worldline of the source essential for the interpretation of the data. Since GRBs present regimes with unprecedently large Lorentz γ factor, also sharply varying with time, particular attention is given to the constitutive equations relating the four time variables: the comoving time, the laboratory time, the arrival time at the detector, duly corrected by the cosmological effects. This paradigm is at the very foundation of any possible interpretation of the data of GRBs.

8. R. Ruffini, C.L. Bianco, P. Chardonnet, F. Fraschetti, S.-S. Xue; "On the interpretation of the burst structure of Gamma-Ray Bursts"; The Astrophysical Journal, 555, L113 (2001).

   Given the very accurate data from the BATSE experiment and RXTE and Chandra satellites, we use the GRB 991216 as a prototypical case to test the EMBH theory linking the origin of the energy of GRBs to the electromagnetic energy of black holes. The fit of the afterglow fixes the only two free parameters of the model and leads to a new paradigm for the interpretation of the burst structure, the IBS paradigm. It leads as well to a reconsideration of the relative roles of the afterglow and burst in GRBs by defining two new phases in this complex phenomenon: a) the injector phase, giving rise to the proper-GRB (P-GRB), and b) the beam-target phase, giving rise to the extended afterglow peak emission (E-APE) and to the afterglow. Such differentiation leads to a

natural possible explanation of the bimodal distribution of GRBs observed by BATSE. The agreement with the observational data in regions extending from the horizon of the EMBH all the way out to the distant observer confirms the uniqueness of the model.

9. R. Ruffini, C.L. Bianco, P. Chardonnet, F. Fraschetti, S.-S. Xue; "On a possible Gamma-Ray Burst-Supernova time sequence"; The Astrophysical Journal, 555, L117 (2001).

   The data from the Chandra satellite on the iron emission lines in the afterglow of GRB 991216 are used to give further support for the EMBH theory, which links the origin of the energy of GRBs to the extractable energy of electromagnetic black holes (EMBHs), leading to an interpretation of the GRB-supernova correlation. Following the relative space-time transformation (RSTT) paradigm and the interpretation of the burst structure (IBS) paradigm, we introduce a paradigm for the correlation between GRBs and supernovae. The following sequence of events is shown as kinematically possible and consistent with the available data: a) the GRB-progenitor star P_1 first collapses to an EMBH, b) the proper GRB (P-GRB) and the peak of the afterglow (E-APE) propagate in interstellar space until the impact on a supernova-progenitor star P_2 at a distance $\leq 2.69 \times 10^{17}$ cm, and they induce the supernova explosion, c) the accelerated baryonic matter (ABM) pulse, originating the afterglow, reaches the supernova remnants 18.5 hours after the supernova explosion and gives rise to the iron emission lines. Some considerations on the dynamical implementation of the paradigm are presented. The concept of induced supernova explosion introduced here specifically for the GRB-supernova correlation may have more general application in relativistic astrophysics.

10. R. Ruffini, C.L. Bianco, P. Chardonnet, F. Fraschetti, S.-S. Xue; "On the physical processes which lie at the bases of time variability of GRBs"; Il Nuovo Cimento B, 116, 99 (2001).

    The relative-space-time-transformation (RSTT) paradigm and the interpretation of the burst-structure (IBS) paradigm are applied to probe the origin of the time variability of GRBs. Again GRB 991216 is used as a prototypical case, thanks to the precise data from the CGRO, RXTE and Chandra satellites. It is found that with the exception of the relatively inconspicuous but scientifically very important signal originating from the initial "proper gamma ray burst" (P-GRB), all the other spikes and time variabilities can be explained by the interaction of the accelerated-baryonic-matter pulse with inhomogeneities in the

interstellar matter. This can be demonstrated by using the RSTT paradigm as well as the IBS paradigm, to trace a typical spike observed in arrival time back to the corresponding one in the laboratory time. Using these paradigms, the identification of the physical nature of the time variablity of the GRBs can be made most convincingly. It is made explicit the dependence of a) the intensities of the afterglow, b) the spikes amplitude and c) the actual time structure on the Lorentz gamma factor of the accelerated-baryonic-matter pulse. In principle it is possible to read off from the spike structure the detailed density contrast of the interstellar medium in the host galaxy, even at very high redshift.

11. R. Ruffini, C.L. Bianco, P. Chardonnet, F. Fraschetti, S.-S. Xue; "On the structures in the afterglow peak emission of gamma ray bursts"; The Astrophysical Journal, 581, L19 (2002).

    Using GRB 991216 as a prototype, it is shown that the intensity substructures observed in what is generally called the "prompt emission" in gamma ray bursts (GRBs) do originate in the collision between the accelerated baryonic matter (ABM) pulse with inhomogeneities in the interstellar medium (ISM). The initial phase of such process occurs at a Lorentz factor $\gamma \sim 310$. The crossing of ISM inhomogeneities of sizes $\Delta R \sim 10^{15}$ cm occurs in a detector arrival time interval of ~ 0.4 s implying an apparent superluminal behavior of $\sim 10^5 c$. The long lasting debate between the validity of the external shock model vs. the internal shock model for GRBs is solved in favor of the first.

12. R. Ruffini, C.L. Bianco, P. Chardonnet, F. Fraschetti, S.-S. Xue; "On the structure of the burst and afterglow of Gamma-Ray Bursts I: the radial approximation"; International Journal of Modern Physics D, 12, 173 (2003).

    We have recently proposed three paradigms for the theoretical interpretation of gamma-ray bursts (GRBs). (1) The relative space-time transformation (RSTT) paradigm emphasizes how the knowledge of the entire world-line of the source from the moment of gravitational collapse is a necessary condition in order to interpret GRB data. (2) The interpretation of the burst structure (IBS) paradigm differentiates in all GRBs between an injector phase and a beam-target phase. (3) The GRB-supernova time sequence (GSTS) paradigm introduces the concept of *induced supernova explosion* in the supernovae-GRB association. In the introduction the RSTT and IBS paradigms are enunciated and illustrated using our theory based on the vacuum polarization process occurring around an electromagnetic black hole (EMBH theory). The results are summarized

using figures, diagrams and a complete table with the space-time grid, the fundamental parameters and the corresponding values of the Lorentz gamma factor for GRB 991216 used as a prototype. In the following sections the detailed treatment of the EMBH theory needed to understand the results of the three above letters is presented. We start from the considerations on the dyadosphere formation. We then review the basic hydrodynamic and rate equations, the equations leading to the relative space-time transformations as well as the adopted numerical integration techniques. We then illustrate the five fundamental eras of the EMBH theory: the self acceleration of the e^+e^- pair-electromagnetic plasma (PEM pulse), its interaction with the baryonic remnant of the progenitor star, the further self acceleration of the e^+e^- pair-electroma--gnetic radiation and baryon plasma (PEMB pulse). We then study the approach of the PEMB pulse to transparency, the emission of the proper GRB (P-GRB) and its relation to the "short GRBs". Particular attention is given to the free parameters of the theory and to the values of the thermodynamical quantities at transparency. Finally the three different regimes of the afterglow are described within the fully radiative and radial approximations: the ultrarelativistic, the relativistic and the nonrelativistic regimes. The best fit of the theory leads to an unequivocal identification of the "long GRBs" as extended emission occurring at the afterglow peak (E-APE). The relative intensities, the time separation and the hardness ratio of the P-GRB and the E-APE are used as distinctive observational test of the EMBH theory and the excellent agreement between our theoretical predictions and the observations are documented. The afterglow power-law indexes in the EMBH theory are compared and contrasted with the ones in the literature, and no beaming process is found for GRB 991216. Finally, some preliminary results relating the observed time variability of the E-APE to the inhomogeneities in the interstellar medium are presented, as well as some general considerations on the EMBH formation. The issue of the GSTS paradigm will be the object of a forthcoming publication and the relevance of the iron-lines observed in GRB 991216 is shortly reviewed. The general conclusions are then presented based on the three fundamental parameters of the EMBH theory: the dyadosphere energy, the baryonic mass of the remnant, the interstellar medium density. An in depth discussion and comparison of the EMBH theory with alternative theories is presented as well as indications of further developments beyond the radial approximation, which will be the subject of paper II in this series. Future needs for specific GRB observations are outlined.

13. R. Ruffini, C.L. Bianco, P. Chardonnet, F. Fraschetti, V. Gurzadyan, S.-S. Xue; "On the instantaneous spectrum of gamma ray bursts"; International Journal of Modern Physics D, 13, 843 (2004).

    A theoretical attempt to identify the physical process responsible for the afterglow emission of Gamma-Ray Bursts (GRBs) is presented, leading to the occurrence of thermal emission in the comoving frame of the shock wave giving rise to the bursts. The determination of the luminosities and spectra involves integration over an infinite number of Planckian spectra, weighted by appropriate relativistic transformations, each one corresponding to a different viewing angle in the past light cone of the observer. The relativistic transformations have been computed using the equations of motion of GRBs within our theory, giving special attention to the determination of the equitemporal surfaces. The only free parameter of the present theory is the "effective emitting area" in the shock wave front. A self consistent model for the observed hard-to-soft transition in GRBs is also presented. When applied to GRB 991216 a precise fit $\left(\chi^2 \simeq 1.078\right)$ of the observed luminosity in the 2–10 keV band is obtained. Similarly, detailed estimates of the observed luminosity in the 50–300 keV and in the 10–50 keV bands are obtained.

4.2 Conference proceedings

1. R. Ruffini; "Beyond the critical mass: The dyadosphere of black holes"; in "Black Holes and High Energy Astrophysics", H. sato, N. Sugiyama, Editors; p. 167; Universal Academy Press (Tokyo, Japan, 1998).

    The "dyadosphere" (from the Greek word "duas-duados" for pairs) is here defined as the region outside the horizon of a black hole endowed with an electromagnetic field (abbreviated to EMBH for "electromagnetic black hole") where the electromagnetic field exceeds the critical value, predicted by Heisenberg and Euler for e^+e^- pair production. In a very short time ($\sim O(\hbar/mc^2)$), a very large number of pairs is created there. I give limits on the EMBH parameters leading to a Dyadosphere for $10M_\odot$ and $10^5 M_\odot$ EMBH's, and give as well the pair densities as functions of the radial coordinate. These data give the initial conditions for the analysis of an enormous pair-electromagnetic-pulse or "PEM-pulse" which naturally leads to relativistic expansion. Basic energy requirements for gamma ray bursts (GRB), including GRB971214 recently observed at $z = 3.4$, can be accounted for by processes occurring in the dyado-

sphere.

2. R. Ruffini, C.L. Bianco, P. Chardonnet, F. Fraschetti, L. Vitagliano, S.-S. Xue; "New perspectives in physics and astrophysics from the theoretical understanding of Gamma-Ray Bursts"; in "COSMOLOGY AND GRAVITATION: Xth Brazilian School of Cosmology and Gravitation; 25th Anniversary (1977-2002)", Proceedings of the Xth Brazilian School on Cosmology and Gravitation, Mangaratiba, Rio de Janeiro (Brazil), July - August 2002, M. Novello, S.E. Perez Bergliaffa, Editors; AIP Conference Proceedings, 668, 16 (2003).

   If due attention is given in formulating the basic equations for the Gamma-Ray Burst (GRB) phenomenon and in performing the corresponding quantitative analysis, GRBs open a main avenue of inquiring on totally new physical and astrophysical regimes. This program is very likely one of the greatest computational efforts in physics and astrophysics and cannot be actuated using shortcuts. A systematic approach is needed which has been highlighted in three basic new paradigms: the relative space-time transformation (RSTT) paradigm, the interpretation of the burst structure (IBS) paradigm, the GRB-supernova time sequence (GSTS) paradigm. From the point of view of fundamental physics new regimes are explored: (1) the process of energy extraction from black holes; (2) the quantum and general relativistic effects of matter-antimatter creation near the black hole horizon; (3) the physics of ultrarelativisitc shock waves with Lorentz gamma factor $\gamma > 100$. From the point of view of astronomy and astrophysics also new regimes are explored: (i) the occurrence of gravitational collapse to a black hole from a critical mass core of mass $M \gtrsim 10M_{\odot}$, which clearly differs from the values of the critical mass encountered in the study of stars "catalyzed at the endpoint of thermonuclear evolution" (white dwarfs and neutron stars); (ii) the extremely high efficiency of the spherical collapse to a black hole, where almost 99.99% of the core mass collapses leaving negligible remnant; (iii) the necessity of developing a fine tuning in the final phases of thermonuclear evolution of the stars, both for the star collapsing to the black hole and the surrounding ones, in order to explain the possible occurrence of the "induced gravitational collapse". New regimes are as well encountered from the point of view of nature of GRBs: (I) the basic structure of GRBs is uniquely composed by a proper-GRB (P-GRB) and the afterglow; (II) the long bursts are then simply explained as the peak of the afterglow (the E-APE) and their observed time variability is explained in terms of inhomogeneities in the interstellar medium (ISM); (III) the short bursts are

identified with the P-GRBs and the crucial information on general relativistic and vacuum polarization effects are encoded in their spectra and intensity time variability. A new class of space missions to acquire information on such extreme new regimes are urgently needed.

3. R. Ruffini, C.L. Bianco, P. Chardonnet, F. Fraschetti, S.-S. Xue; "The EMBH Model in GRB 991216 and GRB 980425"; in Proceedings of "Third Rome Workshop on Gamma-Ray Burst in the Afterglow Era", 17-20 September 2002; M. Feroci, F. Frontera, N. Masetti, L. Piro, Editors; ASP Conference Series, 312, 349 (2004).

   This is a summary of the two talks presented at the Rome GRB meeting by C.L. Bianco and R. Ruffini. It is shown that by respecting the Relative Space-Time Transformation (RSTT) paradigm and the Interpretation of the Burst Structure (IBS) paradigm, important inferences are possible: a) in the new physics occurring in the energy sources of GRBs, b) on the structure of the bursts and c) on the composition of the interstellar matter surrounding the source.

4. M.G. Bernardini, C.L. Bianco, P. Chardonnet, F. Fraschetti, R. Ruffini, S.-S. Xue; "A New Astrophysical 'Triptych': GRB030329/SN2003dh/ URCA-2"; in "GAMMA-RAY BURSTS: 30 YEARS OF DISCOVERY", Proceedings of the Los Alamos "Gamma Ray Burst Symposium", Santa Fe, New Mexico, 8 12 September 2003, E.E. Fenimore, M. Galassi, Editors; AIP Conference Proceedings, 727, 312 (2004).

   We analyze the data of the Gamma-Ray Burst/Supernova GRB030329/ SN2003dh system obtained by HETE-2, R-XTE, XMM and VLT within our theory for GRB030329. By fitting the only three free parameters of the EMBH theory, we obtain the luminosity in fixed energy bands for the prompt emission and the afterglow. Since the Gamma-Ray Burst (GRB) analysis is consistent with a spherically symmetric expansion, the energy of GRB030329 is $E = 2.1 \times 10^{52}$ erg, namely $\sim 2 \times 10^3$ times larger than the Supernova energy. We conclude that either the GRB is triggering an induced-supernova event or both the GRB and the Supernova are triggered by the same relativistic process. In no way the GRB can be originated from the supernova. We also evidence that the XMM observations, much like in the system GRB980425/SN1998bw, are not part of the GRB afterglow, as interpreted in the literature, but are associated to the Supernova phenomenon. A dedicated campaign of observations is needed to confirm the nature of this XMM source as a newly born neutron star cooling by generalized URCA processes.

5. F. Fraschetti, M.G. Bernardini, C.L. Bianco, P. Chardonnet, R. Ruffini, S.-S. Xue; "The GRB980425-SN1998bw Association in the EMBH Model"; in "GAMMA-RAY BURSTS: 30 YEARS OF DISCOVERY", Proceedings of the Los Alamos "Gamma Ray Burst Symposium", Santa Fe, New Mexico, 8 12 September 2003, E.E. Fenimore, M. Galassi, Editors; AIP Conference Proceedings, 727, 424 (2004).

   Our GRB theory, previously developed using GRB 991216 as a prototype, is here applied to GRB 980425. We fit the luminosity observed in the 40–700 keV, 2–26 keV and 2–10 keV bands by the BeppoSAX satellite. In addition the supernova SN1998bw is the outcome of an "induced gravitational collapse" triggered by GRB 980425, in agreement with the GRB-Supernova Time Sequence (GSTS) paradigm. A further outcome of this astrophysically exceptional sequence of events is the formation of a young neutron star generated by the SN1998bw event. A coordinated observational activity is recommended to further enlighten the underlying scenario of this most unique astrophysical system.

6. A. Corsi, M.G. Bernardini, C.L. Bianco, P. Chardonnet, F. Fraschetti, R. Ruffini, S.-S. Xue; "GRB 970228 Within the EMBH Model"; in "GAMMA-RAY BURSTS: 30 YEARS OF DISCOVERY", Proceedings of the Los Alamos "Gamma Ray Burst Symposium", Santa Fe, New Mexico, 8 12 September 2003, E.E. Fenimore, M. Galassi, Editors; AIP Conference Proceedings, 727, 428 (2004).

   We consider the gamma-ray burst of 1997 February 28 (GRB 970228) within the ElectroMagnetic Black Hole (EMBH) model. We first determine the value of the two free parameters that characterize energetically the GRB phenomenon in the EMBH model, that is to say the dyadosphere energy, $E_{dya} = 5.1 \times 10^{52}$ ergs, and the baryonic remnant mass M_B in units of E_{dya}, $B = M_B c^2 / E_{dya} = 3.0 \times 10^{-3}$. Having in this way estimated the energy emitted during the beam-target phase, we evaluate the role of the InterStellar Medium (ISM) number density (n_{ISM}) and of the ratio $\mathcal{R}$ between the effective emitting area and the total surface area of the GRB source, in reproducing the observed profiles of the GRB 970228 prompt emission and X-ray (2-10 keV energy band) afterglow. The importance of the ISM distribution three-dimensional treatment around the central black hole is also stressed in this analysis.

5 Publications (2005–2016)

5.1 Refereed journals

1. R. Ruffini, C.L. Bianco, P. Chardonnet, F. Fraschetti, V. Gurzadyan, S.-S. Xue; "Emergence of a filamentary structure in the fireball from GRB spectra"; International Journal of Modern Physics D, 14, 97 (2005).

   It is shown that the concept of a fireball with a definite filamentary structure naturally emerges from the analysis of the spectra of Gamma-Ray Bursts (GRBs). These results, made possible by the recently obtained analytic expressions of the equitemporal surfaces in the GRB afterglow, depend crucially on the single parameter R describing the effective area of the fireball emitting the X-ray and gamma-ray radiation. The X-ray and gamma-ray components of the afterglow radiation are shown to have a thermal spectrum in the comoving frame of the fireball and originate from a stable shock front described self-consistently by the Rankine-Hugoniot equations. Precise predictions are presented on a correlation between spectral changes and intensity variations in the prompt radiation verifiable, e.g., by the Swift and future missions. The highly variable optical and radio emission depends instead on the parameters of the surrounding medium. The GRB 991216 is used as a prototype for this model.

2. R. Ruffini, M.G. Bernardini, C.L. Bianco, P. Chardonnet, F. Fraschetti, V. Gurzadyan, M. Lattanzi, L. Vitagliano, S.-S. Xue; "Extracting energy from black holes: 'long' and 'short' GRBs and their astrophysical settings"; Il Nuovo Cimento C, 28, 589 (2005).

   The introduction of the three interpretational paradigms for Gamma-Ray Bursts (GRBs) and recent progress in understanding the X- and gamma-ray luminosity in the afterglow allow us to make assessments about the astrophysical settings of GRBs. In particular, we evidence the distinct possibility that some GRBs occur in a binary system. This subclass of GRBs manifests itself in a "tryptich": one component formed by the collapse of a massive star to a black

hole, which originates the GRB; a second component by a supernova and a third one by a young neutron star born in the supernova event. Similarly, the understanding of the physics of quantum relativistic processes during the gravitational collapse makes possible precise predictions about the structure of short GRBs.

3. M.G. Bernardini, C.L. Bianco, P. Chardonnet, F. Fraschetti, R. Ruffini, S.-S. Xue; "Theoretical interpretation of luminosity and spectral properties of GRB 031203"; The Astrophysical Journal, 634, L29 (2005).

   The X-ray and gamma-ray observations of the source GRB 031203 by INTEGRAL are interpreted within our theoretical model. In addition to a complete spacetime parameterization of the GRB, we specifically assume that the afterglow emission originates from a thermal spectrum in the comoving frame of the expanding baryonic matter shell. By determining the two free parameters of the model and estimating the density and filamentary structure of the ISM, we reproduce the observed luminosity in the 20-200 keV energy band. As in previous sources, the prompt radiation is shown to coincide with the peak of the afterglow, and the luminosity substructure is shown to originate in the filamentary structure of the ISM. We predict a clear hard-to-soft behavior in the instantaneous spectra. The time-integrated spectrum over 20 s observed by INTEGRAL is well fitted. Despite the fact that this source has been considered "unusual", it appears to us to be a normal low-energy GRB.

4. R. Ruffini, M.G. Bernardini, C.L. Bianco, P. Chardonnet, F. Fraschetti, S.-S. Xue; Evidence for isotropic emission in GRB991216; Advances in Space Research, 38, 1291 (2006).

   The issue of the possible presence or absence of jets in GRBs is here re-examined for GRB991216. We compare and contrast our theoretically predicted afterglow luminosity in the 2–10 keV band for spherically symmetric versus jetted emission. At these wavelengths the jetted emission can be excluded and data analysis confirms spherical symmetry. These theoretical fits are expected to be improved by the forthcoming data of the Swift mission.

5. R. Ruffini, M.G. Bernardini, C.L. Bianco, P. Chardonnet, F. Fraschetti, R. Guida, S.-S. Xue; "GRB 050315: A step toward understanding the uniqueness of the overall GRB structure"; The Astrophysical Journal, 645, L109 (2006).

Using the Swift data of GRB 050315, we are making progress toward understanding the uniqueness of our theoretically predicted gamma-ray burst (GRB) structure, which is composed of a proper GRB (P-GRB), emitted at the transparency of an electron-positron plasma with suitable baryon loading, and an afterglow comprising the so-called prompt emission due to external shocks. Thanks to the Swift observations, the P-GRB is identified, and for the first time we can theoretically fit detailed light curves for selected energy bands on a continuous timescale ranging over 106 s. The theoretically predicted instantaneous spectral distribution over the entire afterglow is presented, confirming a clear hard-to-soft behavior encompassing, continuously, the "prompt emission" all the way to the latest phases of the afterglow.

6. C.L. Bianco, L. Caito, R. Ruffini; "Theoretical interpretation of GRB 011121"; Il Nuovo Cimento B, 121, 1441 (2006).

   GRB011121 is analyzed as a prototype to understand the "flares" recently observed by Swift in the afterglow of many GRB sources. Detailed theoretical computation of the GRB011121 light curves in selected energy bands are presented and compared and contrasted with observational BeppoSAX data.

7. R. Ruffini, M.G. Bernardini, C.L. Bianco, P. Chardonnet, F. Fraschetti, R. Guida, S.-S. Xue; "GRB 050315: A step toward the uniqueness of the overall GRB structure"; Il Nuovo Cimento B, 121, 1367 (2006).

   Using the *Swift* data of GRB 050315, we progress on the uniqueness of our theoretically predicted Gamma-Ray Burst (GRB) structure as composed by a proper-GRB (P-GRB), emitted at the transparency of an electron-positron plasma with suitable baryon loading, and an afterglow comprising the so called "prompt emission" as due to external shocks. Thanks to the *Swift* observations, we can theoretically fit detailed light curves for selected energy bands on a continuous time scale ranging over 10^6 seconds. The theoretically predicted instantaneous spectral distribution over the entire afterglow confirms a clear hard-to-soft behavior encompassing, continuously, the "prompt emission" all the way to the latest phases of the afterglow. Consequences of the instrumental threshold on the definition of "short" and "long" GRBs are discussed.

8. M.G. Bernardini, C.L. Bianco, L. Caito, P. Chardonnet, A. Corsi, M.G. Dainotti, F. Fraschetti, R. Guida, R. Ruffini, S.-S. Xue; GRB970228 as a prototype for short GRBs with afterglow; Il Nuovo Cimento B, 121, 1439 (2006).

GRB970228 is analyzed as a prototype to understand the relative role of short GRBs and their associated afterglows, recently observed by Swift and HETE-II. Detailed theoretical computation of the GRB970228 light curves in selected energy bands are presented and compared with observational BeppoSAX data.

9. M.G. Dainotti, M.G. Bernardini, C.L. Bianco, L. Caito, R. Guida, R. Ruffini; "GRB060218 and GRBs associated with Supernovae Ib/c"; Astronomy & Astrophysics, 471, L29 (2007).

   Context: The *Swift* satellite has given continuous data in the range 0.3–150 keV from 0 s to 10^6 s for GRB060218 associated with SN2006aj. This Gamma-Ray Burst (GRB) which has an unusually long duration ($T_{90} \sim 2100$ s) fulfills the Amati relation. These data offer the opportunity to probe theoretical models for GRBs connected with Supernovae (SNe).
   Aims: We plan to fit the complete γ- and X-ray light curves of this long duration GRB, including the prompt emission, in order to clarify the nature of the progenitors and the astrophysical scenario of the class of GRBs associated with SNe Ib/c.
   Methods: We apply our "fireshell" model based on the formation of a black hole, giving the relevant references. It is characterized by the precise equations of motion and equitemporal surfaces and by the role of thermal emission.
   Results: The initial total energy of the electron-positron plasma $E_{e^\pm}^{tot} = 2.32 \times 10^{50}$ erg has a particularly low value, similar to the other GRBs associated with SNe. For the first time, we observe a baryon loading $B = 10^{-2}$ which coincides with the upper limit for the dynamical stability of the fireshell. The effective CircumBurst Medium (CBM) density shows a radial dependence $n_{cbm} \propto r^{-\alpha}$ with $1.0 \lesssim \alpha \lesssim 1.7$ and monotonically decreases from 1 to 10^{-6} particles/cm^3. This behavior is interpreted as being due to a fragmentation in the fireshell. Analogies with the fragmented density and filling factor characterizing Novae are outlined. The fit presented is particularly significant in view of the complete data set available for GRB060218 and of the fact that it fulfills the Amati relation.
   Conclusions: We fit GRB060218, usually considered as an X-Ray Flash (XRF), as a "canonical GRB" within our theoretical model. The smallest possible black hole, formed by the gravitational collapse of a neutron star in a binary system, is consistent with the especially low energetics of the class of GRBs associated with SNe Ib/c. We provide the first evidence for a fragmentation in the fireshell. This fragmentation is crucial in explaining both the unusually large T_{90} and the consequently inferred abnormally low value of the CBM effective

density.

10. M.G. Bernardini, C.L. Bianco, L. Caito, M.G. Dainotti, R. Guida, R. Ruffini; "GRB970228 and a class of GRBs with an initial spikelike emission"; Astronomy & Astrophysics, 474, L13 (2007).

    Context: The discovery by *Swift* and HETE-2 of an afterglow emission associated possibly with short GRBs opened the new problematic of their nature and classification. This issue has been further enhanced by the observation of GRB060614 and by a new analysis of the BATSE catalog which led to the identification of a new class of GRBs with "an occasional softer extended emission lasting tenths of seconds after an initial spikelike emission".
    Aims: We plan a twofold task: a) to fit this new class of "hybrid" sources within our "canonical GRB" scenario, where all GRBs are generated by a "common engine" (i.e. the gravitational collapse to a black hole); b) to propose GRB970228 as the prototype of the above mentioned class, since it shares the same morphology and observational features.
    Methods: We analyze *Beppo*SAX data on GRB970228 within the "fireshell" model and we determine the parameters describing the source and the CircumBurst Medium (CBM) needed to reproduce its light curves in the 40–700 keV and 2–26 keV energy bands.
    Results: We find that GRB970228 is a "canonical GRB", like e.g. GRB050315, with the main peculiarity of a particularly low average density of the CBM $\langle n_{cbm} \rangle \sim 10^{-3}$ particles/cm^3. We also simulate the light curve corresponding to a rescaled CBM density profile with $\langle n_{cbm} \rangle = 1$ particle/cm^3. From such a comparison it follows that the total time-integrated luminosity is a faithful indicator of the nature of GRBs, contrary to the peak luminosity which is merely a function of the CBM density.
    Conclusions: We call attention on discriminating the short GRBs between the "genuine" and the "fake" ones. The "genuine" ones are intrinsically short, with baryon loading $B \lesssim 10^{-5}$, as stated in our original classification. The "fake" ones, characterized by an initial spikelike emission followed by an extended emission lasting tenths of seconds, have a baryon loading $10^{-4} \lesssim B \leq 10^{-2}$. They are observed as such only due to an underdense CBM consistent with a galactic halo environment which deflates the afterglow intensity.

11. R. Guida, M.G. Bernardini, C.L. Bianco, L. Caito, M.G. Dainotti, R. Ruffini; "The Amati relation in the "fireshell" model"; Astronomy & Astrophysics, 487, L37 (2008).

Context: The cosmological origin of gamma-ray bursts (GRBs) has been firmly established, with redshifts up to $z = 6.29$. They are possible candidates for use as "distance indicators" for testing cosmological models in a redshift range hardly achievable by other cosmological probes. Asserting the validity of the empirical relations among GRB observables is now crucial for their calibration.
Aims: Motivated by the relation proposed by Amati and collaborators, we look within the "fireshell" model for a relation between the peak energy E_p of the νF_ν total time-integrated spectrum of the afterglow and the total energy of the afterglow E_{aft}, which in our model encompasses and extends the prompt emission.
Methods: The fit within the fireshell model, as for the "canonical" GRB050315, uses the complete arrival time coverage given by the Swift satellite. It is performed simultaneously, self-consistently, and recursively in the four BAT energy bands (15–25 keV, 25–50 keV, 50–100 keV, and 100-150 keV), as well as in the XRT one (0.2–10 keV). It uniquely determines the two free parameters characterizing the GRB source, the total energy $E_{tot}^{e^\pm}$ of the $e^\pm$ plasma and its baryon loading B, as well as the effective CircumBurst Medium (CBM) distribution. We can then build two sets of "gedanken" GRBs varying the total energy of the electron-positron plasma $E_{tot}^{e^\pm}$ and keeping the same baryon loading B of GRB050315. The first set assumes the one obtained in the fit of GRB050315 for the effective CBM density. The second set assumes instead a constant CBM density equal to the average value of the GRB050315 prompt phase.
Results: For the first set of "gedanken" GRBs we find a relation $E_p \propto (E_{aft})^a$, with $a = 0.45 \pm 0.01$, whose slope strictly agrees with the Amati one. Such a relation, in the limit $B \to 10^{-2}$, coincides with the Amati one. Instead, no correlation is found in the second set of "gedanken" GRBs.
Conclusions: Our analysis excludes the proper GRB (P-GRB) from the prompt emission, extends all the way to the latest afterglow phases, and is independent of the assumed cosmological model, since all "gedanken" GRBs are at the same redshift. The Amati relation, on the other hand, includes the P-GRB, focuses only on the prompt emission, being therefore influenced by the instrumental threshold that fixes the end of the prompt emission, and depends on the assumed cosmology. This might explain the intrinsic scatter observed in the Amati relation.

12. L. Caito, M.G. Bernardini, C.L. Bianco, M.G. Dainotti, R. Guida, R. Ruffini; "GRB060614: a "fake" short GRB from a merging binary system"; Astronomy & Astrophysics, 489, 501 (2009).

Context: GRB060614 observations by VLT and by Swift have infringed the traditionally accepted gamma-ray burst (GRB) collapsar scenario that purports the origin of all long duration GRBs from supernovae (SN). GRB060614 is the first nearby long duration GRB clearly not associated with a bright Ib/c SN. Moreover, its duration ($T_{90} \sim 100$ s) makes it hardly classifiable as a short GRB. It presents strong similarities with GRB970228, the prototype of a new class of "fake" short GRBs that appear to originate from the coalescence of binary neutron stars or white dwarfs spiraled out into the galactic halo. *Aims*: Within the "canonical" GRB scenario based on the "fireshell" model, we test if GRB060614 can be a "fake" or "disguised" short GRB. We model the traditionally termed "prompt emission" and discriminate the signal originating from the gravitational collapse leading to the GRB from the process occurring in the circumburst medium (CBM). *Methods*: We fit GRB060614 light curves in Swift's BAT ($15 - 150$ keV) and XRT ($0.2 - 10$ keV) energy bands. Within the fireshell model, light curves are formed by two well defined and different components: the proper-GRB (P-GRB), emitted when the fireshell becomes transparent, and the extended afterglow, due to the interaction between the leftover accelerated baryonic and leptonic shell and the CBM. *Results*: We determine the two free parameters describing the GRB source within the fireshell model: the total $e^{\pm}$ plasma energy ($E_{tot}^{e^{\pm}} = 2.94 \times 10^{51}$erg) and baryon loading ($B = 2.8 \times 10^{-3}$). A small average CBM density $\sim 10^{-3}$ particles/cm^3 is inferred, typical of galactic halos. The first spikelike emission is identified with the P-GRB and the following prolonged emission with the extended afterglow peak. We obtain very good agreement in the BAT ($15 - 150$ keV) energy band, in what is traditionally called "prompt emission", and in the XRT ($0.2 - 10$ keV) one. *Conclusions*: The *anomalous* GRB060614 finds a natural interpretation within our canonical GRB scenario: it is a "disguised" short GRB. The total time-integrated extended afterglow luminosity is greater than the P-GRB one, but its peak luminosity is smaller since it is deflated by the peculiarly low average CBM density of galactic halos. This result points to an old binary system, likely formed by a white dwarf and a neutron star, as the progenitor of GRB060614 and well justifies the absence of an associated SN Ib/c. Particularly important for further studies of the final merging process are the temporal structures in the P-GRB down to 0.1 s.

13. M.G. Bernardini, C.L. Bianco, L. Caito, M.G. Dainotti, R. Guida, R. Ruffini; "GRB970228 in the "canonical GRB" scenario"; Journal of the Korean Physical Society, 56, 1575 (2010).

Within the "fireshell" model, we define a "canonical GRB" light curve with two sharply different components: the proper-GRB (P-GRB), emitted when the optically thick fireshell of an electron-positron plasma originating from the phenomenon reaches transparency, and the afterglow, emitted due to the collision between the remaining optically thin fireshell and the circumburst medium (CBM). On the basis of the recent understanding of GRB970228 as the prototype for a new class of GRBs with "an occasional softer extended emission lasting tenths of seconds after an initial spikelike emission", we outline our "canonical GRB" scenario, originating from the gravitational collapse to a black hole, with special emphasis on the discrimination between "genuine" and "fake" short GRBs. Furthermore, we investigate how the GRB970228 analysis provides a theoretical explanation for the apparent absence of such a correlation for the GRBs belonging to this new class.

14. L. Caito, M.G. Bernardini, C.L. Bianco, M.G. Dainotti, R. Guida, R. Ruffini; "GRB060614: a preliminary result"; Journal of the Korean Physical Society, 56, 1579 (2010).

    The explosion of GRB 060614 produced a deep break in the GRB scenario and opened new horizons of investigation because it can't be traced back to any traditional scheme of classification. In fact, it manifests peculiarities both of long bursts and of short bursts, and above all, it is the first case of a long-duration near GRB without any bright Ib/c associated Supernova. We will show that, in our canonical GRB scenario, this "anomalous" situation finds a natural interpretation and allows us to discuss a possible variation in the traditional classification scheme, introducing a distinction between "genuine" and "fake" short bursts.

15. M.G. Dainotti, M.G. Bernardini, C.L. Bianco, L. Caito, R. Guida, R. Ruffini; "The astrophysical trypthic: GRB, SN and URCA can be extended to GRB060218?"; Journal of the Korean Physical Society, 56, 1588 (2010).

    The *Swift* satellite has given continuous data in the range 0.3–150 keV from 0 s to 10^6 s for GRB060218 associated with SN2006aj. This GRB is the fourth GRB spectroscopically associated with SNe after the cases of GRB980425-SN1998bw, GRB031203-SN2003lw, GRB 030329-SN2003dh. It has an unusually long duration ($T_{90} \sim 2100$ s). These data offer the opportunity to probe theoretical models for Gamma-Ray Bursts (GRBs) connected with Supernovae (SNe). We plan to fit the complete γ- and X-ray light curves of this long duration GRB,

including the prompt emission, in order to clarify the nature of the progenitors and the astrophysical scenario of the class of GRBs associated to SNe Ib/c. We apply our "fireshell" model based on the formation of a black hole, giving the relevant references. The initial total energy of the electron-positron plasma $E_{e^\pm}^{tot} = 2.32 \times 10^{50}$ erg has a particularly low value similarly to the other GRBs associated with SNe. For the first time we observe a baryon loading $B = 10^{-2}$ which coincides with the upper limit for the dynamical stability of the fireshell. The effective CircumBurst Medium (CBM) density shows a radial dependence $n_{cbm} \propto r^{-\alpha}$ with $1.0 \lesssim \alpha \lesssim 1.7$ and monotonically decreases from 1 to 10^{-6} particles/cm^3. Such a behavior is interpreted as due to a fragmentation in the fireshell. Such a fragmentation is crucial in explaining both the unusually large T_{90} and the consequently inferred abnormal low value of the CBM effective density. We fit GRB060218, usually considered as an X-Ray Flash (XRF), as a "canonical GRB" within our theoretical model. The smallest possible black hole, formed by the gravitational collapse of a neutron star in a binary system, is consistent with the especially low energetics of the class of GRBs associated with SNe Ib/c. We present the URCA process and the connection between the GRBs associated with SNe extended also to the case of GRB060218.

16. L. Izzo, M.G. Bernardini, C.L. Bianco, L. Caito, B. Patricelli, R. Ruffini; "GRB 090423 at Redshift 8.1: a Theoretical Interpretation"; Journal of the Korean Physical Society, 57, 551 (2010).

    GRB 090423 is the farthest gamma ray burst ever observed, with a redshift of about 8.1. We present within the fireshell scenario a complete analysis of this GRB. We model the prompt emission and the first rapid flux decay of the afterglow emission as being to the canonical emission of the interaction in the interval $0 \leq t \leq 440$ s by using accelerated baryonic matter with the circumburst medium. After the data reduction of the Swift data in the BAT (15 - 150 keV) and XRT (0.2 - 10 keV) energy bands, we interpret the light curves and the spectral distribution in the context of the fireshell scenario. We also confirm in this source the existence of a second component, a plateau phase, as being responsible for the late emission in the X-ray light curve. This extra component originates from the fact that the ejecta have a range of the bulk Lorentz Γ factor, which starts to interact each other ejecta at the start of the plateau phase.

17. L. Caito, L. Amati, M.G. Bernardini, C.L. Bianco, G. De Barros, L. Izzo, B. Patricelli, R. Ruffini; "GRB 071227: an additional case of a disguised

short burst"; Astronomy & Astrophysics, 521, A80 (2010).

Context: Observations of gamma-ray bursts (GRBs) have shown an hybridization between the two classes of long and short bursts. In the context of the fireshell model, the GRB light curves are formed by two different components: the *proper* GRB (P-GRB) and the extended afterglow. Their relative intensity is linked to the fireshell baryon loading B. The GRBs with P-GRB predominance are the short ones, the remainders are long. A new family of *disguised* short bursts has been identified: long bursts with a protracted low instantaneous luminosity due to a low density CircumBurst Medium (CBM). In the 15–150 keV energy band GRB 071227 exhibits a short duration (about 1.8s) spike-like emission followed by a very soft extended tail up to one hundred seconds after the trigger. It is a faint ($E_{iso} = 5.8 \times 10^{50}$) nearby GRB ($z = 0.383$) that does not have an associated type Ib/c bright supernova (SN). For these reasons, GRB 071227 has been classified as a short burst not fulfilling the Amati relation holding for long burst. *Aims:* We check the classification of GRB 071227 provided by the fireshell model. In particular, we test whether this burst is another example of a *disguised* short burst, after GRB 970228 and GRB 060614, and, for this reason, whether it fulfills the Amati relation. *Methods:* We simulate GRB 071227 light curves in the *Swift* BAT 15–50 keV bandpass and in the XRT (0.3–10 keV) energy band within the fireshell model. *Results:* We perform simulations of the tail in the 15–50 keV bandpass, as well as of the first part of the X-ray afterglow. This infers that: $E_{tot}^{e^{\pm}} = 5.04 \times 10^{51}$ erg, $B = 2.0 \times 10^{-4}$, $E_{P-GRB}/E_{aft} \sim 0.25$, and $\langle n_{cbm} \rangle = 3.33$ particles/cm^3. These values are consistent with those of "long duration" GRBs. We interpret the observed energy of the first hard emission by identifying it with the P-GRB emission. The remaining long soft tail indeed fulfills the Amati relation. *Conclusions:* Previously classified as a short burst, GRB 071227 on the basis of our analysis performed in the context of the fireshell scenario represents another example of a *disguised* short burst, after GRB 970228 and GRB 060614. Further confirmation of this result is that the soft tail of GRB 071227 fulfills the Amati relation.

18. M.G. Bernardini, C.L. Bianco, L. Caito, L. Izzo, B. Patricelli, R. Ruffini; "Analysis of GRB060607A within the fireshell model: prompt emission, X-ray flares and late afterglow phase"; Astronomy & Astrophysics, submitted to.

Context: GRB060607A is a very distant ($z = 3.082$) and energetic event ($E_{iso} \sim 10^{53}$ erg). Its main peculiarity is that the peak of the near-infrared (NIR) af-

terglow has been observed with the REM robotic telescope. This NIR peak has been interpreted as the afterglow onset within the fireball forward shock model, and the initial Lorentz gamma factor of the emitting system has been inferred. *Aims*: We analyze GRB060607A within the fireshell model. We emphasize the central role of the prompt emission in determining the initial Lorentz gamma factor of the extended afterglow and we interpret the X-ray flares as produced by the interaction of the optically thin fireshell with overdense CircumBurst Medium (CBM) clumps. *Methods*: We deal only with the Swift BAT and XRT observations, that are the basic contribution to the GRB emission and that are neglected in the treatment adopted in the current literature. The numerical modeling of the fireshell dynamics allows to calculate all its characteristic quantities, in particular the exact value of the Lorentz gamma factor at the transparency. *Results*: We show that the theoretically computed prompt emission light curves are in good agreement with the observations in all the *Swift* BAT energy bands as well as the spectra integrated over different time intervals. The flares observed in the decaying phase of the X-ray afterglow are also reproduced by the same mechanism, but in a region in which the typical dimensions of the clumps are smaller than the visible area of the fireshell and most energy lies in the X-ray band due to the hard-to-soft evolution. *Conclusions*: We show that it is possible to obtain flares with $\Delta t/t$ compatible with the observations when the three-dimensional structure of the CBM clumps is duly taken into account. We stop our analysis at the beginning of the X-ray plateau phase, since we suppose this originates from the instabilities developed in the collision between different subshells within a structured fireshell.

19. G. de Barros, M. G. Bernardini, C.L. Bianco, L. Caito, L. Izzo, B. Patricelli, R. Ruffini; "On the nature of GRB 050509b: a disguised short GRB"; Astronomy & Astrophyscs, 529, A130 (2011)

    Context: GRB 050509b, detected by the *Swift* satellite, is the first case where an X-ray afterglow has been observed associated with a short gamma-ray burst (GRB). Within the fireshell model, the canonical GRB light curve presents two different components: the proper-GRB (P-GRB) and the extended afterglow. Their relative intensity is a function of the fireshell baryon loading parameter B and of the CircumBurst Medium (CBM) density (n_{CBM}). In particular, the traditionally called short GRBs can be either "genuine" short GRBs (with $B \lesssim 10^{-5}$, where the P-GRB is energetically predominant) or "disguised" short GRBs (with $B \gtrsim 3.0 \times 10^{-4}$ and $n_{CBM} \ll 1$, where the extended afterglow is energetically predominant). *Aims*: We verify whether GRB 050509b can be clas-

sified as a "genuine" short or a "disguised" short GRB, in the fireshell model. *Methods*: We investigate two alternative scenarios. In the first, we start from the assumption that this GRB is a "genuine" short burst. In the second attempt, we assume that this GRB is a "disguised" burst. *Results*: If GRB 050509b were a genuine short GRB, there should initially be very hard emission which is ruled out by the observations. The analysis that assumes that this is a disguised short GRB is compatible with the observations. The theoretical model predicts a value of the extended afterglow energy peak that is consistent with the Amati relation. *Conclusions*: GRB 050509b cannot be classified as a "genuine" short GRB. The observational data are consistent with a "disguised" short GRB classification, i.e., a long burst with a weak extended afterglow "deflated" by the low density of the CBM. We expect that all short GRBs with measured redshifts are disguised short GRBs because of a selection effect: if there is enough energy in the afterglow to measure the redshift, then the proper GRB must be less energetic than the afterglow. The Amati relation is found to be fulfilled only by the extended afterglow excluding the P-GRB.

20. L. Caito, M.G. Bernardini, C.L. Bianco, L. Izzo, B. Patricelli, R. Ruffini; "GRB 071227: another disguised short burst"; International Journal of Modern Physics D, 20, 1931 (2011).

    Observations of Gamma-ray Bursts (GRBs) put forward in the recent years have revealed, with increasing evidence, that the historical classification between long and short bursts has to be revised. Within the Fireshell scenario, both short and long bursts are canonical bursts, consisting of two different phases. First, a Proper-GRB (P-GRB), that is the emission of photons at the transparency of the fireshell. Then, the Extended Afterglow, multiwavelength emission due to the interacion of the baryonic remnants of the fireshell with the CircumBurst Medium (CBM). We discriminate between long and short bursts by the amount of energy stored in the first phase with respect to the second one. Within the Fireshell scenario, we have introduced a third intermediate class: the disguised GRBs. They appear like short bursts, because their morphology is characterized by a first, short, hard episode and a following deflated tail, but this last part — coincident with the peak of the afterglow — is energetically predominant. The origin of this peculiar kind of sources is inferred to a very low average density of the environment (of the order of 10^{-3}). After GRB 970228 and GRB 060614, we find in GRB 071227 a third example of disguised burst.

21. L. Izzo, M.G. Bernardini, C.L. Bianco, L. Caito, B. Patricelli, L.J. Rangel Lemos, R. Ruffini; "GRB 080916C and the high-energy emission in the fireshell scenario"; International Journal of Modern Physics D, 20, 1949 (2011).

    In this paper we discuss a possible explanation for the high energy emission (up to $\sim$ GeV) seen in GRB 080916C. We propose that the GeV emission is originated by the collision between relativistic baryons in the fireshell after the transparency and the nucleons located in molecular clouds near the burst site. This collision should give rise pion production, whose immediate decay provides high energy photons, neutrinos and leptons. Using a public code (SYBILL) we simulate these relativistic collisions in their simple form, so that we can draw our preliminar results in this paper. We will present moreover our hypothesis that the delayed onset of this emission identifies in a complete way the P-GRB emission.

22. B. Patricelli, M.G. Bernardini, C.L. Bianco, L. Caito, L. Izzo, R. Ruffini, G. Vereshchagin; "A new spectral energy distribution of photons in the fireshell model of GRBs"; International Journal of Modern Physics D, 20, 1983 (2011).

    The analysis of various Gamma-Ray Bursts (GRBs) having a low energetics (an isotropic energy $E_{iso} \lesssim 10^{53}$ ergs) within the fireshell model has shown how the $N(E)$ spectrum of their prompt emission can be reproduced in a satisfactory way by a convolution of thermal spectra. Nevertheless, from the study of very energetic bursts ($E_{iso} \lesssim 10^{54}$ ergs) such as, for example, GRB 080319B, some discrepancies between the numerical simulations and the observational data have been observed. We investigate a different spectrum of photons in the comoving frame of the fireshell in order to better reproduce the spectral properties of GRB prompt emission within the fireshell model. We introduce a phenomenologically modified thermal spectrum: a thermal spectrum characterized by a different asymptotic power-law index in the low energy region. Such an index depends on a free parameter α, so that the pure thermal spectrum corresponds to the case $\alpha = 0$. We test this spectrum by comparing the numerical simulations with the observed prompt emission spectra of various GRBs. From this analysis it has emerged that the observational data can be correctly reproduced by assuming a modified thermal spectrum with $\alpha = -1.8$.

23. A.V. Penacchioni, R. Ruffini, L. Izzo, M. Muccino, C.L. Bianco, L. Caito, B. Patricelli, L. Amati; "Evidence for a proto-black hole and a double

astrophysical component in GRB 101023"; Astronomy & Astrophysics, 538, A58 (2012).

Context: It has been recently shown that GRB 090618, observed by AGILE, Coronas Photon, Fermi, Konus, Suzaku and Swift, is composed of two very different components: episode 1, lasting 50 s, shows a thermal plus power-law spectrum with a characteristic temperature evolving in time as a power law; episode 2 (the remaining 100 s) is a canonical long GRB. We have associated episode 1 to the progenitor of a collapsing bare core leading to the formation of a black hole: what was defined as a "proto black hole". *Aims*: In precise analogy with GRB 090618 we aim to analyze the 89s of the emission of GRB 101023, observed by Fermi, Gemini, Konus and Swift, to see if there are two different episodes: the first one presenting a characteristic black-body temperature evolving in time as a broken power law, and the second one consistent with a canonical GRB. *Methods*: To obtain information on the spectra, we analyzed the data provided by the GBM detector onboard the Fermi satellite, and we used the heasoft package XSPEC and RMFIT to obtain their spectral distribution. We also used the numerical code GRBsim to simulate the emission in the context of the fireshell scenario for episode 2. *Results*: We confirm that the first episode can be well fit by a black body plus power-law spectral model. The temperature changes with time following a broken power law, and the photon index of the power-law component presents a soft-to-hard evolution. We estimate that the radius of this source increases with time with a velocity of $1.5 \times 10^4 km/s$. The second episode appears to be a canonical GRB. By using the Amati and the Atteia relations, we determined the cosmological redshift, $z \sim 0.9 \pm 0.084(stat.) \pm 0.2(sys.)$. The results of GRB 090618 are compared and contrasted with the results of GRB 101023. Particularly striking is the scaling law of the soft X-ray component of the afterglow. *Conclusions*: We identify GRB 090618 and GRB 101023 with a new family of GRBs related to a single core collapse and presenting two astrophysical components: a first one related to the proto-black hole prior to the process of gravitational collapse (episode 1), and a second one, which is the canonical GRB (episode 2) emitted during the formation of the black hole. For the first time we are witnessing the process of a black hole formation from the instants preceding the gravitational collapse up to the GRB emission. This analysis indicates progress towards developing a GRB distance indicator based on understanding the P-GRB and the prompt emission, as well as the soft X-ray behavior of the late afterglow.

24. R. Negreiros, R. Ruffini, C. L. Bianco, J. A. Rueda; "Cooling of young

neutron stars in GRB associated to supernovae"; Astronomy & Astrophysics, 540, A12 (2012).

Context: The traditional study of neutron star cooling has been generally applied to quite old objects such as the Crab Pulsar (957 years) or the central compact object in Cassiopeia A (330 years) with an observed surface temperature $\sim 10^6$ K. However, recent observations of the late ($t = 10^8$–10^9 s) emission of the supernovae (SNe) associated to GRBs (GRB-SN) show a distinctive emission in the X-ray regime consistent with temperatures $\sim 10^7$–10^8 K. Similar features have been also observed in two Type Ic SNe SN 2002ap and SN 1994I that are not associated to GRBs. *Aims*: We advance the possibility that the late X-ray emission observed in GRB-SN and in isolated SN is associated to a hot neutron star just formed in the SN event, here defined as a neo-neutron star. *Methods*: We discuss the thermal evolution of neo-neutron stars in the age regime that spans from ~ 1 minute (just after the proto-neutron star phase) all the way up to ages < 10–100 yr. We examine critically the key factor governing the neo-neutron star cooling with special emphasis on the neutrino emission. We introduce a phenomenological heating source, as well as new boundary conditions, in order to mimic the high temperature of the atmosphere for young neutron stars. In this way we match the neo-neutron star luminosity to the observed late X-ray emission of the GRB-SN events: URCA-1 in GRB980425-SN1998bw, URCA-2 in GRB030329-SN2003dh, and URCA-3 in GRB031203-SN2003lw. *Results*: We identify the major role played by the neutrino emissivity in the thermal evolution of neo-neutron stars. By calibrating our additional heating source at early times to $\sim 10^{12}$–10^{15} erg/g/s, we find a striking agreement of the luminosity obtained from the cooling of a neo-neutron stars with the prolonged ($t = 10^8$–10^9 s) X-ray emission observed in GRB associated with SN. It is therefore appropriate a revision of the boundary conditions usually used in the thermal cooling theory of neutron stars, to match the proper conditions of the atmosphere at young ages. The traditional thermal processes taking place in the crust might be enhanced by the extreme high-temperature conditions of a neo-neutron star. Additional heating processes that are still not studied within this context, such as e^+e^- pair creation by overcritical fields, nuclear fusion, and fission energy release, might also take place under such conditions and deserve further analysis. *Conclusions*: Observation of GRB-SN has shown the possibility of witnessing the thermal evolution of neo-neutron stars. A new campaign of dedicated observations is recommended both of GRB-SN and of isolated Type Ic SN.

25. L. Izzo, R. Ruffini, A.V. Penacchioni, C.L. Bianco, L. Caito, S.K. Chakrabarti, J.A. Rueda, A. Nandi, B. Patricelli; "A double component in GRB 090618: a proto-black hole and a genuinely long gamma-ray burst"; Astronomy & Astrophysics, 543, A10 (2012).

Context: The joint X-ray and gamma-ray observations of GRB 090618 by very many satellites offer an unprecedented possibility of testing crucial aspects of theoretical models. In particular, they allow us to test (a) in the process of gravitational collapse, the formation of an optically thick e+e.-baryon plasma self-accelerating to Lorentz factors in the range $200 < \Gamma < 3000$; (b) its transparency condition with the emission of a component of 10^{53-54} baryons in the TeV region and (c) the collision of these baryons with the circumburst medium (CBM) clouds, characterized by dimensions of 10^{15-16} cm. In addition, these observations offer the possibility of testing a new understanding of the thermal and power-law components in the early phase of this GRB. *Aims*: We test the fireshell model of GRBs in one of the closest ($z = 0.54$) and most energetic ($E_{iso} = 2.90 \times 10^{53}$ erg) GRBs, namely GRB 090618. It was observed at ideal conditions by several satellites, namely *Fermi*, *Swift*, Konus-WIND, AGILE, RT-2, and Suzaku, as well as from on-ground optical observatories. *Methods*: We analyzed the emission from GRB 090618 using several spectral models, with special attention to the thermal and power-law components. We determined the fundamental parameters of a canonical GRB within the context of the fireshell model, including the identification of the total energy of the e^+e^- plasma, $E_{tot}^{e^+e^-}$, the proper GRB (P-GRB), the baryon load, the density and structure of the CBM. *Results*: We find evidence of the existence of two different episodes in GRB 090618. The first episode lasts 50 s and is characterized by a spectrum consisting of a thermal component, which evolves between $kT = 54$ keV and $kT = 12$ keV, and a power law with an average index $\gamma = 1.75 \pm 0.04$. The second episode, which lasts for ~ 100 s, behaves as a canonical long GRB with a Lorentz gamma factor at transparency of $\Gamma = 495$, a temperature at transparency of 29.22 keV and with a characteristic size of the surrounding clouds of $R_{cl} \sim 10^{15-16}$ cm and masses of $\sim 10^{22-24}$ g. *Conclusions*: We support the recently proposed two-component nature of GRB 090618, namely, episode 1 and episode 2, with a specific theoretical analysis.We furthermore illustrate that episode 1 cannot be considered to be either a GRB or a part of a GRB event, but it appears to be related to the progenitor of the collapsing bare core, leading to the formation of the black hole, which we call a "proto-black hole". Thus, for the first time, we are witnessing the process of formation of a black

hole from the phases just preceding the gravitational collapse all the way up to the GRB emission.

26. B. Patricelli, M.G. Bernardini, C.L. Bianco, L. Caito, G. De Barros, L. Izzo, R. Ruffini, G.V. Vereshchagin; "Analysis of GRB 080319B and GRB 050904 within the Fireshell Model: Evidence for a Broader Spectral Energy Distribution"; The Astrophysical Journal, 756, 16 (2012).

    The observation of GRB 080319B, with an isotropic energy $E_{iso} = 1.32 \times 10^{54}$ erg, and GRB 050904, with $E_{iso} = 1.04 \times 10^{54}$ erg, offers the possibility of studying the spectral properties of the prompt radiation of two of the most energetic Gamma Ray Bursts (GRBs). This allows us to probe the validity of the fireshell model for GRBs beyond 10^{54} erg, well outside the energy range where it has been successfully tested up to now (10^{49}–10^{53} erg). We find that in the low energy region, the prompt emission spectra observed by *Swift* BAT reveals more power than theoretically predicted. The opportunities offered by these observations to improve the fireshell model are outlined in this paper. One of the distinguishing features of the fireshell model is that it relates the observed GRB spectra to the spectrum in the comoving frame of the fireshell. Originally, a fully radiative condition and a comoving thermal spectrum were adopted. An additional power-law in the comoving thermal spectrum is required due to the discrepancy of the theoretical and observed light curves and spectra in the fireshell model for GRBs 080319B and 050904. A new phenomenological parameter α is correspondingly introduced in the model. We perform numerical simulations of the prompt emission in the *Swift* BAT bandpass by assuming different values of α within the fireshell model. We compare them with the GRB 080319B and GRB 050904 observed time-resolved spectra, as well as with their time-integrated spectra and light curves. Although GRB 080319B and GRB 050904 are at very different redshifts (z=0.937 and z=6.29 respectively), a value of $\alpha = -1.8$ leads for both of them to a good agreement between the numerical simulations and the observed BAT light curves, time-resolved and time-integrated spectra. Such a modified spectrum is also consistent with the observations of previously analyzed less energetic GRBs and reasons for this additional agreement are given. Perspectives for future low energy missions are outlined.

27. M. Muccino, R. Ruffini, C.L. Bianco, L. Izzo, A.V. Penacchioni; "GRB 090227B: The missing link between the genuine short and long GRBs"; The Astrophysical Journal, 763, 125 (2013).

The time-resolved spectral analysis of GRB 090227B, made possible by the *Fermi*-GBM data, allows to identify in this source the missing link between the genuine short and long GRBs. Within the Fireshell model of the Gamma-Ray Bursts (GRBs) we predict genuine short GRBs: bursts with the same inner engine of the long bursts but endowed with a severely low value of the Baryon load, $B \lesssim 5 \times 10^{-5}$. A first energetically predominant emission occurs at the transparency of the e^+e^- plasma, the Proper-GRB (P-GRB), followed by a softer emission, the extended afterglow. The typical separation between the two emissions is expected to be of the order of 10^{-3} – 10^{-2} s. We identify the P-GRB of GRB 090227B in the first 96 ms of emission, where a thermal component with the temperature $kT = (517 \pm 28)$ keV and a flux comparable with the non thermal part of the spectrum is observed. This non thermal component as well as the subsequent emission, where there is no evidence for a thermal spectrum, is identified with the extended afterglow. We deduce a theoretical cosmological redshift $z = 1.61 \pm 0.14$. We then derive the total energy $E^{tot}_{e^+e^-} = (2.83 \pm 0.15) \times 10^{53}$ ergs, the Baryon load $B = (4.13 \pm 0.05) \times 10^{-5}$, the Lorentz Γ factor at transparency $\Gamma_{tr} = (1.44 \pm 0.01) \times 10^4$, and the intrinsic duration $\Delta t' \sim 0.35$ s. We also determine the average density of the CircumBurst Medium (CBM), $\langle n_{CBM} \rangle = (1.90 \pm 0.20) \times 10^{-5}$ particles/cm^3. There is no evidence of beaming in the system. In view of the energetics and of the Baryon load of the source, as well as of the low interstellar medium and of the intrinsic time scale of the signal, we identify the GRB progenitor as a binary neutron star. From the recent progress in the theory of neutron stars, we obtain masses of the stars $m_1 = m_2 = 1.34 M_\odot$ and their corresponding radii $R_1 = R_2 = 12.24$ km and thickness of their crusts ~ 0.47 km, consistent with the above values of the Baryon load, of the energetics and of the time duration of the event.

28. A.V. Penacchioni, R. Ruffini, C.L. Bianco, L. Izzo, M. Muccino, G.B. Pisani, J.A. Rueda; "GRB 110709B in the induced gravitational collapse paradigm"; Astronomy & Astrophysics, 551, A133 (2013).

    Context: GRB 110709B is the first source for which *Swift* BAT triggered twice, with a time separation of ~ 10 minutes. The first emission (called here Episode 1) goes from 40 s before the first trigger up to 60 s after it. The second emission (hereafter Episode 2) goes from 35 s before the second trigger to 100 s after it. These features reproduce the ones of GRB 090618, which has been recently interpreted within the Induced Gravitational Collapse paradigm (IGC). In line with this paradigm we assume the progenitor to be a close binary system composed of a core of an evolved star and a Neutron Star (NS). The evolved star

explodes as a Supernova (SN) and ejects material that is partially accreted by the NS. We identify this process with Episode 1. The accretion process brings the NS over its critical mass, thus gravitationally collapsing to a BH. This process leads to the GRB emission, Episode 2. The double trigger has given for the first time the possibility to have a coverage of the X-ray emission observed by XRT both prior to and during the prompt phase of GRB 110709B. *Aims*: We analyze the spectra and time variability of Episode 1 and 2 and compute the relevant parameters of the binary progenitor, as well as the astrophysical parameters both in the SN and the GRB phase in the IGC paradigm. *Methods*: We perform a time-resolved spectral analysis of Episode 1 by fitting the spectrum with a blackbody (BB) plus a power-law (PL) spectral model. From the BB fluxes and temperatures of Episode 1 and the luminosity distance d_L, we evaluate the evolution with time of the radius of the BB emitter, associated here to the evolution of the SN ejecta. We analyze Episode 2 within the Fireshell model, identifying the Proper-GRB (P-GRB) and simulating the light curve and spectrum. We establish the redshift to be $z = 0.75$, following the phenomenological methods by Amati, by Yonetoku and by Grupe, and our analysis of the late X-ray afterglow. It is most remarkable that the determination of the cosmological redshift on the ground of the scaling of the late X-ray afterglow, already verified in GRB 090618 and GRB 101023, is again verified by this analysis. *Results*: We find for Episode 1 a temperature of the BB component that evolves with time following a broken PL, with the slope of the PL at early times $\alpha = 0$ (constant function) and the slope of the PL at late times $\beta = -4 \pm 2$. The break occurs at $t = 41.21$ s. The total energy of Episode 1 is $E_{iso}^{(1)} = 1.42 \times 10^{53}$ erg. The total energy of Episode 2 is $E_{iso}^{(2)} = 2.43 \times 10^{52}$ erg. We find at transparency a Lorentz factor $\Gamma \sim 1.73 \times 10^2$, laboratory radius of 6.04×10^{13} cm, P-GRB observed temperature $kT_{P-GRB} = 12.36$ keV, baryon load $B = 5.7 \times 10^{-3}$ and P-GRB energy of $E_{P-GRB} = 3.44 \times 10^{50}$ erg. We find a remarkable coincidence of the cosmological redshift by the scaling of the XRT data and with three other phenomenological methods. *Conclusions*: We interpret GRB 110709B as a member of the IGC sources, together with GRB 970828, GRB 090618 and GRB 101023. The existence of the XRT data during the prompt phase of the emission of GRB 110709B (Episode 2) offers an unprecedented tool for improving the diagnostic of GRBs emission.

29. G.B. Pisani, L. Izzo, R. Ruffini, C.L. Bianco, M. Muccino, A.V. Penacchioni, J.A. Rueda, Y. Wang; "Novel distance indicator for gamma-ray bursts associated with supernovae"; Astronomy & Astrophysics, 552,

L5 (2013).

Context: In recent years it has been proposed that the temporal coincidence of a Gamma Ray Burst (GRB) and a type Ib/c supernova (SN) can be explained by the concept of Induced Gravitational Collapse (IGC) of a Neutron Star (NS) to a Black Hole (BH) by accretion of matter ejected by a SN Ib/c. This scenario reveals a possible common behavior in the late time X-ray emission of this subclass of GRBs. *Aims*: We want to test if such a common behavior can actually be present in the sources belonging to this GRB sub-class and if this may lead to a redshift estimator for these sources. *Methods*: We build a sample of GRBs belonging to this sub-class, and we rescale the X-ray light curves of all of them both in time and in flux to a common cosmological redshift. *Results*: We found that the X-ray light curves of all the GRBs of the sample with a measured redshift present a common late time behavior when rescaled to a common redshift $z = 1$. We then use this result to estimate the redshift of the GRBs of the sample with no measured redshift. *Conclusions*: The common behavior in the late decay of the X-ray light curves of the GRBs of the sample points to a common physical mechanism in this particular phase of the GRB emission, possibly related to the SN process. This scenario may represent an invaluable tool to estimate the redshift of GRBs belonging to this sub-class of events. More GRBs are therefore needed in order to enlarge the subclass and to make more stringent constraints on the redshift estimates performed with this method for GRBs pertaining to this class.

30. C.L. Bianco, M. G. Bernardini, L. Caito, G. De Barros, L. Izzo, M. Muccino, B. Patricelli, A.V. Penacchioni, G.B. Pisani, R. Ruffini; "The canonical GRB scenario"; Il Nuovo Cimento C, 36 s01, 21 (2013).

    The canonical GRB scenario implied by the fireshell model is briefly summarized.

31. A.V. Penacchioni, R. Ruffini, L. Izzo, M. Muccino, C.L. Bianco, L. Caito, B. Patricelli; "Evidences for a double component in the emission of GRB 101023"; Il Nuovo Cimento C, 36 s01, 117 (2013).

    In this work we present the results of the analysis of GRB 101023 in the fireshell scenario. Its redshift is not known, so we attempted to infer it from the Amati Relation, obtaining $z = 0.9$. Its light curve presents a double emission, which makes it very similar to the already studied GRB 090618. We called each part Episode 1 and Episode 2. We performed a time-resolved spectral

analysis with RMFIT using different spectral models, and fitted the light curve with a numerical code integrating the fireshell equations of motion. We used Fermi GBM data to build the light curve, in particular the second NaI detector, in the range (8.5–1000 keV). We considered different hypotheses regarding which part of the light curve could be the GRB and performed the analysis of all of them. We noticed a great variation of the temperature with time in the first episode, as well as almost no variation of the progenitor radius. We found that the first emission does not match the requirements for a GRB, while the second part perfectly agrees with being a canonical GRB, with a P-GRB lasting 4 s.

32. M. Muccino, R. Ruffini, C.L. Bianco, L. Izzo, A.V. Penacchioni, G.B. Pisani; "GRB 090510: A Disguised Short Gamma-Ray Burst with the Highest Lorentz Factor and Circumburst Medium"; The Astrophysical Journal, 772, 62 (2013).

    GRB 090510, observed both by Fermi and AGILE satellites, is the first bright short-hard Gamma-Ray Burst (GRB) with an emission from the keV up to the GeV energy range. Within the Fireshell model, we interpret the faint precursor in the light curve as the emission at the transparency of the expanding e^+e^- plasma: the Proper-GRB (P-GRB). From the observed isotropic energy we assume a total plasma energy $E^{tot}_{e^+e^-} = (1.10 \pm 0.06) \times 10^{53}$erg and derive a Baryon load $B = (1.45 \pm 0.28) \times 10^{-3}$ and a Lorentz factor at transparency $\Gamma_{tr} = (6.7 \pm 1.6) \times 10^2$. The main emission $\sim$ 0.4s after the initial spike is interpreted as the extended afterglow, due to the interaction of the ultrarelativistic baryons with the CircumBurst Medium (CBM). Using the condition of fully radiative regime, we infer a CBM average spherically symmetric density of $\langle n_{CBM} \rangle = (1.85 \pm 0.14) \times 10^3$ particles/cm^3, one of the highest found in the Fireshell model. The value of the filling factor, $1.5 \times 10^{-10} \leq \mathcal{R} \leq 3.8 \times 10^{-8}$, leads to the estimate of filaments with densities $n_{fil} = n_{CBM}/\mathcal{R} \approx (10^6 - 10^{14})$ particles/cm^3. The sub-MeV and the MeV emissions are well reproduced. When compared to the canonical GRBs with $\langle n_{CBM} \rangle \approx 1$ particles/cm^3 and to the disguised short GRBs with $\langle n_{CBM} \rangle \approx 10^{-3}$ particles/cm^3, the case of GRB 090510 leads to the existence of a new family of bursts exploding in an over-dense galactic region with $\langle n_{CBM} \rangle \approx 10^3$ particles/cm^3. The joint effect of the high Γ_{tr} and the high density compresses in time and "inflates" in intensity the extended afterglow, making it appear as a short burst, which we here define as "disguised short GRB by excess". The determination of the above parameters values may represent an important step towards the explanation

of the GeV emission.

33. R. Ruffini, M. Muccino, C.L. Bianco, M. Enderli, L. Izzo, M. Kovacevic, A.V. Penacchioni, G.B. Pisani, J.A. Rueda, Y. Wang; "On Binary Driven Hypernovae and their nested late X-ray emission"; Astronomy & Astrophysics, 565, L10 (2014).

    Context: The induced gravitational collapse (IGC) paradigm addresses the very energetic (10^{52}–10^{54} erg) long gamma-ray bursts (GRBs) associated to supernovae (SNe). Unlike the traditional "collapsar" model, an evolved FeCO core with a companion neutron star (NS) in a tight binary system is considered as the progenitor. This special class of sources, here named "binary driven hypernovae" (BdHNe), presents a composite sequence composed of four different episodes with precise spectral and luminosity features.
    Aims: We first compare and contrast the steep decay, the plateau, and the power-law decay of the X-ray luminosities of three selected BdHNe (GRB 060729, GRB 061121, and GRB 130427A). Second, to explain the different sizes and Lorentz factors of the emitting regions of the four episodes, for definiteness, we use the most complete set of data of GRB 090618. Finally, we show the possible role of r-process, which originates in the binary system of the progenitor.
    Methods: We compare and contrast the late X-ray luminosity of the above three BdHNe. We examine correlations between the time at the starting point of the constant late power-law decay t_a^*, the average prompt luminosity $\langle L_{iso} \rangle$, and the luminosity at the end of the plateau L_a. We analyze a thermal emission ($\sim$ 0.97–0.29 keV), observed during the X-ray steep decay phase of GRB 090618.
    Results: The late X-ray luminosities of the three BdHNe, in the rest-frame energy band 0.3–10 keV, show a precisely constrained "nested" structure. In a space-time diagram, we illustrate the different sizes and Lorentz factors of the emitting regions of the three episodes. For GRB 090618, we infer an initial dimension of the thermal emitter of $\sim 7 \times 10^{12}$ cm, expanding at $\Gamma \approx 2$. We find tighter correlations than the Dainotti-Willingale ones.
    Conclusions: We confirm a constant slope power-law behavior for the late X-ray luminosity in the source rest frame, which may lead to a new distance indicator for BdHNe. These results, as well as the emitter size and Lorentz factor, appear to be inconsistent with the traditional afterglow model based on synchrotron emission from an ultra-relativistic ($\Gamma \sim 10^2$–10^3) collimated jet outflow. We argue, instead, for the possible role of r-process, originating in the binary system, to power the mildly relativistic X-ray source.

34. R. Ruffini, L. Izzo, M. Muccino, G.B. Pisani, J.A. Rueda, Y. Wang, C. Barbarino, C.L. Bianco, M. Enderli, M. Kovacevic; "Induced gravitational collapse at extreme cosmological distances: the case of GRB 090423"; Astronomy & Astrophysics, 569, A39 (2014).

    Context: The induced gravitational collapse (IGC) scenario has been introduced in order to explain the most energetic gamma ray bursts (GRBs), $E_{iso} = 10^{52} - 10^{54}$ erg, associated with type Ib/c supernovae (SNe). It has led to the concept of binary-driven hypernovae (BdHNe) originating in a tight binary system composed by a FeCO core on the verge of a SN explosion and a companion neutron star (NS). Their evolution is characterized by a rapid sequence of events: 1) The SN explodes, giving birth to a new NS (νNS). The accretion of SN ejecta onto the companion NS increases its mass up to the critical value; 2) The consequent gravitational collapse is triggered, leading to the formation of a black hole (BH) with GRB emission; 3) A novel feature responsible for the emission in the GeV, X-ray, and optical energy range occurs and is characterized by specific power-law behavior in their luminosity evolution and total spectrum; 4) The optical observations of the SN then occurs.
    Aims: We investigate whether GRB 090423, one of the farthest observed GRB at $z = 8.2$, is a member of the BdHN family.
    Methods: We compare and contrast the spectra, the luminosity evolution, and the detectability in the observations by *Swift* of GRB 090423 with the corresponding ones of the best known BdHN case, GRB 090618.
    Results: Identification of constant slope power-law behavior in the late X-ray emission of GRB 090423 and its overlapping with the corresponding one in GRB 090618, measured in a common rest frame, represents the main result of this article. This result represents a very significant step on the way to using the scaling law properties, proven in Episode 3 of this BdHN family, as a cosmological standard candle.
    Conclusions: Having identified GRB 090423 as a member of the BdHN family, we can conclude that SN events, leading to NS formation, can already occur already at $z = 8.2$, namely at 650 Myr after the Big Bang. It is then possible that these BdHNe originate stem from 40-60 $M_\odot$ binaries. They are probing the Population II stars after the completion and possible disappearance of Population III stars.

35. M. Muccino, C.L. Bianco, L. Izzo, Y. Wang, M. Enderli, M. Kovacevic, G.B. Pisani, A.V. Penacchioni, R. Ruffini; "The Genuine Short GRB 090227B and the Disguised by Excess GRB 090510"; Gravitation and

Cosmology, 20, 197 (2014).

GRB 090227B and GRB 090510, traditionally classified as short gamma-ray Bursts (GRBs), indeed originate from different systems. For GRB 090227B we inferred a total energy of the e^+e^- plasma $E^{tot}_{e^+e^-} = (2.83 \pm 0.15) \times 10^{53}$ erg, a baryon load of $B = (4.1 \pm 0.05) \times 10^{-5}$, and a CircumBurst Medium (CBM) average density $\langle n_{CBM} \rangle = (1.90 \pm 0.20) \times 10^{-5}$ cm^{-3}. From these results we have assumed the progenitor of this burst to be a symmetric neutron stars (NSs) merger with masses $m = 1.34 M_\odot$, radii $R = 12.24$ km. GRB 090510, instead, has $E^{tot}_{e^+e^-} = (1.10 \pm 0.06) \times 10^{53}$ erg, $B = (1.45 \pm 0.28) \times 10^{-3}$, implying a Lorentz factor at transparency of $\Gamma = (6.7 \pm 1.7) \times 10^2$, which are characteristic of the long GRB class, and a very high CBM density, $\langle n_{CBM} \rangle = (1.85 \pm 0.14) \times 10^3$ cm^{-3}. The joint effect of the high values of Γ and of $\langle n_{CBM} \rangle$ compresses in time and "inflates" in intensity in an extended afterglow, making appear GRB 090510 as a short burst, which we here define as "disguised short GRB by excess" occurring an overdense region with 10^3 cm^{-3}.

36. M. Muccino, C.L. Bianco, L. Izzo, Y. Wang, M. Enderli, G.B. Pisani, A.V. Penacchioni, R. Ruffini; "Two short bursts originating from different astrophysical systems: The genuine short GRB 090227B and the disguised short GRB 090510 by excess"; Journal of the Korean Physical Society, 65, 865 (2014).

GRB 090227B and GRB 090510 are two gamma-ray bursts (GRBs) traditionally classified as short bursts. The major outcome of our analysis is that they indeed originate from different systems. In the case of GRB 090227B, from the inferred values of the total energy of the e^+e^- plasma, $E^{tot}_{e^+e^-} = (2.83 \pm 0.15) \times 10^{53}$ erg, the engulfed baryonic mass M_B, expressed as $B = M_B c^2 / E^{tot}_{e^+e^-} = (4.1 \pm 0.05) \times 10^{-5}$, and the circumburst medium (CBM) average density, $\langle n_{CBM} \rangle = (1.90 \pm 0.20) \times 10^{-5}$ cm^{-3}, we have assumed the progenitor of this burst to be a symmetric neutron star (NS) merger with masses $m = 1.34 M_\odot$, radii $R = 12.24$ km, and crustal thicknesses of $\sim$ 0.47 km. In the case of GRB 090510, we have derived the total plasma energy, $E^{tot}_{e^+e^-} = (1.10 \pm 0.06) \times 10^{53}$ erg, the Baryon load, $B = (1.45 \pm 0.28) \times 10^{-3}$, and the Lorentz factor at transparency, $\Gamma = (6.7 \pm 1.7) \times 10^2$, which are characteristic of the long GRB class, as well as a very high CBM density, $\langle n_{CBM} \rangle = (1.85 \pm 0.14) \times 10^3$ cm^{-3}. The joint effect of the high values of Γ and $\langle n_{CBM} \rangle$ compresses in time and "inflates" in intensity the extended afterglow, making GRB 090510 appear to be a short burst, which we here define as a "disguised short GRB by excess", occurring

in an overdense region with 10^3 cm^{-3}.

37. R. Ruffini, Y. Wang, M. Kovacevic, C.L. Bianco, M. Enderli, M. Muccino, A.V. Penacchioni, G.B. Pisani, J. Rueda; "GRB 130427A and SN 2013cq: A Multi-wavelength Analysis of An Induced Gravitational Collapse Event"; The Astrophysical Journal, 798, 10 (2015).

    We have performed our data analysis of the observations by *Swift*, *NuStar* and *Fermi* satellites in order to probe the induced gravitational collapse (IGC) paradigm for GRBs associated with supernovae (SNe), in the "terra incognita" of GRB 130427A. We compare and contrast our data analysis with those in the literature. We have verified that the GRB 130427A conforms to the IGC paradigm by examining the power law behavior of the luminosity in the early 10^4 s of the XRT observations. This has led to the identification of the four different episodes of the "binary driven hypernovae" (BdHNe) and to the prediction, on May 2, 2013, of the occurrence of SN 2013cq, duly observed in the optical band on May 13, 2013. The exceptional quality of the data has allowed the identification of novel features in *Episode 3* including: a) the confirmation and the extension of the existence of the recently discovered "nested structure" in the late X-ray luminosity in GRB 130427A, as well as the identification of a spiky structure at 10^2 s in the cosmological rest-frame of the source; b) a power law emission of the GeV luminosity light curve and its onset at the end of *Episode 2*; c) different Lorentz Γ factors for the emitting regions of the X-ray and GeV emissions in this *Episode 3*. These results make it possible to test the details of the physical and astrophysical regimes at work in the BdHNe: 1) a newly born neutron star and the supernova ejecta, originating in *Episode 1*, 2) a newly formed black hole originating in *Episode 2*, and 3) the possible interaction among these components, observable in the standard features of *Episode 3*.

38. M. Muccino, R. Ruffini, C.L. Bianco, M. Enderli, M. Kovacevic, L. Izzo, A.V. Penacchioni, G.B. Pisani, J.A. Rueda, Y. Wang; "On binary driven hypernovae and their nested late X-ray emission"; Astronomy Reports, 59, 581 (2015).

    The induced gravitational collapse (IGC) paradigm addresses energetic (10^{52}–10^{54} erg), long gamma-ray bursts (GRBs) associated to supernovae (SNe) and proposes as their progenitors tight binary systems composed of an evolved FeCO core and a companion neutron star (NS). Their emission is characterized by four specific episodes: Episode 1, corresponding to the on-set of the FeCO

SN explosion and the accretion of the ejecta onto the companion NS; Episode 2, related the collapse of the companion NS to a black hole (BH) and to the emission of a long GRB; Episode 3, observed in X-rays and characterized by a steep decay, a plateau phase and a late power-law decay; Episode 4, corresponding to the optical SN emission due to the ^{56}Ni decay. We focus on Episode 3 and we show that, from the thermal component observed during the steep decay of the prototype GRB 090618, the emission region has a typical dimension of $\sim 10^{13}$ cm, which is inconsistent with the typical size of the emitting region of GRBs, e.g., $\sim 10^{16}$ cm. We propose, therefore, that the X-ray afterglow emission originates from a spherically symmetric SN ejecta expanding at $\Gamma \sim 2$ or, possibly, from the accretion onto the newly formed black hole, and we name these systems "binary driven hypernovae" (BdHNe). This interpretation is alternative to the traditional afterglow model based on the GRB synchrotron emission from a collimated jet outflow, expanding at ultra-relativistic Lorentz factor of $\Gamma \sim 10^2 - 10^3$ and originating from the collapse of a single object. We show then that the rest-frame energy band 0.3–10 keV X-ray luminosities of three selected BdHNe, GRB 060729, GRB 061121, and GRB 130427A, evidence a precisely constrained "nested" structure and satisfy precise scaling laws between the average prompt luminosity, $< L_{iso} >$, and the luminosity at the end of the plateau, L_a, as functions of the time at the end of the plateau. All these features extend the applicability of the "cosmic candle" nature of Episode 3. The relevance of r-process in fulfilling the demanding scaling laws and the nested structure are indicated.

39. R. Ruffini, J.A. Rueda, C. Barbarino, C. L. Bianco, H. Dereli, M. Enderli, L. Izzo, M. Muccino, A.V. Penacchioni, G.B. Pisani, Y. Wang; "Induced Gravitational Collapse in the BATSE era: the case of GRB 970828"; Astronomy Reports, 59, 626 (2015).

    Following the recently established "Binary-driven HyperNova" (BdHN) paradigm, we here interpret GRB 970828 in terms of the four episodes typical of such a model. The "Episode 1", up to 40 s after the trigger time t_0, with a time varying thermal emission and a total energy of $E_{iso,1st} = 2.60 \times 10^{53}$ erg, is interpreted as due to the onset of an hyper-critical accretion process onto a companion neutron star, triggered by the companion star, an FeCO core approaching a SN explosion. The "Episode 2", observed up t_0+90 s, is interpreted as a canonical gamma ray burst, with an energy of $E_{tot}^{e^+e^-} = 1.60 \times 10^{53}$ erg, a baryon load of $B = 7 \times 10^{-3}$ and a bulk Lorentz factor at transparency of $\Gamma = 142.5$. From this Episode 2, we infer that the GRB exploded in an environment with a large av-

erage particle density $\langle n \rangle \approx 10^3$ particles/cm^3 and dense clouds characterized by typical dimensions of $(4 \div 8) \times 10^{14}$ cm and $\delta n/n \sim 10$. The "Episode 3" is identified from t_0+90 s all the way up to 10^{5-6} s: despite the paucity of the early X-ray data, typical in the BATSE, pre-Swift era, we find extremely significant data points in the late X-ray afterglow emission of GRB 970828, which corresponds to the ones observed in all BdHNe sources. The "Episode 4", related to the Supernova emission, does not appear to be observable in this source, due to the presence of darkening from the large density of the GRB environment, also inferred from the analysis of the Episode 2.

40. Y. Wang, R. Ruffini, M. Kovacevic, C.L. Bianco, M. Enderli, M. Muccino, A.V. Penacchioni, G.B. Pisani, J.A. Rueda; "Predicting supernova associated to gamma-ray burst 130427a"; Astronomy Reports, 59, 667 (2015).

    Binary systems constituted by a neutron star and a massive star are not rare in the universe. The Induced Gravitational Gamma-ray Burst (IGC) paradigm interprets Gamma-ray bursts as the outcome of a neutron star that collapses into a black hole due to the accretion of the ejecta coming from its companion massive star that underwent a supernova event. GRB 130427A is one of the most luminous GRBs ever observed, of which isotropic energy exceeds 10^{54} erg. And it is within one of the few GRBs obtained optical, X-ray and GeV spectra simultaneously for hundreds of seconds, which provides an unique opportunity so far to understand the multi-wavelength observation within the IGC paradigm, our data analysis found low Lorentz factor blackbody emission in the Episode 3 and its X-ray light curve overlaps typical IGC Golden Sample, which comply to the IGC mechanisms. We consider these findings as clues of GRB 130427A belonging to the IGC GRBs. We predicted on GCN the emergence of a supernova on May 2, 2013, which was later successfully detected on May 13, 2013.

41. R. Ruffini, M. Muccino, M. Kovacevic, F.G. Oliveira, J.A. Rueda, C.L. Bianco, M. Enderli, A.V. Penacchioni, G.B. Pisani, Y. Wang, E. Zaninoni; "GRB 140619B: a short GRB from a binary neutron star merger leading to black hole formation"; The Astrophysical Journal, 808, 190 (2015).

    We show the existence of two families of short GRBs, both originating from the merger of binary neutron stars (NSs): family-1 with $E_{iso} < 10^{52}$ erg, leading to a massive NS as the merged core, and family-2 with $E_{iso} > 10^{52}$ erg, leading to a black hole (BH). Following the identification of the prototype

GRB 090227B, we present the details of a new example of family-2 short burst: GRB 140619B. From the spectral analysis of the early ~ 0.2 s, we infer an observed temperature $kT = (324 \pm 33)$ keV of the e^+e^--plasma at transparency (P-GRB), a theoretically derived redshift $z = 2.67 \pm 0.37$, a total burst energy $E^{tot}_{e^+e^-} = (6.03 \pm 0.79) \times 10^{52}$ erg, a rest-frame peak energy $E_{p,i} = 4.7$ MeV, and a baryon load $B = (5.52 \pm 0.73) \times 10^{-5}$. We also estimate the corresponding emission of gravitational waves. Two additional examples of family-2 short bursts are identified: GRB 081024B and GRB 090510, remarkable for its well determined cosmological distance. We show that marked differences exist in the nature of the afterglows of these two families of short bursts: family-2 bursts, leading to BH formation, consistently exhibit high energy emission following the P-GRB emission; family-1 bursts, leading to the formation of a massive NS, should never exhibit high energy emission. We also show that both the families fulfill an $E_{p,i}$–E_{iso} relation with slope $\gamma = 0.59 \pm 0.07$ and a normalization constant incompatible with the one for long GRBs. The observed rate of such family-2 events is $\rho_0 = \left(2.1^{+2.8}_{-1.4}\right) \times 10^{-4}\mathrm{Gpc}^{-3}\mathrm{yr}^{-1}$.

42. R. Ruffini, Y. Aimuratov, C.L. Bianco, M. Enderli, M. Kovacevic, R. Moradi, M. Muccino, A.V. Penacchioni, G.B. Pisani, J.A. Rueda, Y. Wang; "Induced gravitational collapse in FeCO Core-Neutron star binaries and Neutron star-Neutron star binary mergers"; International Journal of Modern Physics A, 30, 1545023 (2015).

    We review the recent progress in understanding the nature of gamma-ray bursts (GRBs). The occurrence of GRB is explained by the Induced Gravitational Collapse (IGC) in FeCO Core-Neutron star binaries and Neutron star-Neutron star binary mergers, both processes occur within binary system progenitors. Making use of this most unexpected new paradigm, with the fundamental implications by the neutron star (NS) critical mass, we find that different initial configurations of binary systems lead to different GRB families with specific new physical predictions confirmed by observations.

43. R. Ruffini, M. Muccino, Y. Aimuratov, C.L. Bianco, C. Cherubini, M. Enderli, M. Kovacevic, R. Moradi, A.V. Penacchioni, G.B. Pisani, J.A. Rueda, Y. Wang; "GRB 090510: A genuine short-GRB from a binary neutron star coalescing into a Kerr-Newman black hole"; The Astrophysical Journal, 831, 178 (2016).

    In a new classification of merging binary neutron stars (NSs) we separate short gamma-ray bursts (GRBs) in two sub-classes. The ones with $E_{\mathrm{iso}} \lesssim 10^{52}$ erg

coalesce to form a massive NS and are indicated as short gamma-ray flashes (S-GRFs). The hardest, with $E_{\rm iso} \gtrsim 10^{52}$ erg, coalesce to form a black hole (BH) and are indicated as genuine short-GRBs (S-GRBs). Within the fireshell model, S-GRBs exhibit three different components: the P-GRB emission, observed at the transparency of a self-accelerating baryon-e^+e^- plasma; the prompt emission, originating from the interaction of the accelerated baryons with the circumburst medium; the high-energy (GeV) emission, observed after the P-GRB and indicating the formation of a BH. GRB 090510 gives the first evidence for the formation of a Kerr BH or, possibly, a Kerr-Newman BH. Its P-GRB spectrum can be fitted by a convolution of thermal spectra whose origin can be traced back to an axially symmetric dyadotorus. A large value of the angular momentum of the newborn BH is consistent with the large energetics of this S-GRB, which reach in the 1–10000 keV range $E_{\rm iso} = (3.95 \pm 0.21) \times 10^{52}$ erg and in the 0.1–100 GeV range $E_{\rm LAT} = (5.78 \pm 0.60) \times 10^{52}$ erg, the most energetic GeV emission ever observed in S-GRBs. The theoretical redshift $z_{\rm th} = 0.75 \pm 0.17$ that we derive from the fireshell theory is consistent with the spectroscopic measurement $z = 0.903 \pm 0.003$, showing the self-consistency of the theoretical approach. All S-GRBs exhibit GeV emission, when inside the *Fermi*-LAT field of view, unlike S-GRFs, which never evidence it. The GeV emission appears to be the discriminant for the formation of a BH in GRBs, confirmed by their observed overall energetics.

44. Ruffini, R.; Rueda, J. A.; Muccino, M.; Aimuratov, Y.; Becerra, L. M.; Bianco, C. L.; Kovacevic, M.; Moradi, R.; Oliveira, F. G.; Pisani, G. B.; Wang, Y.; On the classification of GRBs and their occurrence rates; The Astrophysical Journal, 832, 136 (2016).

    There is mounting evidence for the binary nature of the progenitors of gamma-ray bursts (GRBs). For a long GRB, the induced gravitational collapse (IGC) paradigm proposes as progenitor, or "in-state", a tight binary system composed of a carbon-oxygen core ($CO_{\rm core}$) undergoing a supernova (SN) explosion which triggers hypercritical accretion onto a neutron star (NS) companion. For a short GRB, a NS-NS merger is traditionally adopted as the progenitor. We divide long and short GRBs into two sub-classes, depending on whether or not a black hole (BH) is formed in the merger or in the hypercritical accretion process exceeding the NS critical mass. For long bursts, when no BH is formed we have the sub-class of X-ray flashes (XRFs), with isotropic energy $E_{iso} \lesssim 10^{52}$ erg and rest-frame spectral peak energy $E_{p,i} \lesssim 200$ keV. When a BH is formed we have the sub-class of binary-driven hypernovae (BdHNe),

with $E_{iso} \gtrsim 10^{52}$ erg and $E_{p,i} \gtrsim 200$ keV. In analogy, short bursts are similarly divided into two sub-classes. When no BH is formed, short gamma-ray flashes (S-GRFs) occur, with $E_{iso} \lesssim 10^{52}$ erg and $E_{p,i} \lesssim 2$ MeV. When a BH is formed, the authentic short GRBs (S-GRBs) occur, with $E_{iso} \gtrsim 10^{52}$ erg and $E_{p,i} \gtrsim 2$ MeV. We give examples and observational signatures of these four sub-classes and their rate of occurrence. From their respective rates it is possible that "in-states" of S-GRFs and S-GRBs originate from the "out-states" of XRFs. We indicate two additional progenitor systems: white dwarf-NS and BH-NS. These systems have hybrid features between long and short bursts. In the case of S-GRBs and BdHNe evidence is given of the coincidence of the onset of the high energy GeV emission with the birth of a Kerr BH.

45. Becerra, L.; Bianco, C. L.; Fryer, C. L.; Rueda, J. A.; Ruffini, R.; On the induced gravitational collapse scenario of gamma-ray bursts associated with supernovae; The Astrophysical Journal, 833, 107 (2016).

    Following the induced gravitational collapse (IGC) paradigm of gamma-ray bursts (GRBs) associated with type Ib/c supernovae, we present numerical simulations of the explosion of a carbon-oxygen (CO) core in a binary system with a neutron-star (NS) companion. The supernova ejecta trigger a *hypercritical* accretion process onto the NS thanks to a copious neutrino emission and the trapping of photons within the accretion flow. We show that temperatures 1–10 MeV develop near the NS surface, hence electron-positron annihilation into neutrinos becomes the main cooling channel leading to accretion rates 10^{-9}–10^{-1} $M_\odot$ s^{-1} and neutrino luminosities 10^{43}–10^{52} erg s^{-1} (the shorter the orbital period the higher the accretion rate). We estimate the maximum orbital period, $P_{\max}$, as a function of the NS initial mass, up to which the NS companion can reach by hypercritical accretion the critical mass for gravitational collapse leading to black-hole (BH) formation. We then estimate the effects of the accreting and orbiting NS companion onto a novel geometry of the supernova ejecta density profile. We present the results of a 1.4×10^7 particle simulation which show that the NS induces accentuated asymmetries in the ejecta density around the orbital plane. We elaborate on the observables associated with the above features of the IGC process. We apply this framework to specific GRBs: we find that X-ray flashes (XRFs) and binary-driven hypernovae (BdHNe) are produced in binaries with $P > P_{\max}$ and $P < P_{\max}$, respectively. We analyze in detail the case of XRF 060218.

46. Pisani, G. B.; Ruffini, R.; Aimuratov, Y.; Bianco, C. L.; Kovacevic, M.;

Moradi, R.; Muccino, M.; Penacchioni, A. V.; Rueda, J. A.; Shakeri, S.; Wang, Y.; On the universal late X-ray emission of binary-driven hypernovae and its possible collimation; The Astrophysical Journal, 833, 159 (2016).

It has been previously discovered a universal power-law behaviour of the late X-ray emission (LXRE) of a "golden sample" (GS) of six long energetic GRBs, when observed in the rest-frame of the source. This remarkable feature, independent on the different isotropic energy (E_{iso}) of each GRB, has been used to estimate the cosmological redshift of some long GRBs. This analysis is here extended to a new class of 161 long GRBs, all with $E_{iso} > 10^{52}$ erg. These GRBs are indicated as binary-driven hypernovae (BdHNe) in view of their progenitors: a tight binary systems composed of a carbon-oxigen core (CO_{core}) and a neutron star (NS) undergoing an induced gravitational collapse (IGC) to a black hole (BH) triggered by the CO_{core} explosion as a supernova (SN). We confirm the universal behaviour of the LXRE for the "enlarged sample" (ES) of 161 BdHNe observed up to the end of 2015, assuming a double-cone emitting region. We obtain a distribution of half-opening angles peaking at $\theta = 17.62°$, with mean value 30.05°, and a standard deviation 19.65°. This, in turn, leads to the possible establishment of a new cosmological candle. Within the IGC model, such universal LXRE behaviour is only indirectly related to the GRB and originates from the SN ejecta, of a standard constant mass, being shocked by the GRB emission. The fulfillment of the universal relation in the LXRE and its independence of the prompt emission, further confirmed in this article, establishes a crucial test for any viable GRB model.

47. Y. Aimuratov, R. Ruffini, M. Muccino, C.L. Bianco, A.V. Penacchioni, G.B. Pisani, D. Primorac, J.A. Rueda, Y. Wang; GRB 081024B and GRB 140402A: Two Additional Short GRBs from Binary Neutron Star Mergers; The Astrophysical Journal, 844, 83 (2017).

Theoretical and observational evidences have been recently gained for a twofold classification of short bursts: 1) short gamma-ray flashes (S-GRFs), with isotropic energy $E_{iso} < 10^{52}$ erg and no BH formation, and 2) the authentic short gamma-ray bursts (S-GRBs), with isotropic energy $E_{iso} > 10^{52}$ erg evidencing a BH formation in the binary neutron star merging process. The signature for the BH formation consists in the on-set of the high energy (0.1–100 GeV) emission, coeval to the prompt emission, in all S-GRBs. No GeV emission is expected nor observed in the S-GRFs. In this paper we present

two additional S-GRBs, GRB 081024B and GRB 140402A, following the already identified S-GRBs, i.e., GRB 090227B, GRB 090510 and GRB 140619B. We also return on the absence of the GeV emission of the S-GRB 090227B, at an angle of 71° from the *Fermi*-LAT boresight. All the correctly identified S-GRBs correlate to the high energy emission, implying no significant presence of beaming in the GeV emission. The existence of a common power-law behavior in the GeV luminosities, following the BH formation, when measured in the source rest-frame, points to a commonality in the mass and spin of the newly-formed BH in all S-GRBs.

48. J.A. Rueda, Y. Aimuratov, U. Barres de Almeida, L.M. Becerra, C.L. Bianco, C. Cherubini, S. Filippi, M. Karlica, M. Kovacevic, J.D. Melon Fuksman, R. Moradi, M. Muccino, A.V. Penacchioni, G.B. Pisani, D. Primorac, R. Ruffini, N. Sahakyan, S. Shakeri, Y. Wang; The binary systems associated with short and long gamma-ray bursts and their detectability; International Journal of Modern Physics D, 26, 1730016 (2017).

    Short and long-duration gamma-ray bursts (GRBs) have been recently subclassified into seven families according to the binary nature of their progenitors. For short GRBs, mergers of neutron star binaries (NSNS) or neutron star-black hole binaries (NS-BH) are proposed. For long GRBs, the induced gravitational collapse (IGC) paradigm proposes a tight binary system composed of a carbonoxygen core (COcore) and a NS companion. The explosion of the CO-core as supernova (SN) triggers a hypercritical accretion process onto the NS companion which might reach the critical mass for the gravitational collapse to a BH. Thus, this process can lead either to a NS-BH or to NSNS depending on whether or not the accretion is sufficient to induce the collapse of the NS into a BH. We shall discuss for the above compact object binaries: (1) the role of the NS structure and the equation-of-state on their final fate; (2) their occurrence rates as inferred from the X and gamma-ray observations; (3) the expected number of detections of their gravitational wave (GW) emission by the Advanced LIGO interferometer.

49. R. Ruffini, Y. Aimuratov, L.M. Becerra, C.L. Bianco, M. Karlica, M. Kovacevic, J.D. Melon Fuksman, R. Moradi, M. Muccino, A.V. Penacchioni, G.B. Pisani, D. Primorac, J.A. Rueda, S. Shakeri, G.V. Vereshchagin, Y. Wang, S.-S. Xue; The cosmic matrix in the 50th anniversary of relativistic astrophysics; International Journal of Modern Physics D, 26, 1730019 (2017).

Our concept of induced gravitational collapse (IGC paradigm) starting from a supernova occurring with a companion neutron star, has unlocked the understanding of seven different families of gamma ray bursts (GRBs), indicating a path for the formation of black holes in the universe. An authentic laboratory of relativistic astrophysics has been unveiled in which new paradigms have been introduced in order to advance knowledge of the most energetic, distant and complex systems in our universe. A novel cosmic matrix paradigm has been introduced at a relativistic cosmic level, which parallels the concept of an S-matrix introduced by Feynmann, Wheeler and Heisenberg in the quantum world of microphysics. Here the "in" states are represented by a neutron star and a supernova, while the "out" states, generated within less than a second, are a new neutron star and a black hole. This novel field of research needs very powerful technological observations in all wavelengths ranging from radio through optical, X-ray and gamma ray radiation all the way up to ultra-high-energy cosmic rays.

A.69) R. Ruffini, Y. Wang, Y. Aimuratov, U. Barres de Almeida, L.M. Becerra, C.L. Bianco, Y.C. Chen, M. Karlica, M. Kovacevic, L. Li, J.D. Melon Fuksman, R. Moradi, M. Muccino, A.V. Penacchioni, G.B. Pisani, D. Primorac, J.A. Rueda, S. Shakeri, G.V. Vereshchagin, S.-S. Xue; Early X-Ray Flares in GRBs; The Astrophysical Journal, 852, 53 (2018).

We analyze the early X-ray flares in the GRB "flare-plateau-afterglow" (FPA) phase observed by Swift-XRT. The FPA occurs only in one of the seven GRB subclasses: the binary-driven hypernovae (BdHNe). This subclass consists of long GRBs with a carbon-oxygen core and a neutron star (NS) binary companion as progenitors. The hypercritical accretion of the supernova (SN) ejecta onto the NS can lead to the gravitational collapse of the NS into a black hole. Consequently, one can observe a GRB emission with isotropic energy $E_{iso} \gtrsim 10^{52}$ erg, as well as the associated GeV emission and the FPA phase. Previous work had shown that gamma-ray spikes in the prompt emission occur at $\sim 10^{15}$–10^{17} cm with Lorentz gamma factor $\Gamma \sim 10^2$–10^3. Using a novel data analysis we show that the time of occurrence, duration, luminosity and total energy of the X-ray flares correlate with E_{iso}. A crucial feature is the observation of thermal emission in the X-ray flares that we show occurs at radii $\sim 10^{12}$ cm with $\Gamma \lesssim 4$. These model independent observations cannot be explained by the "fireball" model, which postulates synchrotron and inverse Compton radiation from a single ultra relativistic jetted emission extending from the prompt to the late afterglow and GeV emission phases. We show that

in BdHNe a collision between the GRB and the SN ejecta occurs at $\simeq 10^{10}$ cm reaching transparency at $\sim 10^{12}$ cm with $\Gamma \lesssim 4$. The agreement between the thermal emission observations and these theoretically derived values validates our model and opens the possibility of testing each BdHN episode with the corresponding Lorentz gamma factor.

5.2 Conference proceedings

1. R. Ruffini, M.G. Bernardini, C.L. Bianco, P. Chardonnet, F. Fraschetti, V. Gurzadyan, L. Vitagliano, S.-S. Xue; "The Blackholic energy: long and short Gamma-Ray Bursts (New perspectives in physics and astrophysics from the theoretical understanding of Gamma-Ray Bursts, II)"; in Proceedings of the XIth Brazilian School on Cosmology and Gravitation, Mangaratiba, Rio de Janeiro (Brazil), July August 2004, M. Novello, S.E. Perez Bergliaffa, Editors; AIP Conference Proceedings, 782, 42 (2005).

   We outline the confluence of three novel theoretical fields in our modeling of Gamma-Ray Bursts (GRBs): 1) the ultrarelativistic regime of a shock front expanding with a Lorentz gamma factor ~ 300; 2) the quantum vacuum polarization process leading to an electron-positron plasma originating the shock front; and 3) the general relativistic process of energy extraction from a black hole originating the vacuum polarization process. There are two different classes of GRBs: the long GRBs and the short GRBs. We here address the issue of the long GRBs. The theoretical understanding of the long GRBs has led to the detailed description of their luminosities in fixed energy bands, of their spectral features and made also possible to probe the astrophysical scenario in which they originate. We are specially interested, in this report, to a subclass of long GRBs which appear to be accompanied by a supernova explosion. We are considering two specific examples: GRB980425/SN1998bw and GRB030329/SN2003dh. While these supernovae appear to have a standard energetics of 10^{49} ergs, the GRBs are highly variable and can have energetics $10^4 - 10^5$ times larger than the ones of the supernovae. Moreover, many long GRBs occurs without the presence of a supernova. It is concluded that in no way a GRB can originate from a supernova. The precise theoretical understanding of the GRB luminosity we present evidence, in both these systems, the existence of an independent component in the X-ray emission, usually interpreted in the current literature as part of the GRB afterglow. This compo-

nent has been observed by Chandra and XMM to have a strong decay on scale of months. We have named here these two sources respectively URCA-1 and URCA-2, in honor of the work that George Gamow and Mario Shoenberg did in 1939 in this town of Urca identifying the basic mechanism, the Urca processes, leading to the process of gravitational collapse and the formation of a neutron star and a supernova. The further hypothesis is considered to relate this X-ray source to a neutron star, newly born in the Supernova. This hypothesis should be submitted to further theoretical and observational investigation. Some theoretical developments to clarify the astrophysical origin of this new scenario are outlined. We turn then to the theoretical developments in the short GRBs: we first report some progress in the understanding the dynamical phase of collapse, the mass-energy formula and the extraction of blackholic energy which have been motivated by the analysis of the short GRBs. In this context progress has also been accomplished on establishing an absolute lower limit to the irreducible mass of the black hole as well as on some critical considerations about the relations of general relativity and the second law of thermodynamics. We recall how this last issue has been one of the most debated in theoretical physics in the past thirty years due to the work of Bekenstein and Hawking. Following these conceptual progresses we analyze the vacuum polarization process around an overcritical collapsing shell. We evidence the existence of a separatrix and a dyadosphere trapping surface in the dynamics of the electron-positron plasma generated during the process of gravitational collapse. We then analyze, using recent progress in the solution of the Vlasov-Boltzmann-Maxwell system, the oscillation regime in the created electron-positron plasma and their rapid convergence to a thermalized spectrum. We conclude by making precise predictions for the spectra, the energy fluxes and characteristic time-scales of the radiation for short-bursts. If the precise luminosity variation and spectral hardening of the radiation we have predicted will be confirmed by observations of short-bursts, these systems will play a major role as standard candles in cosmology. These considerations will also be relevant for the analysis of the long-bursts when the baryonic matter contribution will be taken into account.

2. R. Ruffini, M.G. Bernardini, C.L. Bianco, P. Chardonnet, F. Fraschetti, V. Gurzadyan, L. Vitagliano, S.-S. Xue; "Black hole physics and astrophysics: The GRB-Supernova connection and URCA-1 URCA-2"; in Proceedings of the Tenth Marcel Grossmann Meeting on General Relativity, Rio de Janeiro, Brazil, July 2003, M. Novello, S.E. Perez-Bergliaffa,

Editors; p. 369; World Scientific, (Singapore, 2006).

We outline the confluence of three novel theoretical fields in our modeling of Gamma-Ray Bursts (GRBs): 1) the ultrarelativistic regime of a shock front expanding with a Lorentz gamma factor ~ 300; 2) the quantum vacuum polarization process leading to an electron-positron plasma originating the shock front; and 3) the general relativistic process of energy extraction from a black hole originating the vacuum polarization process. There are two different classes of GRBs: the long GRBs and the short GRBs. We here address the issue of the long GRBs. The theoretical understanding of the long GRBs has led to the detailed description of their luminosities in fixed energy bands, of their spectral features and made also possible to probe the astrophysical scenario in which they originate. We are specially interested, in this report, to a subclass of long GRBs which appear to be accompanied by a supernova explosion. We are considering two specific examples: GRB980425/SN1998bw and GRB030329/SN2003dh. While these supernovae appear to have a standard energetics of 10^{49} ergs, the GRBs are highly variable and can have energetics 10^4 – 10^5 times larger than the ones of the supernovae. Moreover, many long GRBs occurs without the presence of a supernova. It is concluded that in no way a GRB can originate from a supernova. The precise theoretical understanding of the GRB luminosity we present evidence, in both these systems, the existence of an independent component in the X-ray emission, usually interpreted in the current literature as part of the GRB afterglow. This component has been observed by Chandra and XMM to have a strong decay on scale of months. We have named here these two sources respectively URCA-1 and URCA-2, in honor of the work that George Gamow and Mario Shoenberg did in 1939 in this town of Urca identifying the basic mechanism, the Urca processes, leading to the process of gravitational collapse and the formation of a neutron star and a supernova. The further hypothesis is considered to relate this X-ray source to a neutron star, newly born in the Supernova. This hypothesis should be submitted to further theoretical and observational investigation. Some theoretical developments to clarify the astrophysical origin of this new scenario are outlined.

3. M.G. Bernardini, C.L. Bianco, P. Chardonnet, F. Fraschetti, R. Ruffini, S.-S. Xue; "General features of GRB 030329 in the EMBH model"; in Proceedings of the Tenth Marcel Grossmann Meeting on General Relativity, Rio de Janeiro, Brazil, July 2003, M. Novello, S.E. Perez-Bergliaffa, Editors; p. 2459; World Scientific, (Singapore, 2006).

GRB 030329 is considered within the EMBH model. We determine the three free parameters and deduce its luminosity in given energy bands comparing it with the observations. The observed substructures are compared with the predictions of the model: by applying the result that substructures observed in the extended afterglow peak emission (E-APE) do indeed originate in the collision of the accelerated baryonic matter (ABM) pulse with the inhomogeneities in the interstellar medium around the black-hole, masks of density inhomogeneities are considered in order to reproduce the observed temporal substructures. The induced supernova concept is applied to this system and the general consequences that we are witnessing are the formation of a cosmological thriptych of a black hole originating the GRB 030329, the supernova SN2003dh and a young neutron star. Analogies to the system GRB 980425–SN1998bw are outlined.

4. R. Ruffini, M.G. Bernardini, C.L. Bianco, P. Chardonnet, A. Corsi, F. Fraschetti, S.-S. Xue; "GRB 970228 and its associated Supernova in the EMBH model"; in Proceedings of the Tenth Marcel Grossmann Meeting on General Relativity, Rio de Janeiro, Brazil, July 2003, M. Novello, S.E. Perez-Bergliaffa, Editors; p. 2465; World Scientific, (Singapore, 2006).

   The γ-ray burst of 1997 February 28 is analyzed within the Electromagnetic Black Hole model. We first estimate the value of the total energy deposited in the dyadosphere, E_{dya}, and the amount of baryonic matter left over by the EMBH progenitor star, $B = M_B c^2 / E_{dya}$. We then consider the role of the interstellar medium number density n_{ISM} and of the ratio R between the effective emitting area and the total surface area of the γ-ray burst source, in reproducing the prompt emission and the X-ray afterglow of this burst. Some considerations are also done concerning the possibility of explaining, within the theory, the observed evidence for a supernova in the optical afterglow.

5. F. Fraschetti, M.G. Bernardini, C.L. Bianco, P. Chardonnet, R. Ruffini, S.-S. Xue; "Inferences on the ISM structure around GRB980425 and GRB980425-SN1998bw association in the EMBH Model"; in Proceedings of the Tenth Marcel Grossmann Meeting on General Relativity, Rio de Janeiro, Brazil, July 2003, M. Novello, S.E. Perez-Bergliaffa, Editors; p. 2451; World Scientific, (Singapore, 2006).

   We determine the four free parameters within the EMBH model for GRB 980425 and deduce its luminosity in given energy bands, its spectra and its time variability in the prompt radiation. We compute the basic kinematical parameters

of GRB 980425. In the extended afterglow peak emission the Lorentz γ factor is lower than the critical value 150 which has been found in Ruffini et al. (2002) to be necessary in order to perform the tomography of the ISM surrounding the GRB as suggested by Dermer & Mitman (1999). The detailed structure of the density inhomogeneities as well as the effects of radial apparent superluminal effects are evaluated within the EMBH model. Under the assumption that the energy distribution of emitted radiation is thermal in the comoving frame, time integrated spectra of EMBH model for prompt emission are computed. The induced supernova concept is applied to this system and general consequences on the astrophysical and cosmological scenario are derived.

6. R. Ruffini, M.G. Bernardini, C.L. Bianco, P. Chardonnet, F. Fraschetti, R. Guida, S.-S. Xue; "GRB 050315: A step in the proof of the uniqueness of the overall GRB structure"; in "GAMMA-RAY BURSTS IN THE SWIFT ERA: Sixteenth Maryland Astrophysics Conference", Washington, DC, USA, November 29th December 2nd 2005, Stephen S. Holt, Neil Gehrels, John A. Nousek, Editors; AIP Conference Proceedings, 836, 103 (2006).

   Using the Swift data of GRB 050315, we progress in proving the uniqueness of our theoretically predicted Gamma-Ray Burst (GRB) structure as composed by a proper-GRB, emitted at the transparency of an electron-positron plasma with suitable baryon loading, and an afterglow comprising the "prompt radiation" as due to external shocks. Detailed light curves for selected energy bands are theoretically fitted in the entire temporal region of the Swift observations ranging over 10^6 seconds.

7. R. Ruffini, M.G. Bernardini, C.L. Bianco, P. Chardonnet, F. Fraschetti, S.-S. Xue; "Theoretical Interpretation of GRB 031203 and URCA-3"; in "Relativistic Astrophysics and Cosmology - Einsteins Legacy", B. Aschenbach, V. Burwitz, G. Hasinger, B. Leibundgut, Editors; Springer-Verlag (2007).

8. R. Ruffini, M.G. Bernardini, C.L. Bianco, L. Caito, P. Chardonnet, M.G. Dainotti, F. Fraschetti, R. Guida, M. Rotondo, G. Vereshchagin, L. Vita--gliano, S.-S. Xue; "The Blackholic energy and the canonical Gamma-Ray Burst"; in Proceedings of the XIIth Brazilian School on Cosmology and Gravitation, Mangaratiba, Rio de Janeiro (Brazil), September 2006, M. Novello, S.E. Perez Bergliaffa, Editors; AIP Conference Proceedings, 910, 55 (2007).

Gamma-Ray Bursts (GRBs) represent very likely "the" most extensive computational, theoretical and observational effort ever carried out successfully in physics and astrophysics. The extensive campaign of observation from space based X-ray and γ-ray observatory, such as the *Vela*, CGRO, BeppoSAX, HETE-II, INTEGRAL, *Swift*, R-XTE, *Chandra*, XMM satellites, have been matched by complementary observations in the radio wavelength (e.g. by the VLA) and in the optical band (e.g. by VLT, Keck, ROSAT). The net result is unprecedented accuracy in the received data allowing the determination of the energetics, the time variability and the spectral properties of these GRB sources. The very fortunate situation occurs that these data can be confronted with a mature theoretical development. Theoretical interpretation of the above data allows progress in three different frontiers of knowledge: **a)** the ultrarelativistic regimes of a macroscopic source moving at Lorentz gamma factors up to ~ 400; **b)** the occurrence of vacuum polarization process verifying some of the yet untested regimes of ultrarelativistic quantum field theories; and **c)** the first evidence for extracting, during the process of gravitational collapse leading to the formation of a black hole, amounts of energies up to 10^{55} ergs of black-holic energy — a new form of energy in physics and astrophysics. We outline how this progress leads to the confirmation of three interpretation paradigms for GRBs proposed in July 2001. Thanks mainly to the observations by *Swift* and the optical observations by VLT, the outcome of this analysis points to the existence of a "canonical" GRB, originating from a variety of different initial astrophysical scenarios. The communality of these GRBs appears to be that they all are emitted in the process of formation of a black hole with a negligible value of its angular momentum. The following sequence of events appears to be canonical: the vacuum polarization process in the dyadosphere with the creation of the optically thick self accelerating electron-positron plasma; the engulfment of baryonic mass during the plasma expansion; adiabatic expansion of the optically thick "fireshell" of electron-positron-baryon plasma up to the transparency; the interaction of the accelerated baryonic matter with the interstellar medium (ISM). This leads to the canonical GRB composed of a proper GRB (P-GRB), emitted at the moment of transparency, followed by an extended afterglow. The sole parameters in this scenario are the total energy of the dyadosphere E_{dya}, the fireshell baryon loading M_B defined by the dimensionless parameter $B \equiv M_B c^2 / E_{dya}$, and the ISM filamentary distribution around the source. In the limit $B \to 0$ the total energy is radiated in the P-GRB with a vanishing contribution in the afterglow. In this limit, the canonical GRBs explain as well the short GRBs. In these lecture notes we systematically

outline the main results of our model comparing and contrasting them with the ones in the current literature. In both cases, we have limited ourselves to review already published results in refereed publications. We emphasize as well the role of GRBs in testing yet unexplored grounds in the foundations of general relativity and relativistic field theories.

9. R. Ruffini, M.G. Bernardini, C.L. Bianco, L. Caito, P. Chardonnet, M.G. Dainotti, F. Fraschetti, R. Guida, G. Vereshchagin, S.-S. Xue; "The role of GRB 031203 in clarifying the astrophysical GRB scenario"; in Proceedings of the 6th Integral Workshop - The Obscured Universe, Moscow, (Russia), July 2006, S. Grebenev, R. Sunyaev, C. Winkler, A. Parmar, L. Ouwehand, Editors; ESA Special Publication, SP-622, 561 (2007).

   The luminosity and the spectral distribution of the afterglow of GRB 031203 have been presented within our theoretical framework, which envisages the GRB structure as composed by a proper-GRB, emitted at the transparency of an electron-positron plasma with suitable baryon loading, and an afterglow comprising the "prompt emission" as due to external shocks. In addition to the GRB emission, there appears to be a prolonged soft X-Ray emission lasting for 10^6–10^7 seconds followed by an exponential decay. This additional source has been called by us URCA-3. It is urgent to establish if this component is related to the GRB or to the Supernova (SN). In this second case, there are two possibilities: either the interaction of the SN ejecta with the interstellar medium or, possibly, the cooling of a young neutron star formed in the SN 2003lw process. The analogies and the differences between this triptych GRB 031203 / SN 2003lw / URCA-3 and the corresponding ones GRB 980425 / SN 1998bw / URCA-1 and GRB 030329 / SN 2003dh / URCA-2, as well as GRB 060218 / SN 2006aj are discussed.

10. M.G. Bernardini, C.L. Bianco, L. Caito, M.G. Dainotti, R. Guida, R. Ruffini; "GRB970228 and the class of GRBs with an initial spikelike emission: do they follow the Amati relation?"; in Relativistic Astrophysics Proceedings of the 4th Italian-Sino Workshop, Pescara (Italy), July 2007, C.L. Bianco, S.-S. Xue, Editors; AIP Conference Proceedings, 966, 7 (2008).

    On the basis of the recent understanding of GRB050315 and GRB060218, we return to GRB970228, the first Gamma-Ray Burst (GRB) with detected afterglow. We proposed it as the prototype for a new class of GRBs with "an occasional softer extended emission lasting tenths of seconds after an initial spikelike emission". Detailed theoretical computation of the GRB970228 light

curves in selected energy bands for the prompt emission are presented and compared with observational *Beppo*SAX data. From our analysis we conclude that GRB970228 and likely the ones of the above mentioned new class of GRBs are "canonical GRBs" have only one peculiarity: they exploded in a galactic environment, possibly the halo, with a very low value of CBM density. Here we investigate how GRB970228 unveils another peculiarity of this class of GRBs: they do not fulfill the "Amati relation". We provide a theoretical explanation within the fireshell model for the apparent absence of such correlation for the GRBs belonging to this new class.

11. C.L. Bianco, M.G. Bernardini, L. Caito, M.G. Dainotti, R. Guida, R. Ruffini; "The "Fireshell" Model and the "Canonical" GRB Scenario; in Relativistic Astrophysics Proceedings of the 4th Italian-Sino Workshop, Pescara (Italy), July 2007, C.L. Bianco, S.-S. Xue, Editors; AIP Conference Proceedings, 966, 12 (2008).

    In the "fireshell" model we define a "canonical GRB" light curve with two sharply different components: the Proper-GRB (P-GRB), emitted when the optically thick fireshell of electron-positron plasma originating the phenomenon reaches transparency, and the afterglow, emitted due to the collision between the remaining optically thin fireshell and the CircumBurst Medium (CBM). We outline our "canonical GRB" scenario, originating from the gravitational collapse to a black hole, with a special emphasis on the discrimination between "genuine" and "fake" short GRBs.

12. L. Caito, M.G. Bernardini, C.L. Bianco, M.G. Dainotti, R. Guida, R. Ruffini; "GRB 060614: A Progress Report"; in Relativistic Astrophysics Proceedings of the 4th Italian-Sino Workshop, Pescara (Italy), July 2007, C.L. Bianco, S.-S. Xue, Editors; AIP Conference Proceedings, 966, 16 (2008).

    The explosion of GRB 060614, detected by the Swift satellite, produced a deep break in the GRB scenario opening new horizons of investigation, because it can't be traced back to any traditional scheme of classification. In fact, it manifests peculiarities both of long bursts and of short bursts. Above all, it is the first case of long duration near GRB without any bright Ib/c associated Supernova. We will show that, in our canonical GRB scenario, this "anomalous" situation finds a natural interpretation and allows us to discuss a possible variation to the traditional classification scheme, introducing the distinction between "genuine" and "fake" short bursts.

13. M.G. Dainotti, M.G. Bernardini, C.L. Bianco, L. Caito, R. Guida, R. Ruffini; "GRB 060218 and the Binaries as Progenitors of GRB-SN Systems"; in Relativistic Astrophysics Proceedings of the 4th Italian-Sino Workshop, Pescara (Italy), July 2007, C.L. Bianco, S.-S. Xue, Editors; AIP Conference Proceedings, 966, 25 (2008).

    We study the Gamma-Ray Burst (GRB) 060218: a particularly close source at $z = 0.033$ with an extremely long duration, namely $T_{90} \sim 2000$ s, related to SN 2006aj. This source appears to be a very soft burst, with a peak in the spectrum at 4.9 keV, therefore interpreted as an X-Ray Flash (XRF). It fullfills the Amati relation. I present the fitting procedure, which is time consuming. In order to show its sensitivity I also present two examples of fits with the same value of B and different value of $E^{tot}_{e^\pm}$. We fit the X- and γ-ray observations by *Swift* of GRB 060218 in the 0.1–150 keV energy band during the entire time of observations from 0 all the way to 10^6 s within a unified theoretical model. The free parameters of our theory are only three, namely the total energy $E^{tot}_{e\pm}$ of the $e^\pm$ plasma, its baryon loading $B \equiv M_B c^2/E^{tot}_{e\pm}$, as well as the CircumBurst Medium (CBM) distribution. We justify the extremely long duration of this GRB by a total energy $E^{tot}_{e\pm} = 2.32 \times 10^{50}$ erg, a very high value of the baryon loading $B = 1.0 \times 10^{-2}$ and the effective CircumBurst Medium (CBM) density which shows a radial dependence $n_{cbm} \propto r^{-\alpha}$ with $1.0 \leq \alpha \leq 1.7$ and monotonically decreases from 1 to 10^{-6} particles/cm^3. We recall that this value of the B parameter is the highest among the sources we have analyzed and it is very close to its absolute upper limit expected. By our fit we show that there is no basic differences between XRFs and more general GRBs. They all originate from the collapse process to a black hole and their difference is due to the variability of the three basic parameters within the range of full applicability of the theory. We also think that the smallest possible black hole, formed by the gravitational collapse of a neutron star in a binary system, is consistent with the especially low energetics of the class of GRBs associated with SNe Ib/c.

14. R. Guida, M.G. Bernardini, C.L. Bianco, L. Caito, M.G. Dainotti, R. Ruffini; "The Amati Relation within the Fireshell Model"; in Relativistic Astrophysics Proceedings of the 4th Italian-Sino Workshop, Pescara (Italy), July 2007, C.L. Bianco, S.-S. Xue, Editors; AIP Conference Proceedings, 966, 46 (2008).

    In this work we show the existence of a spectral-energy correlation within our "fireshell" model for GRBs. The free parameters of the model are the total

energy $E_{tot}^{e\pm}$ of the $e^{\pm}$ plasma and its baryon loading $B \equiv M_B\, c^2 / E_{tot}^{e\pm}$, characterizing the source, and the parameters describing the effective CircumBurst medium (CBM) distribution, namely its particle number density ρ and its effective emitting area R. We build a sample of pseudo-GRBs, i.e. a set of theoretically simulated light curves, varying the total energy of the electron-positron plasma $E_{tot}^{e\pm}$ and keeping the same baryon loading; the parametrization used to describe the distribution of the CircumBurst medium is the same as well for all the pseudo-GRBs. The values of these parameters (B, ρ and R) used in this work are equal to the ones assumed to fit GRB050315, a *Swift* burst representing a good example of what in the literature has been addressed as "canonical light curve". For each GRB of the sample we calculate the νF_ν spectrum integrating the theoretically computed light curve over the total time, namely from our T_0, the end of the Proper-GRB (P-GRB), up to the end of our afterglow phase, when the fireshell Lorentz gamma factor is close to unity; we exclude the P-GRB from this spectral computation because, following our "canonical" GRB scenario, this component of the GRB emission is physically different from the other component, that is our afterglow component, so one should take care in no mixing them. We find that the maximum of this spectrum, that is the observed peak energy $E_{p,tot}$, correlates with the initial electron-positron plasma energy $E_{tot}^{e\pm}$ in a way very similar to the Amati one: $E_{p,tot} \propto (E_{tot}^{e\pm})^{0.5}$.

15. R. Guida, M.G. Bernardini, C.L. Bianco, L. Caito, M.G. Dainotti, R. Ruffini; "Theoretical interpretation of the Amati relation within the fireshell model"; in GAMMA-RAY BURSTS 2007: Proceedings of the Santa Fe Conference, Santa Fe (NM, USA), November 2007, M. Galassi, D. Palmer, E. Fenimore, Editors; AIP Conference Proceedings, 1000, 60 (2008).

    We discuss within our theoretical "fireshell" model for Gamma-Ray Bursts (GRBs) the theoretical interpretation of the phenomenological correlation between the isotropic-equivalent radiated energy of the prompt emission E_{iso} and the cosmological rest-frame νF_ν spectrum peak energy E_p observed by Amati and collaborators. Possible reasons for some of the outliers of this relation are given.

16. L. Caito, M.G. Bernardini, C.L. Bianco, M.G. Dainotti, R. Guida, R. Ruffini; "GRB 060614: a Fake Short Gamma-Ray Burst"; in GAMMA-RAY BURSTS 2007: Proceedings of the Santa Fe Conference, Santa Fe (NM, USA), November 2007, M. Galassi, D. Palmer, E. Fenimore, Editors; AIP Conference Proceedings, 1000, 301 (2008).

The explosion of GRB 060614 produced a deep break in the GRB scenario and opened new horizons of investigation because it can't be traced back to any traditional scheme of classification. In fact, it manifests peculiarities both of long bursts and of short bursts and, above all, it is the first case of long duration near GRB without any bright Ib/c associated Supernova. We will show that, in our canonical GRB scenario, this "anomalous" situation finds a natural interpretation and allows us to discuss a possible variation to the traditional classification scheme, introducing the distinction between "genuine" and "fake" short bursts.

17. C.L. Bianco, M.G. Bernardini, L. Caito, M.G. Dainotti, R. Guida, R. Ruffini; "Short and canonical GRBs"; in GAMMA-RAY BURSTS 2007: Proceedings of the Santa Fe Conference, Santa Fe (NM, USA), November 2007, M. Galassi, D. Palmer, E. Fenimore, Editors; AIP Conference Proceedings, 1000, 305 (2008).

    Within the "fireshell" model for the Gamma-Ray Bursts (GRBs) we define a "canonical GRB" light curve with two sharply different components: the Proper-GRB (P-GRB), emitted when the optically thick fireshell of electron-positron plasma originating the phenomenon reaches transparency, and the afterglow, emitted due to the collision between the remaining optically thin fireshell and the CircumBurst Medium (CBM). We outline our "canonical GRB" scenario, with a special emphasis on the discrimination between "genuine" and "fake" short GRBs.

18. C.L. Bianco, M.G. Bernardini, L. Caito, M.G. Dainotti, R. Guida, R. Ruffini, G. Vereshchagin, S.-S. Xue; "The Equations of motion of the "fireshell""; in OBSERVATIONAL EVIDENCE FOR BLACK HOLES IN THE UNIVERSE: Proceedings of the 2nd Kolkata Conference, Kolkata (India), February 2008, S.K. Chakrabarti, A.S. Majumdar, Editors; AIP Conference Proceedings, 1053, 259 (2008).

    The Fireshell originating a Gamma-Ray Burst (GRB) encompasses an optically thick regime followed by an optically thin one. In the first one the fireshell self-accelerates from a Lorentz gamma factor equal to 1 all the way to 200-300. The physics of this system is based on the continuous annihilation of electron-positron pairs in an optically thick e^+e^- plasma with a small baryon loading. In the following regime, the optically thin fireshell, composed by the baryons left over after the transparency point, ballistically expands into the CircumBurst Medium (CBM). The dynamics of the fireshell during both regimes will

be analyzed. In particular we will re-examine the validity of the constant-index power-law relation between the fireshell Lorentz gamma factor and its radial coordinate, usually adopted in the current literature on the grounds of an "ultrarelativistic" approximation. Such expressions are found to be mathematically correct but only approximately valid in a very limited range of the physical and astrophysical parameters and in an asymptotic regime which is reached only for a very short time, if any.

19. M.G. Bernardini, C.L. Bianco, L. Caito, M.G. Dainotti, R. Guida, R. Ruffini; "The "Canonical" GRBs within the fireshell model"; in OBSERVATIONAL EVIDENCE FOR BLACK HOLES IN THE UNIVERSE: Proceedings of the 2nd Kolkata Conference, Kolkata (India), February 2008, S.K. Chakrabarti, A.S. Majumdar, Editors; AIP Conference Proceedings, 1053, 267 (2008).

    Within the fireshell model we define a "canonical" GRB light curve with two sharply different components: the Proper-GRB (P-GRB), emitted when the optically thick fireshell of electron-positron plasma originating the phenomenon reaches transparency, and the afterglow, emitted due to the collision between the remaining optically thin fireshell and the CircumBurst Medium (CBM). On the basis of the recent understanding of GRB970228 as the prototype for a new class of GRBs with "an occasional softer extended emission lasting tenths of seconds after an initial spikelike emission" we outline our "canonical" GRB scenario, originating from the gravitational collapse to a black hole, with a special emphasis on the discrimination between short GRBs and the ones appearing as such due to their peculiar astrophysical setting.

20. M.G. Dainotti, M.G. Bernardini, C.L. Bianco, L. Caito, R. Guida, R. Ruffini; "GRB 060218: the density mask and its peculiarity compared to the other sources"; in OBSERVATIONAL EVIDENCE FOR BLACK HOLES IN THE UNIVERSE: Proceedings of the 2nd Kolkata Conference, Kolkata (India), February 2008, S.K. Chakrabarti, A.S. Majumdar, Editors; AIP Conference Proceedings, 1053, 283 (2008).

    The Swift satellite has given continuous data in the range 0.3150 keV from 0 s to 106 s for GRB060218 associated with SN2006aj. It has an unusually long duration ($T_{90} \sim 2100$ s). We plan to fit the complete γ- and X-ray light curves of this long duration GRB, including the prompt emission and we give peculiar attention to the afterglow lightcurve in order to better constrain the density mask. We apply our "fireshell" model based on the formation of a black hole, giving the relevant references. The initial total energy of the electron-positron

plasma $E_{e^\pm}^{tot} == 2.32 \times 10^{50}$ erg has a particularly low value similarly to the other GRBs associated with SNe. For the first time we observe a baryon loading $B = 10^{-2}$ which coincides with the upper limit for the dynamical stability of the fireshell. The effective CircumBurst Medium (CBM) density shows a radial dependence $n_{cbm} \propto r^{-a}$ with $1.0 \leq a \leq 1.7$ and monotonically decreases from 1 to 10^{-6} particles/cm^3. Such a behavior is interpreted as due to a fragmentation in the fireshell. Such a fragmentation is crucial in explaining both the unusually large T_{90} and the consequently inferred abnormal low value of the CBM effective density. We present the comparison between the density mask of this source and the ones of a normal GRB 050315 and a fake short, GRB 970228, making some assumptions on the CBM behaviour in the surrounding of the Black hole.

21. L. Caito, M.G. Bernardini, C.L. Bianco, M.G. Dainotti, R. Guida, R. Ruffini; "GRB 060614 in the canonical fireshell model"; in OBSERVATIONAL EVIDENCE FOR BLACK HOLES IN THE UNIVERSE: Proceedings of the 2nd Kolkata Conference, Kolkata (India), February 2008, S.K. Chakrabarti, A.S. Majumdar, Editors; AIP Conference Proceedings, 1053, 291 (2008).

    Gamma-Ray Burst (GRB) 060614 is the first nearby long duration GRB clearly not associated to any bright Ib/c Supernova. The explosion of this burst undermines one of the fundamental assumptions of the standard scenario and opens new horizons and hints of investigation. GRB 060614, hardly classifiable as a short GRB, is not either a "typical" long GRB since it occurs in a low star forming region. Moreover, it presents deep similarities with GRB 970228, which is the prototype of the "fake" short bursts, or better canonical GRBs disguised as short ones. Within the "fireshell" model, we test if this "anomalous" source can be a disguised short GRB.

22. L.J. Rangel Lemos, S. Casanova, R. Ruffini, S.S. Xue; "Fermis approach to the study of pp interactions"; in OBSERVATIONAL EVIDENCE FOR BLACK HOLES IN THE UNIVERSE: Proceedings of the 2nd Kolkata Conference, Kolkata (India), February 2008, S.K. Chakrabarti, A.S. Majumdar, Editors; AIP Conference Proceedings, 1053, 275 (2008).

    The physics of hadronic interactions found much difficulties for explain the experimental data. In this work we study the approach of Fermi (1950) about the multiplicity of pions emitted in pp interactions and in follow we compare with the modern approach

23. R. Ruffini, A.G. Aksenov, M.G. Bernardini, C.L. Bianco, L. Caito, M.G. Dainotti, G. De Barros, R. Guida, G.V. Vereshchagin, S.-S. Xue; "The canonical Gamma-Ray Bursts and their 'precursors"'; in 2008 NANJING GAMMA-RAY BURST CONFERENCE, Proceedings of the 2008 Nanjing Gamma-Ray Burst Conference, Nanjing (China), June 2008, Y.-F. Huang, Z.-G. Dai, B. Zhang, Editors; AIP Conference Proceedings, 1065, 219 (2008).

    The fireshell model for Gamma-Ray Bursts (GRBs) naturally leads to a canonical GRB composed of a proper-GRB (P-GRB) and an afterglow. P-GRBs, introduced by us in 2001, are sometimes considered "precursors" of the main GRB event in the current literature. We show in this paper how the fireshell model leads to the understanding of the structure of GRBs, with precise estimates of the time sequence and intensities of the P-GRB and the of the afterglow. It leads as well to a natural classification of the canonical GRBs which overcomes the traditional one in short and long GRBs.

24. M.G. Bernardini, C.L. Bianco, L. Caito, M.G. Dainotti, R. Guida, R. Ruffini; "Preliminary analysis of GRB060607A within the fireshell model"; in 2008 NANJING GAMMA-RAY BURST CONFERENCE; Proceedings of the 2008 Nanjing Gamma-Ray Burst Conference, Nanjing (China), June 2008, Y.-F. Huang, Z.-G. Dai, B. Zhang, Editors; AIP Conference Proceedings, 1065, 227 (2008).

    GRB060607A is a very distant ($z = 3.082$) and energetic event ($E_{iso} \sim 10^{53}$ erg). Its main peculiarity is that the peak of the near-infrared afterglow has been observed with the REM robotic telescope, allowing to infer the initial Lorentz gamma factor of the emitting system. We present a preliminary analysis of the spectra and light curves of GRB060607A prompt emission within the fireshell model. We show that the N(E) spectrum of the prompt emission, whose behavior is usually described as "simple power-law", can also be fitted in a satisfactory way by a convolution of thermal spectra as predicted by the model we applied. The theoretical time-integrated spectrum of the prompt emission as well as the light curves in the BAT and XRT energy band are in good agreement with the observations, enforcing the plausibility of our approach. Furthermore, the initial value of Lorentz gamma factor we predict is compatible with the one deduced from the REM observations.

25. C.L. Bianco, M.G. Bernardini, L. Caito, M.G. Dainotti, R. Guida, R. Ruffini; "The "fireshell" model and the "canonical GRB" scenario"; in 2008 NAN-

JING GAMMA-RAY BURST CONFERENCE; Proceedings of the 2008 Nanjing Gamma-Ray Burst Conference, Nanjing (China), June 2008, Y.-F. Huang, Z.-G. Dai, B. Zhang, Editors; AIP Conference Proceedings, 1065, 223 (2008).

The Swift observation of GRB 060614, as well as the catalog analysis by Norris & Bonnell (2006), opened the door "on a new Gamma-Ray Bursts (GRBs) classification scheme that straddles both long and short bursts" (Gehrels et al. 2006). Within the "fireshell" model for the Gamma-Ray Bursts (GRBs) we define a "canonical GRB" light curve with two sharply different components: the Proper-GRB (P-GRB), emitted when the optically thick fireshell of electron-positron plasma originating the phenomenon reaches transparency, and the afterglow, emitted due to the collision between the remaining optically thin fireshell and the CircumBurst Medium (CBM). We here outline our "canonical GRB" scenario, which implies three different GRB classes: the "genuine" short GRBs, the "fake" or "disguised" short GRBs and the other (so-called "long") GRBs. We also outline some implications for the theoretical interpretation of the Amati relation.

26. G. De Barros, M.G. Bernardini, C.L. Bianco, L. Caito, M.G. Dainotti, R. Guida, R. Ruffini; "Is GRB 050509b a genuine short GRB?"; in 2008 NANJING GAMMA-RAY BURST CONFERENCE; Proceedings of the 2008 Nanjing Gamma-Ray Burst Conference, Nanjing (China), June 2008, Y.-F. Huang, Z.-G. Dai, B. Zhang, Editors; AIP Conference Proceedings, 1065, 231 (2008).

    Within our "fireshell" model we introduced a "canonical" GRB scenario which differentiates physically the "proper GRB" (P-GRB) emission when photons decouple, and the afterglow emission due to interaction of the accelerated baryons with the CircumBurst Medium (CBM). The ratio between energetics of the two components is ruled by the baryon loading of the fireshell. We here analyse the possibility that GRB050509b is the first case of a "genuine" short GRB the ones with smaller baryon loading. In such a case, the GRB050509b "prompt emission" would be dominated by the "proper GRB" and, moreover, the P-GRB total energy would be greater than the afterglow one. Our fit of the afterglow data and of the P-GRB energetics indicates that this source present the smallest baryon loading we ever encountered so far, being on the order of 10^{-4}.

27. G. De Barros, A.G. Aksenov, C.L. Bianco, R. Ruffini, G.V. Vereshchagin;

"Fireshell versus Fireball scenarios"; in 2008 NANJING GAMMA-RAY BURST CONFERENCE; Proceedings of the 2008 Nanjing Gamma-Ray Burst Conference, Nanjing (China), June 2008, Y.-F. Huang, Z.-G. Dai, B. Zhang, Editors; AIP Conference Proceedings, 1065, 234 (2008).

We revisit Cavallo and Rees classification based on the analysis of initial conditions in electron-positron-photon plasma which appears suddenly around compact astrophysical objects and gives origin to GRBs. These initial conditions were recently studied in [1,2] by numerical integration of relativistic Boltzmann equations with collision integrals, including binary and triple interactions between particles. The main conclusion is that the pair plasma in GRB sources quickly reaches thermal equilibrium well before its expansion starts. In light of this work we comment on each of the four scenarios proposed by Cavallo and Rees and discuss their applicability to describe evolution of GRB sources.

28. M.G. Bernardini, C.L. Bianco, L. Caito, M.G. Dainotti, R. Guida, R. Ruffini; "GRB970228 as a prototype for the class of GRBs with an initial spike-like emission"; in Proceedings of the Eleventh Marcel Grossmann Meeting on General Relativity, Berlin, Germany, July 2006, H. Kleinert, R.T. Jantzen, Editors; World Scientific, (Singapore, 2008).

    We interpret GRB970228 prompt emission within our "canonical" GRB scenario, identifying the initial spikelike emission with the Proper-GRB (P-GRB) and the following bumps with the afterglow peak emission. Furthermore, we emphasize the necessity to consider the "canonical" GRB as a whole due to the highly non-linear nature of the model we applied.

29. M.G. Bernardini, C.L. Bianco, L. Caito, M.G. Dainotti, R. Guida, R. Ruffini; "GRB980425 and the puzzling URCA1 emission"; in Proceedings of the Eleventh Marcel Grossmann Meeting on General Relativity, Berlin, Germany, July 2006, H. Kleinert, R.T. Jantzen, Editors; World Scientific, (Singapore, 2008).

    We applied our "fireshell" model to GRB980425 observational data, reproducing very satisfactory its prompt emission. We use the results of our analysis to provide a possible interpretation for the X-ray emission of the source S1. The effect on the GRB analysis of the lack of data in the pre-Swift observations is also outlined.

30. C.L. Bianco, M.G. Bernardini, L. Caito, P. Chardonnet, M.G. Dainotti,

F. Fraschetti, R. Guida, R. Ruffini, S.-S. Xue; "Theoretical interpretation of 'long' and 'short' GRBs"; in Proceedings of the Eleventh Marcel Grossmann Meeting on General Relativity, Berlin, Germany, July 2006, H. Kleinert, R.T. Jantzen, Editors; World Scientific, (Singapore, 2008).

Within the "fireshell" model we define a "canonical GRB" light curve with two sharply different components: the Proper-GRB (P-GRB), emitted when the optically thick fireshell of electron-positron plasma originating the phenomenon reaches transparency, and the afterglow, emitted due to the collision between the remaining optically thin fireshell and the CircumBurst Medium (CBM). We here present the consequences of such a scenario on the theoretical interpretation of the nature of "long" and "short" GRBs.

31. C.L. Bianco, M.G. Bernardini, P. Chardonnet, F. Fraschetti, R. Ruffini, S.-S. Xue; "Theoretical interpretation of luminosity and spectral properties of GRB 031203"; in Proceedings of the Eleventh Marcel Grossmann Meeting on General Relativity, Berlin, Germany, July 2006, H. Kleinert, R.T. Jantzen, Editors; World Scientific, (Singapore, 2008).

    We show how an emission endowed with an instantaneous thermal spectrum in the co-moving frame of the expanding fireshell can reproduce the time-integrated GRB observed non-thermal spectrum. An explicit example in the case of GRB 031203 is presented.

32. C.L. Bianco, R. Ruffini; "The 'Fireshell' model in the Swift era"; in Proceedings of the Eleventh Marcel Grossmann Meeting on General Relativity, Berlin, Germany, July 2006, H. Kleinert, R.T. Jantzen, Editors; World Scientific, (Singapore, 2008).

    We here re-examine the validity of the constant-index power-law relation between the fireshell Lorentz gamma factor and its radial coordinate, usually adopted in the current Gamma-Ray Burst (GRB) literature on the grounds of an "ultrarelativistic" approximation. Such expressions are found to be mathematically correct but only approximately valid in a very limited range of the physical and astrophysical parameters and in an asymptotic regime which is reached only for a very short time, if any.

33. L. Caito, M.G. Bernardini, C.L. Bianco, M.G. Dainotti, R. Guida, R. Ruffini; "Theoretical interpretation of GRB011121"; in Proceedings of the Eleventh Marcel Grossmann Meeting on General Relativity, Berlin, Germany, July

2006, H. Kleinert, R.T. Jantzen, Editors; World Scientific, (Singapore, 2008).

GRB 011121, detected by the BeppoSAX satellite, is studied as a prototype to understand the presence of flares observed by Swift in the afterglow of many GRB sources. Detailed theoretical analysis of the GRB 011121 light curves in selected energy bands are presented and compared with observational data. An interpretation of the flare of this source is provided by the introduction of the three-dimensional structure of the CircumBurst Medium(CBM).

34. M.G. Dainotti, M.G. Bernardini, C.L. Bianco, L. Caito, R. Guida, R. Ruffini; "On GRB 060218 and the GRBs related to Supernovae Ib/c"; in Proceedings of the Eleventh Marcel Grossmann Meeting on General Relativity, Berlin, Germany, July 2006, H. Kleinert, R.T. Jantzen, Editors; World Scientific, (Singapore, 2008).

    We study the Gamma-Ray Burst (GRB) 060218: a particularly close source at $z = 0.033$ with an extremely long duration, namely $T_{90} \sim 2000$ s, related to SN 2006aj. This source appears to be a very soft burst, with a peak in the spectrum at 4.9 keV, therefore interpreted as an X-Ray Flash (XRF) and it obeys to the Amati relation. We fit the X- and γ-ray observations by Swift of GRB 060218 in the 0.1150 keV energy band during the entire time of observations from 0 all the way to 106 s within a unified theoretical model. The details of our theoretical analysis have been recently published in a series of articles. The free parameters of the theory are only three, namely the total energy $E^{tot}_{e\pm}$ of the $e^{\pm}$ plasma, its baryon loading $B = M_B c^2 / E^{tot}_{e\pm}$, as well as the CircumBurst Medium (CBM) distribution. We fit the entire light curve, including the prompt emission as an essential part of the afterglow. We recall that this value of the B parameter is the highest among the sources we have analyzed and it is very close to its absolute upper limit expected. We successfully make definite predictions about the spectral distribution in the early part of the light curve, exactly we derive the instantaneous photon number spectrum N(E) and we show that although the spectrum in the co-moving frame of the expanding pulse is thermal, the shape of the final spectrum in the laboratory frame is clearly non thermal. In fact each single instantaneous spectrum is the result of an integration of thousands of thermal spectra over the corresponding EQuiTemporal Surfaces (EQTS). By our fit we show that there is no basic differences between XRFs and more general GRBs. They all originate from the collapse process to a black hole and their difference is due to the variability of the three basic parameters within

the range of full applicability of the theory.

35. R. Guida, M.G. Bernardini, C.L. Bianco, L. Caito, M.G. Dainotti, R. Ruffini; "Theoretical interpretation of GRB060124"; in Proceedings of the Eleventh Marcel Grossmann Meeting on General Relativity, Berlin, Germany, July 2006, H. Kleinert, R.T. Jantzen, Editors; World Scientific, (Singapore, 2008).

    We show the preliminary results of the application of our "fireshell" model to GRB060124. This source is very peculiar because it is the first event for which both the prompt and the afterglow emission were observed simultaneously by the three Swift instruments: BAT (15 - 350 keV), XRT (0,2 - 10 keV) and UVOT (170 - 650 nm), due to the presence of a precursor $\sim$ 570 s before the main burst. We analyze GRB060124 within our "canonical" GRB scenario, identifying the precursor with the P-GRB and the prompt emission with the afterglow peak emission. In this way we reproduce correctly the energetics of both these two components. We reproduce also the observed time delay between the precursor (P-GRB) and the main burst. The effect of such a time delay in our model will be discussed.

36. R. Ruffini, M.G. Bernardini, C.L. Bianco, L. Caito, P. Chardonnet, C. Cherubini, M.G. Dainotti, F. fraschetti, A. Geralico, R. Guida, B. Patricelli, M. Rotondo, J. Rueda Hernandez, G. Vereshchagin, S.-S. Xue; "Gamma-Ray Bursts"; in Proceedings of the Eleventh Marcel Grossmann Meeting on General Relativity, Berlin, Germany, July 2006, H. Kleinert, R.T. Jantzen, Editors; World Scientific, (Singapore, 2008).

    We show by example how the uncoding of Gamma-Ray Bursts (GRBs) offers unprecedented possibilities to foster new knowledge in fundamental physics and in astrophysics. After recalling some of the classic work on vacuum polarization in uniform electric fields by Klein, Sauter, Heisenberg, Euler and Schwinger, we summarize some of the efforts to observe these effects in heavy ions and high energy ion collisions. We then turn to the theory of vacuum polarization around a Kerr-Newman black hole, leading to the extraction of the blackholic energy, to the concept of dyadosphere and dyadotorus, and to the creation of an electron-positron-photon plasma. We then present a new theoretical approach encompassing the physics of neutron stars and heavy nuclei. It is shown that configurations of nuclear matter in bulk with global charge neutrality can exist on macroscopic scales and with electric fields close to the

critical value near their surfaces. These configurations may represent an initial condition for the process of gravitational collapse, leading to the creation of an electron-positron-photon plasma: the basic self-accelerating system explaining both the energetics and the high energy Lorentz factor observed in GRBs. We then turn to recall the two basic interpretational paradigms of our GRB model: 1) the Relative Space-Time Transformation (RSTT) paradigm and 2) the Interpretation of the Burst Structure (IBS) paradigm. These paradigms lead to a "canonical" GRB light curve formed from two different components: a Proper-GRB (P-GRB) and an extended afterglow comprising a raising part, a peak, and a decaying tail. When the P-GRB is energetically predominant we have a "genuine" short GRB, while when the afterglow is energetically predominant we have a so-called long GRB or a "fake" short GRB. We compare and contrast the description of the relativistic expansion of the electron-positron plasma within our approach and within the other ones in the current literature. We then turn to the special role of the baryon loading in discriminating between "genuine" short and long or "fake" short GRBs and to the special role of GRB 991216 to illustrate for the first time the "canonical" GRB bolometric light curve. We then propose a spectral analysis of GRBs, and proceed to some applications: GRB 031203, the first spectral analysis, GRB 050315, the first complete light curve fitting, GRB 060218, the first evidence for a critical value of the baryon loading, GRB 970228, the appearance of "fake" short GRBs. We finally turn to the GRB-Supernova Time Sequence (GSTS) paradigm: the concept of induced gravitational collapse. We illustrate this paradigm by the systems GRB 980425 / SN 1998bw, GRB 030329 / SN 2003dh, GRB 031203 / SN 2003lw, GRB 060218 / SN 2006aj, and we present the enigma of the URCA sources. We then present some general conclusions.

37. R. Ruffini, A.G. Aksenov, M.G. Bernardini, C.L. Bianco, L. Caito, M.G. Dainotti, G. De Barros, R. Guida, G. Vereshchagin, S.-S. Xue; "The canonical Gamma-Ray Bursts: long, 'fake'-'disguised' and 'genuine' short bursts; in PROBING STELLAR POPULATIONS OUT TO THE DISTANT UNIVERSE: CEFALU 2008, Proceedings of the International Conference; Cefal (Italy), September 2008, G. Giobbi, A. Tornambe, G. Raimondo, M. Limongi, L. A. Antonelli, N. Menci, E. Brocato, Editors; AIP Conference Proceedings, 1111, 325 (2009).

    The Gamma-Ray Bursts (GRBs) offer the unprecedented opportunity to observe for the first time the blackholic energy extracted by the vacuum polarization during the process of gravitational collapse to a black hole leading to

the formation of an electron-positron plasma. The uniqueness of the Kerr-Newman black hole implies that very different processes originating from the gravitational collapse a) of a single star in a binary system induced by the companion, or b) of two neutron stars, or c) of a neutron star and a white dwarf, do lead to the same structure for the observed GRB. The recent progress of the numerical integration of the relativistic Boltzmann equations with collision integrals including 2-body and 3-body interactions between the particles offer a powerful conceptual tool in order to differentiate the traditional "fireball" picture, an expanding hot cavity considered by Cavallo and Rees, as opposed to the "fireshell" model, composed of an internally cold shell of relativistically expanding electron-positron-baryon plasma. The analysis of the fireshell naturally leads to a canonical GRB composed of a proper-GRB and an extended afterglow. By recalling the three interpretational paradigms for GRBs we show how the fireshell model leads to an understanding of the GRB structure and to an alternative classification of short and long GRBs.

38. M.G. Bernardini, M.G. Dainotti, C.L. Bianco, L. Caito, R. Guida, R. Ruffini; "Prompt emission and X-ray flares: the case of GRB 060607 A"; in PROBING STELLAR POPULATIONS OUT TO THE DISTANT UNIVERSE: CEFALU 2008, Proceedings of the International Conference; Cefal (Italy), September 2008, G. Giobbi, A. Tornambe, G. Raimondo, M. Limongi, L. A. Antonelli, N. Menci, E. Brocato, Editors; AIP Conference Proceedings, 1111, 383 (2009).

    GRB 060607A is a very distant and energetic event. Its main peculiarity is that the peak of the near-infrared (NIR) afterglow has been observed with the REM robotic telescope, allowing to estimate the initial Lorentz gamma factor within the fireball forward shock model. We analyze GRB 060607A within the fireshell model. The initial Lorentz gamma factor of the fireshell can be obtained adopting the exact solutions of its equations of motion, dealing only with the BAT and XRT observations, that are the basic contribution to the afterglow emission, up to a distance from the progenitor $r \sim 10^{18}$ cm. According to the "canonical GRB" scenario we interpret the whole prompt emission as the peak of the afterglow emission, and we show that the observed temporal variability of the prompt emission can be produced by the interaction of the fireshell with overdense CircumBurst Medium (CBM) clumps. This is indeed the case also of the X-ray flares which are present in the early phases of the afterglow light curve.

39. C.L. Bianco, M.G. Bernardini, L. Caito, M.G. Dainotti, R. Guida, R. Ruffini; "The 'fireshell' model and the 'canonical GRB' scenario. Implications for the Amati relation"; in PROBING STELLAR POPULATIONS OUT TO THE DISTANT UNIVERSE: CEFALU 2008, Proceedings of the International Conference; Cefal (Italy), September 2008, G. Giobbi, A. Tornambe, G. Raimondo, M. Limongi, L. A. Antonelli, N. Menci, E. Brocato, Editors; AIP Conference Proceedings, 1111, 587 (2009).

    Within the "fireshell" model for GRBs we define a "canonical GRB" light curve with two sharply different components: the Proper-GRB (P-GRB), emitted when the optically thick fireshell reaches transparency, and the extended afterglow, emitted due to the collision between the remaining optically thin fireshell and the CircumBurst Medium (CBM). We here outline our "canonical GRB" scenario, which implies three different GRB classes: the "genuine" short GRBs, the "fake" or "disguised" short GRBs and the other (so-called "long") GRBs. We will also outline the corresponding implications for the Amati relation, which are opening its use for cosmology.

40. R. Ruffini, A.G. Aksenov, M.G. Bernardini, C.L. Bianco, L. Caito, P. Chardonnet, M.G. Dainotti, G. De Barros, R. Guida, L. Izzo, B. Patricelli, L.J. Rangel Lemos, M. Rotondo, J.A. Rueda Hernandez, G. Vereshchagin, S.-S. Xue; "The Blackholic energy and the canonical Gamma-Ray Burst IV: the 'long', 'genuine short' and 'fake disguised short' GRBs"; in Proceedings of the XIIIth Brazilian School on Cosmology and Gravitation, Mangaratiba, Rio de Janeiro (Brazil), July-August 2008, M. Novello, S.E. Perez Bergliaffa, Editors; AIP Conference Proceedings, 1132, 199 (2009).

    We report some recent developments in the understanding of GRBs based on the theoretical framework of the "fireshell" model, already presented in the last three editions of the "Brazilian School of Cosmology and Gravitation". After recalling the basic features of the "fireshell model", we emphasize the following novel results: 1) the interpretation of the X-ray flares in GRB afterglows as due to the interaction of the optically thin fireshell with isolated clouds in the CircumBurst Medium (CBM); 2) an interpretation as "fake - disguised" short GRBs of the GRBs belonging to the class identified by Norris & Bonnell; we present two prototypes, GRB 970228 and GRB 060614; both these cases are consistent with an origin from the final coalescence of a binary system in the halo of their host galaxies with particularly low CBM density $n_{cbm} \sim 10^{-3}$

particles/cm^3; 3) the first attempt to study a genuine short GRB with the analysis of GRB 050509B, that reveals indeed still an open question; 4) the interpretation of the GRB-SN association in the case of GRB 060218 via the "induced gravitational collapse" process; 5) a first attempt to understand the nature of the "Amati relation", a phenomenological correlation between the isotropic-equivalent radiated energy of the prompt emission E_{iso} with the cosmological rest-frame νF_ν spectrum peak energy $E_{p,i}$. In addition, recent progress on the thermalization of the electron-positron plasma close to their formation phase, as well as the structure of the electrodynamics of Kerr-Newman Black Holes are presented. An outlook for possible explanation of high-energy phenomena in GRBs to be expected from the AGILE and the Fermi satellites are discussed. As an example of high energy process, the work by Enrico Fermi dealing with ultrarelativistic collisions is examined. It is clear that all the GRB physics points to the existence of overcritical electrodynamical fields. In this sense we present some progresses on a unified approach to heavy nuclei and neutron stars cores, which leads to the existence of overcritical fields under the neutron star crust.

41. A.G. Aksenov, M.G. Bernardini, C.L. Bianco, L. Caito, C. Cherubini, G. De Barros, A. Geralico, L. Izzo, F.A. Massucci, B. Patricelli, M. Rotondo, J.A. Rueda Hernandez, R. Ruffini, G. Vereshchagin, S.-S. Xue; "The fireshell model for Gamma-Ray Bursts"; in The Shocking Universe, Proceedings of the conference held in Venice (Italy), September 2009, G. Chincarini, P. DAvanzo, R. Margutti, R. Salvaterra, Editors; SIF Conference Proceedings, 102, 451 (2010).

    The fireshell model for GRBs is briefly outlined, and the currently ongoing developments are summarized.

42. M.G. Bernardini, C.L. Bianco, L. Caito, L. Izzo, B. Patricelli, R. Ruffini; "The end of the prompt emission within the fireshell model"; in The Shocking Universe, Proceedings of the conference held in Venice (Italy), September 2009, G. Chincarini, P. DAvanzo, R. Margutti, R. Salvaterra, Editors; SIF Conference Proceedings, 102, 489 (2010)

    The shallow decay emission, revealed by the Swift satellite in the X-ray afterglow of a good sample of bursts, is a puzzle. Within the fireshell model it has been recently proposed an alternative explanation: if we assume that after the prompt phase the system has a range of Lorentz factors, the plateau phase is simply the product of the injection of slower material into the fireshell. This

injection produces a modification both in the dynamics of the fireshell and in the spectrum of the emitted radiation. We postulate that this spread in the fireshell Lorentz factor occurs when the fireshell becomes transparent and do not depend on a prolonged activity of the central engine. The aim of this paper is to characterize dynamically the system in order to understand the nature of that material.

43. L. Izzo, M.G. Bernardini, C.L. Bianco, L. Caito, B. Patricelli, R. Ruffini; "GRB 090423 in the fireshell scenario"; in The Shocking Universe, Proceedings of the conference held in Venice (Italy), September 2009, G. Chincarini, P. DAvanzo, R. Margutti, R. Salvaterra, Editors; SIF Conference Proceedings, 102, 537 (2010).

44. B. Patricelli, M.G. Bernardini, C.L. Bianco, L. Caito, L. Izzo, R. Ruffini, G. Vereshchagin; "A new spectral energy distribution of photons in the fireshell model of GRBs"; in The Shocking Universe, Proceedings of the conference held in Venice (Italy), September 2009, G. Chincarini, P. DAvanzo, R. Margutti, R. Salvaterra, Editors; SIF Conference Proceedings, 102, 559 (2010).

    The fireshell model of Gamma Ray Bursts (GRBs) postulates that the emission process is thermal in the comoving frame of the fireshell, but this is just a first approximation. We investigate a different spectrum of photons in the comoving frame in order to better reproduce the observed spectral properties of GRB prompt emission. We introduce a modified thermal spectrum whose low energy slope depends on an index α, left as a free parameter. We test it by comparing the numerical simulations with observed BAT spectra integrated over different intervals of time. We find that the observational data can be correctly reproduced by assuming $\alpha = -1.8$.

45. C.L. Bianco, M.G. Bernardini, L. Caito, G. De Barros, L. Izzo, B. Patricelli, R. Ruffini; "Disguised Short Bursts and the Amati Relation"; in Deciphering the ancient universe with Gamma-Ray Bursts, Proceedings of the conference held in Kyoto (Japan), April 2010, N. Kawai, S. Nagataki, Editors; AIP Conference Proceedings, 1279, 299 (2010).

    The class of "Disguised short" GRBs implied by the fireshell scenario is presented, with special emphasis on the implications for the Amati relation.

46. L. Izzo, M.G. Bernardini, C.L. Bianco, L. Caito, B. Patricelli, L.J. Rangel Lemos, R. Ruffini; "On GRB 080916C and GRB 090902B observed by the

Fermi satellite"; in Deciphering the ancient universe with Gamma-Ray Bursts, Proceedings of the conference held in Kyoto (Japan), April 2010, N. Kawai, S. Nagataki, Editors; AIP Conference Proceedings, 1279, 343 (2010).

We propose a possible explanation, in the context of the Fireshell scenario, for the high-energy emission observed in GRB 080916C and GRB 090902B. The physical process underlying this emission consists mainly in the interaction of the baryon in the Fireshell with some high-density region around the burst site. Moreover we associate the observed delay of the onset of the high-energy emission as due to the P-GRB emission.

47. B. Patricelli, M.G. Bernardini, C.L. Bianco, L. Caito, G. De Barros, L. Izzo, R. Ruffini; "Black Holes in Gamma Ray Bursts"; in Deciphering the ancient universe with Gamma-Ray Bursts, Proceedings of the conference held in Kyoto (Japan), April 2010, N. Kawai, S. Nagataki, Editors; AIP Conference Proceedings, 1279, 406 (2010).

    Within the fireshell model, Gamma Ray Bursts (GRBs) originate from an optically thick $e^{\pm}$ plasma created by vacuum polarization process during the formation of a Black Hole (BH). Here we briefly recall the basic features of this model, then we show how it is possible to interpret GRB observational properties within it. In particular we present, as a specific example, the analysis of GRB 050904 observations of the prompt emission light curve and spectrum in the Swift BAT energy band (15-150 keV).

48. M.G. Bernardini, C.L. Bianco, L. Caito, M.G. Dainotti, R. Guida, R. Ruffini; "The GRB classification within the "fireshell" model: short, long and "fake" short GRBs"; in Proceedings of the 3rd Stueckelberg Workshop on Relativistic Field Theories, Pescara, Italy, July 2008, N. Carlevaro, R. Ruffini, G.V. Vereshchagin, Editors; Cambridge Scientific Publishers, (UK, 2011).

49. C.L. Bianco, M.G. Bernardini, L. Caito, M.G. Dainotti, R. Guida, R. Ruffini, G.V. Vereshchagin, S.-S. Xue; "Equations of motion of the "fireshell""; in Proceedings of the 3rd Stueckelberg Workshop on Relativistic Field Theories, Pescara, Italy, July 2008, N. Carlevaro, R. Ruffini, G.V. Vereshchagin, Editors; Cambridge Scientific Publishers, (UK, 2011).

50. L. Caito, M.G. Bernardini, C.L. Bianco, M.G. Dainotti, R. Guida, R. Ruffini; "GRB 060614: another example of "fake" short burst from a merging

binary system"; in Proceedings of the 3rd Stueckelberg Workshop on Relativistic Field Theories, Pescara, Italy, July 2008, N. Carlevaro, R. Ruffini, G.V. Vereshchagin, Editors; Cambridge Scientific Publishers, (UK, 2011).

51. G. De Barros, M.G. Bernardini, C.L. Bianco, L. Caito, R. Guida, R. Ruffini; "Analysis of GRB 050509b"; in Proceedings of the 3rd Stueckelberg Workshop on Relativistic Field Theories, Pescara, Italy, July 2008, N. Carlevaro, R. Ruffini, G.V. Vereshchagin, Editors; Cambridge Scientific Publishers, (UK, 2011).

52. R. Ruffini, L. Izzo, A.V. Penacchioni, C.L. Bianco, L. Caito, S.K. Chakrabarti, A. Nandi; "GRB 090618: a possible case of multiple GRB?"; in Proceedings of the 25th Texas Symposium on Relativistic Astrophysics, held in Heidelberg (Germany), December 2010, F.M. Rieger, C. van Eldik, W. Hofmann, Editors; PoS(Texas2010), 101.

53. L.J. Rangel Lemos, C.L. Bianco, H.J. Mosquera Cuesta, J.A. Rueda, R. Ruffini; "Luminosity function of BATSE GRBs dominated by extended afterglow"; in Proceedings of the 25th Texas Symposium on Relativistic Astrophysics, held in Heidelberg (Germany), December 2010, F.M. Rieger, C. van Eldik, W. Hofmann, Editors; PoS(Texas2010), 204.

54. R. Ruffini, A.G. Aksenov, M.G. Bernardini, C.L. Bianco, L. Caito, P. Chardonnet, M.G. Dainotti, G. De Barros, R. Guida, L. Izzo, B. Patricelli, L.J. Rangel Lemos, M. Rotondo, J.A. Rueda Hernandez, G. Vereshchagin, She-Sheng Xue; "Black Holes Energetics and GRBs"; in The Sun, the Stars, the Universe and General Relativity: Proceedings of Sobral 2009; S.E. Perez Bergliaffa, M. Novello , R. Ruffini, Editors; Cambridge Scientific Publishers (UK, 2011).

55. C.L. Bianco, L. Amati, M.G. Bernardini, L. Caito, G. De Barros, L. Izzo, B. Patricelli, R. Ruffini; "The class of 'disguised' short GRBs and its implications for the Amati relation"; in GRBs as probes - from the progenitors environment to the high redshift Universe, Proceedings of the conference held in Como (Italy), May 2011, S. Campana, P. DAvanzo, A. Melandri, Editors; Mem. S.A.It. Suppl., 21, 139 (2012).

56. A.V. Penacchioni, R. Ruffini, L. Izzo, M. Muccino, C.L. Bianco, L. Caito, B. Patricelli; "Evidences for a double component in the emission of GRB

101023"; in GRBs as probes - from the progenitors environment to the high redshift Universe, Proceedings of the conference held in Como (Italy), May 2011, S. Campana, P. DAvanzo, A. Melandri, Editors; Mem. S.A.It. Suppl., 21, 230 (2012).

57. M.G. Bernardini, C.L. Bianco, L. Caito, L. Izzo, B. Patricelli, R. Ruffini; "The X-Ray Flares of GRB 060607A within the Fireshell Model"; in Proceedings of the Twelfth Marcel Grossmann Meeting on General Relativity, Paris, France, July 2009, T. Damour, R.T. Jantzen, R. Ruffini, Editors; World Scientific, (Singapore, 2012).

58. L. Izzo, M.G. Bernardini, C.L. Bianco, L. Caito, B. Patricelli, R. Ruffini; "GRB 090423 in the Fireshell Scenario: A Canonical GRB at Redshift 8.2"; in Proceedings of the Twelfth Marcel Grossmann Meeting on General Relativity, Paris, France, July 2009, T. Damour, R.T. Jantzen, R. Ruffini, Editors; World Scientific, (Singapore, 2012).

59. B. Patricelli, M.G. Bernardini, C.L. Bianco, L. Caito, L. Izzo, R. Ruffini, G.V. Vereshchagin; "A New Spectral Energy Distribution of Photons in the Fireshell Model of GRBs"; in Proceedings of the Twelfth Marcel Grossmann Meeting on General Relativity, Paris, France, July 2009, T. Damour, R.T. Jantzen, R. Ruffini, Editors; World Scientific, (Singapore, 2012).

60. C.L. Bianco, M.G. Bernardini, L. Caito, G. De Barros, L. Izzo, M. Muccino, B. Patricelli, A.V. Penacchioni, G.B. Pisani, R. Ruffini; "Needs for a new GRB classification following the fireshell model: genuine short, disguised short and long GRBs"; in Proceedings of the Gamma-Ray Bursts 2012 Conference, held in Munich (Germany), May 2012, A. Rau, J. Greiner, Editors; PoS(GRB 2012), 043.

61. A.V. Penacchioni, G.B. Pisani, R. Ruffini, C.L. Bianco, L. Izzo, M. Muccino; "The proto-black hole concept in GRB 101023 and its possible extension to GRB 110709B"; in Proceedings of the Gamma-Ray Bursts 2012 Conference, held in Munich (Germany), May 2012, A. Rau, J. Greiner, Editors; PoS(GRB 2012), 042.

62. B. Patricelli, M.G. Bernardini, C.L. Bianco, L. Caito, L. Izzo, R. Ruffini; "GRB 050904: The study of a high redshift GRB within the Fireshell Model"; in Proceedings of the Twelfth Marcel Grossmann Meeting on

General Relativity, Paris, France, July 2009, T. Damour, R.T. Jantzen, R. Ruffini, Editors; World Scientific, (Singapore, 2012).

63. L. Izzo, G.B. Pisani, M. Muccino, J.A. Rueda, Y.Wang, C.L. Bianco, A.V. Penacchioni, R. Ruffini; "A common behavior in the late X-ray afterglow of energetic GRB-SN systems"; EAS Publications Series, Volume 61, 595-597 (2013).

64. R. Ruffini; "Black Holes, Supernovae and Gamma Ray Bursts"; in Proceedings of the Thirteenth Marcel Grossmann Meeting on General Relativity, Stockholm, Sweden, July 2012, R.T. Jantzen, K. Rosquist, R. Ruffini, Editors; World Scientific, (Singapore, 2015).

65. M. Muccino, R. Ruffini, C.L. Bianco, L. Izzo, A.V. Penacchioni, G.B. Pisani; "GRB 090227B: The missing link between the genuine short and long GRBs"; in Proceedings of the Thirteenth Marcel Grossmann Meeting on General Relativity, Stockholm, Sweden, July 2012, R.T. Jantzen, K. Rosquist, R. Ruffini, Editors; World Scientific, (Singapore, 2015).

66. A.V. Penacchioni, R. Ruffini, C.L. Bianco, L. Izzo, M. Muccino, G.B. Pisani, J.A. Rueda; "The family of the Induced Gravitational Collapse scenario: The case of GRB 110709B"; in Proceedings of the Thirteenth Marcel Grossmann Meeting on General Relativity, Stockholm, Sweden, July 2012, R.T. Jantzen, K. Rosquist, R. Ruffini, Editors; World Scientific, (Singapore, 2015).

67. A.V. Penacchioni, R. Ruffini, C.L. Bianco, L. Izzo, M. Muccino, G.B. Pisani; "GRB 111228, analysis within the Induced Gravitational Collapse scenario and association with a supernova"; in Proceedings of the Thirteenth Marcel Grossmann Meeting on General Relativity, Stockholm, Sweden, July 2012, R.T. Jantzen, K. Rosquist, R. Ruffini, Editors; World Scientific, (Singapore, 2015).

68. G.B. Pisani, L. Izzo, R. Ruffini, C.L. Bianco, M. Muccino, A.V. Penacchioni, J.A. Rueda, Y. Wang; "On a novel distance indicator for Gamma-Ray Bursts associated with supernovae"; in Proceedings of the Thirteenth Marcel Grossmann Meeting on General Relativity, Stockholm, Sweden, July 2012, R.T. Jantzen, K. Rosquist, R. Ruffini, Editors; World Scientific, (Singapore, 2015).

69. M. Muccino, R. Ruffini, C.L. Bianco, L. Izzo, A.V. Penacchioni, G.B. Pisani; "GRB 090510, explosion of a GRB in the highest circumburst medium even inferred: a disguised short GRB"; in Proceedings of the Thirteenth Marcel Grossmann Meeting on General Relativity, Stockholm, Sweden, July 2012, R.T. Jantzen, K. Rosquist, R. Ruffini, Editors; World Scientific, (Singapore, 2015).

70. L. Izzo, G.B. Pisani, M. Muccino, R. Ruffini, C.L. Bianco, M. Enderli, Y. Wang; "Hints for a physically based GRB distance indicator"; in Proceedings of the Thirteenth Marcel Grossmann Meeting on General Relativity, Stockholm, Sweden, July 2012, R.T. Jantzen, K. Rosquist, R. Ruffini, Editors; World Scientific, (Singapore, 2015).

The Astrophysical Journal, 844:83 (15pp), 2017 July 20 https://doi.org/10.3847/1538-4357/aa7a9f

GRB 081024B and GRB 140402A: Two Additional Short GRBs from Binary Neutron Star Mergers

Y. Aimuratov[1,2], R. Ruffini[1,2,3,4], M. Muccino[1,3], C. L. Bianco[1,3], A. V. Penacchioni[3,5,6], G. B. Pisani[1,3], D. Primorac[1,3], J. A. Rueda[1,3,4], and Y. Wang[1,3]

[1] ICRA and Dipartimento di Fisica, Sapienza Università di Roma and ICRA, Piazzale Aldo Moro 5, I-00185 Roma, Italy
[2] Université de Nice Sophia-Antipolis, Grand Château Parc Valrose, Nice, CEDEX 2, France
[3] ICRA Net, Piazza della Repubblica 10, I-65122 Pescara, Italy
[4] ICRA Net-Rio, Centro Brasileiro de Pesquisas Físicas, Rua Dr. Xavier Sigaud 150, 22290-180 Rio de Janeiro, Brazil
[5] ASI Science Data Center, Via del Politecnico s.n.c., I-00133 Rome, Italy
[6] Department of Physical Sciences, Earth and Environment, University of Siena, Via Roma 56, I-53100 Siena, Italy
Received 2017 April 26; revised 2017 June 13; accepted 2017 June 18; published 2017 July 25

Abstract

Theoretical and observational evidences for a two-fold classification of short bursts have been recently obtained: (1) short gamma-ray flashes (S-GRFs), with isotropic energy $E_{\rm iso} < 10^{52}$ erg and no black hole (BH) formation, and (2) authentic short gamma-ray bursts (S-GRBs), with isotropic energy $E_{\rm iso} > 10^{52}$ erg showing evidence of BH formation in the binary neutron star merging process. The signature for BH formation is the onset of high-energy (0.1–100 GeV) emission, coeval to the prompt emission, in all S-GRBs. No GeV emission is expected nor observed in S-GRFs. In this paper, we present two S-GRBs, GRB 081024B and GRB 140402A, in addition to the already identified S-GRBs, GRB 090227B, GRB 090510, and GRB 140619B. We also return to the absence of GeV emission in the S-GRB 090227B, at an angle of 71° from the *Fermi*-LAT boresight. All of the correctly identified S-GRBs correlate with high-energy emission, implying no significant presence of beaming in GeV emission. The existence of a common power-law behavior in the GeV luminosities, following the BH formation, when measured in the source rest frame, points to a commonality in the mass and spin of the newly formed BHs in all S-GRBs.

Key words: gamma-ray burst: general – gamma-ray burst: individual (GRB 081024B, GRB 140402A) – stars: neutron

1. Introduction

Gamma-ray bursts (GRBs) have been historically divided into a two-fold classification based on the observed T_{90} duration of their prompt emission: short GRBs with $T_{90} \lesssim 2$ s and long GRBs with $T_{90} \gtrsim 2$ s (Mazets et al. 1981; Dezalay et al. 1992; Klebesadel 1992; Kouveliotou et al. 1993; Tavani 1998).

The progenitor systems of short bursts have traditionally been identified with binary neutron star (NS) and NS−black hole (BH) mergers (see, e.g., Goodman 1986; Paczynski 1986; Eichler et al. 1989; Narayan et al. 1991; Meszaros & Rees 1997; Rosswog et al. 2003; Lee et al. 2004; Belczynski et al. 2006; Berger 2014). This assumption has received observational support from their localization, made possible by the X-ray emission of the afterglow, with large offsets from their hosts galaxies, both late- and early-type galaxies with no star formation evidence (see, e.g., Fox et al. 2005; Gehrels et al. 2005; Berger 2014).

A vast activity of numerical work on relativistic magnetohydrodynamical (MHD) simulation using the largest facilities in the world (equipped with supercomputers with peak performances of 6.8 PFLOPS,[7] see Siegel et al. 2014; 13.3 PFLOPS, see Ruiz et al. 2016; and 10.51 PFLOPS, see Kiuchi et al. 2014) have been developed with the declared goal of finding a jetted emission, which they considered, without convincing observational support, to be a necessary step in developing short GRB models in merging binary NS–NS or binary BH–NS systems (see, e.g., Rezzolla et al. 2011; Shibata et al. 2011; Kiuchi et al. 2014; Siegel et al. 2014; Paschalidis et al. 2015; Ruiz et al. 2016). It is interesting that they themselves recognized the shortcoming of their approach: "...there is microphysics that we do not model here, such as the effects of a realistic hot, nuclear EOS [equation of state] and neutrino transport" (see, e.g., Ruiz et al. 2016, p. 5). They also expected that such models would be further confirmed by the observation of gravitational waves (GWs) by aLIGO (see, e.g., Brown et al. 2004).

There is no observational signature for the role of MHD activities in GRBs, nor, as we show in this paper, for jetted emission in X-rays and γ-rays, as well as in the ultrarelativistic GeV emission of short bursts (see Section 5). On the contrary, also in the case of short GRBs, we have strong evidence for the necessary occurrence of hypercritical accretion processes, as already shown in long GRBs, with the fundamental roles played by neutrino emission (Zel'dovich et al. 1972; Ruffini & Wilson 1973; Rueda & Ruffini 2012; Fryer et al. 2014) and the value of the NS critical mass $M_{\rm crit}^{\rm NS}$ (Rotondo et al. 2011a, 2011b; Rueda et al. 2011, 2014; Belvedere et al. 2012, 2014, 2015; Rueda & Ruffini 2013; Cipolletta et al. 2015; see also Fryer et al. 2014, 2015b; Becerra et al. 2015, 2016). We also established firm upper limits on the observation of GWs from short GRBs by aLIGO (Oliveira et al. 2014; Ruffini et al. 2015, 2016b).

Our approach is markedly different from traditional ones. Since Ruffini et al. (2001a, 2001b, 2001c). we started:

(a) daily systematic and independent analyses of the GRB data in X-rays and γ-rays and GeV emission from *Beppo-SAX*

[7] The acronym PFLOPS means Peta (10^{15}) Floating Point Operations per second.

(see, e.g., Frontera 2015), *Swift* (Barthelmy et al. 2005), *Fermi* (Meegan et al. 2009), Konus-*WIND* (Aptekar et al. 1995), and *AGILE* (Tavani et al. 2009). We extended our data analysis to optical and radio data.

(b) We have developed theoretical and astrophysical models based on quantum and classical relativistic field theories.

(c) At every step, we verified that the theoretical considerations are consistent with the observational data.

In this article, we mainly address the study of NS–NS mergers and only at the end do we refer to BH–NS binaries.

In Ruffini et al. (2015), a further division of the short bursts into two different subclasses has been proposed, and specific observable criteria characterizing this division have been given there:

1. The first subclass of short bursts is characterized by isotropic energies $E_{\rm iso} \lesssim 10^{52}$ erg and rest-frame spectral peak energies $E_{p,i} \lesssim 2$ MeV (Zhang et al. 2012; Calderone et al. 2015). In this case, the outcome of the NS–NS merger is a massive NS (MNS) with additional orbiting material (Ruffini et al. 2016c). An alternative scenario leads to a new binary system comprising an MNS and a less massive NS or a white dwarf (WD). For specific mass ratios, a stable mass-transfer process may occur from the less massive to the MNS (see, e.g., Clark & Eardley 1977; Bildsten & Cutler 1992, and references therein). Consequently, the donor NS moves outward by losing mass and may also reach beta-decay instability, becoming a low-mass WD. In view of their moderate hardness and their low energetics, we have indicated such short bursts as short gamma-ray flashes (S-GRFs; see Ruffini et al. 2016c). There, the local rate of S-GRFs has been estimated to be $\rho_0 = 3.6^{+1.4}_{-1.0}$ Gpc^{-3} yr^{-1}.
2. The second subclass corresponds to the authentic short GRBs (S-GRBs) with $E_{\rm iso} \gtrsim 10^{52}$ erg and $E_{p,i} \gtrsim 2$ MeV (Zhang et al. 2012; Calderone et al. 2015). In this system, the NS–NS merger leads to the formation of a Kerr BH with additional orbiting material, in order to conserve energy and angular momentum (Ruffini et al. 2016a, 2016c). A further characterizing feature of S-GRBs absent in S-GRFs is the presence of 0.1–100 GeV emission, coeval to their prompt emission and showing evidence of the activity of a newly born BH. In Ruffini et al. (2016c), the local rate of S-GRBs has been estimated to be $\rho_0 = (1.9^{+2.8}_{-1.1}) \times 10^{-3}$ Gpc^{-3} yr^{-1}. The impossibility of detecting the observed short GRB 140619B with LIGO was evident (see Figure 12 in Ruffini et al. 2015). We return again in this article to the issue of non-detectability of GWs for S-GRBs.

The above relative rate of these two subclasses of short bursts has been discussed and presented in Ruffini et al. (2016c). There, it has been shown that S-GRFs are the most frequent events among short bursts. This conclusion is in good agreement with the NS–NS binaries observed within our Galaxy: only a subset of them has a total mass larger than $M^{\rm NS}_{\rm crit}$ and can form a BH in their merging process (Ruffini et al. 2015). There, in Figure 3, it was assumed that $M^{\rm NS}_{\rm crit} = 2.67\, M_\odot$ for a non-rotating NS by imposing global charge neutrality and using the NL3 nuclear model (see, e.g., Cipolletta et al. 2015). Similar conclusions have also been independently reached by Fryer et al. (2015a) and Lawrence et al. (2015).

We have identified three authentic S-GRBs: GRB 090227B (Muccino et al. 2013), GRB 090510 (Ruffini et al. 2016a), and GRB 140619B (Ruffini et al. 2015). All of them populate the high-energy part of the $E_{p,i}$–$E_{\rm iso}$ relation for short bursts (Zhang et al. 2012; Calderone et al. 2015; Ruffini et al. 2016a) and have $E_{\rm iso} > 10^{52}$ erg. We have analyzed the above three S-GRBs within the fireshell model (see, e.g., Ruffini et al. 2010). The transparency emission of the e^+e^- plasma (the P-GRB emission), the onset of prompt emission, and the correlation between the spike emission of the prompt and CBM inhomogeneities have led to the most successful test and applicability of the fireshell model.

A further and independent distinguishing feature between S-GRFs and S-GRBs has been found thanks to *Fermi* data: when these three S-GRBs fall within the *Fermi*-LAT field of view (FoV), GeV emission related to the emission from a newly born BH occurs, starting soon after the P-GRB emission.

In this paper, we present two additional S-GRBs: GRB 081024B and GRB 140402A. The S-GRB 081024 is historically important since that source provided the first clear detection of a GeV temporally extended emission from a short burst (Abdo et al. 2010). From the application of the fireshell model to this S-GRB, we theoretically derived its redshift, $z = 3.12 \pm 1.82$, and, therefore, $E_{\rm iso} = (2.6 \pm 1.0) \times 10^{52}$ erg, $E_{p,i} = (9.6 \pm 4.9)$ MeV, and $E_{\rm LAT} = (2.79 \pm 0.98) \times 10^{52}$ erg. For the S-GRB 140402A, we theoretically derived a redshift $z = 5.52 \pm 0.93$, which gives $E_{\rm iso} = (4.7 \pm 1.1) \times 10^{52}$ erg and $E_{p,i} = (6.1 \pm 1.6)$ MeV. A long-lived GeV emission with 800 s has been reported (Bissaldi et al. 2014). The total energy of the brightest GeV emission is $E_{\rm LAT} = (4.5 \pm 2.2) \times 10^{52}$ erg.

We also updated the analysis of the GeV emission of the S-GRB 090227B. The apparent absence of GeV emission has already been discussed in Ruffini et al. (2015), recalling that this source was outside the nominal LAT FoV, and only photons in the LAT low-energy (LLE) channel and a single transient-class event with energy above 100 MeV were associated with this GRB (Ackermann et al. 2013). A further updated analysis would indicate that, in view of the missing observations, in no way can the absence of GeV emission before ∼40 s in the source rest frame can be inferred.

From the analyses of the two additional S-GRBs, 081024B and 140402A, and the further check for GeV emission associated with the S-GRB 090227B, we conclude that all S-GRBs correlate with high-energy emission, implying no significant presence of beaming in GeV emission.

In Section 2, we briefly recall the fireshell model and its implications for S-GRBs. In Sections 3 and 4, we report the data analyses of the S-GRBs 081024B and 140402A, respectively, and show their theoretical interpretation within the fireshell model: from the theoretical inference of their cosmological redshift, their transparency emission parameters, to the details of the circumburst media where they occurred. In Section 5, we summarize the properties of the GeV emission of all S-GRBs and show the characteristic common power-law behavior of the rest-frame 0.1–100 GeV luminosity light curves. We also discuss the minimum Lorentz factor of the GeV emission $\Gamma^{\rm min}_{\rm GeV}$ obtained by requiring that the outflow must be optically thin to GeV photons (namely, to the pair-creation process), as well as its possible energy source, i.e., the matter accreting onto the newly formed BH. In Section 6, we indicate that there is no evidence in favor of or against a common behavior of X-ray afterglows of S-GRBs in view of the limited

observations. In Section 7, we briefly address the issue of the possible emission of short bursts from BH–NS binaries leading to ultrashort GRBs (U-GRBs; see Fryer et al. 2015b; Ruffini et al. 2016c). In Section 8, we infer our conclusions.

2. The Fireshell Model

In the fireshell model (Ruffini et al. 2001a, 2001b, 2001c), the GRB acceleration process consists of the dynamics of an optically thick e^+e^- plasma of total energy $E^{\rm tot}_{e^+e^-}$—the *fireshell*. Its expansion and self-acceleration are due to the gradual e^+e^- annihilation, which has been described in Ruffini et al. (1999). The effect of baryonic contamination on the dynamics of the fireshell has been considered in Ruffini et al. (2000), where it was shown that even after the engulfment of baryonic mass M_B, quantified by the baryon load $B = M_B c^2/E^{\rm tot}_{e^+e^-}$, the fireshell still remains optically thick and continues its self-acceleration up to ultrarelativistic velocities (Aksenov et al. 2007, 2009). The dynamics of the fireshell in the optically thick phase up to the transparency condition is fully described by $E^{\rm tot}_{e^+e^-}$ and B (Ruffini et al. 2000). In the case of long bursts, it is characterized by $10^{-4} \lesssim B < 10^{-2}$ (Izzo et al. 2012; Patricelli et al. 2012; Penacchioni et al. 2012, 2013), while for short bursts, we have $10^{-5} \lesssim B \lesssim 10^{-4}$ (Muccino et al. 2013; Ruffini et al. 2015, 2016a).

The fireshell continues its self-acceleration until the transparency condition is reached; then, a first flash of thermal radiation, the P-GRB, is emitted (Ruffini et al. 1999, 2000, 2001b). The spectrum of the P-GRB is determined by the geometry of the fireshell, which is dictated, in turn, by the geometry of the pair-creation region. In the case of a spherically symmetric dyadosphere, the P-GRB spectrum is generally described by a single thermal component in good agreement with the spectral data (see, e.g., Muccino et al. 2013; Ruffini et al. 2015). In the case of an axially symmetric dyadotorus, the resulting P-GRB spectrum, which resembles more a power-law spectral energy distribution with an exponential cutoff (Ruffini et al. 2016a), is a convolution of thermal spectra of different temperatures.

After transparency, the accelerated baryons (and leptons) propagate through the circumburst medium (CBM). The collisions with the CBM, assumed to occur in the fully radiative regime, give rise to the prompt emission (Ruffini et al. 2001b). The spectrum of these collisions, in the comoving frame of the shell, is modeled with a modified blackbody (BB) spectrum, obtained by introducing an additional power law at low energy with a phenomenological index $\bar{\alpha}$, which describes the departure from the purely thermal case (see Patricelli et al. 2012 for details). The structures observed in the prompt emission of a GRB depend on the CBM density $n_{\rm CBM}$ and its inhomogeneities (Ruffini et al. 2004), described by the fireshell filling factor $\mathcal{R}$. This parameter is defined as the ratio between the effective fireshell emitting area $A_{\rm eff}$ and the total visible area $A_{\rm vis}$ (Ruffini et al. 2002, 2005). The $n_{\rm CBM}$ profile determines the temporal behavior (the *spikes*) of the light curve. The observed prompt emission spectrum results from the convolution of a large number of modified BB spectra over the surfaces of constant arrival time for photons at the detector (EQuiTemporal Surfaces, EQTS; Bianco & Ruffini 2005a, 2005b) over the entire observation time. Each modified BB spectrum is deduced from the interaction with the CBM and it is characterized by decreasing temperatures and Lorentz and Doppler factors.

The duration and, consequently, the moment at which the burst emission stops are determined by the dynamics of the e^+e^- plasma. The short duration is essentially due to the low baryon load of the plasma and the high Lorentz factor $\Gamma \approx 10^4$ (see Figure 2 in Ruffini et al. 2001b and Figure 4 in Muccino et al. 2013).

The description of both the P-GRB and the prompt emission requires the appropriate relative spacetime transformation paradigm introduced in Ruffini et al. (2001c): it relates the observed GRB signal to its past light cone, defining the events on the worldline of the source that is essential for the interpretation of the data. This requires knowledge of the correct equations relating the comoving time, the laboratory time, the arrival time, and the arrival time at the detector corrected by the cosmological effects.

It is interesting to compare and contrast the masses, densities, thicknesses, and distances of the CBM clouds from the BH, both in short and long bursts. In S-GRBs, we infer CBM clouds with masses of 10^{22}–10^{24} g and sizes of $\approx 10^{15}$–10^{16} cm, at typical distances from the BH of $\approx 10^{16}$–10^{17} cm (see Sections 3.2.2 and 4.2.2, and Ruffini et al. 2016a)— indeed, these are very similar to the values inferred in long GRBs (see, e.g., Izzo et al. 2012). The different durations of the spikes in the prompt emission of S-GRBs and long bursts depend, indeed, only on the different values of Γ of the accelerated baryons and not on the structure of the CBM: in long bursts, we have $\Gamma \approx 10^2$–10^3 (see, e.g., Izzo et al. 2012), while in S-GRBs it reaches the value of $\Gamma \approx 10^4$ (see, e.g., Ruffini et al. 2016a; see Sections 3.2.2 and 4.2.2).

The evolution of an optically thick baryon-loaded pair plasma is generally described in terms of $E^{\rm tot}_{e^+e^-}$ and B, and it is independent of the way the pair plasma is created. This general formalism can also be applied to any optically thick e^+e^- plasma, like the one created via the $\nu\bar{\nu} \leftrightarrow e^+e^-$ mechanism in an NS merger as described in Narayan et al. (1992), Salmonson & Wilson (2002), and Rosswog et al. (2003).

Only in the case where a BH is formed does an additional component to the fireshell emission occur in both S-GRBs and binary-driven hypernovae (BdHNe; long GRBs with $E_{\rm iso} > 10^{52}$ erg—details in Ruffini et al. 2017); at the end of the P-GRB phase: the GeV emission observed by *Fermi*-LAT and AGILE. As outlined in this article, this component has a Lorentz factor $\Gamma > 300$ and, as we will show in Section 5, it appears to have a behavior universal to both S-GRBs and BdHNe. It is, however, important to recall that the different geometries present in S-GRBs and BdHNe lead, in the case of BdHNe, to the absorption of the GeV emission in some specific cases (Ruffini et al. 2017).

3. The S-GRB 081024B

3.1. Observations and Data Analysis

The short-hard GRB 081024B was detected on 2008 October 24 at 21:22:41 (UT) by the *Fermi*-GBM (Connaughton & Briggs 2008). It has a duration $T_{90} \approx 0.8$ s long and exhibits two main peaks, the first one lasting $\approx$0.2 s. Its location (R.A., decl.) = (322°.9, 21°.204) (J2000) is consistent with that reported by the *Fermi*-LAT (Omodei 2008). The LAT recorded 11 events with energy above 100 MeV within 15° from the position of the burst and within 3 s from the trigger time (Abdo et al. 2010). Emission up to 3 GeV was seen within ~5 s after the trigger (Omodei 2008).

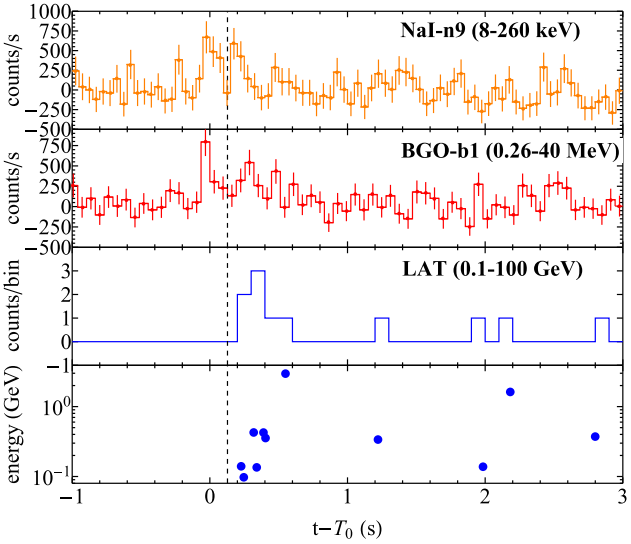

Figure 1. Background-subtracted light curves and high-energy photons of GRB 081024B: the 50 ms binned light curves from the Na I−n9 (8–260 keV, top panel) and BGO–b1 (0.26–40 MeV, second panel) detectors, the 100 ms binned high-energy channel light curve (0.1–100 GeV, third panel, without error bars), and the high-energy photons detected by *Fermi*-LAT (bottom panel). The vertical dashed line marks the end of the first *Fermi*-GBM light curve pulse, before the onset of the LAT light curve.

GRB 081024B also triggered the *Suzaku*-WAM, showing a double peaked light curve with a duration of ∼0.4 s (Hanabata et al. 2008). *Swift*-XRT began observing the field of the *Fermi*-LAT ∼ 70.3 ks after the trigger, in Photon Counting (PC) mode for 9.9 ks (Guidorzi et al. 2008b). Three uncataloged sources were detected within the *Fermi*-LAT error circle (Guidorzi et al. 2008b), but a series of follow-up observations established that none of them could be the X-ray counterpart because they were not fading (Guidorzi 2008; Guidorzi & Margutti 2008; Guidorzi et al. 2008a).

The above possible associations have also been discarded by the optical observations performed in the R_c band (Fatkhullin et al. 2008). Consequently, no host galaxy has been associated with this burst and, therefore, no spectroscopic redshift has been determined.

3.1.1. Time-integrated Spectral Analysis of the Fermi-GBM Data

We analyzed the data from the *Fermi*-GBM detectors, i.e., Na I−n6 and n9 (8–900 keV), and BGO–b1 (0.25–40 MeV), and LAT data[8] in the energy range 0.1–100 GeV. In order to obtain detailed *Fermi*-GBM light curves, we analyzed the `TTE` (Time-Tagged Events) files[9] with the `RMFIT` package.[10]

In Figure 1, we reproduced the 50 ms binned GBM light curves corresponding to the Na I−n9 (8–260 keV, top panel) and the BGO–b1 (0.26–40 MeV, second panel) detectors. We also reproduced the 100 ms binned LAT light curve (0.1–100 GeV, third panel) and the corresponding high-energy detected photons (bottom panel), both consistent with those reported in Abdo et al. (2010). All the light curves are background subtracted. The GBM light curves show one narrow spike of about 0.1 s, followed by a longer pulse lasting around ∼0.7 s.

[8] http://fermi.gsfc.nasa.gov/ssc/data/analysis/documentation/Cicerone/
[9] ftp://legacy.gsfc.nasa.gov/fermi/data/gbm/bursts
[10] http://fermi.gsfc.nasa.gov/ssc/data/analysis/rmfit/vc_rmfit_tutorial.pdf

The time-integrated analysis was performed in the time interval from $T_0 - 0.064$ s to $T_0 + 0.768$ s which corresponds to the T_{90} duration of the burst and T_0 is the trigger time. We have fitted the corresponding spectrum with two spectral models: Comptonized (Compt; i.e., a power-law model with an exponential cutoff) and Band (Band et al. 1993); see Figure 2 and Table 1. The Compt and the Band models provide similar values of the C-STAT (see Table 1). Therefore, the best fit is the Compt model because it has one parameter fewer than the Band one.

3.1.2. Time-resolved Spectral Analysis of the Fermi-GBM Data

We have also performed the time-resolved analysis using 16 ms bins. After the rebinning, the GBM light curves still exhibit two pulses: the first pulse observed before the onset of the LAT emission, from $T_0 - 0.064$ s to $T_0 + 0.128$ s, and the following emission, from $T_0 + 0.128$ s to $T_0 + 0.768$ s, hereafter dubbed the ΔT_1 and ΔT_2 time intervals, respectively.

As proposed in Ruffini et al. (2015), the emission before the onset of the LAT emission corresponds to the P-GRB emission, while the following emission is attributed to the prompt emission (see Section 2).

The spectrum of the ΔT_1 time interval, which can be interpreted as the P-GRB emission, is equally best fit, among all the possible models, by a BB model and by a Compt spectral model. Figure 3 and Table 1 illustrate the results of this time-resolved analysis. From the difference in the C-STAT values between the BB and the Compt models (ΔC-STAT = 9.88; see Table 1), we conclude that the simpler BB model can be excluded at $>3\sigma$ confidence level. Therefore, the best fit is the Compt model.

As in the case of GRB 090510, a Compt spectrum for the P-GRB emission can be interpreted as the result of the convolution of BB spectra at different Doppler factors arising from a spinning BH (see Section 2 and Ruffini et al. 2016a).

The spectrum of the ΔT_2 time interval, which can be interpreted as the prompt emission, is equally best fit by a power-law (PL) model and a Compt spectral model (see Figure 4 and Table 1). The PL and the Compt models are equivalent, though the Compt model slightly improves the C-STAT statistic. However, because of the unconstrained value for the peak energy of the Compt model E_p, we conclude that the PL model represents an acceptable fit to the data.

3.2. Theoretical Interpretation within the Fireshell Model

We proceed to the interpretation of the data analysis performed in Section 3.1 within the fireshell model.

3.2.1. The Estimate of the Redshift

Identifying the P-GRB and the prompt emission is fundamental in order to estimate the source cosmological redshift and, consequently, to determine all of the physical properties of the e^+e^- plasma at the transparency point (Muccino et al. 2013; Ruffini et al. 2015). The method introduced in Muccino et al. (2013) allows the source redshift from the two main observational constraints, the observed P-GRB temperature kT, related to the theoretically computed rest-frame temperature $kT_{\rm blue} = kT(1+z)$, and the ratio between the P-GRB fluence $S_{\rm BB} = F(\Delta T_1)\Delta T_1$ and the total one $S_{\rm tot} = F(T_{90})T_{90}$, which represents a good redshift independent approximation for the ratio $E_{\rm P\text{-}GRB}/E_{e^+e^-}$ (see Table 1), to be determined. A trial and

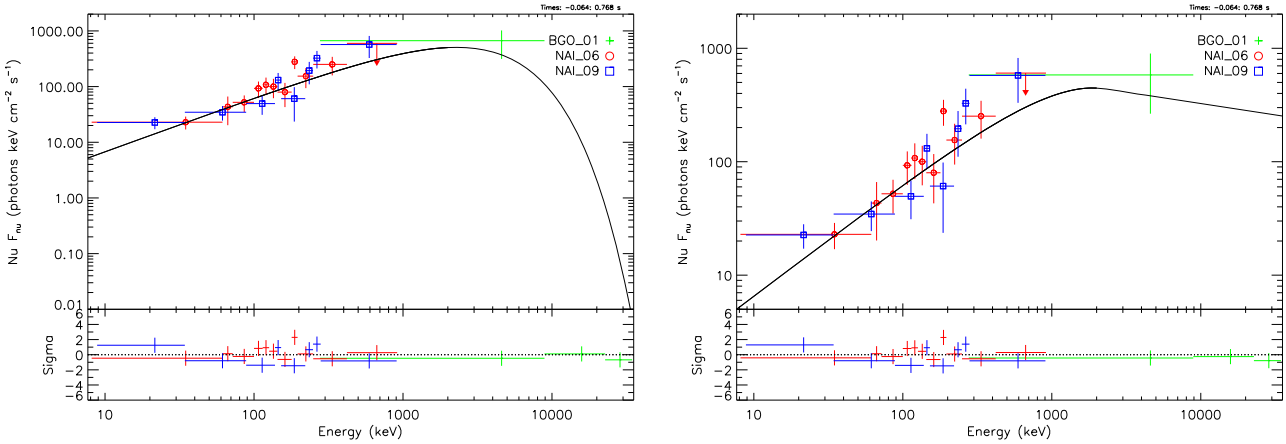

Figure 2. Compt (left plot) and the Band (right plot) spectral fits on the combined Na I–n6 and n9+BGO–b0 νF_ν data of GRB 081024B in the T_{90} time interval.

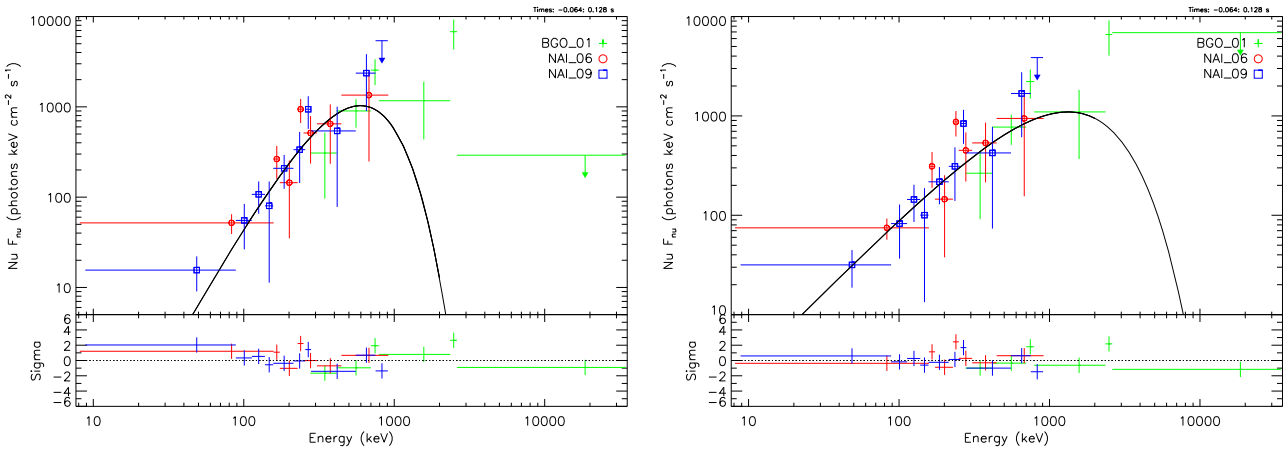

Figure 3. Same as in Figure 2, in the ΔT_1 time interval. A comparison between the BB (left panel) and Compt (right panel) models.

Table 1
Results of the Spectral Analyses of the S-GRB 081024B

S-GRB 081024B								
ΔT	Model	K (ph keV^{-1} cm^{-2} s^{-1})	kT (keV)	E_p (MeV)	α	β	F (erg cm^{-2} s^{-1})	C-STAT/DOF
T_{90}	Compt	$(6.39 \pm 0.69) \times 10^{-3}$		2.3 ± 1.2	-1.02 ± 0.11		$(2.27 \pm 0.87) \times 10^{-6}$	383.89/356
	Band	$(6.51 \pm 0.92) \times 10^{-3}$		1.9 ± 1.7	-1.01 ± 0.15	-2.2 ± 1.1	$(2.9 \pm 1.5) \times 10^{-6}$	383.23/355
ΔT_1	BB	$(4.0 \pm 1.7) \times 10^{-7}$	152 ± 20				$(2.24 \pm 0.40) \times 10^{-6}$	343.54/357
	Compt	$(9.8 \pm 1.9) \times 10^{-3}$		1.33 ± 0.59	-0.48 ± 0.27		$(3.8 \pm 1.4) \times 10^{-6}$	333.78/356
ΔT_2	PL	$(4.60 \pm 0.53) \times 10^{-3}$			-1.37 ± 0.07		$(5.0 \pm 1.5) \times 10^{-6}$	392.2/357
	Compt	$(4.80 \pm 0.59) \times 10^{-3}$		10.95(unc)	-1.28 ± 0.11		$(3.5 \pm 2.0) \times 10^{-6}$	390.57/356

Note. Each column lists the GRB, the time interval ΔT, the spectral model, the normalization constant K, the BB temperature kT, the Compt peak energy E_p, the low-energy α and the high-energy β photon indexes, the 8 keV–40 MeV energy flux F, and the value of the C-STAT over the number of degrees of freedom (DOF).

error procedure is then started, using various sets of values for $E^{\rm tot}_{e^+e^-}$ and B to reproduce the observational constraints. Each of these sets of values provides various possible values for the redshift z from the relation between kT and $kT_{\rm blue}$. The closure condition is represented by $E_{\rm iso}(z) \equiv E^{\rm tot}_{e^+e^-}$, where $E_{\rm iso}$ is computed taking into account the K-correction on $S_{\rm tot}$ (Schaefer 2007). The redshift verifying the last condition and the corresponding values of $E^{\rm tot}_{e^+e^-}$ and B is the correct one for the source. The theoretical redshift $z = 3.12 \pm 1.82$ together with all of the other quantities so far determined are summarized in Table 2 (for further details on the method, see, e.g., Ruffini et al. 2015). The analogy with the prototypical source GRB 090227B ($B = 4.13 \times 10^{-5}$; Muccino et al. 2013), GRB 140619B ($B = 5.52 \times 10^{-5}$; Ruffini et al. 2015), and GRB 090510 ($B = 5.54 \times 10^{-5}$; Ruffini et al. 2016a) is very striking.

The self-consistency of the above theoretical method to estimate the redshift has been tested in S-GRB 090510 (Ruffini

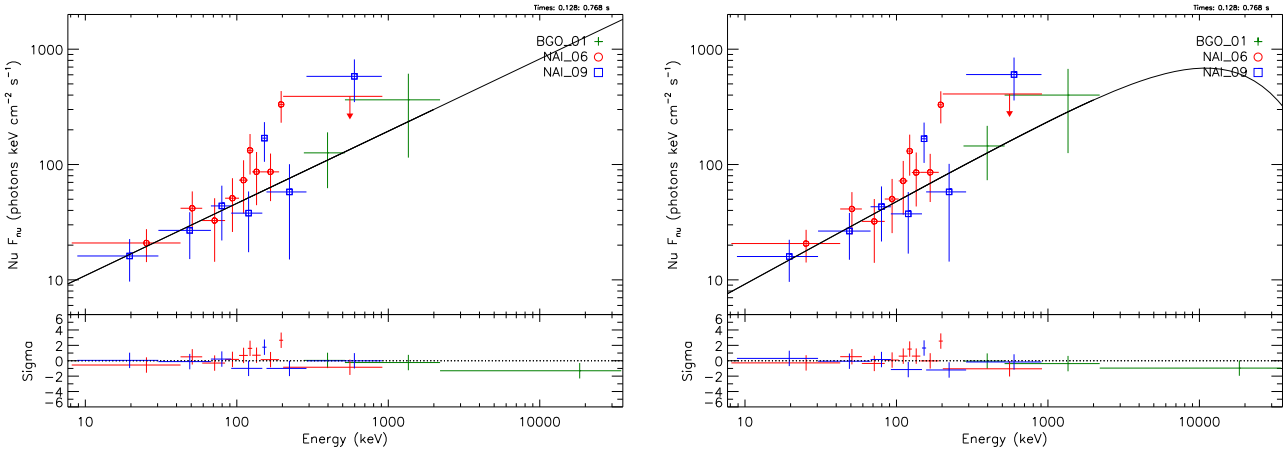

Figure 4. Same as in Figure 3, in the ΔT_2 time interval. A comparison between the PL (left panel) and Compt (right panel) models.

Table 2
P-GRB and Prompt Emission Parameters of the S-GRBs 081024B within the Fireshell Model

P-GRB							
z	$E^{\rm tot}_{e^+e^-}/(10^{52}$ erg)	$B/10^{-5}$	$M_{\rm B}/(10^{-7}\ M_\odot)$	$E_{\rm P\text{-}GRB}/E_{e^+e^-}$ (%)	$\Gamma_{\rm tr}/10^4$	$r_{\rm tr}/(10^{12}$ cm)	$kT_{\rm blue}$ (MeV)
3.12 ± 1.82	2.64 ± 1.00	4.6 ± 2.8	6.7 ± 4.8	50 ± 26	1.10 ± 0.24	5.6 ± 2.1	1.39 ± 0.76
Prompt							
Cloud	r (cm)	Δr (cm)	$n_{\rm CBM}/(10^{-4}$ cm$^{-3})$	$M_{\rm CBM}/(10^{22}$ g)	$\mathcal{R}/10^{-12}$	$\Gamma/10^4$	$d_{\rm v}$ (cm)
1st	5.5×10^{16}	0.5×10^{16}	0.90 ± 0.70	3.1 ± 2.4	9.0 ± 7.0	1.10	2.90×10^{10}
2nd	6.0×10^{16}	0.8×10^{16}	0.10 ± 0.02	0.69 ± 0.14		0.52	6.60×10^{14}
3rd	6.8×10^{16}	0.7×10^{16}	1.00 ± 0.20	7.5 ± 1.5		0.51	7.68×10^{14}
4th	7.5×10^{16}	0.3×10^{16}	3.5 ± 0.70	12.9 ± 2.6	98 ± 53	0.40	1.08×10^{15}
5th	7.8×10^{16}	0.7×10^{16}	20.0 ± 4.00	196 ± 39		0.29	1.55×10^{15}
average			3.18 ± 0.74				

Note. The list of P-GRB parameters (upper part of the table): the inferred redshift z, the e^+e^- plasma energy $E^{\rm tot}_{e^+e^-}$, the baryon load B and the corresponding baryonic mass $M_{\rm B}$, the P-GRB energy $E_{\rm P\text{-}GRB}$ over $E^{\rm tot}_{e^+e^-}$, the Lorentz factor $\Gamma_{\rm tr}$, the radius of the fireshell $r_{\rm tr}$, and the temperature blueshifted toward the observed $kT_{\rm Blue}$ computed at the transparency point. The CBM properties inferred from the prompt emission simulation (lower part of the table) are the number of CBM clouds, the distance r from the BH, the thickness Δr, the number density distribution $n_{\rm CBM}$, the total mass $M_{\rm CBM}$, the filling factors $\mathcal{R}$, the Lorentz factor after each collision Γ, and the total transversal sizes $d_{\rm v}$ of the fireshell visible area. The average number density is indicated at the end of the $n_{\rm CBM}$ column.

et al. 2016a). In this case, a theoretical redshift $z_{\rm th} = 0.75 \pm 0.17$ has been derived, in agreement with the spectroscopic measurement $z = 0.903 \pm 0.003$ (Rau et al. 2009).

3.2.2. Analysis of the Prompt Emission

In the fireshell model, the prompt emission light curve is the result of the interaction of the accelerated baryons with the CBM (see above and, e.g., Ruffini et al. 2002, 2006; Patricelli et al. 2012). After the determination of the initial conditions for the fireshell, i.e., $E^{\rm tot}_{e^+e^-}$ and B (see Table 2), to simulate the prompt emission light curve of the S-GRB 081024B (see Figure 1) and its corresponding spectrum, we derived the CBM number density and the filling factor $\mathcal{R}$ distributions and the corresponding attached errors (see Table 2 and Figure 5, top panel). The average CBM number density inferred from the prompt emissions of GRB 081024B is $\langle n_{\rm CBM}\rangle = (3.18 \pm 0.74) \times 10^{-4}$ (see Table 2) and is larger than that of GRB 140619B, $\langle n_{\rm CBM}\rangle = (4.7 \pm 1.2) \times 10^{-5}$ cm^{-3} (Ruffini et al. 2015), and GRB 090227B, $\langle n_{\rm CBM}\rangle = (1.90 \pm 0.20) \times 10^{-5}$ cm^{-3} (Muccino et al. 2013), but still typical of S-GRB galactic halo environments.

The simulation of the prompt emission light curve of the Na I −n9 (8–900 keV) data of GRB 081024B is shown in Figure 5 (middle panel). The short timescale variability observed in the S-GRB light curves is the result of the large values of the Lorentz factor ($\Gamma \approx 10^4$; see Table 2). Under these conditions, the total transversal size of the visible fireshell area, d_v, is smaller than the thickness of the inhomogeneities ($\approx 10^{16}$ cm; see the values indicated in Table 2), justifying the spherical symmetry approximation (Ruffini et al. 2002, 2006; Patricelli et al. 2012) and explaining the insignificant "broadening" in the arrival time of the luminosity peaks.

The corresponding spectrum is simulated by using the spectral model described in Patricelli et al. (2012) with the phenomenological parameters $\bar{\alpha} = -1.99$. The rebinned data within the ΔT_2 time interval agree with the simulation, as shown by the residuals around the simulated fireshell spectrum (see Figure 5, bottom panel).

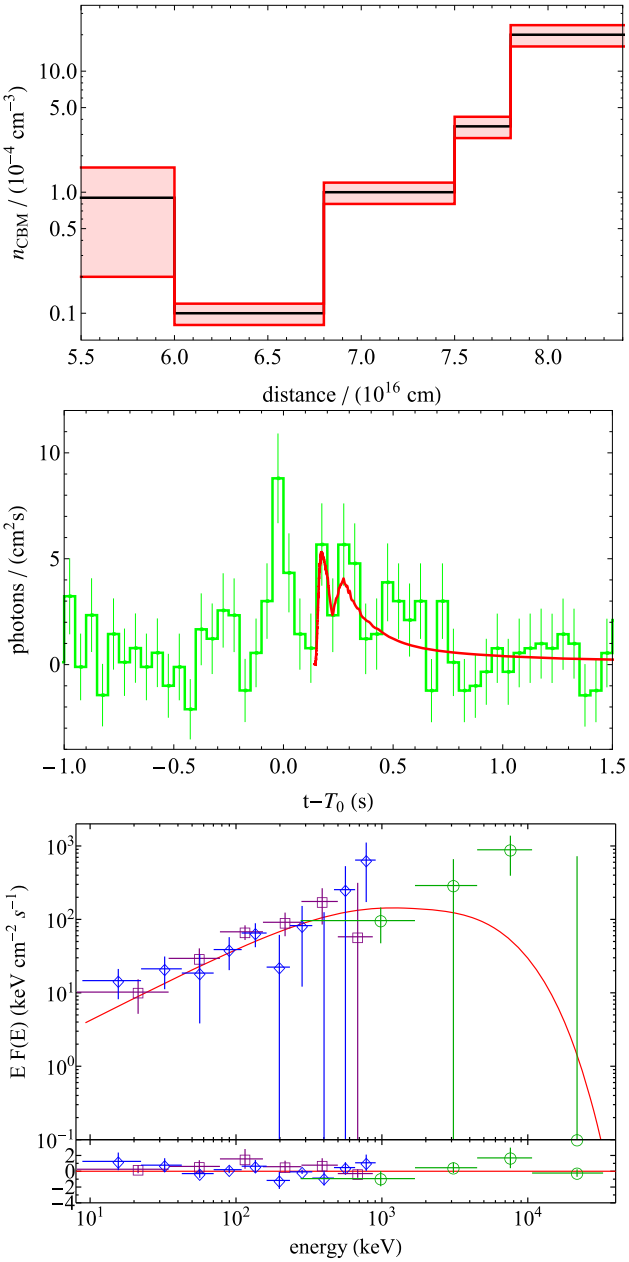

Figure 5. Results of the prompt emission simulation of the S-GRB 081024B. Top: the CBM number density (black line) and errors (red shaded region). Middle: comparison between the simulated prompt emission light curve (solid red curves) and the Na I−n9 (8–900 keV) data. Bottom: comparison between the simulated spectrum (solid red curve) and the Na I−n6 (purple squares), Na I −n9 (blue diamonds), and the BGO–b1 (green circles) spectra within the ΔT_2 time interval. The residuals are shown in the subplot.

4. S-GRB 140402A

4.1. Observations and Data Analysis

The short-hard GRB 140402A was detected on 2014 April 2 at 00:10:07.00 (UT) by *Fermi*-GBM (Jenke & Yu 2014). The duration of this S-GRB in 50–300 keV is $T_{90} = 0.3$ s. It was also detected by *Fermi*-LAT (Bissaldi et al. 2014) with a best on-ground location (R.A., decl.) = (207°.47, 5°.87) (J2000), consistent with that from the GBM. More than 10 photons were detected above 100 MeV and within 10° from the GBM

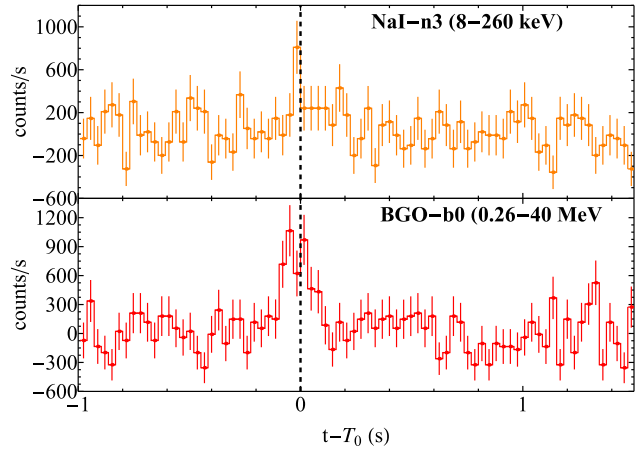

Figure 6. Background-subtracted light curves of GRB 140402A: the 16 ms binned light curves from the Na I−n3 (8–260 keV, upper panel) and BGO–b0 (0.26–20 MeV, lower panel) detectors. The vertical dashed line marks the onset of the LAT light curve (see Figure 7).

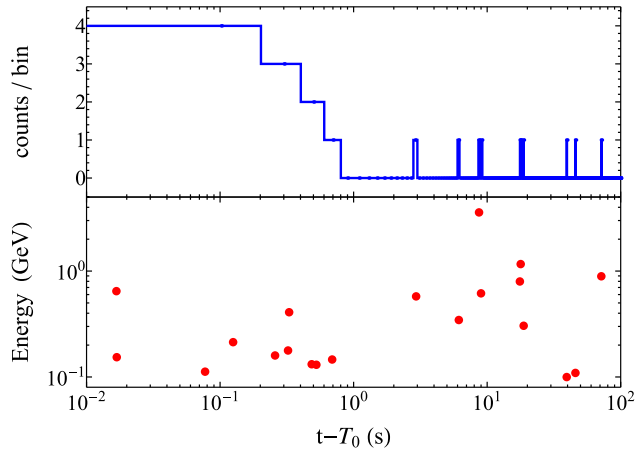

Figure 7. Upper panel: the background-subtracted 200 ms binned high-energy (0.1–100 GeV) light curve, without error bars. Lower panel: the energy light curve of the detected high-energy photons.

location, which spatially and temporally correlates with the GBM emission with high significance (Bissaldi et al. 2014).

This burst was also detected by *Swift*-BAT (Cummings 2014), with a best location (R.A., decl.) = (207°.592, 5°.971) (J2000). No source was detected in the *Swift*-XRT data (Pagani 2014a) after two pointings in PC mode, from 33.3 ks to 51.2 ks and from 56 ks to 107 ks. These two observation sets are within the 3σ upper limit of the count rate of 3.6×10^{-3} counts s^{-1} and 3.0×10^{-3} counts s^{-1}, respectively (Pagani 2014a). Optical exposures at the full refined BAT position (Cummings 2014) taken by *Swift*-UVOT (during both XRT pointings; Breeveld & Pagani 2014) and by *Magellan* (at 1.21 days after the burst; Fong et al. 2014) showed no optical afterglow. This allowed, respectively, 3σ upper limits of $v > 19.8$ mag and of $r > 25.0$ mag to be set. Consequently, no host galaxy has been associated with this burst and, therefore, no spectroscopic redshift has been determined.

4.1.1. Time-integrated Spectral Analysis of the Fermi-GBM Data

In Figure 6, we reproduced the 16 ms binned GBM light curves corresponding to the detectors Na I−n3 (8–260 keV, top

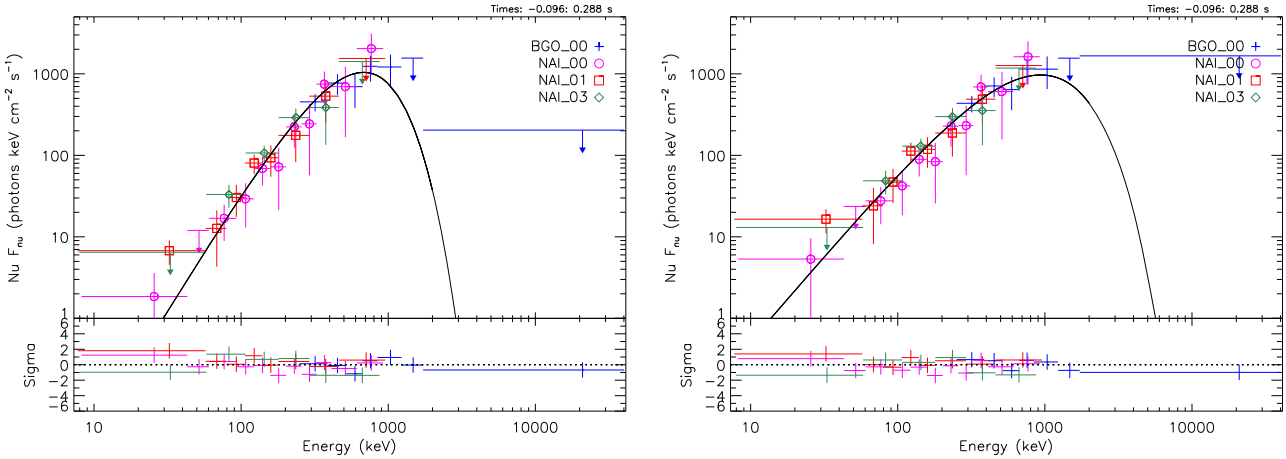

Figure 8. BB (left plot) and Compt (right plot) spectral fits on the combined Na I–n0, n1, and n3+BGO–b1 νF_ν data of GRB 140402A in the T_{90} time interval.

Table 3
Results of the Spectral Analyses of the S-GRB 140402A

S-GRB 140402A							
ΔT	Model	K (ph keV^{-1} cm^{-2} s^{-1})	kT (keV)	E_p (MeV)	α	F (erg cm^{-2} s^{-1})	C-STAT/DOF
T_{90}	BB	$(2.43 \pm 0.75) \times 10^{-7}$	173 ± 18			$(2.26 \pm 0.31) \times 10^{-6}$	527.65/483
	Compt	$(7.0 \pm 1.4) \times 10^{-3}$		0.94 ± 0.24	0.12 ± 0.37	$(2.77 \pm 0.62) \times 10^{-6}$	521.66/482
ΔT_1	BB	$(1.67 \pm 0.69) \times 10^{-7}$	242 ± 34			$(6.0 \pm 1.1) \times 10^{-6}$	441.01/483
	Compt	$(7.1 \pm 2.6) \times 10^{-3}$		1.20 ± 0.32	0.43 ± 0.51	$(6.9 \pm 1.8) \times 10^{-6}$	439.61/482
ΔT_2	BB	$(5.0 \pm 2.2) \times 10^{-7}$	122 ± 18			$(1.17 \pm 0.22) \times 10^{-6}$	500.42/483
	Compt	$(7.5 \pm 2.0) \times 10^{-3}$		0.70 ± 0.25	0.07 ± 0.54	$(1.52 \pm 0.46) \times 10^{-6}$	497.57/482

Note. Each column lists the GRB, the time interval ΔT, the spectral model, the normalization constant K, the BB temperature kT, the compt peak energy E_p, the low-energy photon index α, the 8 keV–40 MeV energy flux F, and the value of the C-STAT over the number of degrees of freedom (DOF).

panel) and BGO–b0 (0.26–20 MeV, second panel), and the 0.2 s binned high-energy light curve (0.1–100 GeV, bottom panel). Also, for this burst, all of the light curves are background subtracted.

The Na I light curve shows a very weak and short pulse, almost at the background level, while the BGO signal exhibits two substructures with a total duration of ≈0.3 s. The vertical dashed line in Figure 6 represents the onset of the LAT emission, soon after the first pulse seen in both GBM light curves. The background-subtracted LAT light curve within 100 s after the GBM trigger and the corresponding 20 photons with energies higher than 0.1 GeV are shown in Figure 7.

We performed the time-integrated spectral analysis in the time interval from $T_0 - 0.096$ s to $T_0 + 0.288$ s (hereafter T_{90}). To increase the poor statistics at energies $\lesssim$260 keV, we also included the data from the Na I–n0 and n1 detectors in the spectral analysis. Among all of the possible models, BB and Compt equally best fit the above data (see Figure 8 and the results listed in Table 3). From the value ΔC-STAT = 5.99 between the above two models (see Table 3), we conclude that the Compt model is an acceptable fit to the data. Similar to GRB 140619B (Ruffini et al. 2015), in the case of GRB 140402A, the low-energy index of the Compt model is consistent with $\alpha \sim 0$. From theoretical and observational considerations of the onset of the GeV emission (see Section 2 and Figure 6), we investigate the presence of a spectrum consistent with a BB one, which corresponds to the signature of the P-GRB emission for a moderately spinning BH (see Ruffini et al. 2016a).

4.1.2. Time-resolved Spectral Analysis of the Fermi-GBM Data

The first spike (see Figure 6), observed before the onset of the GeV emission, extends from $T_0 - 0.096$ s to T_0 (hereafter ΔT_1). Again, the BB and Compt spectral models equally best fit the above data. As shown in Figure 9 and Table 3, the above two models are almost indistinguishable, with the low-energy index of the Compt model $\alpha = 0.43 \pm 0.51$ being consistent within almost the 1σ level with the low-energy index of a BB ($\alpha = 1$). We conclude that the BB model is an acceptable fit to the data and identify the first pulse in the light curve with the P-GRB emission.

The spectrum of the emission in the time interval from T_0 to $T_0 + 0.288$ s (hereafter ΔT_2) reveals that a Compt model slightly better fits the data points at ≈1 MeV, and its low-energy index $\alpha = 0.07 \pm 0.54$ indicates that the energy distribution is somehow broader than that of a BB model (see Figure 10 and Table 3). The Compt model is consistent with the modified BB spectrum adopted in the fireshell model for the prompt emission (Patricelli et al. 2012). Therefore, we identify the ΔT_2 time interval with the prompt emission.

4.2. Theoretical Interpretation within the Fireshell Model

We proceed to the interpretation of the data analysis performed in Section 4.1 within the fireshell model.

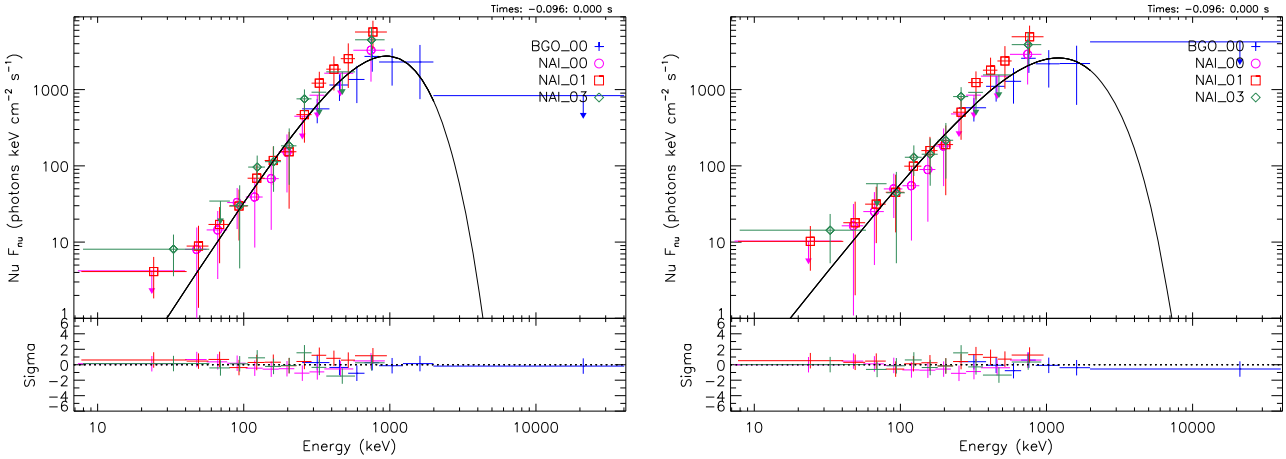

Figure 9. Same as in Figure 8, in the ΔT_1 time interval. A comparison between the BB (left panel) and Compt (right panel) models.

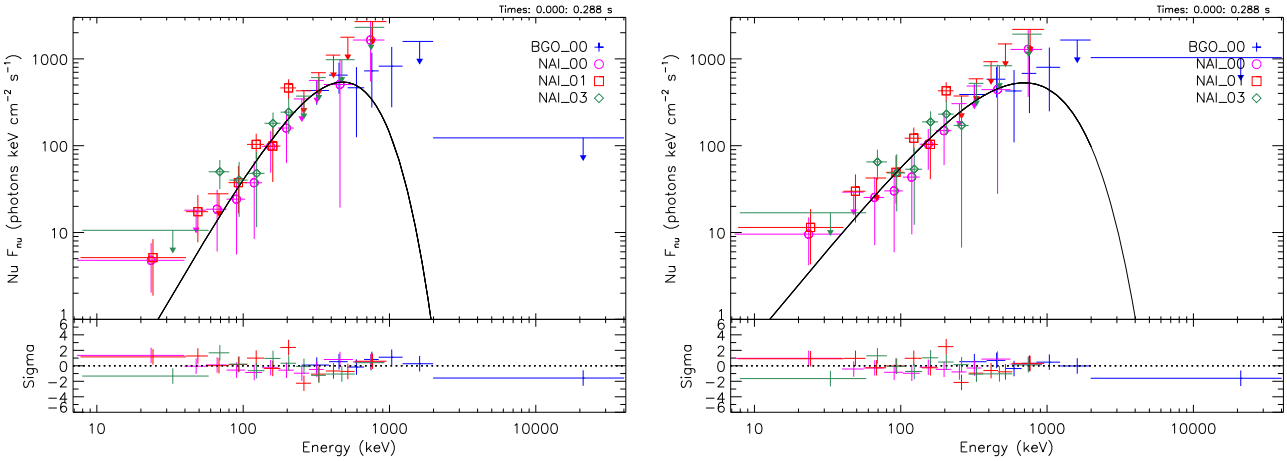

Figure 10. Same as in Figure 8, in the ΔT_2 time interval. A comparison between the BB (left panel) and Compt (right panel) models.

Table 4
P-GRB and Prompt Emission Parameters of the S-GRB 140402A within the Fireshell Model

P-GRB							
z	$E^{\rm tot}_{e^+e^-}/(10^{52}$ erg)	$B/10^{-5}$	$M_{\rm B}/(10^{-7}\ M_\odot)$	$E_{\rm P\text{-}GRB}/E_{e^+e^-}$ (%)	$\Gamma_{\rm tr}/10^4$	$r_{\rm tr}/(10^{12}$ cm)	$kT_{\rm blue}$ (MeV)
5.52 ± 0.93	4.7 ± 1.1	3.6 ± 1.0	9.5 ± 3.4	54 ± 16	1.30 ± 0.13	6.66 ± 0.91	1.58 ± 0.22
Prompt							
Cloud	r (cm)	Δr (cm)	$n_{\rm CBM}/(10^{-4}$ cm$^{-3})$	$M_{\rm CBM}/(10^{22}$ g)	$\mathcal{R}/10^{-9}$	$\Gamma/10^4$	$d_{\rm v}$ (cm)
1st	1.0×10^{16}	1.4×10^{16}	6.0 ± 2.0	5.4 ± 1.8	4.7 ± 0.45	1.30	6.64×10^{10}
2nd	2.4×10^{16}	2.6×10^{16}	24.0 ± 3.0	187 ± 23		0.92	1.49×10^{14}
average			15.4 ± 2.5				

Note. For the P-GRB parameters (upper part of the table) and the CBM properties (lower part of the table), inferred from the prompt emission simulation, we refer to Table 2.

4.2.1. The Estimate of the Redshift

After having identified the P-GRB emission of the S-GRB 140402A (see Section 4.1.2), we follow the same loop procedure recalled in Section 3.2.1 to infer the redshift, $E^{\rm tot}_{e^+e^-}$, and B of the source. The results of this method are summarized in Table 4. In particular, the theoretically derived redshift for this source is $z = 5.52 \pm 0.93$. Again, the analogy with the S-GRBs 081024B (see Section 3.1.2), GRB 090227B (Muccino et al. 2013), 140619B (Ruffini et al. 2015), and 090510 (Ruffini et al. 2016a) is very striking.

4.2.2. Analysis of the Prompt Emission

Similarly to the case of the S-GRB 081024B (see Section 3.2.2), to simulate the prompt emission light curve of the S-GRB 140402A (see Figure 6) and its corresponding spectrum, we derived the CBM number density and the filling

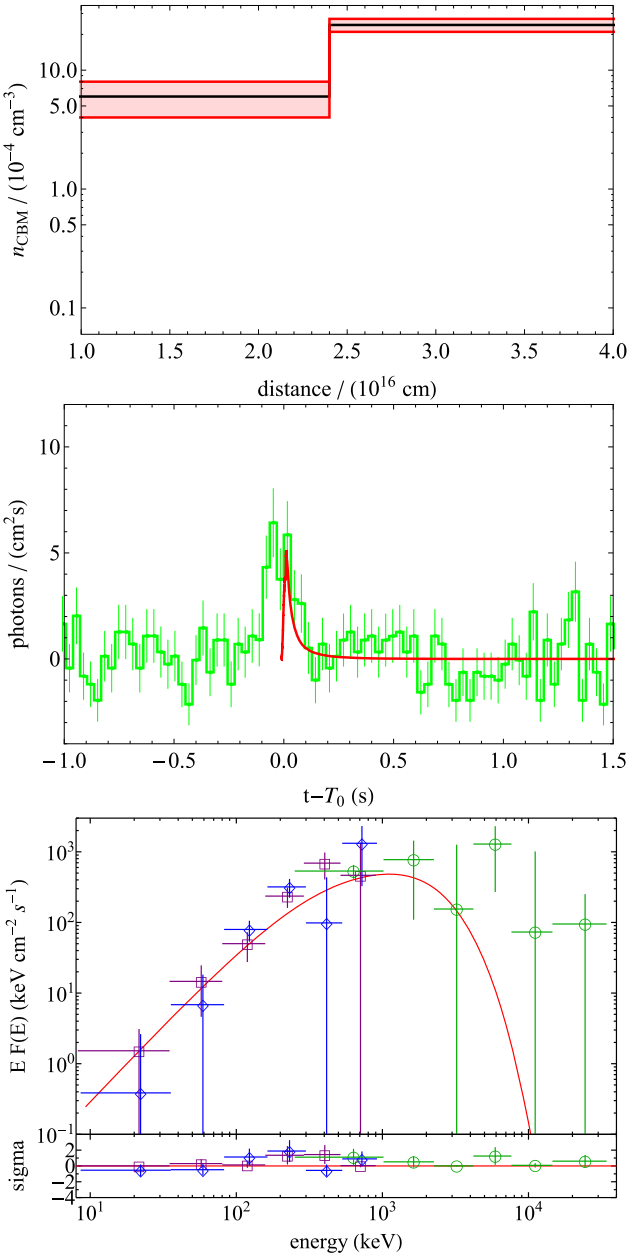

Figure 11. Results of the prompt emission simulation of the S-GRB 140402A. Top: the CBM number density (black line) and errors (red shaded region). Middle: comparison between the simulated prompt emission light curve (solid red curves) and the BGO–b0 (0.26–40 MeV) data. Bottom: comparison between the simulated spectrum (solid red curve) and the Na I−n1 (purple squares), Na I−n3 (blue diamonds), and the BGO–b0 (green circles) spectra within the ΔT_2 time interval. The residuals are shown in the subplot.

factor $\mathcal{R}$ distributions (see Table 4 and Figure 11, top panel). Also, in this case, the inferred values fully justify the adopted spherical symmetry approximation (Ruffini et al. 2002, 2006; Patricelli et al. 2012) and explain the negligible "dispersion" in arrival time of the luminosity peak.

The average CBM number density in the case of GRB 140402A is $\langle n_{\rm CBM}\rangle = (1.54 \pm 0.25) \times 10^{-3}$ (see Table 4), which is similar to that inferred from GRB 081024B. The simulation of the prompt emission light curve of the BGO–b0 (0.26–40 MeV) data of GRB 140402A is shown in Figure 11 (middle panel). The simulation of the corresponding spectrum requires a phenomenological parameter $\bar{\alpha} = -0.9$. Figure 11 (bottom panel) displays the agreement between the rebinned data from the ΔT_2 time interval and the simulation.

5. The GeV Emission in S-GRBs

Before going into more detail on the general properties of the S-GRB GeV emission, we briefly summarize the observational features and the data analysis of the high-energy emission of the S-GRBs 081024B and 140402A, and then we turn to a new analysis of the absence of the GeV emission in the S-GRB 090227B.

5.1. The GeV Emission of the S-GRBs 081024B and 140402A

We downloaded the LAT event and spacecraft data[11] selecting the observational time, the energy range, and the source coordinates (Bissaldi et al. 2014). We then made cuts on the data set time and energy range, position (Bissaldi et al. 2014), region of interest (ROI) radius (typically10°), and maximum zenith angle.[12] Within the event selection recommendations for the analysis of LAT data using the Pass 8 Data (P8R2), we adopted the burst and transient analysis (for events lasting <200 s) with an energy selection of 0.1–500 GeV, an ROI-based zenith angle cut of 100°, event class 16, and the instrument response function `P8R2_TRANSIENT020_V6`.[13] The additional selection of the good time intervals (GTIs) when the data quality is good (`DATA_QUAL>0`) is introduced to exclude time periods when some spacecraft event has affected the quality of the data (in addition to the time selection to the maximum zenith angle cut introduced above).

In the case of the S-GRB 081024B, we obtained the GeV light curve and the observed photon energies shown in Figure 1 (third and fourth panels), which are in agreement with those reported in Ackermann et al. (2013). In the case of the S-GRB 140402A, we obtained the GeV light curve shown in Figure 7 (upper plot). About 20 photons with energies higher than 0.1 GeV have been detected within 100 s after the GBM trigger (see Figure 7, lower panel). The highest energy photon is a 3.7 GeV event, which is observed at $T_0 + 8.7$ s.

Then, we built up the rest-frame 0.1–100 GeV light curve of the S-GRBs 081024B and 140402A. For the S-GRB 081024B, we rebinned its GeV emission luminosity light curve into two bins, as displayed in Ackermann et al. (2013). For the S-GRB 140402A, we rebinned it into two time bins with enough photons to perform a spectral anlysis: from T_0 to $T_0 + 0.6$ s, and from $T_0 + 0.6$ s to $T_0 + 20$ s.

The resulting luminosity light curves follow a common power-law trend with the rest-frame time which goes as $t^{-1.29\pm0.06}$ (see dashed black line in Figure 12). All the light curves are shown from the burst trigger times on, while in the case of the S-GRB 090510 it starts after the precursor emission, i.e., from the P-GRB emission on (see Ruffini et al. 2016a for details). The GeV emission of the S-GRB 140402A is the second longest in time duration after GRB 090510, which exhibits a behavior in common with the light curves of the other S-GRBs after the ∼1 s rest-frame time (see Figure 12).

[11] http://fermi.gsfc.nasa.gov/cgi-bin/ssc/LAT/LATDataQuery.cgi
[12] The maximum zenith angle selection excludes any portion of the ROI that is too close to the Earth's limb, resulting in elevated background levels.
[13] http://fermi.gsfc.nasa.gov/ssc/data/analysis/documentation/Cicerone/Cicerone_Data_Exploration/Data_preparation.html

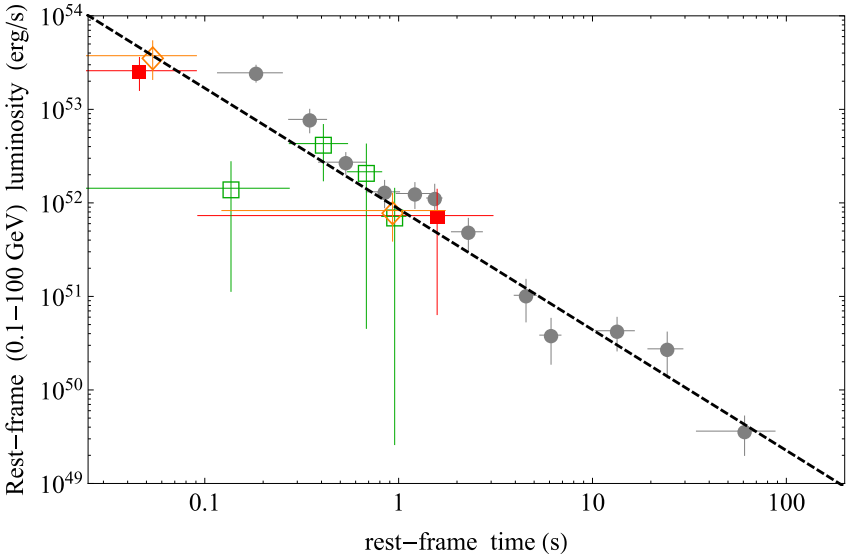

Figure 12. Rest-frame 0.1–100 GeV isotropic luminosities of the S-GRBs 081024B (orange empty diamonds), 090510 (gray filled circles), 140402A (red filled squares), and 140619B (green empty squares). All of the light curves are shown from the burst trigger times on, while in the case of the S-GRB 090510 it starts after the precursor emission, i.e., from the P-GRB emission on (see Ruffini et al. 2016a for details). The dashed black line marks the common behavior of all of the S-GRB light curves, which goes as $t^{-1.29\pm0.06}$.

Table 5
S-GRB Prompt and GeV Emission Properties

GRB	z	$E_{\rm p,i}$ (MeV)	$E_{\rm iso}$ (10^{52} erg)	$E_{\rm GeV}^{\rm max}$ (GeV)	$\Gamma_{\rm GeV}^{\rm min}$	$E_{\rm LAT}$ (10^{52} erg)	$M_{\rm acc}^{\eta_+}$ ($M_\odot$)	$M_{\rm acc}^{\eta_-}$ ($M_\odot$)
081024B	3.12 ± 1.82	9.56 ± 4.94	2.64 ± 1.00	3	$\gtrsim$779	$\gtrsim$2.79 ± 0.98	$\gtrsim$0.04	$\gtrsim$0.41
090227B	1.61 ± 0.14	5.89 ± 0.30	28.3 ± 1.5	…	…	…	…	…
090510	0.903 ± 0.003	7.89 ± 0.76	3.95 ± 0.21	31	$\gtrsim$551	$\gtrsim$5.78 ± 0.60	$\gtrsim$0.08	$\gtrsim$0.86
140402A	5.52 ± 0.93	6.1 ± 1.6	4.7 ± 1.1	3.7	$\gtrsim$354	$\gtrsim$4.5 ± 2.2	$\gtrsim$0.06	$\gtrsim$0.66
140619B	2.67 ± 0.37	5.34 ± 0.79	6.03 ± 0.79	24	$\gtrsim$471	$\gtrsim$2.34 ± 0.91	$\gtrsim$0.03	$\gtrsim$0.35

Note. The columns list z, $E_{\rm p,i}$, the maximum GeV photon observed energy $E_{\rm GeV}^{\rm max}$, the minimum Lorentz factor of the GeV emission $\Gamma_{\rm GeV}^{\rm min}$, $E_{\rm iso}$, $E_{\rm LAT}$, and the amount of infalling accreting mass corotating (counterrotating) with the BH $M_{\rm acc}^{\eta_+}$ ($M_{\rm acc}^{\eta_-}$), needed to explain $E_{\rm LAT}$.

Table 5 lists the redshift, $E_{p,i}$, $E_{\rm iso}$ (in the rest-frame energy band 1–10,000 keV), and the GeV isotropic emission energy $E_{\rm LAT}$ in the rest-frame energy band 0.1–100 GeV of the five authentic S-GRBs discussed here. These values of $E_{\rm LAT}$ are simply obtained by multiplying the average luminosity in each time bin by the corresponding rest-frame duration and then by summing up all the contributions for each bin. However, these estimates represent lower limits to the actual GeV isotropic emission energies, since at late times the observations of GeV emission could be prevented due to the instrumental threshold of the LAT.

5.2. Reanalyzing the GeV Emission of the S-GRB 090227B

We performed the unbinned likelihood analysis method,[14] which is preferred when the number of events is expected to be small, for the S-GRB 090227B. We took spectra within 1 s, 10 s, 100 s, and 1000 s after the burst trigger. The background point-like sources and diffuse (galactic and extragalactic) emission within 10° from the GRB position are taken from the LAT 4-year Point Source Catalog (3FGL). The test statistic (TS) computed from the above likelihood analysis is TS $\lesssim$ 1 in each time interval (TS > 25 corresponds to 5σ of significance); therefore, no significant GeV emission can be associated with this GRB. A single GeV photon with energy 1.59 GeV at time 896 s after the trigger and within 1° from the GRB has been found. Considering the above background models, we computed the probability of this photon belonging to this GRB. The likelihood analysis gives a probability of this photon correlating with GRB 090227B of 0.36%, while its probability of being a photon from the diffuse background is >99%.

The results of this analysis are in agreement with those reported in Ackermann et al. (2013). There, it is also stated that an autonomous repoint request by *Fermi*-GBM brought the LAT down to ≃20° after ∼300 s and, therefore, the source entered the optimal LAT FoV. Using the S-GRB common power-law trend $t^{-1.29\pm0.06}$ (see the dashed black line in Figure 12), we computed the expected energy fluxes of the GeV emission of the S-GRB 090227B, f_1, at the time of ∼300 s when the source entered the LAT FoV, and f_2, at 896 s when the diffuse background photon was detected. We assumed a power-law spectrum with a typical value of the photon index of −2 and obtained $f_1 = (1.09 \pm 0.16) \times 10^{-9}$ erg cm^{-2} s^{-1} and $f_2 = (2.65 \pm 0.39) \times 10^{-10}$ erg cm^{-2} s^{-1}. These computed

[14] https://fermi.gsfc.nasa.gov/ssc/data/analysis/scitools/lat_grb_analysis.html

fluxes are within the *Fermi*-LAT sensitivity of the Pass 8 Release 2 Version 6 Instrument Response Functions,[15] which is approximately 10^{-11} erg cm^{-2} s^{-1}. Therefore, we can conclude that the GeV emission associated with the S-GRB 090227B ceased before 300 s, when the source entered the LAT FoV.

5.3. Lower Limits on the GeV Emission Lorentz Factors in S-GRBs

Following Lithwick & Sari (2001), it is possible to derive a lower limit on the Lorentz factor of the GeV emission $\Gamma_{\rm GeV}^{\rm min}$ by requiring that the outflow must be optically thin to high-energy photons, namely, to the pair-creation process. Using the maximum GeV photon observed energy $E_{\rm GeV}^{\rm max}$ in Table 5, for each S-GRB, various lower limits on the GeV Lorentz factors can be derived from the time-resolved spectral analysis. For each S-GRB, we estimate lower limits in each time interval of the GeV luminosity light curves in Figure 12. Then, the $\Gamma_{\rm GeV}^{\rm min}$ for each S-GRB was then determined as the largest among the inferred lower limits (see Table 5). The GeV photons are produced in ultrarelativistic outflows with $\Gamma_{\rm GeV}^{\rm min} \gtrsim 300$.

5.4. The Energy Budget of the GeV Emission in S-GRBs

Ruffini et al. (2016a) proposed that the 0.1–100 GeV in S-GRBs (see Figure 12) is produced by the mass accretion onto the newborn Kerr–Newman BH. The amount of mass that remains bound to the BH is given by the conservation of energy and angular momentum from the merger moment to the BH birth. We can estimate lower limits of the needed mass to explain the energy requirements $E_{\rm LAT}$ in Table 5 by considering the above accretion process onto a maximally rotating Kerr BH. In this case, depending whether the infalling material is in a co- or counterrotating orbit with the spinning BH, the maximum efficiency of the conversion of gravitational energy into radiation is $\eta_+ = 42.3\%$ or $\eta_- = 3.8\%$, respectively (see Ruffini & Wheeler 1969 in problem 2 of Section 104 in Landau & Lifshitz 2003). Therefore, $E_{\rm LAT}$ can be expressed as

$$E_{\rm LAT} = f_{\rm b}^{-1}\eta_{\pm}M_{\rm acc}^{\eta_{\pm}}c^2, \tag{1}$$

where $f_{\rm b}$ is the beaming factor which depends on the geometry of the GeV emission and $M_{\rm acc}^{\eta_{\pm}}$ is the amount of accreted mass corresponding to the choice of the efficiency $\eta_{\pm}$. The observational evidence that the totality of S-GRBs exhibit GeV emission and that its absence is due to the instrumental absence of alignment between the LAT and the source at the time of the GRB emission (see Section 5.2) suggests that no beaming is necessary in Equation (1). Therefore, in the following, we set $f_{\rm b} \equiv 1$. The corresponding estimates of $M_{\rm acc}^{\eta_{\pm}}$ in our sample of S-GRBs are listed in Table 5.

6. On the Detectability of the X-Ray Emission of S-GRBs

GRB 090510 is the only S-GRB with a complete X-ray afterglow (see Figure 13(a) and Ruffini et al. 2016a). Only upper limits exist for the X-ray afterglow emission of the other S-GRBs and no special features are identifiable.

As an example to give evidence of the difficulty of measuring the X-ray afterglow in S-GRBs, we computed the observed X-ray flux light curve of GRB 090510, actually observed at $z_{\rm in} = 0.903$, as if it occurred at the redshifts of the other S-GRBs, i.e., $z_{\rm fin} = 1.61$, 2.67, 3.12, and 5.52. This can be attained in four steps.

(1) In each time interval of the X-ray flux light curve $f_{\rm obs}^{\rm in}$ of GRB 090510, we assume that the best fit to the spectral energy distribution is a power-law function with photon index γ, i.e., $N(E) \sim E^{-\gamma}$.
(2) In the rest-frame of GRB 090510, we identify the spectral energy range for a source at redshift $z_{\rm fin}$, which corresponds to the 0.3–10 keV observed by *Swift*-XRT, i.e.,

$$0.3\left(\frac{1+z_{\rm fin}}{1+z_{\rm in}}\right) - 10\left(\frac{1+z_{\rm fin}}{1+z_{\rm in}}\right)\text{keV}.$$

(3) We rescale the fluxes for the different luminosity distance $d_{\rm l}$. Therefore, the observed 0.3–10 keV X-ray flux light curve $f_{\rm obs}^{\rm fin}$ for a source at redshift $z_{\rm fin}$ is given by

$$f_{\rm obs}^{\rm fin} = f_{\rm obs}^{\rm in}\left[\frac{d_{\rm l}(z_{\rm in})}{d_{\rm l}(z_{\rm fin})}\right]^2 \frac{\int_{0.3\frac{1+z_{\rm fin}}{1+z_{\rm in}}\,\text{keV}}^{10\frac{1+z_{\rm fin}}{1+z_{\rm in}}\,\text{keV}} N(E)EdE}{\int_{0.3\,\text{keV}}^{10\,\text{keV}} N(E)EdE} = f_{\rm obs}^{\rm in}\left[\frac{d_{\rm l}(z_{\rm in})}{d_{\rm l}(z_{\rm fin})}\right]^2\left(\frac{1+z_{\rm fin}}{1+z_{\rm in}}\right)^{2-\gamma}. \tag{2}$$

(4) We transform the observational time $t_{\rm in}$ of GRB 090510 at $z_{\rm in}$ into the observational time $t_{\rm fin}$ for a source at $z_{\rm fin}$ by taking into account the time dilation due to the cosmological redshift effect, i.e.,

$$t_{\rm fin} = \left(\frac{1+z_{\rm fin}}{1+z_{\rm in}}\right)t_{\rm in}. \tag{3}$$

Figure 13 shows that all of the computed flux light curves are well below the observational upper limits provided by the *Swift*-XRT repointings.

1. S-GRB 090227B, no repointings (see Figure 13(b)).
2. S-GRB 140619B, a repointing from 48.7 to 71.6 ks after the GBM trigger with an upper limit of 2.9×10^3 counts s^{-1} (see Maselli & D'Avanzo 2014 and Figure 13(c)).
3. S-GRB 081024B, two repointings within the flux light curve in Figure 13(d). Each upper limit was set by using the lowest count rate among those of the uncataloged sources within the LAT FoV, later on confirmed as not being the burst X-ray counterparts: the first one at ~70.3 ks after the trigger for ~9.9 ks with a count rate of 1.3×10^{-3} counts s^{-1} (Guidorzi et al. 2008b), and the second one from 1.5 to 6.1 days with an average count rate of 7.4×10^{-4} counts s^{-1} (Guidorzi et al. 2008a).
4. S-GRB 140402A, two repointings (Pagani 2014a): the first from 33.3 to 51.2 ks with a count rate upper limit of 3.6×10^{-3} counts s^{-1}, and the second from 56 to 107 ks with an upper limit of 3.0×10^{-3} counts s^{-1} (see Figure 13(d)).

[15] http://www.slac.stanford.edu/exp/glast/groups/canda/lat_Performance_files/broadband_flux_sensitivity_p8r2_source_v6_all_10yr_zmax100_n03.0_e1.50_ts25.png

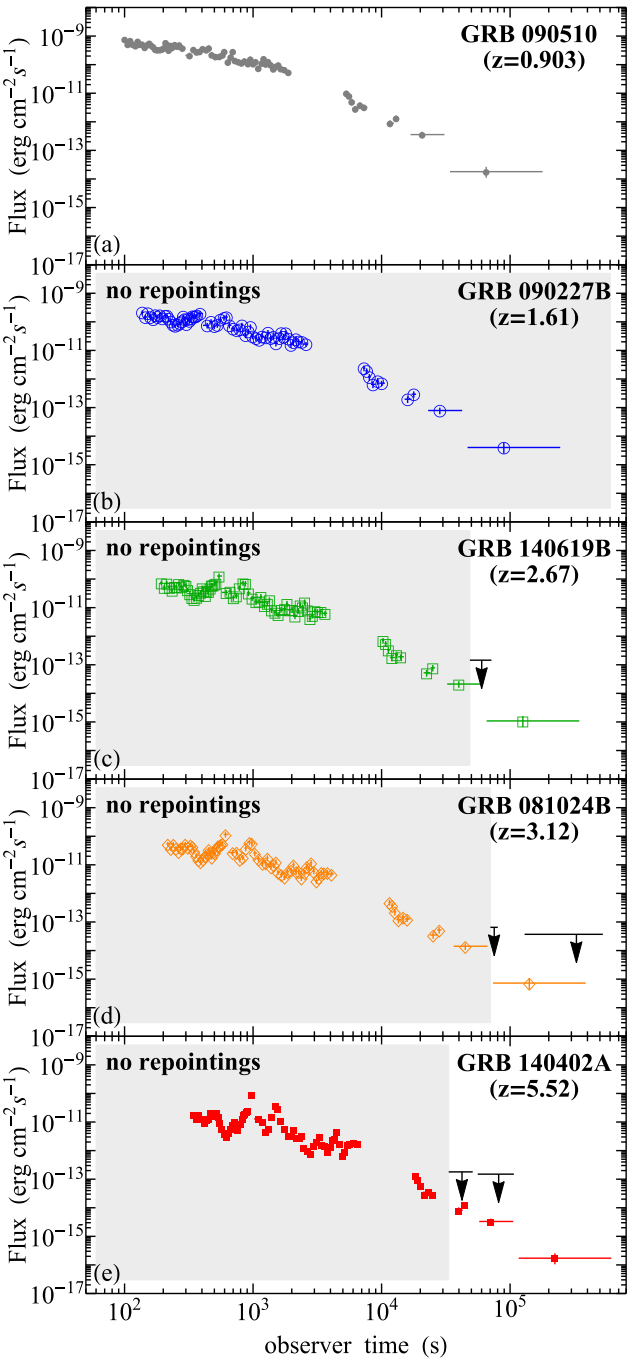

Figure 13. Observed 0.3–10 keV energy flux light curves of (a) the S-GRB 090510, located at $z_{\rm in} = 0.903$, and the corresponding predicted ones for the S-GRBs (b) 090227B at $z_{\rm in} = 1.61$, (c) 140619B at $z_{\rm in} = 2.67$, (d) 081024B at $z_{\rm in} = 3.12$, and (e) 140402A at $z_{\rm in} = 5.52$ (same symbols as in Figure 12). The shaded areas correspond to the epochs before the observational upper limits set by the available *Swift*-XRT repointings (black arrows; see text for details).

We converted the above count rate upper limits into fluxes by multiplying with a typical conversion factor 5×10^{-11} erg/cm^2/count (see, e.g., Pagani 2014b).

We conclude that there is no evidence in favor of or against a common behavior of the X-ray afterglows of S-GRBs in view of the limited observations.

These aspects are noteworthy since in the case of long GRBs, the X-ray emission has a very crucial role (Pisani et al. 2016; Ruffini et al. 2017), which is not testable in the case of S-GRBs.

7. On the Short Bursts Originating in BH–NS Mergers

As pointed out in Fryer et al. (2015b) and Ruffini et al. (2016c, 2016b), U-GRBs are expected to originate in the BH–NS binaries produced by the further evolution of BdHNe (see, e.g., Becerra et al. 2016; Ruffini et al. 2016c). We recall that BdHN progenitor systems are composed of a carbon−oxygen core ($CO_{\rm core}$) and an NS in a close binary system. When the $CO_{\rm core}$ explodes as a supernova (SN) Ib/c, its ejecta starts a hypercritical accretion process onto the companion NS, pushing its mass beyond the value $M_{\rm crit}^{\rm NS}$, and leading to the formation of a BH. This BH, together with the new NS (νNS) produced from the SN event, leads to the progenitor systems of the U-GRBs.

The orbital velocities of the BH–NS binaries formed from BdHNe are high and even large kicks are unlikely to make these systems unbound (Fryer et al. 2015b). U-GRBs represent a new family of BH–NS binaries unaccounted for in current standard population synthesis analyses (see, e.g., Fryer et al. 2015b).

U-GRBs are expected to lead to harder and shorter bursts in γ-rays, which explains the lack of their observational identification (Fryer et al. 2015b), and possibly pose a great challenge as they are considered to emit fast radio bursts. They also could manifest themselves, before the merging, as pulsar −BH binaries (see, e.g., Tauris et al. 2015 and references therein).

8. Conclusions

We first recalled the division of short bursts into two different sub-lasses (Ruffini et al. 2015): S-GRFs, with $E_{\rm iso} \lesssim 10^{52}$ erg, $E_{p,i} \lesssim 2$ MeV, and no GeV emission; and authentic S-GRBs, with $E_{\rm iso} \gtrsim 10^{52}$ erg, $E_{p,i} \gtrsim 2$ MeV, and with GeV emission present, which is always detected by *Fermi*-LAT, when operative (Ruffini et al. 2015).

We then focus on two additional examples of S-GRBs: GRB 081024B, with $E_{\rm iso} = (2.6 \pm 1.0) \times 10^{52}$ erg and $E_{p,i} = (9.6 \pm 4.9)$ MeV (see Section 3), and GRB 140402A, with $E_{\rm iso} = (4.7 \pm 1.1) \times 10^{52}$ erg and $E_{p,i} = (6.1 \pm 1.6)$ MeV (see Section 4).

We perform time-integrated and time-resolved spectral analyses on both of these sources (see Sections 3.1.1–3.1.2 and 4.1.1–4.1.2) and infer their cosmological redshifts ($z = 3.12$ for the S-GRB 081024B and $z = 5.52$ for the S-GRB 140402A; see Sections 3.2.1 and 4.2.1, respectively). We also identify their P-GRB spectral emission. The P-GRB emission of S-GRB 081024B exhibit the convolution of BB spectra at different Doppler factors arising from a spinning BH, in total analogy with S-GRB 090510 (see Sections 2 and 3.1.2 and Ruffini et al. 2016a). The P-GRB emission of S-GRB 140402A is consistent with a single BB, expected to occur for a moderately spinning BH (see Section 4.1.2 SND Ruffini et al. 2016a).

The baryon load mass M_B, the Lorentz Γ factor, and the properties of the CBM clouds are in agreement with those of the other S-GRBs: $M_B \approx 10^{-6}\ M_\odot$, $\Gamma \approx 10^4$ (see Sections 3.2.1 and 4.2.1), distances of the CBM clouds $r \approx 10^{16}$ cm, and CBM densities $n_{\rm CBM} \approx 10^{-3}$ cm^{-3} (see Sections 3.2.2 and

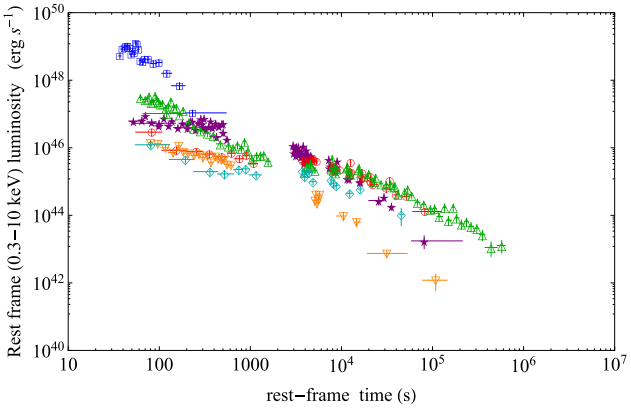

Figure 14. Rest-frame 0.3–10 keV X-ray luminosity light curves of selected S-GRFs: GRB 051210 (blue squares), GRB 051221 (green triangles), GRB 061201 (orange inverted triangles), GRB 070809 (cyan diamonds), and GRB 130603B (purple stars).

4.2.2), typical of galactic halo environments (see, e.g., Muccino et al. 2013; Ruffini et al. 2015).

In analogy to the other S-GRBs, we confirm that the GeV emission turns on after the P-GRB emission and is coeval with the occurrence of the prompt emission (see Section 5). All of these coincidences point to the fact that the GeV emission originates from the onset of the BH formation (see the spacetime diagrams in Figure 3 of Ruffini et al. 2016a).

Most noteworthy is that the existence of a common power-law behavior in the rest-frame 0.1–100 GeV luminosities (see Figure 12 in Section 5), following the BH formation, points to a commonality in the mass and spin of the newly formed BH in all of these S-GRBs. This result is explainable with the expected mass of the merging NSs, each one of $M \approx 1.3$–$1.5\,M_\odot$ (Özel & Freire 2016), and the expected range of the non-rotating NS critical mass $M_{\rm crit}^{\rm NS} \sim 2.2$–$2.7\,M_\odot$ leading to a standard value of the BH mass and of its Kerr parameter $a/M \sim 1$ (Ruffini et al. 2015).

Finally, in all S-GRBs, the energetics of the GeV emission implies the accretion of $M \gtrsim 0.03$–$0.08\,M_\odot$ or $M \gtrsim 0.35$–$0.86\,M_\odot$ for co- or counterrotating orbits with a maximally rotating BH, respectively (see Section 5). This accretion process, occurring in both S-GRBs and BdHNe (Becerra et al. 2016), is currently being analyzed for the occurrence of r-process (Ruffini et al. 2014; Becerra et al. 2016).

In all of the identified S-GRBs, within the *Fermi*-LAT FoV, GeV photons are always observed (Ruffini et al. 2016a, 2016c). This implies that no intrinsic beaming is necessary for the S-GRB GeV emission. The Lorentz factor of the GeV emission is $\Gamma_{\rm GeV}^{\rm min} \gtrsim 300$.

From Figure 13 for S-GRBs and from Figure 14 for S-GRFs, we conclude that in both systems there is no evidence for the early X-ray flares observed in BdHNe (Ruffini et al. 2017).

Before closing, we return to the issue of GW detectability by aLIGO from S-GRBs. We have already shown evidence of their non-detectability by aLIGO in GRB 090227B (Oliveira et al. 2014) and GRB 140619B (Ruffini et al. 2015) by computing the signal-to-noise ratio (S/N) up to the contact point of the binary NS components. In both cases, each NS has been assumed to have mass $M_{\rm NS} = 1.34\,M_\odot = 0.5 M_{\rm crit}^{\rm NS}$. There, it was concluded that the GW signals emitted in such systems were well below the S/N = 8 value needed for a positive detection.

These considerations have been extended in Ruffini et al. (2016b) to all S-GRBs. It was concluded there that such signals might be detectable for sources located at $z \lesssim 0.14$ (i.e., at distances smaller than the GW detection horizon of 640 Mpc) for the aLIGO 2022+ run. GRB 090510, to date the closest S-GRB, is located at $z = 0.903$ (i.e., 5842 Mpc) and, therefore, it is outside such a GW detection horizon. We can then conclude that for sources at distances larger than that of GRB 090510, like GRB 081024B (at $z = 3.12$) and GRB 140402A (at $z = 5.52$) analyzed in this paper, no GW emission can be detected.

We thank the referee for pleasant and expert advice. M.M. and J.A.R. acknowledge the partial support of the project N 3101/GF4 IPC-11 and the target program F.0679 0073-6/PTsF of the Ministry of Education and Science of the Republic of Kazakhstan. Y.A. is supported by the Erasmus Mundus Joint Doctorate Program Grant Number 2014-0707 from the agency EACEA of the European Commission.

References

Abdo, A. A., Ackermann, M., Ajello, M., et al. 2010, ApJ, 712, 558
Ackermann, M., Ajello, M., Asano, K., et al. 2013, ApJS, 209, 11
Aksenov, A. G., Ruffini, R., & Vereshchagin, G. V. 2007, PhRvL, 99, 125003
Aksenov, A. G., Ruffini, R., & Vereshchagin, G. V. 2009, PhRvD, 79, 043008
Aptekar, R. L., Frederiks, D. D., Golenetskii, S. V., et al. 1995, SSRv, 71, 265
Band, D., Matteson, J., Ford, L., et al. 1993, ApJ, 413, 281
Barthelmy, S. D., Chincarini, G., Burrows, D. N., et al. 2005, Natur, 438, 994
Becerra, L., Bianco, C. L., Fryer, C. L., Rueda, J. A., & Ruffini, R. 2016, ApJ, 833, 107
Becerra, L., Cipolletta, F., Fryer, C. L., Rueda, J. A., & Ruffini, R. 2015, ApJ, 812, 100
Belczynski, K., Perna, R., Bulik, T., et al. 2006, ApJ, 648, 1110
Belvedere, R., Boshkayev, K., Rueda, J. A., & Ruffini, R. 2014, NuPhA, 921, 33
Belvedere, R., Pugliese, D., Rueda, J. A., Ruffini, R., & Xue, S.-S. 2012, NuPhA, 883, 1
Belvedere, R., Rueda, J. A., & Ruffini, R. 2015, ApJ, 799, 23
Berger, E. 2014, ARA&A, 52, 43
Bianco, C. L., & Ruffini, R. 2005a, ApJL, 633, L13
Bianco, C. L., & Ruffini, R. 2005b, ApJL, 620, L23
Bildsten, L., & Cutler, C. 1992, ApJ, 400, 175
Bissaldi, E., Vianello, G., & Chiang, J. 2014, GCN, 16069, 1
Breeveld, A. A., & Pagani, C. 2014, GCN, 16077, 1
Brown, D. A., Babak, S., Brady, P. R., et al. 2004, CQGra, 21, S1625
Calderone, G., Ghirlanda, G., Ghisellini, G., et al. 2015, MNRAS, 448, 403
Cipolletta, F., Cherubini, C., Filippi, S., Rueda, J. A., & Ruffini, R. 2015, PhRvD, 92, 023007
Clark, J. P. A., & Eardley, D. M. 1977, ApJ, 215, 311
Connaughton, V., & Briggs, M. 2008, GCN, 8408, 1
Cummings, J. R. 2014, GCN, 16073, 1
Dezalay, J.-P., Barat, C., Talon, R., et al. 1992, in AIP Conf. Ser. 265 Gamma-ray bursts, ed. W. S. Paciesas & G. J. Fishman (Melville, NY: AIP), 304
Eichler, D., Livio, M., Piran, T., & Schramm, D. N. 1989, Natur, 340, 126
Fatkhullin, T., Moskvitin, A., & Castro-Tirado, A. J. 2008, GCN, 8456, 1
Fong, W., Ehlert, S., Osip, D., et al. 2014, GCN, 16080, 1
Fox, D. B., Frail, D. A., Price, P. A., et al. 2005, Natur, 437, 845
Frontera, F. 2015, in Proc. of the MG13 Meeting on General Relativity (in 3 Volumes), Thirteenth Marcel Grossmann Meeting: On Recent Developments in Theoretical and Experimental General Relativity, Astrophysics and Relativistic Field Theories, ed. K. Rosquist (Singapore: World Scientific), 33
Fryer, C. L., Belczynski, K., Ramirez-Ruiz, E., et al. 2015a, ApJ, 812, 24
Fryer, C. L., Oliveira, F. G., Rueda, J. A., & Ruffini, R. 2015b, PhRvL, 115, 231102
Fryer, C. L., Rueda, J. A., & Ruffini, R. 2014, ApJ, 793, L36
Gehrels, N., Sarazin, C. L., O'Brien, P. T., et al. 2005, Natur, 437, 851
Goodman, J. 1986, ApJL, 308, L47
Guidorzi, C. 2008, GCN, 8513, 1
Guidorzi, C., Mao, J., & Margutti, R. 2008a, GCN, 8454, 1
Guidorzi, C., & Margutti, R. 2008, GCN, 8416, 1

Guidorzi, C., Margutti, R., & Mao, J. 2008b, GCN, 8410, 1
Hanabata, Y., Uehara, T., Takahashi, T., et al. 2008, GCN, 8444, 1
Izzo, L., Ruffini, R., Penacchioni, A. V., et al. 2012, A&A, 543, A10
Jenke, P. A., & Yu, H.-F. 2014, GCN, 16070, 1
Kiuchi, K., Kyutoku, K., Sekiguchi, Y., Shibata, M., & Wada, T. 2014, PhRvD, 90, 041502
Klebesadel, R. W. 1992, in Gamma-Ray Bursts—Observations, Analyses and Theories, ed. C. Ho, R. I. Epstein, & E. E. Fenimore (Cambridge: Cambridge Univ. Press), 161
Kouveliotou, C., Meegan, C. A., Fishman, G. J., et al. 1993, ApJL, 413, L101
Landau, L. D., & Lifshitz, E. M. 2003, The Classical Theory of Fields (4th ed.; Oxford: Butterworth-Heinemann)
Lawrence, S., Tervala, J. G., Bedaque, P. F., & Miller, M. C. 2015, ApJ, 808, 186
Lee, W. H., Ramirez-Ruiz, E., & Page, D. 2004, ApJL, 608, L5
Lithwick, Y., & Sari, R. 2001, ApJ, 555, 540
Maselli, A., & D'Avanzo, P. 2014, GCN, 16424, 1
Mazets, E. P., Golenetskii, S. V., Ilinskii, V. N., et al. 1981, Ap&SS, 80, 3
Meegan, C., Lichti, G., Bhat, P. N., et al. 2009, ApJ, 702, 791
Meszaros, P., & Rees, M. J. 1997, ApJL, 482, L29
Muccino, M., Ruffini, R., Bianco, C. L., Izzo, L., & Penacchioni, A. V. 2013, ApJ, 763, 125
Narayan, R., Paczynski, B., & Piran, T. 1992, ApJL, 395, L83
Narayan, R., Piran, T., & Shemi, A. 1991, ApJL, 379, L17
Oliveira, F. G., Rueda, J. A., & Ruffini, R. 2014, ApJ, 787, 150
Omodei, N. 2008, GCN, 8407, 1
Özel, F., & Freire, P. 2016, ARA&A, 54, 401
Paczynski, B. 1986, ApJL, 308, L43
Pagani, C. 2014a, GCN, 16078, 1
Pagani, C. 2014b, GCN, 16075
Paschalidis, V., Ruiz, M., & Shapiro, S. L. 2015, ApJL, 806, L14
Patricelli, B., Bernardini, M. G., Bianco, C. L., et al. 2012, ApJ, 756, 16
Penacchioni, A. V., Ruffini, R., Bianco, C. L., et al. 2013, A&A, 551, A133
Penacchioni, A. V., Ruffini, R., Izzo, L., et al. 2012, A&A, 538, A58
Pisani, G. B., Ruffini, R., Aimuratov, Y., et al. 2016, ApJ, 833, 159
Rau, A., McBreen, S., & Kruehler, T. 2009, GCN, 9353, 1
Rezzolla, L., Giacomazzo, B., Baiotti, L., et al. 2011, ApJL, 732, L6
Rosswog, S., Ramirez-Ruiz, E., & Davies, M. B. 2003, MNRAS, 345, 1077
Rotondo, M., Rueda, J. A., Ruffini, R., & Xue, S.-S. 2011a, PhRvC, 83, 045805
Rotondo, M., Rueda, J. A., Ruffini, R., & Xue, S.-S. 2011b, PhLB, 701, 667
Rueda, J. A., & Ruffini, R. 2012, ApJL, 758, L7
Rueda, J. A., & Ruffini, R. 2013, IJMPD, 22, 1360007
Rueda, J. A., Ruffini, R., Wu, Y.-B., & Xue, S.-S. 2014, PhRvC, 89, 035804
Rueda, J. A., Ruffini, R., & Xue, S.-S. 2011, NuPhA, 872, 286
Ruffini, R., Bernardini, M. G., Bianco, C. L., et al. 2005, in AIP Conf. Ser. 782, XIth Brazilian School of Cosmology and Gravitation, ed. M. Novello & S. E. Perez Bergliaffa (Melville, NY: AIP), 42
Ruffini, R., Bernardini, M. G., Bianco, C. L., et al. 2006, in AIP Conf. Ser. 836, Gamma-Ray Bursts in the Swift Era, ed. S. S. Holt, N. Gehrels, & J. A. Nousek (Melville, NY: AIP), 103
Ruffini, R., Bianco, C. L., Chardonnet, P., Fraschetti, F., & Xue, S. 2002, ApJL, 581, L19
Ruffini, R., Bianco, C. L., Fraschetti, F., Xue, S.-S., & Chardonnet, P. 2001a, ApJL, 555, L117
Ruffini, R., Bianco, C. L., Fraschetti, F., Xue, S.-S., & Chardonnet, P. 2001b, ApJL, 555, L113
Ruffini, R., Bianco, C. L., Fraschetti, F., Xue, S.-S., & Chardonnet, P. 2001c, ApJL, 555, L107
Ruffini, R., Bianco, C. L., Xue, S.-S., et al. 2004, IJMPD, 13, 843
Ruffini, R., Muccino, M., Aimuratov, Y., et al. 2016a, ApJ, 831, 178
Ruffini, R., Muccino, M., Bianco, C. L., et al. 2014, A&A, 565, L10
Ruffini, R., Muccino, M., Kovacevic, M., et al. 2015, ApJ, 808, 190
Ruffini, R., Rodriguez, J., Muccino, M., et al. 2016b, arXiv:1602.03545
Ruffini, R., Rueda, J. A., Muccino, M., et al. 2016c, ApJ, 832, 136
Ruffini, R., Salmonson, J. D., Wilson, J. R., & Xue, S. 2000, A&A, 359, 855
Ruffini, R., Salmonson, J. D., Wilson, J. R., & Xue, S.-S. 1999, A&A, 350 334
Ruffini, R., Vereshchagin, G., & Xue, S. 2010, PhR, 487, 1
Ruffini, R., Wang, Y., Aimuratov, Y., et al. 2017, arXiv:1704.03821
Ruffini, R., & Wheeler, J. A. 1971, ESRSP, 52, 45
Ruffini, R., & Wilson, J. 1973, PhRvL, 31, 1362
Ruiz, M., Lang, R. N., Paschalidis, V., & Shapiro, S. L. 2016, ApJL, 824, L6
Salmonson, J. D., & Wilson, J. R. 2002, ApJ, 578, 310
Schaefer, B. E. 2007, ApJ, 660, 16
Shibata, M., Suwa, Y., Kiuchi, K., & Ioka, K. 2011, ApJL, 734, L36
Siegel, D. M., Ciolfi, R., & Rezzolla, L. 2014, ApJL, 785, L6
Tauris, T. M., Kaspi, V. M., Breton, R. P., et al. 2015, in Advancing Astrophysics with the Square Kilometre Array (AASKA14), 39
Tavani, M. 1998, ApJL, 497, L21
Tavani, M., Barbiellini, G., Argan, A., et al. 2009, A&A, 502, 995
Zel'dovich, Y. B., Ivanova, L. N., & Nadezhin, D. K. 1972, SvA, 16, 209
Zhang, F.-W., Shao, L., Yan, J.-Z., & Wei, D.-M. 2012, ApJ, 750, 88

Review

International Journal of Modern Physics D
Vol. 26, No. 9 (2017) 1730016 (19 pages)

DOI: 10.1142/S0218271817300166

The binary systems associated with short and long gamma-ray bursts and their detectability*

Jorge A. Rueda[†,‡,§,***], Y. Aimuratov[†,‡,¶], U. Barres de Almeida[‖], L. Becerra[†,‡], C. L. Bianco[†,‡], C. Cherubini[**,††], S. Filippi[**,††], M. Karlica[†,‡,¶], M. Kovacevic[†,‡,¶], J. D. Melon Fuksman[†,‡], R. Moradi[†,‡], M. Muccino[†,‡], A. V. Penacchioni[‡‡,§§], G. B. Pisani[†,‡], D. Primorac[†,‡], R. Ruffini[†,‡,§], N. Sahakyan[¶¶], S. Shakeri[†,‖‖] and Y. Wang[†,‡]

[†]*ICRANet, Piazza Della Repubblica 10, I-65122 Pescara, Italy*

[‡]*Dip. di Fisica and ICRA, Sapienza Università di Roma, P.le Aldo Moro 5, I-00185 Rome, Italy*

[§]*ICRANet-Rio, Centro Brasileiro de Pesquisas Físicas, Rua Dr. Xavier Sigaud 150, 22290–180 Rio de Janeiro, Brazil*

[¶]*Université de Nice Sophia Antipolis, CEDEX 2, Grand Château Parc Valrose, Nice, France*

[‖]*Centro Brasileiro de Pesquisas Físicas, Rua Dr. Xavier Sigaud 150, 22290–180 Rio de Janeiro, Brazil*

[**]*Unit of Nonlinear Physics and Mathematical Modeling, Università Campus Bio-Medico di Roma, Via A. del Portillo 21, I-00128 Rome, Italy*

[††]*ICRA, Università Campus Bio-Medico di Roma, Via A. del Portillo 21, I-00128 Rome, Italy*

[‡‡]*ASI Science Data Center, Via del Politecnico s.n.c., I-00133 Rome, Italy*

[§§]*Dept. of Physical Sciences, Earth and Environment, University of Siena, Via Roma 56, I-53100 Siena, Italy*

[¶¶]*ICRANet-Yerevan, Marshall Baghramian Avenue 24a, Yerevan 0019, Republic of Armenia*

[‖‖]*Department of Physics, Isfahan University of Technology, 84156–83111, Iran*

[***]*jorge.rueda@icra.it*

Received 2 March 2017
Accepted 3 March 2017
Published 13 April 2017

Short and long-duration gamma-ray bursts (GRBs) have been recently sub-classified into seven families according to the binary nature of their progenitors. For short GRBs, mergers of neutron star binaries (NS–NS) or neutron star-black hole binaries (NS-BH) are proposed. For long GRBs, the induced gravitational collapse (IGC) paradigm proposes

*Based on a talks presented at the Fourteenth Marcel Grossmann Meeting on General Relativity, Rome, July 2015.

a tight binary system composed of a carbon–oxygen core (CO_{core}) and a NS companion. The explosion of the CO_{core} as supernova (SN) triggers a hypercritical accretion process onto the NS companion which might reach the critical mass for the gravitational collapse to a BH. Thus, this process can lead either to a NS-BH or to NS–NS depending on whether or not the accretion is sufficient to induce the collapse of the NS into a BH. We shall discuss for the above compact object binaries: (1) the role of the NS structure and the equation-of-state on their final fate; (2) their occurrence rates as inferred from the X and gamma-ray observations; (3) the expected number of detections of their gravitational wave (GW) emission by the Advanced LIGO interferometer.

Keywords: Gamma-ray bursts; neutron stars; black holes.

PACS Number(s): 04.30.Tv, 04.40.Dg, 97.60.Bw, 97.60.Jd, 97.60.Lf, 98.62.Mw

1. Introduction

There has been a traditional phenomenological classification of GRBs based on the observed prompt duration, T_{90}: long GRBs for $T_{90} > 2\,\mathrm{s}$ and short GRBs for $T_{90} < 2\,\mathrm{s}$.[1–5] In this paper, we shall review the recent progress reached in the understanding of the nature of long and short GRBs that has led to a physical GRB classification, proposed in Refs. 6–8. Such a classification, as we will see below, is based on the possible outcomes in the final stages of the evolution of the progenitor systems.

1.1. *Long GRBs*

The induced gravitational collapse (IGC) scenario introduces, as the progenitor of the long GRBs associated with SNe Ib/c, binaries composed of a carbon–oxygen core (CO_{core}) on the verge of supernova with a NS companion.[9–15] The explosion of the CO_{core} as SN, forming at its center a newly-born NS called hereafter νNS, triggers an accretion process onto the NS binary companion. Depending on the parameters of the *in-state*, i.e. of CO_{core}-NS binary, two sub-classes of long GRBs with corresponding *out-states* are envisaged[6]:

- *X-ray flashes* (*XRFs*). Long bursts with $E_{iso} \lesssim 10^{52}$ erg are produced by CO_{core}-NS binaries with relatively large binary separations ($a \gtrsim 10^{11}$ cm). The accretion rate of the SN ejecta onto the NS in these systems is not high enough to bring the NS mass to the critical value M_{crit}, hence no BH is formed. The out-state of this GRB sub-class can be either a νNS–NS binary if the system keeps bound after the SN explosion, or two runaway NSs if the binary system is disrupted.
- *Binary driven hypernovae* (*BdHNe*). Long bursts with $E_{iso} \gtrsim 10^{52}$ erg are instead produced by more compact CO_{core}-NS binaries ($a \lesssim 10^{11}$ cm, see e.g. Refs. 13 and 15). In this case, the SN triggers a larger accretion rate onto the NS companion, e.g. $\gtrsim 10^{-2}$–$10^{-1}\,M_{\odot}\,\mathrm{s}^{-1}$, bringing the NS to its critical mass M_{crit},[11–13] namely to the point of gravitational collapse with consequent formation of a BH. Remarkably, in Ref. 14, it was recently shown that the large majority of BdHNe leads naturally to NS-BH binaries owing to the high compactness of the binary that avoids the disruption of it even in cases of very high mass loss exceeding 50% of the total mass of the initial CO_{core}-NS binary.

In addition, it exists the possibility of BH-SNe.[6] Long burst with $E_{\rm iso} \gtrsim 10^{54}$ erg occurring in close $\rm CO_{core}$-BH binaries in which the hypercritical accretion produces, as *out-states*, a more massive BH and a νNS. These systems have been considered in Ref. 6 as a subset of the BdHNe but no specific example have been yet observationally identified.

1.2. *Short GRBs*

There is the consensus within the GRB community that the progenitors of short GRBs are mergers of NS–NS and/or NS-BH binaries (see, e.g. Refs. 16–20 for a recent review). Similarly to the case of long GRBs, in Ref. 6 short GRBs have been split into different sub-classes:

- *Short gamma-ray flashes* (*S-GRFs*). Short bursts with energies $E_{\rm iso} \lesssim 10^{52}$ erg, produced when the post-merger core do not surpass the NS critical mass $M_{\rm crit}$, hence there is no BH formation. Thus, these systems left as byproduct a massive NS and possibly, due to the energy and angular momentum conservation, orbiting material in a disk-like structure or a low-mass binary companion.
- *Authentic short gamma-ray bursts* (*S-GRBs*). Short bursts with $E_{\rm iso} \gtrsim 10^{52}$ erg, produced when the post-merger core reaches or overcome $M_{\rm crit}$, hence forming a Kerr or Kerr–Newman BH,[8] and also in this case possibly orbiting material.
- *Ultra-short GRBs* (*U-GRBs*). A new sub-class of short bursts originating from νNS-BH merging binaries. They can originate from BdHNe (see Ref. 14) or from BH-SNe.

In addition, it exists the possibility of *gamma-ray flashes* (*GRFs*). These are bursts with hybrid properties between short and long, they have $10^{51} \lesssim E_{\rm iso} \lesssim 10^{52}$ erg. This sub-class of sources originates in NS-WD mergers.[6]

Table 1 summarized some observational aspects of the GRB sub-classes including the occurrence rate calculated in Ref. 6.

Table 1. Some observational aspects of the GRB sub-classes. In the first three columns, we indicate the GRB sub-class and their corresponding *in-states* and the *out-states*. In column 4, we list the $E_{\rm iso}$ (rest-frame 1–10^4 keV), columns 5–6 list, for each GRB sub-class, the maximum observed redshift and the local occurrence rate computed in Ref. 6.

GRB sub-class	In-state	Out-state	$E_{\rm iso}$ (erg)	$z_{\rm max}$	$\rho_{\rm GRB}$ ($\rm Gpc^{-3}yr^{-1}$)
XRFs	$\rm CO_{core}$-NS	νNS-NS	10^{48}–10^{52}	1.096	100^{+45}_{-34}
BdHNe	$\rm CO_{core}$-NS	νNS-BH	10^{52}–10^{54}	9.3	$0.77^{+0.09}_{-0.08}$
BH-SN	$\rm CO_{core}$-BH	νNS-BH	$>10^{54}$	9.3	$\lesssim 0.77^{+0.09}_{-0.08}$
S-GRFs	NS-NS	MNS	10^{49}–10^{52}	2.609	$3.6^{+1.4}_{-1.0}$
S-GRBs	NS-NS	BH	10^{52}–10^{53}	5.52	$(1.9^{+1.8}_{-1.1}) \times 10^{-3}$
U-GRBs	νNS-BH	BH	$>10^{52}$	—	$\gtrsim 0.77^{+0.09}_{-0.08}$
GRFs	NS-WD	MNS	10^{51}–10^{52}	2.31	$1.02^{+0.71}_{-0.46}$

We focus here on the physical properties of the above progenitors, as well as on the main properties of NSs that play a relevant role in the dynamics of these systems and that lead to the above different GRB sub-classes. We shall discuss as well recent estimates of the rates of occurrence on all the above subclasses based on X and gamma-ray observations, and also elaborate on the possibility of detecting the gravitational wave (GW) emission originated in these systems.

2. IGC, Hypercritical Accretion, and Long GRBs

We turn now to the details of the accretion process within the IGC scenario. Realistic simulations of the IGC process were performed in Ref. 12, including: (1) detailed SN explosions of the CO_{core}; (2) the hydrodynamic details of the hypercritical accretion process; (3) the evolution of the SN ejecta material entering the Bondi–Hoyle region all the way up to its incorporation into the NS. Here, the concept of hypercritical accretion refers to the fact the accretion rates are highly super-Eddington. The accretion process in the IGC scenario is allowed to exceed the Eddington limit mainly for two reasons: (i) the photons are trapped within the infalling material impeding them to transfer momentum; (ii) the accreting material creates a very hot NS atmosphere ($T \sim 10^{10}\,\mathrm{K}$) that triggers a very efficient neutrino emission which become the main energy sink of these systems unlike photons.

The hypercritical accretion process in the above simulations was computed within a spherically symmetric approximation. A further step was given in Ref. 13 by estimating the angular momentum that the SN ejecta carries and transfer to the NS via accretion, and how it affects the evolution and fate of the system. The calculations are as follows: first the accretion rate onto the NS is computed adopting an homologous expansion of the SN ejecta and introducing the pre-SN density profile of the CO_{core} envelope from numerical simulations. Then, it is estimated the angular momentum that the SN material might transfer to the NS: it comes out that the ejecta have enough angular momentum to circularize for a short time and form a disc around the NS. Finally, the evolution of the NS central density and rotation angular velocity (spin-up) is followed computing the equilibrium configurations from the numerical solution of the axisymmetric Einstein equations in full rotation, until the critical point of collapse of the NS to a BH taking into due account the equilibrium limits given by mass-shedding and the secular axisymmetric instability.

Now we enter into the details of each of the above steps. The accretion rate of the SN ejecta onto the NS can be estimated via the Bondi–Hoyle–Lyttleton accretion formula:

$$\dot{M}_B(t) = \pi \rho_{\rm ej} R_{\rm cap}^2 \sqrt{v_{\rm rel}^2 + c_{\rm s,ej}^2}, \quad R_{\rm cap}(t) = \frac{2GM_{\rm NS}(t)}{v_{\rm rel}^2 + c_{\rm s,ej}^2}, \tag{1}$$

where G is the gravitational constant, $\rho_{\rm ej}$ and $c_{\rm s,ej}$ are the density and sound speed of the SN ejecta, $R_{\rm cap}$ is the NS gravitational capture radius (Bondi–Hoyle radius), $M_{\rm NS}$, the NS mass, and $v_{\rm rel}$ the ejecta velocity relative to the NS: $\mathbf{v}_{\rm rel} = \mathbf{v}_{\rm orb} - \mathbf{v}_{\rm ej}$,

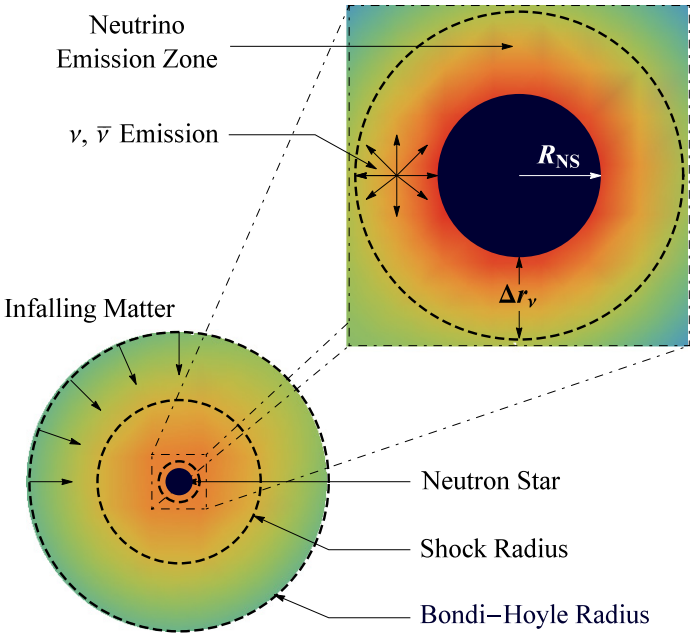

Fig. 1. Scheme of the IGC scenario: the CO_{core} undergoes SN explosion, the NS accretes part of the SN ejecta and then reaches the critical mass for gravitational collapse to a BH, with consequent emission of a GRB. The SN ejecta reach the NS Bondi–Hoyle radius and fall toward the NS surface. The material shocks and decelerates as it piles over the NS surface. At the neutrino emission zone, neutrinos take away most of the infalling matter gravitational energy gain. The neutrinos are emitted above the NS surface in a region of thickness Δr_ν about half the NS radius that allow the material to reduce its entropy to be finally incorporated to the NS. The image is not to scale. For further details and numerical simulations of the above process, see Refs. 12–15.

with $|\mathbf{v}_{\rm orb}| = \sqrt{G(M_{\rm core} + M_{\rm NS})/a}$, the module of the NS orbital velocity around the CO_{core}, and $\mathbf{v}_{\rm ej}$ the velocity of the supernova ejecta (see Fig. 1).

Extrapolating the results for the accretion process from stellar wind accretion in binary systems, the angular momentum per unit time that crosses the NS capture region can be approximated by: $\dot{L}_{\rm cap} = (\pi/2)(\epsilon_\rho/2 - 3\epsilon_\nu)\rho_{\rm ej}(a,t)v^2_{\rm rel}(a,t)R^4_{\rm cap}(a,t)$, where ϵ_ρ and ϵ_ν are parameters measuring the inhomogeneity of the flow (see Ref. 13 for details).

In order to simulate the hypercritical accretion, it is adopted an homologous expansion of the SN ejecta, i.e. the ejecta velocity evolves as $v_{\rm ej}(r,t) = nr/t$, where r is the position of every ejecta layer from the SN center and n is called expansion parameter. The ejecta density is given by $\rho_{\rm ej}(r,t) = \rho^0_{\rm ej}(r/R_{\rm star}(t), t_0)\frac{M_{\rm env}(t)}{M_{\rm env}(0)}(\frac{R_{\rm star}(0)}{R_{\rm star}(t)})^3$, where $M_{\rm env}(t)$ the mass of the CO_{core} envelope, namely the mass of the ejected material in the SN explosion and available to be accreted by the NS, $R_{\rm star}(t)$ is the position of the outermost layer of the ejected material, and $\rho^0_{\rm ej}$ is the pre-SN density profile. The latter can be approximated with a power law: $\rho_{\rm ej}(r,t_0) = \rho_{\rm core}(R_{\rm core}/r)^m$, where $\rho_{\rm core}$, $R_{\rm core}$ and m are the profile parameters which are fixed by fitting the pre-SN profiles obtained from numerical simulations.

For the typical parameters of pre-SN CO_{core} and assuming a velocity of the outermost SN layer $v_{\rm sn}(R_{\rm star}, t_0) \sim 10^9\,{\rm cm\,s^{-1}}$ and a free expansion $n = 1$ (for details

of typical initial conditions of the binary system see Refs. 12 and 13), Eq. (1) gives accretion rates around the order of $10^{-4} - 10^{-2} M_\odot\,\mathrm{s}^{-1}$, and an angular momentum per unit time crossing the capture region $\dot{L}_{\rm cap} \sim 10^{46}$–$10^{49}\,\mathrm{g\,cm^2\,s^{-2}}$.

We consider the NS companion of the $\mathrm{CO_{core}}$ initially as nonrotating, thus at the beginning, the NS exterior spacetime is described by the Schwarzschild metric. The SN ejecta approach the NS with specific angular momentum, $l_{\rm acc} = \dot{L}_{\rm cap}/\dot{M}_B$, thus they will circularize at a radius $r_{\rm st}$ if they have enough angular momentum. What does the word "enough" means here? The last stable circular orbit (LSO) around a nonrotating NS is located at a distance $r_{\rm lso} = 6GM_{\rm NS}/c^2$ and has an angular momentum per unit mass $l_{\rm lso} = 2\sqrt{3}GM_{\rm NS}/c$. The radius $r_{\rm lso}$ is larger than the NS radius for masses larger than $1.67\,M_\odot$, $1.71\,M_\odot$, and $1.78\,M_\odot$ for the GM1, TM1, and NL3 nuclear equation-of-state (EOS).[13] If $l_{\rm acc} \geq l_{\rm lso}$, the material circularizes around the NS at locations $r_{\rm st} \geq r_{\rm lso}$. For the values of the IGC systems under discussion here, $r_{\rm st}/r_{\rm lso} \sim 10 - 10^3$, thus the SN ejecta have enough angular momentum to form a sort of disc around the NS. Even in this case, the viscous forces and other angular momentum losses that act on the disk will allow the matter in the disk to reach the inner boundary at $r_{\rm in} \sim r_{\rm lso}$, to then be accreted by the NS.

Within this picture, the NS accretes the material from $r_{\rm in}$ and the NS mass and angular momentum evolve as:

$$\dot{M}_{\rm NS} = \left(\frac{\partial M_{\rm NS}}{\partial M_b}\right)_{J_{\rm NS}} \dot{M}_b + \left(\frac{\partial M_{\rm NS}}{\partial J_{\rm NS}}\right)_{M_b} \dot{J}_{\rm NS}, \quad \dot{J}_{\rm NS} = \xi l(r_{\rm in})\dot{M}_{\rm B}, \tag{2}$$

where M_b is the NS baryonic mass, $l(r_{\rm in})$ is the specific angular momentum of the accreted material at $r_{\rm in}$, which corresponds to the angular momentum of the LSO, and $\xi \leq 1$ is a parameter that measures the efficiency of angular momentum transfer. We assume in our simulations $\dot{M}_b = \dot{M}_B$.

In order to integrate Eqs. (1) and (2), we have to supply the two above partial derivatives which are obtained from the relation of the NS gravitational mass with M_b and $J_{\rm NS}$, namely from the NS binding energy. The general relativistic calculations of rotating NSs in Ref. 21 show that, independent on the nuclear EOS, this relation is well approximated by the formula

$$\frac{M_b}{M_\odot} = \frac{M_{\rm NS}}{M_\odot} + \frac{13}{200}\left(\frac{M_{\rm NS}}{M_\odot}\right)^2 \left(1 - \frac{1}{137} j_{\rm NS}^{1.7}\right), \tag{3}$$

where $j_{\rm NS} \equiv cJ_{\rm NS}/(GM_\odot^2)$. In addition, since the NS will spin up with accretion, we need information of the dependence of the specific angular momentum of the LSO as a function of both the NS mass and angular momentum. For corotating orbits, the following relation is valid for all the aforementioned EOS[13]:

$$l_{\rm lso} = \frac{GM_{\rm NS}}{c}\left[2\sqrt{3} - 0.37\left(\frac{j_{\rm NS}}{\frac{M_{\rm NS}}{M_\odot}}\right)^{0.85}\right]. \tag{4}$$

The NS accretes mass until it reaches a region of instability. There are two main instability limits for rotating NSs: mass-shedding or Keplerian limit and the secular

Table 2. Critical NS mass in the nonrotating case and constants k and p needed to compute the NS critical mass in the nonrotating case given by Eq. (5). The values are given for the NL3, GM1 and TM1 EOS.

EOS	$M_{\rm crit}^{J=0}$ $(M_\odot)$	p	k
NL3	2.81	1.68	0.006
GM1	2.39	1.69	0.011
TM1	2.20	1.61	0.017

axisymmetric instability. The critical NS mass along the secular instability line is approximately given by[21]:

$$M_{\rm NS}^{\rm crit} = M_{\rm NS}^{J=0}(1 + k j_{\rm NS}^{p}), \tag{5}$$

where the parameters k and p depends of the nuclear EOS (see Table 2). These formulas fit the numerical results with a maximum error of 0.45%.

Along the mass-shedding sequence, the NS has the maximum possible angular momentum[21]: $J_{\rm NS,max} \approx 0.7 G M_{\rm NS}^2/c$. Figure 2 shows the evolution of the NS dimensionless angular momentum, $cJ_{\rm NS}/(GM_{\rm NS}^2)$, as a function of the NS mass for $\xi = 0.5$ and for selected values of the initial NS mass. The NS fate depends of the NS initial mass and the efficiency parameter ξ. The less massive initial configurations reach the mass-shedding limit with a maximum dimensionless angular momentum value while the initially more massive configurations reach the secular axisymmetric instability. It is interesting to note that the total angular momentum of the SN ejecta entering the Bondi–Hoyle region, $L_{\rm cap}$, is much larger than the

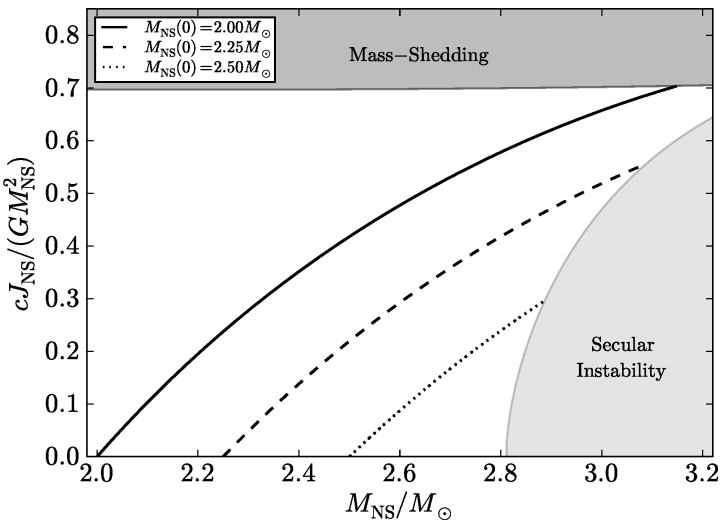

Fig. 2. Evolution of NSs of different initial masses $M_{\rm NS} = 2.0, 2.25$ and $2.5\,M_\odot$ during the hypercritical accretion in a BdHN.[13] It is shown the dimensionless angular momentum as a function of the NS mass. The binary parameters are: $\rm CO_{core}$ of a $M_{\rm ZAMS} = 30\,M_\odot$ progenitor star ($m = 2.801$, $M_{\rm env} = 7.94\,M_\odot$, $\rho_{\rm core} = 3.08 \times 10^8\,{\rm g\,cm^{-3}}$ and $R_{0_{\rm star}} = 7.65 \times 10^9\,{\rm cm}$), a free expansion ($n = 1$) and a SN outermost ejecta velocity $v_{0_{\rm star}} = 2 \times 10^9\,{\rm cm\,s^{-1}}$. The orbital period is of approximately 5 min.

maximum angular momentum that a uniformly rotating NS can support, $J_{\rm NS,max}$. The numerical simulations in Ref. 13 indicate $L_{\rm cap} \sim 10 J_{\rm NS,max}$. Thus, part of this angular momentum must be lost or redistributed before the material can reach the NS surface. This result leads to a clear prediction: the BHs produced through the IGC mechanism, namely those formed in BdHNe, have initial dimensionless spin $\sim$0.7 and the excess of angular momentum could lead to a jetted emission with possible high-energy signatures and/or to the presence of a disk-like structure first around the NS as shown above and possibly also around the BH originated from the gravitational collapse of the NS.

2.1. *Most recent simulations of the IGC process*

Additional details and improvements of the hypercritical accretion process leading to XRFs and BdHNe have been recently presented in Ref. 15. In particular:

(1) It was there improved the accretion rate estimate including the density profile finite size/thickness and additional $\rm CO_{core}$ progenitors leading to different SN ejecta masses were also considered.
(2) It was shown in Ref. 13, the existence of a maximum orbital period, $P_{\rm max}$, over which the accretion onto NS companion is not high enough to bring it to the critical mass for gravitational collapse to a BH. Therefore, $\rm CO_{core}$-NS binaries with $P > P_{\rm max}$ lead to XRFs while the ones with $P \lesssim P_{\rm max}$ lead to BdHNe. In Ref. 15, the determination of $P_{\rm max}$ was extended to all the possible initial values of the mass of the NS companion and the angular momentum transfer efficiency parameter was also allowed to vary.
(3) It was computed the expected luminosity during the hypercritical accretion process for a wide range of binary periods covering XRFs and BdHNe.
(4) It was there shown that the presence of the NS companion originates large asymmetries (see, e.g. simulation in Fig. 3) in the SN ejecta leading to observable signatures in the X-rays.

Figure 3 shows a simulation of an IGC process presented in Ref. 15. We considered the effects of the gravitational field of the NS on the SN ejecta including the orbital motion as well as the changes in the NS gravitational mass owing to the accretion process via the Bondi formalism. The supernova matter was described as formed by point-like particles whose trajectory was computed by solving the Newtonian equation of motion. The initial conditions of the SN ejecta are computed assuming an homologous velocity distribution in free expansion. The initial power-law density profile of the CO envelope is simulated by populating the inner layers with more particles. For the $M_{\rm ZAMS} = 30\,M_\odot$ progenitor which gives a $\rm CO_{core}$ with envelope profile $\rho^0_{\rm ej} \approx 3.1 \times 10^8 (8.3 \times 10^7/r)^{2.8}\,{\rm g\,cm^{-3}}$, we adopt for the simulation a total number of $N = 10^6$ particles. We assume that particles crossing the Bondi–Hoyle radius are captured and accreted by the NS so we removed them from the system as they reach that region. We removed these particles according to the

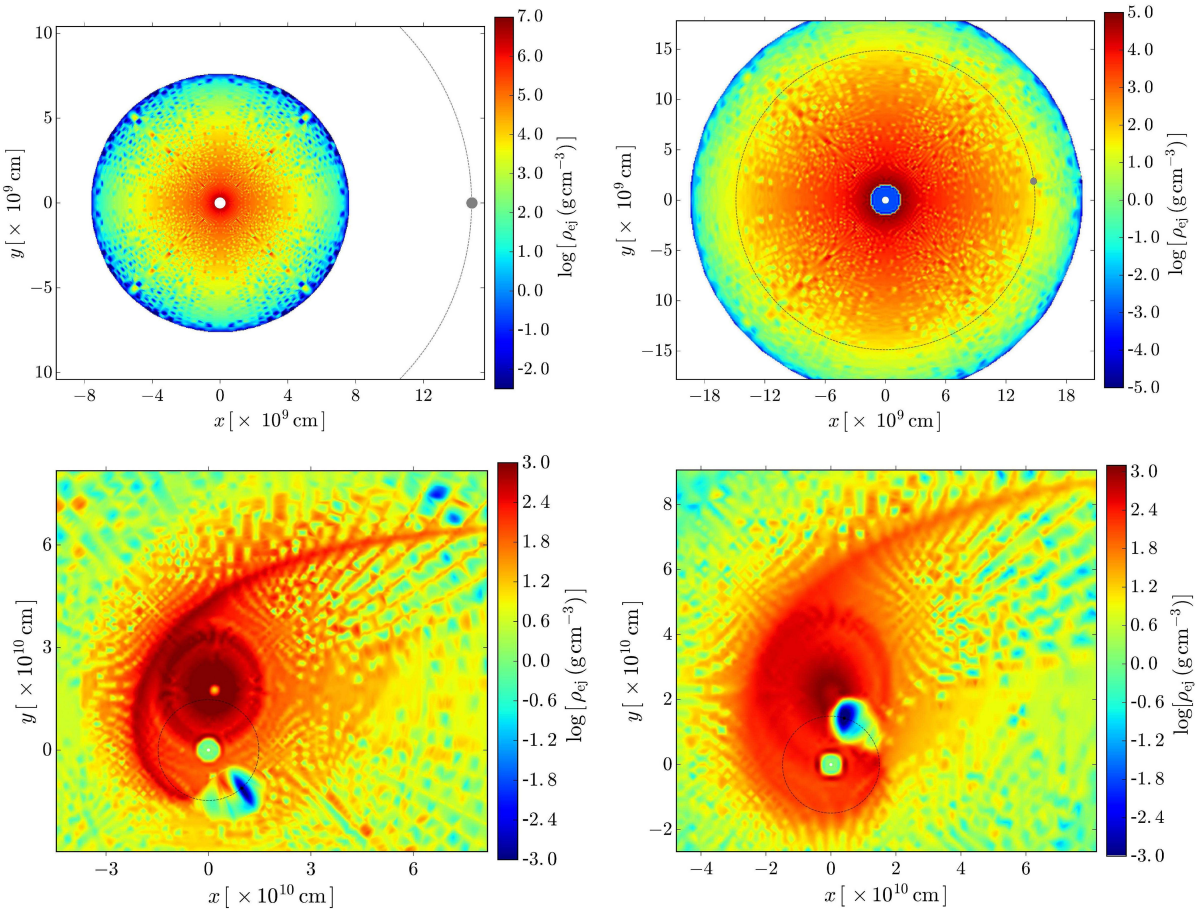

Fig. 3. Hypercritical accretion process in the IGC binary system at selected evolution times. In this example, the $\mathrm{CO_{core}}$ has a total mass of $9.44\,M_\odot$ divided in an ejecta mass of $7.94\,M_\odot$ and a νNS of $1.5\,M_\odot$ formed by the collapsed high density core. The supernova ejecta evolve homologously with outermost layer velocity $v_{0,\mathrm{star}} = 2\times 10^9\,\mathrm{cm\,s^{-1}}$. The NS binary companion has an initial mass of $2.0\,M_\odot$. The binary period is $P \approx 5\,\mathrm{min}$, which corresponds to a binary separation $a \approx 1.5\times 10^{10}$ cm. The system of coordinates is centered on the νNS represented by the white-filled circle at $(0,0)$. The NS binary companion, represented by the gray-filled circle, orbits counterclockwise following the thin-dashed circular trajectory. The colorbar indicates values of ejecta density in logarithmic scale. *Left upper panel*: initial time of the process. The supernova ejecta expand radially outward and the NS binary companion is at $(a,0)$. *Right upper panel*: the accretion process starts when the first supernova layers reach the Bondi–Hoyle region. This happens at $t = t_{\mathrm{acc},0} \approx a/v_{0,\mathrm{star}} \approx 7.7\,\mathrm{s}$. *Left lower panel*: the NS binary companion reaches the critical mass by accreting matter from the SN with consequent collapse to a BH. This happens at $t = t_{\mathrm{coll}} \approx 254\,\mathrm{s} \approx 0.85\,P$. The newly-formed BH of mass $M_{\mathrm{BH}} = M_{\mathrm{crit}} \approx 3\,M_\odot$ is represented by the black-filled circle. It is here evident the asymmetry of the supernova ejecta induced by the presence of the accreting NS companion at close distance. *Right lower panel*: $t = t_{\mathrm{coll}} + 100\,\mathrm{s} = 354\,\mathrm{s} \approx 1.2\,P$, namely $100\,\mathrm{s}$ after the BH formation. It appears here the new binary system composed of the νNS and the newly-formed BH.

results obtained from the numerical integration explained above. Figure 3 shows the orbital plane of an IGC binary at selected times of its evolution. The NS has an initial mass of $2.0\,M_\odot$; the $\mathrm{CO_{core}}$ leads to a total ejecta mass $7.94\,M_\odot$ and a νNS of $1.5\,M_\odot$. The orbital period of the binary is $P \approx 5\,\mathrm{min}$, i.e. a binary separation $a \approx 1.5\times 10^{10}\,\mathrm{cm}$. For these parameters, the NS reaches the critical mass and collapses to form a BH.

2.2. *Hydrodynamics and neutrino inside the accretion region*

We turn now to give some details on the properties of the system inside the Bondi–Hoyle accretion region. We have seen that the accretion rate onto the NS can be as high as $\sim 10^{-2}$–$10^{-1}\, M_\odot\, \mathrm{s}^{-1}$. For these accretion rates:

(1) We can neglect the effect of the NS magnetic field since the magnetic pressure remains much smaller than the random pressure of the infalling material.[11,22]
(2) The photons are trapped in the accretion flow. The trapping radius, defined at which the photons emitted diffuse outward at a slower velocity than the one of the infalling material, is[23]: $r_{\mathrm{trapping}} = \min\{\dot{M}_B \kappa/(4\pi c), R_{\mathrm{cap}}$, where κ is the opacity. For the $\mathrm{CO_{core}}$, in Ref. 12, a Rosseland mean opacity roughly $5 \times 10^3\, \mathrm{cm}^2\, \mathrm{g}^{-1}$ was estimated. For the range of accretion rates, we obtain that $\dot{M}_B \kappa/(4\pi c) \sim 10^{13}$–$10^{19}\, \mathrm{cm}$, a radius much bigger than the NS capture radius which is in our simulations at most 1/3 of the binary separation. Thus, in our systems, the trapping radius extends all the way to the Bondi–Hoyle region, hence the Eddington limit does not apply and hypercritical accretion onto the NS occurs.
(3) Under these conditions, the gain of gravitational energy of the accreted material is mainly radiated via neutrino emission (see below).[11,12,22,24,25]

2.2.1. *Convective instabilities*

As the material piles onto the NS and the atmosphere radius, the accretion shock moves outward. The post-shock entropy is a decreasing function of the shock radius position which creates an atmosphere unstable to Rayleigh–Taylor convection during the initial phase of the accretion process. These instabilities can accelerate above the escape velocity driving outflows from the accreting NS with final velocities approaching the speed of light.[26,27] Assuming that radiation dominates, the entropy of the material at the base of the atmosphere is[22]: $S_{\mathrm{bubble}} \approx 16(1.4\, M_\odot/M_{\mathrm{NS}})^{-7/8}(M_\odot\, \mathrm{s}^{-1}/\dot{M}_{\mathrm{B}})^{1/4}(10^6\, \mathrm{cm}/r)^{3/8}$, in units of k_B per nucleon. This material will rise and expand, cooling adiabatically, i.e. $T^3/\rho =$ constant, for radiation dominated gas. If we assume a spherically symmetric expansion, then $\rho \propto 1/r^3$ and we obtain $k_B T_{\mathrm{bubble}} = 195\, S_{\mathrm{bubble}}^{-1}(10^6\, \mathrm{cm}/r)\, \mathrm{MeV}$. However, it is more likely that the bubbles expand in the lateral but not in the radial direction,[27] thus we have $\rho \propto 1/r^2$, i.e. $T_{\mathrm{bubble}} = T_0(S_{\mathrm{bubble}})(r_0/r)^{2/3}$, where $T_0(S_{\mathrm{bubble}})$ is given by the above equation evaluated at $r = r_0 \approx R_{\mathrm{NS}}$. This temperature implies a bolometric blackbody flux at the source from the bubbles

$$F_{\mathrm{bubble}} \approx 2 \times 10^{40} \left(\frac{M_{\mathrm{NS}}}{1.4\, M_\odot}\right)^{-7/2} \left(\frac{\dot{M}_{\mathrm{B}}}{M_\odot\, \mathrm{s}^{-1}}\right) \left(\frac{R_{\mathrm{NS}}}{10^6\, \mathrm{cm}}\right)^{3/2} \times \left(\frac{r_0}{r}\right)^{8/3} \mathrm{erg\, s^{-1} cm^{-2}}, \tag{6}$$

where σ is the Stefan–Boltzmann constant.

In Ref. 12, it was shown that the above thermal emission from the rising bubbles produced during the hypercritical accretion process can explain the early ($t \lesssim 50\,\mathrm{s}$) thermal X-ray emission observed in GRB 090618.[10,28] In that case, T_{bubble} drops from 50 keV to 15 keV expanding from $r \approx 10^9$ cm to 6×10^9 cm, for an accretion rate $10^{-2}\,M_\odot\,\mathrm{s}^{-1}$.

It is interesting that also r-process nucleosynthesis can occur in these outflows.[26] This implies that long GRBs can be also r-process sites with specific signatures from the decay of the produced heavy elements, possibly similar as in the case of the *kilonova* emission in short GRBs.[29] The signatures of this phenomenon in XRFs and BdHNe, and its comparison with kilonovae, deserves to be explored.

2.2.2. *Neutrino emission*

Most of the energy from the accretion is lost through neutrino emission. For the accretion rate conditions characteristic of our models $\sim 10^{-4}$–$10^{-2}\,M_\odot\,\mathrm{s}^{-1}$, e^+e^- pair annihilation dominates the neutrino emission and electron neutrinos remove the bulk of the energy. The temperature of these neutrinos can be roughly approximated by assuming that the inflowing material generally flows near to the NS surface before shocking and emitting neutrinos. For accretion rates $\sim 10^{-4}$–$10^{-2}\,M_\odot\,\mathrm{s}^{-1}$, neutrino energies $\sim$5–20 MeV are obtained.[15] A detailed study of the neutrino emission will be the presented elsewhere.

For the developed temperatures (say $k_B T \sim$ 1–10 MeV) near the NS surface, the dominant neutrino emission process is the e^+e^-annihilation leading to $\nu\bar{\nu}$. This process produces a neutrino emissivity proportional to the ninth power of the temperature. The accretion atmosphere near the NS surface is characterized by a temperature gradient with a typical scale height $\Delta r_\nu \approx 0.7\,R_{\mathrm{NS}}$.[15] Owing to the aforementioned strong dependence of the neutrino emission on temperature, most of the neutrino emission occurs in the region Δr_ν above the NS surface.

These conditions lead to the neutrinos to be efficient in balancing the gravitational potential energy gain allowing the hypercritical accretion rates. The effective accretion onto the NS can be estimated as[22]: $\dot{M}_{\mathrm{eff}} \approx \Delta M_\nu (L_\nu/E_\nu)$, where ΔM_ν and L_ν are the mass and neutrino luminosity in the emission region (i.e. Δr_ν). E_ν is half the gravitational potential energy gained by the material falling from infinity to the $R_{\mathrm{NS}} + \Delta r_\nu$. Since $L_\nu \approx 2\pi R_{\mathrm{NS}}^2 \Delta r_\nu \epsilon_{\mathrm{e^-e^+}}$ with $\epsilon_{\mathrm{e^-e^+}}$ the e^+e^- pair annihilation process emissivity, and $E_\nu = (1/2) G M_{\mathrm{NS}} \Delta M_\nu / (R_{\mathrm{NS}} + \Delta r_\nu)$, it can be checked that for $M_{\mathrm{NS}} = 1.4\,M_\odot$ this accretion rate leads to values $\dot{M}_{\mathrm{eff}} \approx 10^{-9}$–$10^{-1}\,M_\odot\,\mathrm{s}^{-1}$ for temperatures $k_B T =$ 1–10 MeV.

2.3. *Accretion luminosity*

The gain of gravitational potential energy in the accretion process is the total one available to be released, e.g. by neutrinos and photons. The total energy released in the star in a time-interval dt during the accretion of an amount of mass dM_b with

angular momentum $l\dot{M}_b$, is given by[13,30]

$$L_{\rm acc} = (\dot{M}_b - \dot{M}_{\rm NS})c^2 = \dot{M}_b c^2 \left[1 - \left(\frac{\partial M_{\rm NS}}{\partial J_{\rm NS}}\right)_{M_b} l - \left(\frac{\partial M_{\rm NS}}{\partial M_b}\right)_{J_{\rm NS}}\right]. \quad (7)$$

This upper limit to the energy released is just the amount of gravitational energy gained by the accreted matter by falling to the NS surface and which is not spent in changing the gravitational binding energy of the NS. The total energy releasable during the accretion process, say $\Delta E_{\rm acc} \equiv \int L_{\rm acc} dt$, is given by the difference in binding energies of the initial and final NS configurations. The typical luminosity will be $L_{\rm acc} \approx \Delta E_{\rm acc}/\Delta t_{\rm acc}$ where $\Delta t_{\rm acc}$ is the duration of the accretion process.

The duration of the accretion process is given approximately by the flow time of the slowest layers of the supernova ejecta to the NS. If the velocity of these layers is $v_{\rm inner}$, then $\Delta t_{\rm acc} \sim a/v_{\rm inner}$, where a is the binary separation. For $a \sim 10^{11}$ cm and $v_{\rm inner} \sim 10^8\,{\rm cm\,s^{-1}}$, we obtain $\Delta t_{\rm acc} \sim 10^3$ s, while for shorter binary separation, e.g. $a \sim 10^{10}$ cm ($P \sim 5$ min), $\Delta t_{\rm acc} \sim 10^2$ s, as validated by the results of our numerical integrations.

For instance, the NS in the system with $P = 5$ min accretes $\approx 1\,M_\odot$ in $\Delta t_{\rm acc} \approx 100$ s. With the aid of Eq. (3), we estimate a difference in binding energies between a $2\,M_\odot$ and a $3\,M_\odot$ NS, i.e. $\Delta E_{\rm acc} \approx 13/200(3^2 - 2^2)\,M_\odot c^2 \approx 0.32\,M_\odot c^2$ leading to a maximum luminosity $L_{\rm acc} \approx 3 \times 10^{-}3\,M_\odot c^2 \approx 0.1\dot{M}_b c^2$. This accretion power, which could be as high as $L_{\rm acc} \sim 0.1\dot{M}_b c^2 \sim 10^{47}$–$10^{51}\,{\rm erg\,s^{-1}}$ for accretion rates in the range $\dot{M}_b \sim 10^{-6}$–$10^{-2}\,M_\odot\,{\rm s^{-1}}$, necessarily leads to signatures observable in long GRBs (see, e.g. Refs. 10 and 12).

2.4. *Post-explosion orbits and formation of NS-BH binaries*

We turn now to discuss the out-states of the IGC process. The SN explosion of the $\rm CO_{core}$ leaves as a central remnant, the νNS, while the IGC process triggered by the hypercritical accretion of the SN ejecta onto the NS companion leads to the formation of a BH. Thus, the question arises if BdHNe are natural sites for the formation of NS-BH binaries or if these binaries become disrupted during the SN explosion and the consequent IGC process. The answer to this question was recently given in Ref. 14, where it was shown that indeed most of BdHN form NS-BH binaries since the high compactness of the orbit avoids the unbinding of the orbit.

In typical systems, most of the binaries become unbound during the SN explosion because of the ejected mass and momentum imparted (kick) on the newly formed compact object in the explosion of the massive star. Under the instantaneous explosion assumption, if half of the binary system's mass is lost in the SN explosion, the system is disrupted. In general, the fraction of massive binaries that can produce double compact object binaries is thought to be low: ∼0.001–1%.[31–33]

The mass ejected during the SN alters the binary orbit, causing it to become wider and more eccentric. Assuming that the mass is ejected instantaneously, the

post-explosion semi-major axis is $a/a_0 = (M_0 - \Delta M)/(M_0 - 2a_0\Delta M/r)$, where a_0 and a are the initial and final semi-major axes respectively, M_0 is the total initial mass of the binary system, ΔM is the change of mass (equal to the amount of mass ejected in the SN), and r is the orbital separation at the time of explosion.[34] For circular orbits, the system is unbound if it loses half of its mass. However, for very tight binaries as the one proposed in the IGC scenario, a number of additional effects can alter the fate of the binary.

The time it takes for the ejecta to flow past a companion in a SN is roughly 10–1000 s. Although the shock front is moving above $10^4\,\mathrm{km\,s^{-1}}$, the denser, lower-velocity ejecta can be moving at $10^3\,\mathrm{km\,s^{-1}}$.[12] The broad range of times arises because the SN ejecta velocities varies from 10^2–$10^4\,\mathrm{km\,s^{-1}}$. The accretion peaks as the slow-moving (inner) ejecta flows past the NS companion. For normal (wide) binaries, this time is a small fraction of the orbital period and the "instantaneous" mass-loss assumption is perfectly valid. However, in the compact binary systems considered in the IGC scenario, the orbital period ranges from only 100–1000 s, and the mass loss from the SN explosion can no longer be assumed to be instantaneous.

We have seen how in BdHNe, the accretion process can lead to BH formation in a time-interval as short as the orbital period. We here deepen this analysis to study the effect of the SN explosion in such a scenario with a specific example of Ref. 14. Figure 4 shows as the ejecta timescale becomes just a fraction of the orbital timescale, the fate of the post-explosion binary is altered. For these models, we assumed very close binaries with an initial orbital separation of 7×10^9 cm in circular orbits. With $\mathrm{CO_{core}}$ radii of 1–4×10^9 cm, such a separation is small, but achievable. We assume the binary consists of a $\mathrm{CO_{core}}$ and a $2.0\,M_\odot$ NS companion. When the $\mathrm{CO_{core}}$ collapses, it forms a $1.5\,M_\odot$ NS, ejecting the rest of the core. We then vary the ejecta mass and time required for most of the ejected matter to move out of the binary. Note that even if 70% of the mass is lost from the system (the $8\,M_\odot$ ejecta case), the system remains bound as long as the explosion time is just above the orbital time ($T_{\mathrm{orbit}} = 180$ s) with semi-major axes of less than 10^{11} cm.

The short orbits (on ejecta timescales) are not the only feature of these binaries that alters the post-explosion orbit. The NS companion accretes both matter and momentum from the SN ejecta, reducing the mass lost from the system with respect to typical binaries with larger orbital separations and much less accretion. In addition, as with common envelope scenarios, the bow shock produced by the accreting NS transfers orbital energy into the SN ejecta. Figure 4 shows the final orbital separation of our same three binaries, including the effects of mass accretion (we assume $0.5\,M_\odot$ is accreted with the momentum of the SN material) and orbit coupling (30% of the orbital velocity is lost per orbit). With these effects, not only do the systems remain bound even for explosion times greater than 1/2 the orbital period but, if the explosion time is long, the final semi-major axis can be on par with the initial orbital separation.

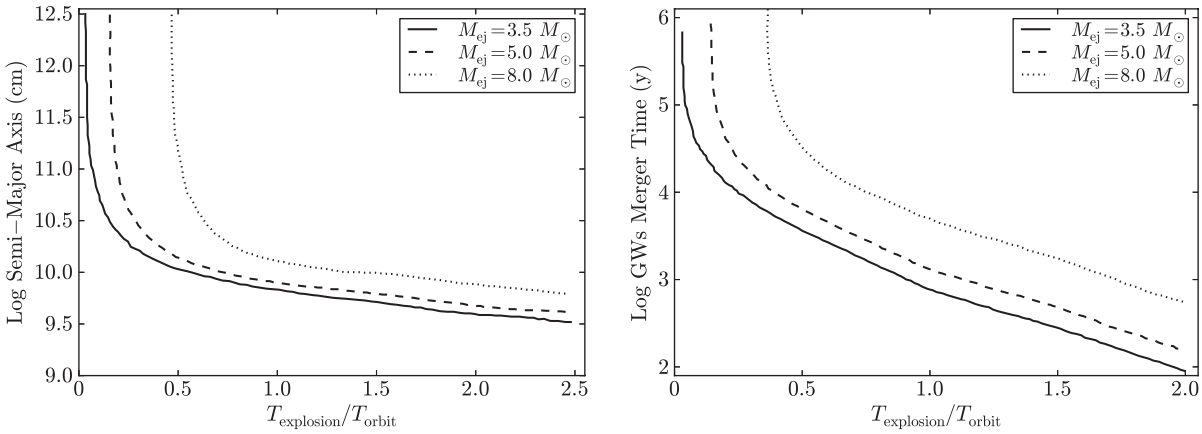

Fig. 4. Left panel: semi-major axis versus explosion time for three binary systems including mass accretion and momentum effects. Including these effects, all systems with explosion times above 0.7 times, the orbital time are bound and the final separations are on par with the initial separations. Right panel: merger time due to GW emission as a function of explosion time. Beyond a critical explosion time (0.1–0.6 $T_{\rm orbit}$ depending on the system), the merger time is less than roughly 10,000 yr. For most of our systems, the explosion time is above this limit and we expect most of these systems to merge quickly.

The tight compact binaries produced in these explosions will emit GW emission, ultimately causing the system to merge. For typical massive star binaries, the merger time is many Myr. For BdHNe, the merger time is typically 10,000 yr, or less, as shown in the right panel of Fig. 4. Since the merger should occur within the radius swept clean by the BdHN, we expect a small baryonic contamination around the merger site which might lead to a new family of events which we term ultrashort GRBs, U-GRBs. to this new family of events.

3. NS–NS/NS-BH Mergers and Short GRBs

Let us turn to short GRBs. We have mentioned that the most viable progenitors of short GRBs appear to be mergers of NS–NS and/or NS-BH binaries. Specifically, in the case of NS–NS mergers, the value of the critical mass of the NS, which crucially depends on the nuclear EOS, has been also found to be a most relevant parameter since it defines the fate of the post-merger object.[8] In this section, we discuss the conditions that determine the fate of the NS–NS binary merger by estimating the mass and angular momentum of the post-merger object. Once we know these values, we can compare the mass of the merged core with the value of the NS critical mass obtained for uniformly rotating NSs. Based on this, we can asses whether a massive NS or a BH is formed from the merger.

We proceed to estimate the mass and the angular momentum of the post-merger core via baryonic mass and angular momentum conservation of the system. We adopt for simplicity that nonrotating binary components. We first compute the total baryonic mass of the NS–NS binary $M_b = M_{b_1} + M_{b_2}$ using the relation between the gravitational mass M_i and the baryonic mass M_{b_i} $(i = 1, 2)$ recently obtained in Ref. 21 and given in Eq. (3) assuming $j_{\rm NS} = cJ_{\rm NS}/(GM_\odot^2) = 0$. The

post-merger core will have approximately the entire baryonic mass of the initial binary, i.e. $M_{b,\mathrm{core}} \approx M_b$, since little mass is expected to be ejected during the coalescence process. However, the gravitational mass of the post-merger core cannot be estimated using again the above formula since, even assuming nonrotating binary components, the post-merger core will necessarily acquire a fraction $\eta \leq 1$ of the binary angular momentum at the merger point. One expects a value of η smaller than unity since, during the coalesce, angular momentum is lost, e.g. by gravitational wave emission and it can be also redistributed, e.g. into a surrounding disk.

To obtain the gravitational mass of the post-merger core, we can use again Eq. (3) relating the baryonic mass $M_{b,\mathrm{NS}}$ and the gravitational mass M_{NS} in this case with $j_{\mathrm{NS}} \neq 0$. The mass and angular momentum of the post-merger core, respectively M_{core} and J_{core}, are therefore obtained from baryon mass and angular momentum conservation, i.e.

$$M_{\mathrm{core}} = M_{\mathrm{NS}}, \quad M_{b,\mathrm{core}} = M_{b,\mathrm{NS}} = M_{b_1} + M_{b_2}, \quad J_{\mathrm{core}} = J_{\mathrm{NS}} = \eta J_{\mathrm{merger}}, \quad (8)$$

where J_{merger} is the system angular momentum at the merger point. The value of J_{merger} is approximately given by $J_{\mathrm{merger}} = \mu r^2_{\mathrm{merger}} \Omega_{\mathrm{merger}}$, where $\mu = M_1 M_2/M$ is the binary reduced mass, $M = M_1 + M_2$ is the total binary mass, and r_{merger} and Ω_{merger} are the binary separation and angular velocity at the merger point. If we adopt the merger point where the two stars enter into contact we have $r_{\mathrm{merger}} = R_1 + R_2$, where R_i is the radius (which depend on the EOS) of the i-component of the binary.

Given the parameters of the merging binary, the above equations lead to the merged core properties M_{core} and J_{core} (or j_{core}). These values can be therefore confronted with the values of uniformly rotating, stable NSs to check if such a merger will lead either to a new massive NS or to an unstable merged core collapsing to a BH.

For the sake of exemplifying, let us assume a mass-symmetric binary, $M_1 = M_2 = M/2$. In this case, Eq. (8) together with the above estimate of J_{merger} lead to the angular momentum of the merged core $J_{\mathrm{core}} = (\eta/4)(GM^2/c)\mathcal{C}^{-1/2}$, where $\mathcal{C} \equiv GM_1/(c^2 R_1) = GM_2/(c^2 R_2)$ is the compactness of the merging binary components. Therefore, if we adopt $M_1 = 1.4\ M_\odot$ and $\mathcal{C} = 0.15$ the above equations imply a merged core mass $M_{\mathrm{core}} = (2.61, 2.65)\ M_\odot$ for $\eta = (0, 1)$, i.e. for a dimensionless angular momentum of the merged core $j_{\mathrm{core}} = (0, 5.06)$. Whether or not these pairs $(M_{\mathrm{core}}, j_{\mathrm{core}})$ correspond to stable NSs depend on the nuclear EOS. A similar analysis can be done for any other pair of binary masses.

4. Detectability of GWs Produced by the GRB Progenitors

Having established the nature of the progenitors of each GRB sub-class, we turn now to briefly discuss the detectability of their associated GW emission. The minimum GW frequency detectable by the broadband aLIGO interferometer is

$f_{\rm min}^{\rm aLIGO} \approx 10\,{\rm Hz}$.[35] Since during the binary inspiral, the GW frequency is twice the orbital one, this implies that a binary enters the aLIGO band for orbital periods $P_{\rm orb} \lesssim 0.2\,{\rm s}$. Thus, $\rm CO_{core}$-NS binaries, *in-states* of XRFs and BdHNe, and $\rm CO_{core}$-BH binaries, *in-states* of BH-SN, are not detectable by aLIGO since they have orbital periods $P_{\rm orb} \gtrsim 5\,{\rm min} \gg 0.2\,{\rm s}$. Concerning their *out-states* after the corresponding hypercritical accretion processes, namely νNS–NS, *out-states* of XRFs, and νNS-BH, *out-states* of BdHNe and BH-SNe, they are not detectable by aLIGO at their birth but only when approaching the merger. Clearly, the analysis of the νNS–NS mergers is included in the analysis of the S-GRFs and S-GRBs and, likewise, the merger of νNS-BH binaries is included in the analysis of U-GRBs. In the case of NS-WD binaries, the WD is tidally disrupted by the NS making their GW emission hard to be detected (see, e.g. Ref. 36).

A coalescing binary evolves first through the *inspiral regime* to then pass over a *merger regime*, the latter composed by the plunge leading to the merger itself and by the ringdown (oscillations) of the newly formed object. During the inspiral regime, the system evolves through quasi-circular orbits and is well described by the traditional point-like quadrupole approximation.[37–39] The GW frequency is twice the orbital frequency ($f_s = 2f_{\rm orb}$) and grows monotonically. The energy spectrum during the inspiral regime is: $dE/df_s = (1/3)(\pi G)^{2/3} M_c^{5/3} f_s^{-1/3}$, where $M_c = \mu^{3/5} M^{2/5} = \nu^{3/5} M$ is the so-called *chirp mass* and $\nu \equiv \mu/M$ is the symmetric mass-ratio parameter. A symmetric binary ($m_1 = m_2$) corresponds to $\nu = 1/4$ and the test-particle limit is $\nu \to 0$. The GW spectrum of the merger regime is characterized by a GW burst.[40] Thus, one can estimate the contribution of this regime to the signal-to-noise ratio with the knowledge of the location of the GW burst in the frequency domain and of the energy content. The frequency range spanned by the GW burst is $\Delta f = f_{\rm qnm} - f_{\rm merger}$, where $f_{\rm merger}$ is the frequency at which the merger starts and $f_{\rm qnm}$ is the frequency of the ringing modes of the newly formed object after the merger, and the energy emitted is $\Delta E_{\rm merger}$. With these quantities defined, one can estimate the typical value of the merger regime spectrum as: $dE/df_s \approx \Delta E_{\rm merger}/\Delta f$. Unfortunately, the frequencies and energy content of the merger regime of the above merging binaries are such that it is undetectable by LIGO.[41]

Since the GW signal is deep inside the detector noise, the signal-to-noise ratio (ρ) is usually estimated using the matched filter technique.[42] The exact position of the binary relative to the detector and the orientation of the binary rotation plane are usually unknown, thus it is a common practice to average over all the possible locations and orientations, i.e.[42]: $\langle \rho^2 \rangle = 4 \int_0^\infty \langle |\tilde{h}(f)|^2 \rangle / S_n(f) df = 4 \int_0^\infty h_c^2(f)/[f^2 S_n(f)] df$, where f is the GW frequency in the detector frame, $\tilde{h}(f)$ is the Fourier transform of $h(t)$, and $\sqrt{S_n(f)}$ is the one-sided amplitude spectral density of the detector noise, and $h_c(f)$ is the characteristic strain, $h_c = (1+z)/(\pi d_l)\sqrt{(1/10)(G/c^3)(dE/df_s)}$. We recall that in the detector frame, the GW frequency is redshifted by a factor $1+z$ with respect to the one in the source frame,

f_s, i.e. $f = f_s/(1+z)$ and d_l is the luminosity distance to the source. We adopt a ΛCDM cosmology with $H_0 = 71\,\mathrm{km\,s^{-1}\,Mpc^{-1}}$, $\Omega_M = 0.27$ and $\Omega_\Lambda = 0.73$.[43]

A threshold $\rho_0 = 8$ in a single detector is adopted by LIGO.[44] This minimum ρ_0 defines a maximum detection distance or GW horizon distance, say d_{GW}, that corresponds to the most optimistic case when the binary is just above the detector and the binary plane is parallel to the detector plane. In order to give an estimate, the annual number of merging binaries associated with the above GRB subclasses detectable by aLIGO, we can use the lower and upper values of the aLIGO *search volume* defined by $\mathcal{V}_s = V_{\mathrm{max}}^{\mathrm{GW}}\mathcal{T}$, where $V_{\mathrm{max}}^{\mathrm{GW}} = (4\pi/3)\mathcal{R}^3$, where $\mathcal{T}$ is the observing time and $\mathcal{R}$ is the so-called *detector range* defined by $\mathcal{R} = \mathcal{F}d_{\mathrm{GW}}$, with $\mathcal{F}^{-1} = 2.2627$ (see, Refs. 44 and 45, for details). For a $(1.4+1.4)\,M_\odot$ NS binary and the three following different observational campaigns we have[44]: 2015/2016 (O1; $\mathcal{T} = 3\,\mathrm{months}$) $\mathcal{V}_S = (0.5\text{–}4)\times 10^5\,\mathrm{Mpc^3\,yr}$, 2017/2018 (O3; $\mathcal{T} = 9\,\mathrm{months}$) $\mathcal{V}_S = (3\text{–}10)\times 10^6\,\mathrm{Mpc^3\,yr}$, and the entire network including LIGO-India at design sensitivity (2022+; $\mathcal{T} = 1\,\mathrm{yr}$) $\mathcal{V}_S = 2\times 10^7\,\mathrm{Mpc^3\,yr}$. The maximum possible sensitivity reachable in 2022+ leads to $d_{\mathrm{GW}} \approx 0.2\,\mathrm{Gpc}$, hence $V_{\mathrm{max}}^{\mathrm{GW}} \approx 0.033\,\mathrm{Gpc^3}$, for such a binary. One can use this information for other binaries with different masses taking advantage of the fact that d_{GW} scales with the binary chirp mass as $M_c^{5/6}$. The expected GW detection rate by aLIGO can be thus estimated as: $\dot{N}_{\mathrm{GW}} \equiv \rho_{\mathrm{GRB}} V_{\mathrm{max}}^{\mathrm{GRB}}$, where ρ_{GRB} is the inferred occurrence rate of GRBs shown in Table 1 computed in Ref. 6. Bearing the above in mind, it is easy to check that there is a low probability for aLIGO to detect the GW signals associated with the GRB binary progenitors: indeed in the best case of the 2022+ observing rung one obtains, respectively, $\sim$1 detection every 3 and 5 yr for U-GRBs and S-GRFs.

5. Conclusions

There is accumulated evidence on the binary nature of long and short GRBs. Such binaries are composed of $\mathrm{CO_{cores}}$, NSs, BHs and WDs in different combinations. We have here focused on the salient aspects of the NS physics relevant for the understanding of these binaries and their implications in GRB astrophysics, including their associated GW emission. We have discussed the crucial role of the NS critical mass in discriminating the GRB sub-classes. Therefore, we expect that the increasing amount of GRB high-quality data will help in constraining the NS critical mass with high accuracy with the most welcome result of constraining the NS matter content and the corresponding nuclear EOS.

Acknowledgments

M. Karlica, M. Kovacevic and Y. A. are supported by the Erasmus Mundus Joint Doctorate Program Grant Nos. 2013–1471, 2013–1471 and 2014–0707, respectively, from EACEA of the European Commission. M. M. and J. A. R. acknowledge the partial support of the Project No. 3101/GF4 IPC-11, and the target program F.0679

of the Ministry of Education and Science of the Republic of Kazakhstan. C. C. and S. F. acknowledge INdAM-GNFM for support.

References

1. E. P. Mazets, S. V. Golenetskii, V. N. Ilinskii, V. N. Panov, R. L. Aptekar, I. A. Gurian, M. P. Proskura, I. A. Sokolov, Z. I. Sokolova and T. V. Kharitonova, *Astrophys. Space Sci.* **80** (1981) 3.
2. R. W. Klebesadel, The durations of gamma-ray bursts, in *Gamma-Ray Bursts — Observations, Analyses and Theories*, eds. C. Ho, R. I. Epstein and E. E. Fenimore (Cambridge University Press, 1992).
3. J.-P. Dezalay, C. Barat, R. Talon, R. Syunyaev, O. Terekhov and A. Kuznetsov, *AIP Conference Proceedings* **265** (1991) 304–309.
4. C. Kouveliotou, C. A. Meegan, G. J. Fishman, N. P. Bhat, M. S. Briggs, T. M. Koshut, W. S. Paciesas and G. N. Pendleton, *Astrophys. J.* **413** (1993) L101.
5. M. Tavani, *Astrophys. J.* **497** (1998) L21.
6. R. Ruffini, J. A. Rueda, M. Muccino, Y. Aimuratov, L. M. Becerra, C. L. Bianco, M. Kovacevic, R. Moradi, F. G. Oliveira, G. B. Pisani and Y. Wang, *Astrophys. J.* **832** (2016) 136.
7. R. Ruffini, Y. Wang, M. Enderli, M. Muccino, M. Kovacevic, C. L. Bianco, A. V. Penacchioni, G. B. Pisani and J. A. Rueda, *Astrophys. J.* **798** (2015) 10.
8. R. Ruffini, M. Muccino, M. Kovacevic, F. G. Oliveira, J. A. Rueda, C. L. Bianco, M. Enderli, A. V. Penacchioni, G. B. Pisani, Y. Wang and E. Zaninoni, *Astrophys. J.* **808** (2015) 190.
9. R. Ruffini, M. G. Bernardini, C. L. Bianco, L. Vitagliano, S.-S. Xue, P. Chardonnet, F. Fraschetti and V. Gurzadyan, Black hole physics and astrophysics: The GRB-Supernova connection and URCA-1–URCA-2, in *The Tenth Marcel Grossmann Meeting*, eds. M. Novello, S. Perez Bergliaffa and R. Ruffini (World Scientific, Singapore, 2006).
10. L. Izzo, J. A. Rueda and R. Ruffini, *Astron. Astrophys.* **548** (2012) L5.
11. J. A. Rueda and R. Ruffini, *Astrophys. J.* **758** (2012) L7.
12. C. L. Fryer, J. A. Rueda and R. Ruffini, *Astrophys. J.* **793** (2014) L36.
13. L. Becerra, F. Cipolletta, C. L. Fryer, J. A. Rueda and R. Ruffini, *Astrophys. J.* **812** (2015) 100.
14. C. L. Fryer, F. G. Oliveira, J. A. Rueda and R. Ruffini, *Phys. Rev. Lett.* **115** (2015) 231102.
15. L. Becerra, C. L. Bianco, C. L. Fryer, J. A. Rueda and R. Ruffini, *Astrophys. J.* **833** (2016) 107.
16. J. Goodman, *Astrophys. J.* **308** (1986) L47.
17. B. Paczynski, *Astrophys. J.* **308** (1986) L43.
18. D. Eichler, M. Livio, T. Piran and D. N. Schramm, *Nature* **340** (1989) 126.
19. R. Narayan, T. Piran and A. Shemi, *Astrophys. J.* **379** (1991) L17.
20. E. Berger, *Annu. Rev. Astron. Astrophys.* **52** (2014) 43.
21. F. Cipolletta, C. Cherubini, S. Filippi, J. A. Rueda and R. Ruffini, *Phys. Rev. D* **92** (2015) 023007.
22. C. L. Fryer, W. Benz and M. Herant, *Astrophys. J.* **460** (1996) 801.
23. R. A. Chevalier, *Astrophys. J.* **346** (1989) 847.
24. Y. B. Zel'dovich, L. N. Ivanova and D. K. Nadezhin, *Sov. Astron.* **16** (1972) 209.
25. R. Ruffini and J. Wilson, *Phys. Rev. Lett.* **31** (1973) 1362.

26. C. L. Fryer, F. Herwig, A. Hungerford and F. X. Timmes, *Astrophys. J.* **646** (2006) L131.
27. C. L. Fryer, *Astrophys. J.* **699** (2009) 409.
28. L. Izzo, R. Ruffini, A. V. Penacchioni, C. L. Bianco, L. Caito, S. K. Chakrabarti, J. A. Rueda, A. Nandi and B. Patricelli, *Astron. Astrophys.* **543** (2012) A10.
29. N. R. Tanvir, A. J. Levan, A. S. Fruchter, J. Hjorth, R. A. Hounsell, K. Wiersema and R. L. Tunnicliffe, *Nature* **500** (2013) 547.
30. N. R. Sibgatullin and R. A. Sunyaev, *Astron. Lett.* **26** (2000) 772.
31. C. L. Fryer, S. E. Woosley and D. H. Hartmann, *Astrophys. J.* **526** (1999) 152.
32. M. Dominik, K. Belczynski, C. Fryer, D. E. Holz, E. Berti, T. Bulik, I. Mandel and R. O'Shaughnessy, *Astrophys. J.* **759** (2012) 52.
33. K. A. Postnov and L. R. Yungelson, *Living Rev. Rel.* **17** (2014) 3.
34. J. G. Hills, *Astrophys. J.* **267** (1983) 322.
35. LIGO Scientific Collab. (J. Aasi *et al.*), *Class. Quantum Grav.* **32** (2015) 074001.
36. V. Paschalidis, M. MacLeod, T. W. Baumgarte and S. L. Shapiro, *Phys. Rev. D* **80** (2009) 024006.
37. P. C. Peters and J. Mathews, *Phys. Rev.* **131** (1963) 435.
38. P. C. Peters, *Phys. Rev.* **136** (1964) 1224.
39. M. Rees, R. Ruffini and J. A. Wheeler, *Black Holes*, *Gravitational Waves and Cosmology* (Gordon and Breach Science Publishers, New York, 1974).
40. M. Davis, R. Ruffini, W. H. Press and R. H. Price, *Phys. Rev. Lett.* **27** (1971) 1466.
41. R. Ruffini, J. Rodriguez, M. Muccino, J. A. Rueda, Y. Aimuratov, U. Barres de Almeida, L. Becerra, C. L. Bianco, C. Cherubini, S. Filippi, D. Gizzi, M. Kovacevic, R. Moradi, F. G. Oliveira, G. B. Pisani and Y. Wang, arXiv:1602.03545.
42. É. É. Flanagan and S. A. Hughes, *Phys. Rev. D* **57** (1998) 4535.
43. M. Rigault, G. Aldering, M. Kowalski, Y. Copin, P. Antilogus, C. Aragon, S. Bailey, C. Baltay, D. Baugh, S. Bongard, K. Boone, C. Buton, J. Chen, N. Chotard, H. K. Fakhouri, U. Feindt, P. Fagrelius, M. Fleury, D. Fouchez, E. Gangler, B. Hayden, A. G. Kim, P.-F. Leget, S. Lombardo, J. Nordin, R. Pain, E. Pecontal, R. Pereira, S. Perlmutter, D. Rabinowitz, K. Runge, D. Rubin, C. Saunders, G. Smadja, C. Sofiatti, N. Suzuki, C. Tao and B. A. Weaver, *Astrophys. J.* **802** (2015) 20.
44. B. P. Abbott *et al.*, *Living Rev. Rel.* **19** (2016) 1.
45. L. S. Finn and D. F. Chernoff, *Phys. Rev. D* **47** (1993) 2198.

Review

International Journal of Modern Physics D
Vol. 26, No. 10 (2017) 1730019 (47 pages)

DOI: 10.1142/S0218271817300191

The cosmic matrix in the 50th anniversary of relativistic astrophysics*

R. Ruffini[†,‡,§,‡‡], Y. Aimuratov[†,‡,¶], L. Becerra[†,‡], C. L. Bianco[†,‡], M. Karlica[†,‡,¶], M. Kovacevic[†,‡,¶], J. D. Melon Fuksman[†,‡], R. Moradi[†,‡], M. Muccino[†,‡], A. V. Penacchioni[‖,**], G. B. Pisani[†,‡], D. Primorac[†,‡], J. A. Rueda[†,‡,§], S. Shakeri[†,††], G. V. Vereshchagin[†], Y. Wang[†,‡] and S.-S. Xue[†]

[†]*ICRANet, Piazza della Repubblica 10, I-65122 Pescara, Italy*

[‡]*Dip. di Fisica and ICRA, Sapienza Università di Roma, P.le Aldo Moro 5, I-00185 Rome, Italy*

[§]*ICRANet-Rio, Centro Brasileiro de Pesquisas Físicas, Rua Dr. Xavier Sigaud 150, 22290–180 Rio de Janeiro, Brazil*

[¶]*Université de Nice Sophia Antipolis, CEDEX 2, Grand Château Parc Valrose, Nice, France*

[‖]*ASI Science Data Center, Via del Politecnico s.n.c., I-00133 Rome, Italy*

[**]*Department of Physical Sciences, Earth and Environment, University of Siena, Via Roma 56, I-53100 Siena, Italy*

[††]*Department of Physics, Isfahan University of Technology, 84156–83111, Iran*

[‡‡]*ruffini@icra.it*

Received 24 March 2017
Accepted 28 March 2017
Published 11 May 2017

Our concept of induced gravitational collapse (IGC paradigm) starting from a supernova occurring with a companion neutron star, has unlocked the understanding of seven different families of gamma ray bursts (GRBs), indicating a path for the formation of black holes in the universe. An authentic laboratory of relativistic astrophysics has been unveiled in which new paradigms have been introduced in order to advance knowledge of the most energetic, distant and complex systems in our universe. A novel cosmic matrix paradigm has been introduced at a relativistic cosmic level, which parallels the concept of an S-matrix introduced by Feynmann, Wheeler and Heisenberg in the quantum world of microphysics. Here the "in" states are represented by a neutron star and a supernova, while the "out" states, generated within less than a second, are a new neutron star and a black hole. This novel field of research needs very powerful technological observations in all wavelengths ranging from radio through optical, X-ray and gamma ray radiation all the way up to ultra-high-energy cosmic rays.

Keywords: Binaries; black hole physics; gamma-ray bursts; neutron stars; supernovae; white dwarfs.

PACS Number(s): 04.70.−s, 98.70.Rz, 97.60.Bw, 97.80.−d, 97.60.Jd, 97.20.Rp

*Based on talks presented at the Fourteenth Marcel Grossmann Meeting on General Relativity, Rome, July 2015.

1. Introduction and the First Paradigm

We begin with a personal historical overview by the lead author.

Supernovae (SNe) have been known and studied for a long time, from 1054 A.D. to the classic work of Baade and Zwicky in 1934[1,2] and of Oppenheimer and his students in 1939, and to the 1968 detection of the first pulsar, first in radio and then in optical wavelengths, located at the center of the Crab Nebula. The explanation of the energetics of pulsars as originating from the rotational energy of neutron stars (NSs) gave the first clear evidence for the existence of NSs through this discovery and led to the conclusion that the Crab supernova originated from gravitational collapse to a NS.

The next fundamental discovery came from the pioneering work of Riccardo Giacconi and his group with the X-ray astronomy detection of Sco X-1.[3] In 1967, this X-ray source was theoretically interpreted by Shklovskii[4] as originating from a binary system containing a NS. This was followed by the launch of the UHURU satellite on December 12, 1970. The coordination of the X-ray observations with ground-based optical telescope observations has since led to the discovery of a large number of binary X-ray sources in our galaxy.[5] These systems give evidence for: (a) an X-ray emission due to accretion in a binary system composed of a massive star and a gravitational collapsed star, with X-ray luminosities originating from gravitational energy a million times more intense than those expected from the star's thermonuclear evolution; (b) the first determination of NS masses well above the value of the critical mass expected by Oppenheimer and Volkoff, see e.g. Fig. 1 on Cen X-3 and (c) the first identification of a black hole in Cygnus X-1.[6–8]

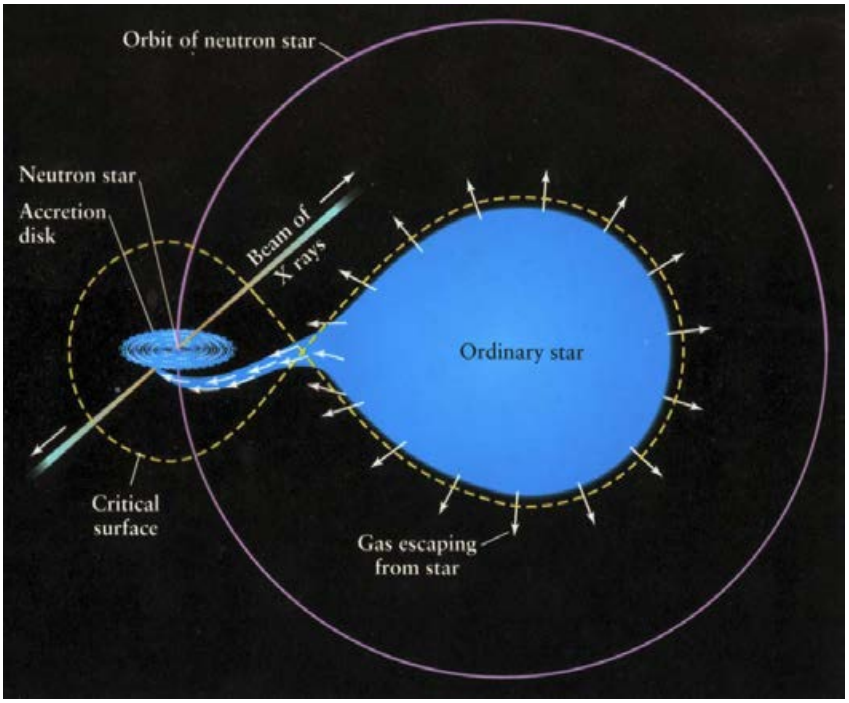

Fig. 1. X-ray binary Centaurus X3 detected by UHURU satellite. The pulse period is 4.84 s. A binary motion signature was found with a 1.7 day orbital period, thanks to UHURU.

Observations of GRBs only date back to their detection by the Vela satellites in the early 1970s, see e.g. Ref. 9 and references therein. It was only after the observations in 1997 by the BeppoSAX satellite[10] which allowed the optical identification of GRBs. From the estimates of their cosmological distances, their enormous energetics is 10^3–10^4 times larger than those of supernovas, were able to be determined: energies of the order of 10^{54} erg, equivalent to the release of $\sim M_\odot c^2$ in few tens of seconds. This result had been predicted already in 1975 on purely theoretical grounds assuming that GRBs originated from an electron–positron plasma in the gravitational collapse to a Kerr–Newman black hole, see Ruffini, "Physics outside the horizon of a black hole" in Refs. 5 and 11. From these experiences, I had formulated a basic paradigm to serve as a guideline to interpret unitarily and consistently the occurrence of supernovae, the existence of binary X-ray sources and also possibly the nature of GRBs[12–14]:

First paradigm

- *Supernovae originate from gravitational collapse to a neutron star.*
- *GRBs originate during the gravitational collapse to a black hole (BH).*
- *In studying a massive star, its binary nature and possibly the multiple systems involved in its behavior should of necessity be properly taken into account.*

We will see that the enforcement of this minimal set of assumptions has been extremely valuable. As the knowledge of these systems has evolved, I introduced two new and more specific paradigms narrowing in on the nature of the sources — each new paradigm being in clear agreement with the previous ones. I was well aware of a vast literature contemplating the possibility of relating different supernovae types to black holes over an extremely wide range of masses but I was very doubtful about these considerations since they violated more then one principle of my paradigm, they neglected a wealth of observational data, and they were based on a somewhat restrictive property related to metallicity in the thermonuclear evolution expected in a single star system (see e.g. Ref. 15). Moreover, after the splendid observations of the Hubble Space Telescope,[16] today we begin to understand that even Eta Carinae is a binary system[17,18] and that massive single stars are very likely a set of measure zero: massiveness implies multiplicity.

This situation has become even more interesting since the unexpected observation of a temporal and spatial coincidence between the occurrence of a GRB and a SN explosion, see e.g. GRB 980425[19] and SN 1998bw,[20,21] see Fig. 2. The explanation of this coincidence has led our group to introduce the induced gravitational collapse (IGC) paradigm (paradigm 1), a many-cosmic-body-interaction, and consequently we introduced a cosmic matrix: a C-matrix; see Fig. 3. The many-particle interaction in the S-matrix is confronted with this new concept of C-matrix involving a many-body interaction among astrophysical systems. This unprecedented situation has led to a series of new conceptual paradigms and the opening up of a new

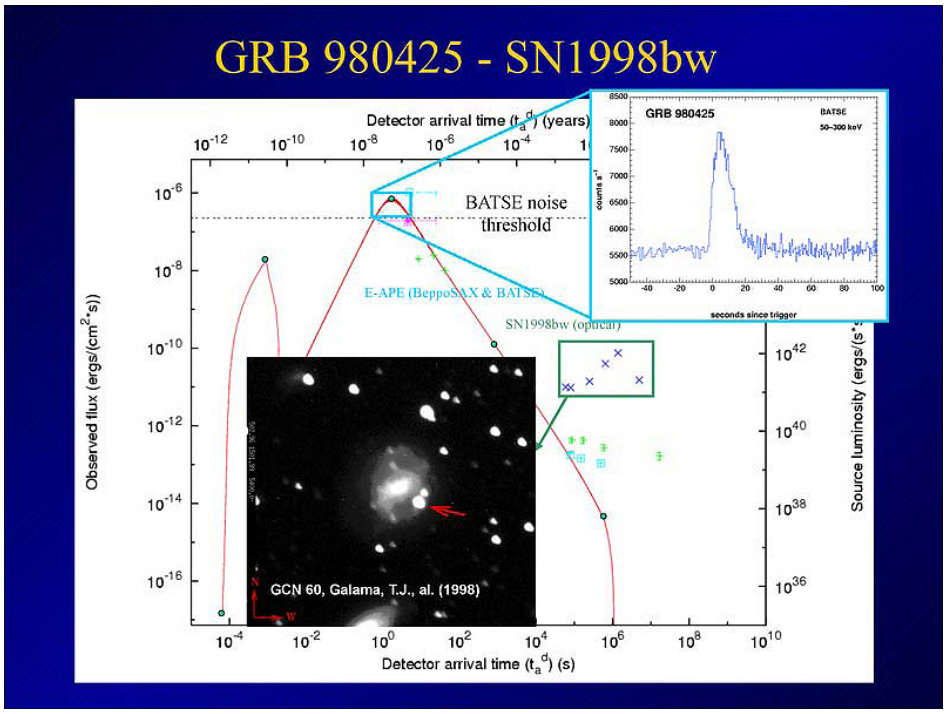

Fig. 2. GRB980425 and supernova SN 1998bw.

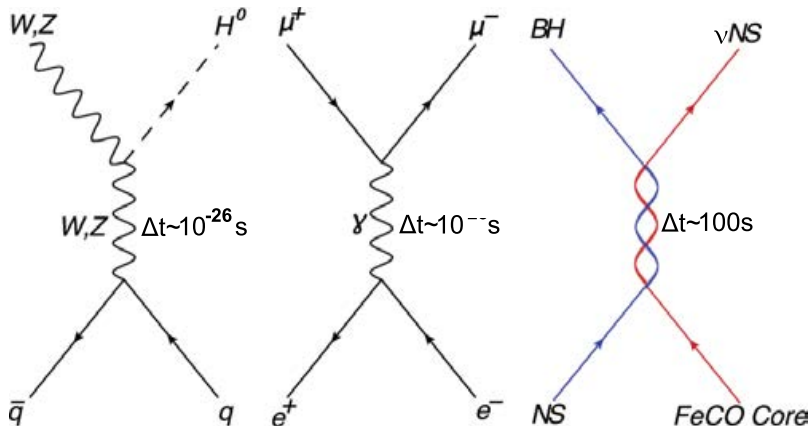

Fig. 3. The new concept of "C-matrix", compared with the usual S-matrix. From Ref. 23.

understanding of a vast number of previously unknown domains within physics and astrophysics, see e.g. Ref. 22 and references therein.

1.1. *Crab pulsar: A neutron star and a black hole*

That NSs exist in nature has been proven by the discovery of pulsars. The year 1967 marked the discovery of the first pulsar, observed at radio wavelengths in November 28, 1967 by Jocelyn Bell Burnell and Antony Hewish.[24] Just a few months later, the pulsar NP0532 was found in the center of the Crab Nebula and observed first at radio wavelengths and soon after at optical wavelengths, see Fig. 4.

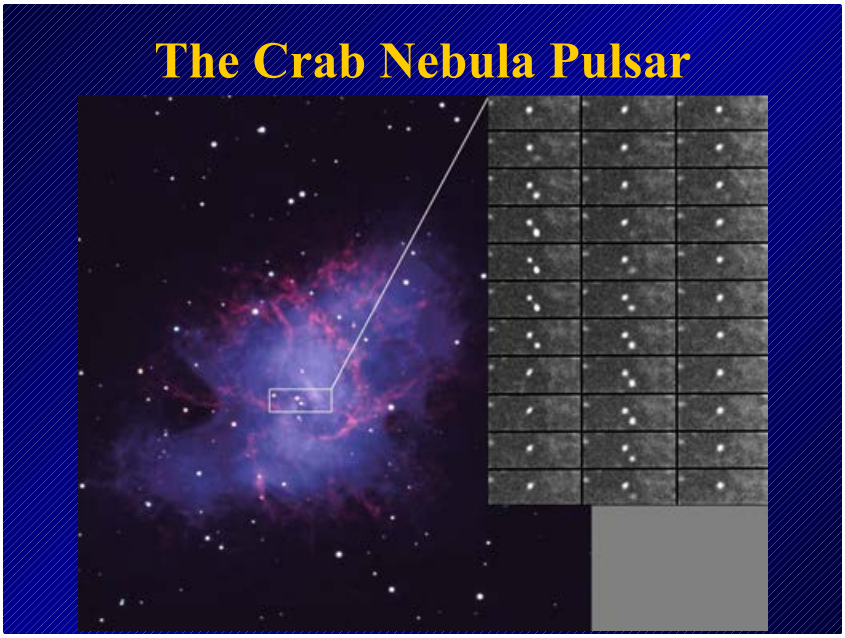

Fig. 4. The sequence of black and white images on the right is separated by one ms intervals, from which it is clear that the left star is a pulsar with a period of $P = 33$ ms. This period changes with a rate dP/dt of 12.5 ms per year. The fact that the loss of rotational energy of a NS with moment of inertia I is given by $dE/dt \propto -I(1/P^3)dP/dt$ explains precisely the energetics of the pulsar and proves at once the existence of NSs.[27]

The discovery of NSs led our small group working around John Wheeler in Princeton to direct our main attention to go further and address the study of continuous gravitational collapse to a black hole as first introduced by Oppenheimer and his students (see Fig. 5). The work in Princeton addressed the topic of black holes, gravitational waves (GWs) and cosmology. A summary of that work can be found in Refs. 25 and 26, where a wide range of topics in relativistic astrophysics was reconsidered, including the possible sources of GWs, the cross-sections of GW detectors, and especially, an entirely new family of astrophysical phenomena occurring around NSs and black holes and in cosmology.

One of the most important results in the physics and astrophysics of BHs has been the BH mass-energy formula (see Fig. 6). From this, indeed, it became clear that up to 50% of the mass-energy of a BH could be extracted by using reversible transformations.[28] It then followed that during the formation of a BH, some of the most energetic processes in the universe should exist, releasing an energy of the order of $\sim 10^{54}$ erg for a $1\,M_\odot$ BH (see Fig. 6).

1.2. *The Vela and CGRO satellites and GRBs*

In Ref. 29, I described how the observations of the Vela satellites were fundamental in discovering GRBs, see Fig. 7. Just a few months after the public announcement of their discovery,[9] I formulated a theoretical model with T. Damour, a collaborator in Princeton, based on the extractable energy of a Kerr–Newmann black hole through a vacuum polarization process giving rise to GRBs, see Fig. 8. In our paper,[11]

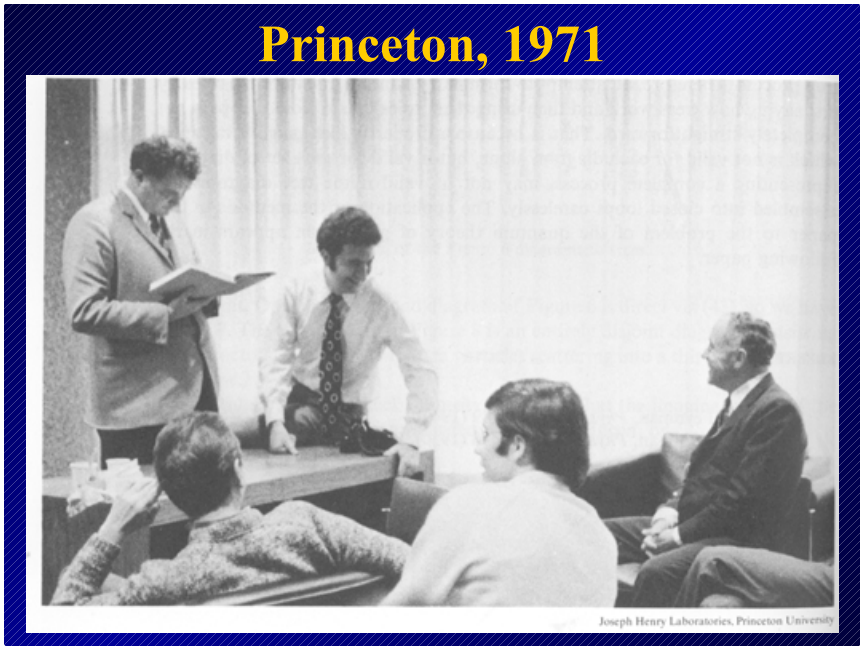

Fig. 5. Standing to the left Tullio Regge, sitting on the desk myself and sitting on the chair John Wheeler.

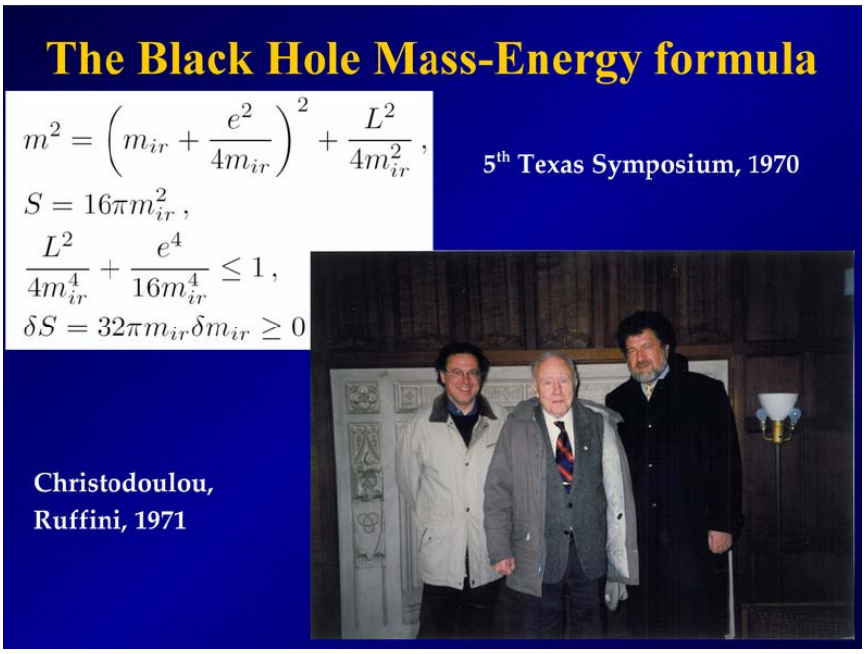

Fig. 6. The black hole mass-energy formula. From Ref. 28.

we pointed out that vacuum polarization occurring in the field of electromagnetic BHs could release an enormous e^+e^- plasma which self-accelerates and gives origin to the GRB phenomenon. Energetics for GRBs all the way up to $\sim 10^{55}$ ergs was theoretically predicted for a $10\,M_\odot$ BH.[12] The dynamics of this e^-e^+ plasma was first studied by J. R. Wilson and myself with the collaboration of Xue and Salmonson.[30,31]

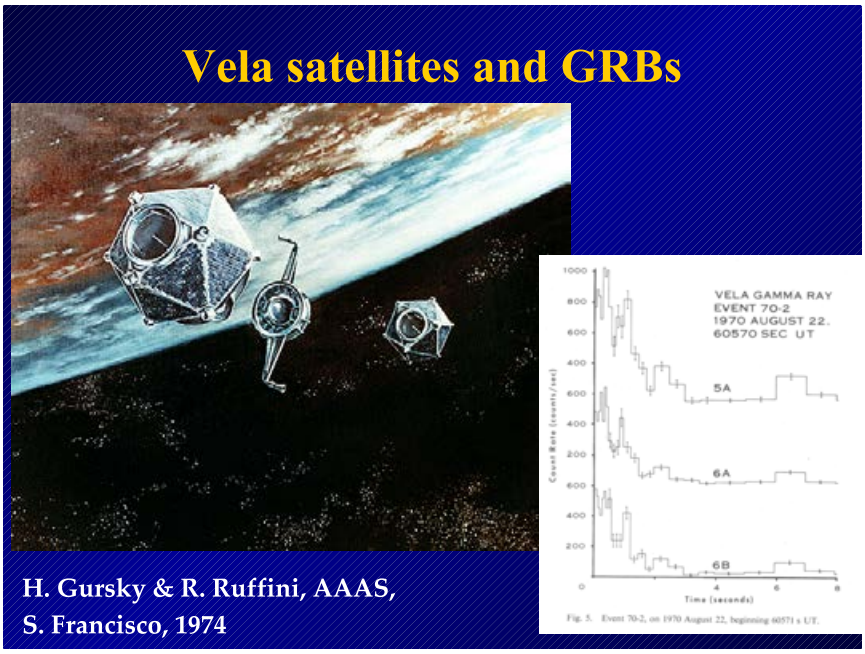

Fig. 7. The Vela satellites, see e.g. the Ian Strong chapter in Ref. 9.

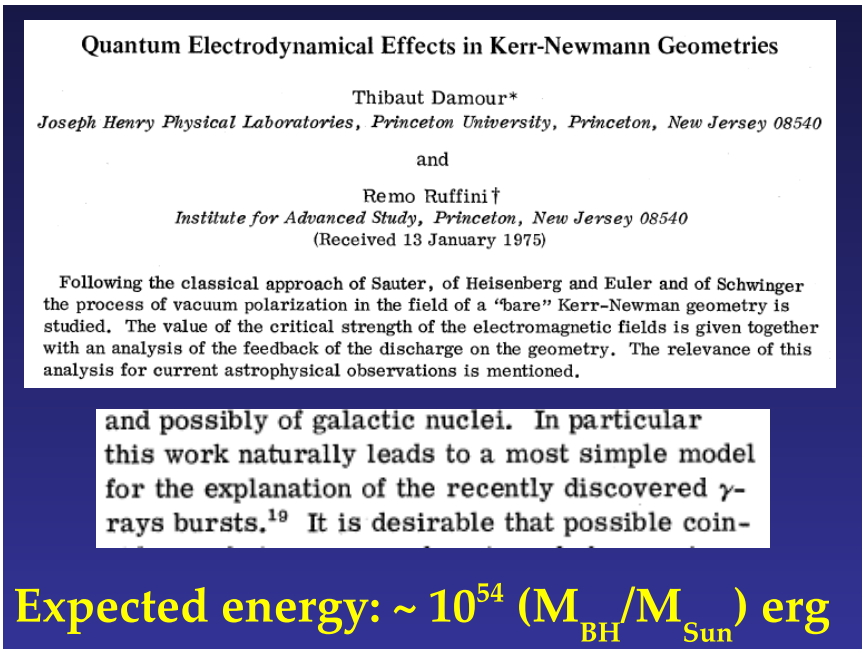

Fig. 8. The classic paper Ref. 11 on the extractable energy of a Kerr–Newmann black hole through vacuum polarization.

Initially it was difficult to model GRBs to understand their nature since their distances from the Earth were unknown, and thousands of models were presented[32] attempting to explain the mystery they presented. The launching of the Compton Gamma Ray Observatory (CGRO) with the BATSE detectors on-board (see Fig. 9) led to the following important discoveries:

(1) there is a homogeneous distribution of GRBs in the universe,

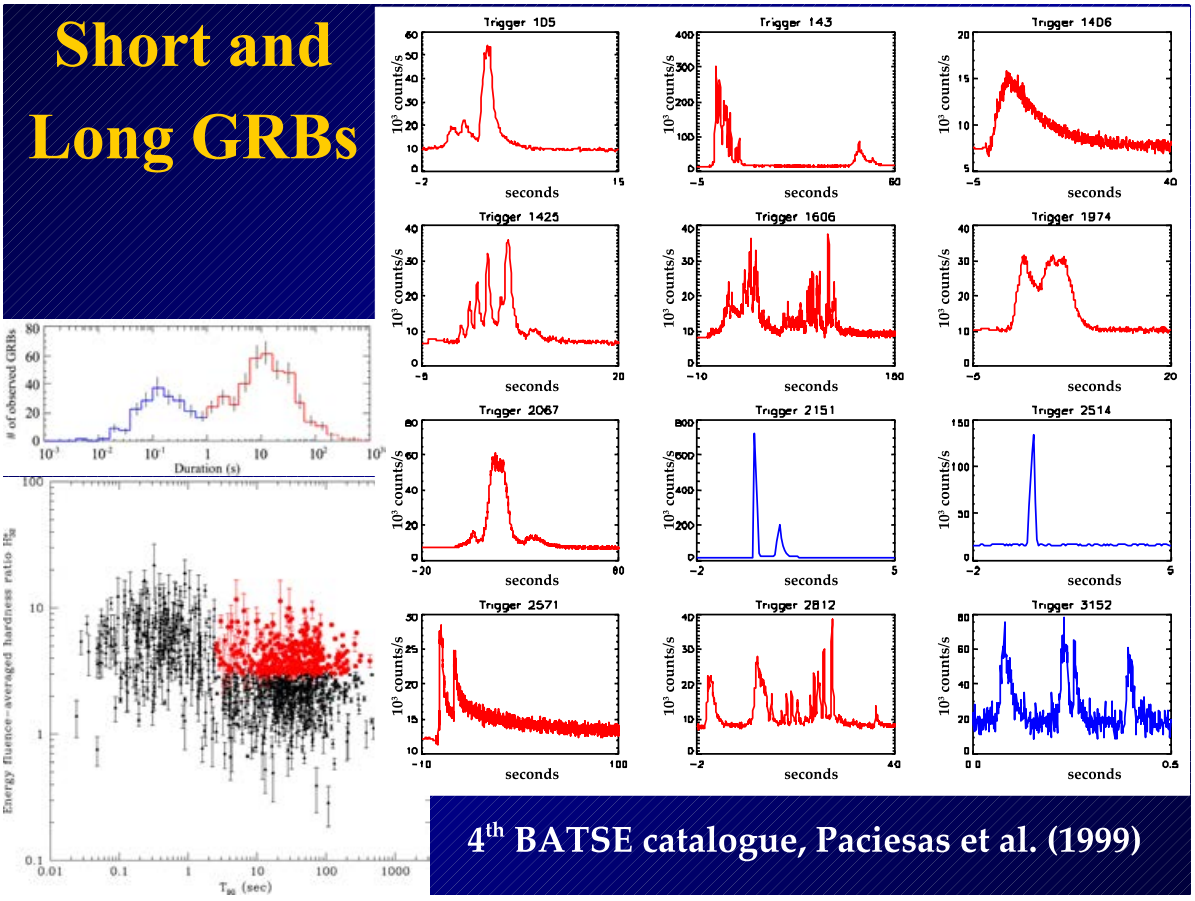

Fig. 9. Short and long GRB light curves and their temporal distribution from the 4th BATSE catalog, Ref. 33.

(2) short GRBs exist lasting less than a second, and
(3) long GRBs exist lasting more than one second.

The crucial contribution to interpreting GRBs came from the Italian-Dutch BeppoSAX satellite, see Fig. 10 (e.g. Ref. 34) which led to a much more precise definition of their position in the sky obtained using a wide field X-ray camera and narrow field instrumentation. This enabled the optical identification of GRBs and the determination of their cosmological redshift, and consequently of their energetics, which turned out to be up to $\sim 10^{55}$ erg, previously predicted in Ref. 11. Since that time no fewer than 10 different X- and γ-ray observatory missions and numerous observations at optical and radio wavelengths have allowed us to reach a deeper understanding of the nature of GRBs, see Fig. 10.

After reviewing below the basic differences between the most quoted "fireball model" of GRBs and our "fireshell model", we will describe the IGC paradigm (the "second paradigm") and the analysis of the GRB 090618 in the fireshell scenario.[35] This will show the first application of the IGC paradigm to it.[36] We will then indicate some recent results on a possible distance indicator inferred from a GRB-SN correlation within the IGC paradigm,[37] and then give some additional evidence coming from the identification of the NS created by the supernova and its use as a

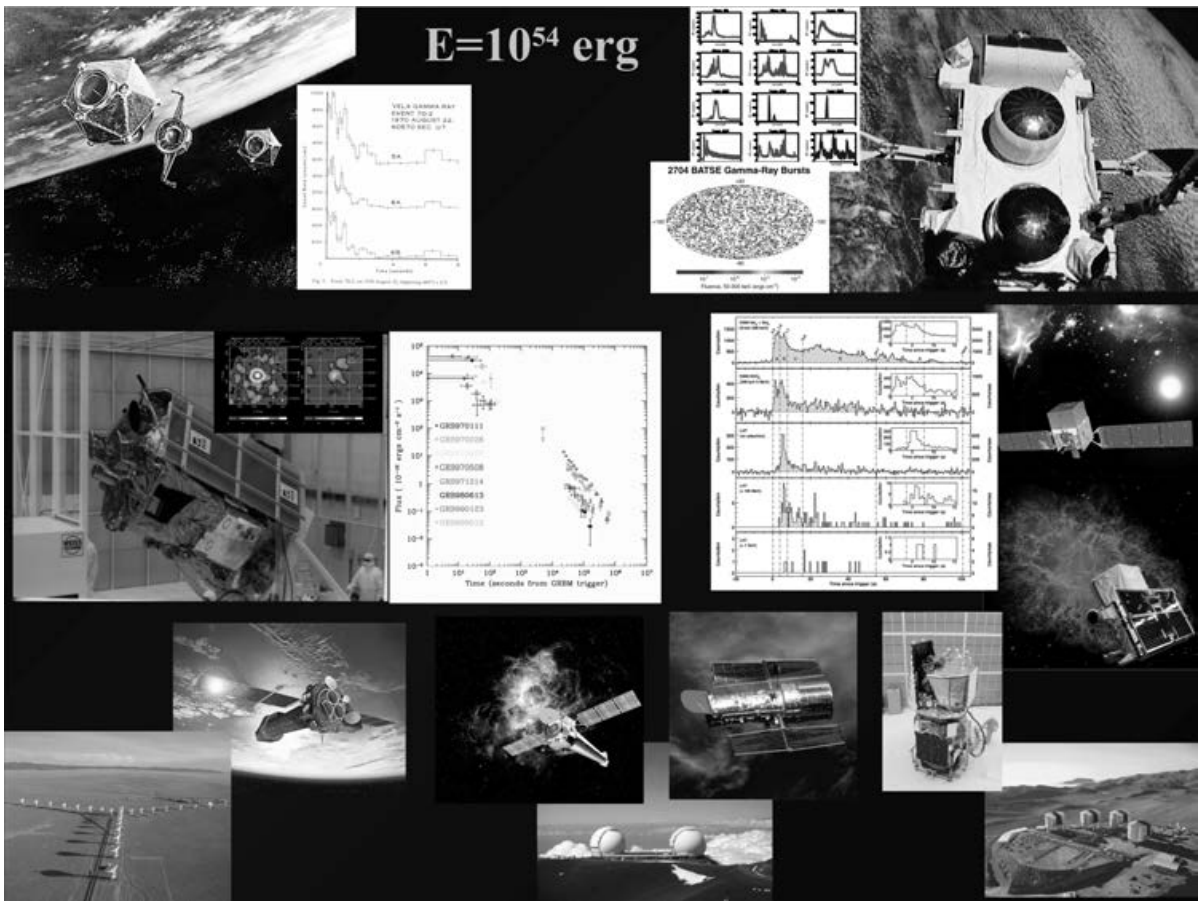

Fig. 10. The flotilla of space missions and the principal optical and radio astronomical observatories which participated in establishing the cosmological distances and energetics of GRBs extending up to the limit of 10^{55} Erg predicted in 1975, see Fig. 8. Most significant has been the central role played by the BeppoSAX mission through its coordinate observations of the narrow high energy field instruments and the wide field X-ray cameras, which led to the discovery of prolonged GRB emission and consequently to the optical identification of the GRB sources.

cosmological distance candle. Next we will turn to the first example of the genuine short GRB 090227B[38] leading to black hole formation. Finally, we will illustrate a brand new paradigm dealing with the two families of short and long GRBs and a special role of the formation or not of a black hole.

1.3. *The fireball model compared and contrasted with the fireshell model*

A variety of models have been developed to theoretically explain the observational properties of GRBs, among which the fireball model[39] is one of those most often used. In Refs. 40–43, it was proposed that the sudden release of a large quantity of energy in a compact region can lead to an optically thick photon–lepton plasma and to the production of e^+e^- pairs. The sudden initial total annihilation of the e^+e^- plasma was assumed by Cavallo and Rees,[40] leading to an enormous release of energy pushing on the circumburst medium (CBM): the "fireball", see e.g. Ref. 43 and references therein.

An alternative approach originating from the gravitational collapse to a black hole is the fireshell model, see e.g. Refs. 22 and 44. Here the GRB originates from an optically thick e^+e^- plasma in thermal equilibrium, with a total energy of $E_{\rm tot}^{e^\pm}$. This plasma is initially confined between the radius r_h of a black hole and its dyadosphere[45,46] radius

$$r_{ds} = r_h \left[2\alpha \frac{E_{\rm tot}^{e^+e^-}}{m_e c^2} \left(\frac{\hbar}{\frac{m_e c}{r_h}} \right)^3 \right]^{1/4} , \tag{1}$$

where α is the usual fine structure constant, $\hbar$ is the Planck's constant, c is the speed of light, and m_e is the mass of the electron. The lower limit of $E_{\rm tot}^{e^\pm}$ is assumed to coincide with the observed isotropic energy $E_{\rm iso}$ emitted in X-rays and gamma rays alone in the GRB. The condition of thermal equilibrium assumed in this model[47] distinguishes it from alternative ones, e.g. Ref. 40.

1.3.1. *The fireball model*

In the fireball model, the prompt emission, including the sharp luminosity variations,[48] is caused by the prolonged and variable activity of the "inner engine".[39,49] The conversion of the fireball energy to radiation is made by shocks, either internally (when faster moving matter overtakes a slower moving shell, see Ref. 49) or externally (when the moving matter is slowed down by the external medium surrounding the burst, see Ref. 50).

Synchrotron emission from relativistic electrons in the CBM has been given much attention, possibly accompanied by self-synchrotron Compton (SSC) emission, in order to explain the observed GRB spectra. These processes were purported to be consistent with the observational data of some GRBs.[51,52] However, several limitations have been reported in relation to the low-energy spectral slopes of time-integrated spectra[53–56] and the time-resolved spectra.[56] Additional limitations on SSC emission have also been pointed out in Refs. 57 and 58.

The latest phases of the afterglow are described in the fireball model by a single ultrarelativistic jetted emission assuming an equation of motion given by the Blandford-McKee self-similar power-law solution.[59] The maximum Lorentz factor of the fireball is estimated from the temporal occurrence of the peak of the optical emission, which is identified with the peak of the forward external shock emission[60,61] in the thin shell approximation.[62]

Several partly alternative and/or complementary scenarios have been developed independent of the fireball model, e.g. based on quasi-thermal Comptonization,[63] Compton drag emission,[64,65] synchrotron emission from a decaying magnetic field,[66] jitter radiation,[67] Compton scattering of synchrotron self-absorbed photons,[68,69] and photospheric emission.[70–76] In particular, it was pointed out in Ref. 75 that photospheric emission overcomes some of the difficulties of purely nonthermal emission models. The collapsar model, leading to the astrophysical framework of the

"fireball" model characterized by a jetted ultrarelativistic (Lorentz gamma factor 100–500) emission, was then introduced.

1.3.2. *The fireshell model*

Let us turn to the fireshell model. The rate equation for the e^+e^- pair plasma and its dynamics (the pair-electromagnetic pulse or PEM pulse for short) have been described in Refs. 30 and 31. This equation applies to any electron–positron plasma giving rise to the GRB phenomena, independent of whether it is generated by vacuum polarization around a Kerr–Newman black hole[11] or other mechanisms, e.g. electron–positron pairs from a neutrino–antineutrino annihilation mechanism. This plasma engulfs the baryonic material of mass M_B left over from the process of gravitational collapse, while still maintaining thermal equilibrium between electrons, positrons and baryons.

The baryon load is measured by the dimensionless parameter $B = M_B c^2/E_{\rm tot}^{e^+e^-}$. References 31 and 77 showed that no relativistic expansion of the plasma exists for $B > 10^{-2}$, see Fig. 11. The fireshell is still optically thick and self-accelerates to ultrarelativistic velocities (the pair-electromagnetic-baryonic pulse or PEMB pulse for short.[31,77]) Then the fireshell becomes transparent and the "proper GRB" (P-GRB) is emitted.[78] The final Lorentz gamma factor reached at transparency can vary over a wide range between 10^2 and 10^4 as a function of $E_{\rm tot}^{e^+e^-}$ and B. To determine this final value, it is necessary to integrate explicitly the rate equation

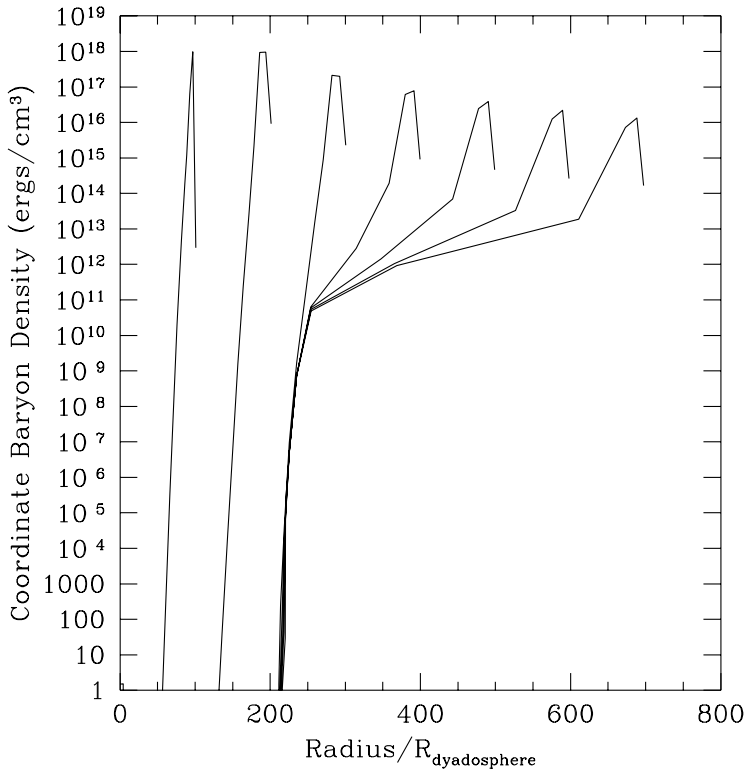

Fig. 11. The turbulent expansion for $B = 10^{-2}$. See details in Ref. 31.

for the e^+e^- annihilation process and evaluate, for a given black hole mass and given e^+e^- plasma radius, at what point the transparency condition is reached.[31]

The fireshell scenario does not require any prolonged activity of the inner engine and applies in generality to any confined amount of e^+e^- in a dyadosphere. After transparency, the remaining accelerated baryonic matter still expands ballistically and starts to slow down from collisions with the CBM of average density $n_{\rm CBM}$. In the standard fireball scenario,[43] the spiky light curve is assumed instead to be caused by internal shocks.

In the fireshell model, the entire extended prompt emission is assumed to originate from an expanding thin baryonic shell, which maintains energy and momentum conservation during its collision with the CBM. The condition of a fully radiative regime is assumed.[78] This in turn allows one to estimate the characteristic inhomogeneities of the CBM, as well as its average density. It is appropriate to point out another difference between our treatment and others in the current literature. The complete analytic solution of the equations of motion of the baryonic shell were developed in Refs. 79 and 80, while elsewhere the Blandford–McKee self-similar approximate solution is almost always adopted without justification.[72,81–89] The analogies and differences between the two approaches have been explicitly explained in Ref. 90.

In our general approach, a canonical GRB bolometric light curve is composed of two different parts: the P-GRB and the prompt radiation phase. The relative energetics of these two components and the observed temporal separation between the corresponding peaks is a function of the above three parameters $E_{\rm tot}^{e^+e^-}$, B, and the average value of the CBM density $n_{\rm CBM}$. The first two parameters are inherent to the accelerator mechanism characterizing the GRB, i.e. the optically thick phase, while the third parameter is inherent to the environment surrounding the GRB which gives rise to the prompt radiation phase by colliding with the baryonic fireshell.

For the observational properties of a relativistically expanding fireshell model, a crucial concept has been the introduction of the equi-temporal surfaces (EQTS). Here too our model differs from those in the literature by having derived an analytic expression for the EQTS obtained from the solutions to the equations of motion.[80,90]

Details of the P-GRB and GRB prompt radiation are given in Ref. 13. Before closing it is appropriate to recall the fundamental diagram comparing and contrasting the P-GRB and the prompt radiation, see Fig. 12, characterizing the difference between short and long GRBs in the fireshell model as a function of the baryon load.

2. Unveiling the GRB-SN Connection: The Second Paradigm

2.1. *Introduction*

Until 1998 the study and GRBs and supernovae continued in parallel but disjoint from one another. Conceptually we have adopted the first paradigm mentioned

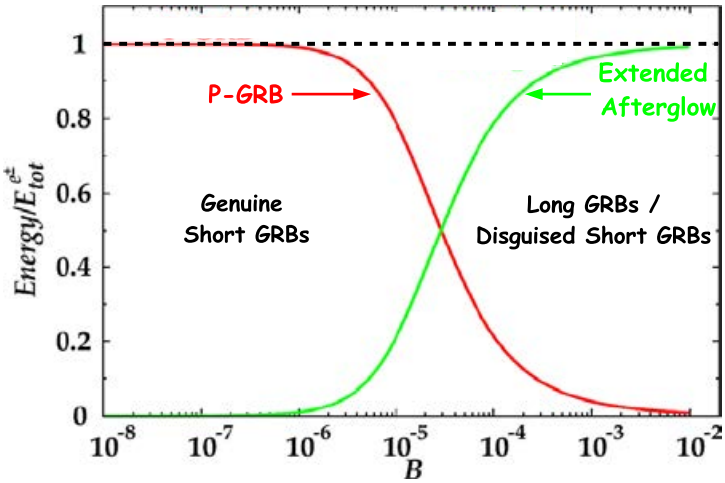

Fig. 12. (Color online) The energy emitted in the extended afterglow (solid green curve) and in the P-GRB (solid red curve) in units of $E^{\rm tot}_{e^+e^-} = 1.77 \times 10^{53}$ erg (dashed horizontal line), as functions of B. The crossing point, corresponding to the condition $E_{P\text{-GRB}} \equiv 50\% E^{\rm tot}_{e^+e^-}$, marks the division between the genuine short GRB region and the disguised short and long GRB region. The upper limit for B of 10^{-2} is determined by the onset of instabilities as shown in Fig. 11. From Ref. 38.

above: that supernovae originate from the formation of a NS and that GRBs are generated by the formation of a black hole. Something totally unexpected happened on April 25, 1998: the occurrence of GRB 980425 and the simultaneous observation of SN 1998bw, see Refs. 19–21. This coincidence has become extremely common for all long GRBs at values of the cosmological redshift less than 1.

While the collapsar proponents and other groups started to attempt hybrid models of NSs and black holes, supernovae creating black holes and similar ideas, we maintained our first paradigm and introduced a new "second paradigm":

Second paradigm

- *All long GRBs are necessarily associated with supernovas of type* ***SN Ic*** *and are components of a "****cosmic matrix****".*
- *They originate from a massive binary system, which evolves through a binary X-ray source, and finally leads to a binary system composed of an* ***FeCO*** *core* $> 2.8\,M_\odot$ *and a* ***NS*** *companion separated by* $b_{\rm crit} \sim 10^{11}$ *cm. For* $b < b_{\rm crit}$ *hypercritical accretion of the SN ejecta onto the NS leads to* ***BH*** *formation and to the consequent emission of a GRB. For* $b > b_{\rm crit}$ no ***BH*** *is formed.*
- *For* $b < b_{\rm crit}$ *a binary-driven hypernova (****BdHN****) occurs characterized by:* ***Episode 1*** *the hypercritical accretion,* ***Episode 2*** *the GRB,* ***Episode 3*** *the universal behavior, and* ***Episode 4*** *the optical* ***SN*** *observed. For* $b > b_{\rm crit}$ *only* ***Episode 1*** *and* ***Episode 4*** *exist, and an* ***X-ray Flash*** *occurs".*

Our present paradigm has recently evolved from an earlier formulation,[91] see Fig. 14. All these theoretical works and their observational feedback have recently

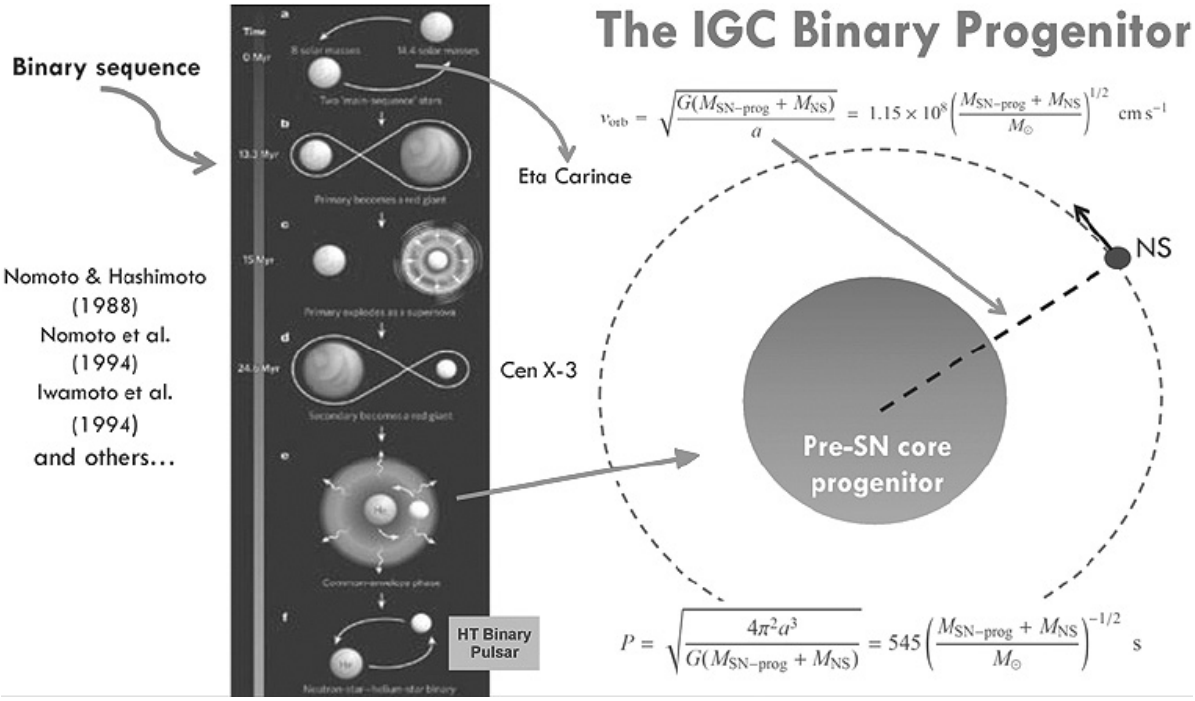

Fig. 13. The IGC binary progenitor. For details see Refs. 36 and 94.

led to the binary-driven hypernova model (BdHN).[92,93] Contrary to the collapsar model which envisions a single object and a single event characterizing the GRB-supernova association, the IGC paradigm assumes as its progenitor a binary system containing an evolved Fe-Co core and a tightly bound neutron star binary companion, see Fig. 13. What was previously conceived for the GRB as a single ultra-relativistic event characterized by jetted emission appears to be a much more complex and rich system composed generally of four different episodes distinctively different in their astrophysical nature and with very specific signatures in their spectral and time varying luminosity emissions in selected wavelengths.

In conclusion, the IGC binary scenario applied here to the specific case of GRB 090618 naturally leads to understanding the energetics and the temporal coincidence of SNs and GRBs, as well as their astrophysical scenario and makes their correlation a direct consequence of the binary nature of the progenitor. In summary, we present in Figs. 15 and 16 the full interpretation of GRB 090618 observations as the four different episodes of the IGC paradigm.

Let us identify these four events in GRB 090618, the prototype of this most energetic family of GRBs, with an $E_{\rm iso}$ energy larger than 10^52 erg, associated with supernovae. We describe a few key moments in the recent evolution of our understanding of this system which is very unique within physics and astrophysics. Some 20 additional examples of such a GRBs associated with supernovae have been identified by our group leading to the concept of binary driven-hypernovae.

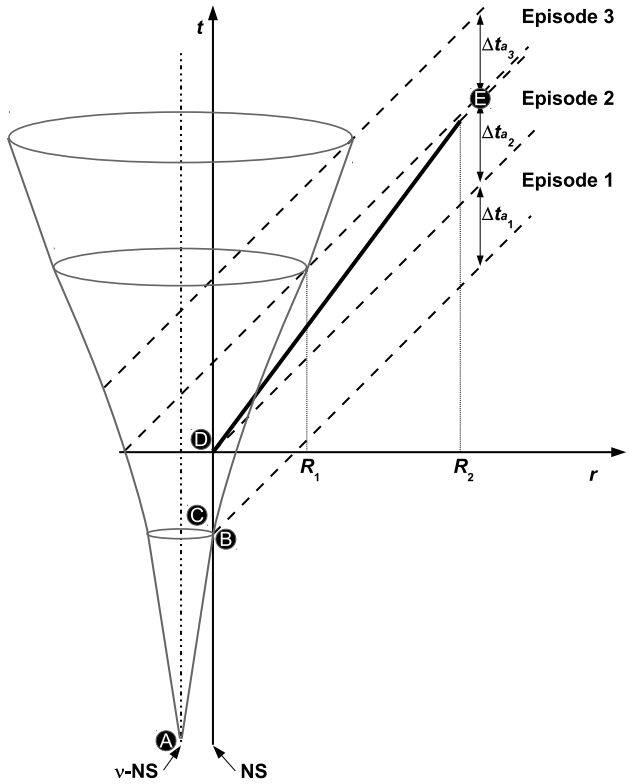

Fig. 14. The initial IGC spacetime diagram (not to scale), from Ref. 92. *Episode* 1 corresponds to the onset of the FeCO core SN explosion, creating a new NS (ν-NS, see A). Part of the SN ejecta triggers an accretion process onto the NS companion (see B and Refs. 36 and 94), and a prolonged interaction between the ν-NS and the NS binary companion occurs (see C). This leads to a spectrum with an expanding thermal component plus an extra power law component (see Fig. 16 in Ref. 35). *Episode* 2 occurs when the companion NS reaches its critical mass and collapses to a BH, emitting the GRB (D) with Lorentz factors $\Gamma \approx 10^2$–10^3 (for details, see e.g. Refs. 22 and 35). *Episode* 3, observed in the X-rays, shows very precise behavior consisting of a steep decay, starting at the end point of the prompt emission (see E), and then a plateau phase, followed by a late constant power-law decay (see Refs. 35 and 95). The figure illustrates the relativistic motion of Episode 2 ($\Gamma \approx 500$, thick line) and the nonrelativistic Episode 1 ($\Gamma \approx 1$) and Episode 3 ($\Gamma \approx 2$). Emissions from different radii, R_1 ($\sim 10^{13}$ cm) and R_2 ($\sim 10^{16}$–10^{17} cm), contribute to the transition point (E). Clearly, the X-ray luminosity originates from the SN remnant or in the newly born BH, but not from the GRB.

2.2. *The case of GRB* 090618

The GRB 090618 discovered by the Swift satellite[98] represents the prototype of a class of energetic ($10^{52} \leq E_{\rm iso} \leq 10^{55}$ erg) GRBs, characterized by the presence of a supernova observed 10 $(1+z)$ days after the trigger time, and the observation of four distinct emission episodes in their Gev emission, hard X-ray light curve, soft X-ray and optical emission (see details in Ref. 35). The BAT light curve shows a multi-peak structure, whose total estimated duration is $\sim$320 s and whose T_{90} duration in the (15–350) keV range was 113 s.[99] The first 50 s of the light curve shows a smooth decay trend followed by a spiky emission, with three prominent peaks at 62, 80 and 112 s after the trigger time, respectively, and each has the typical appearance of a

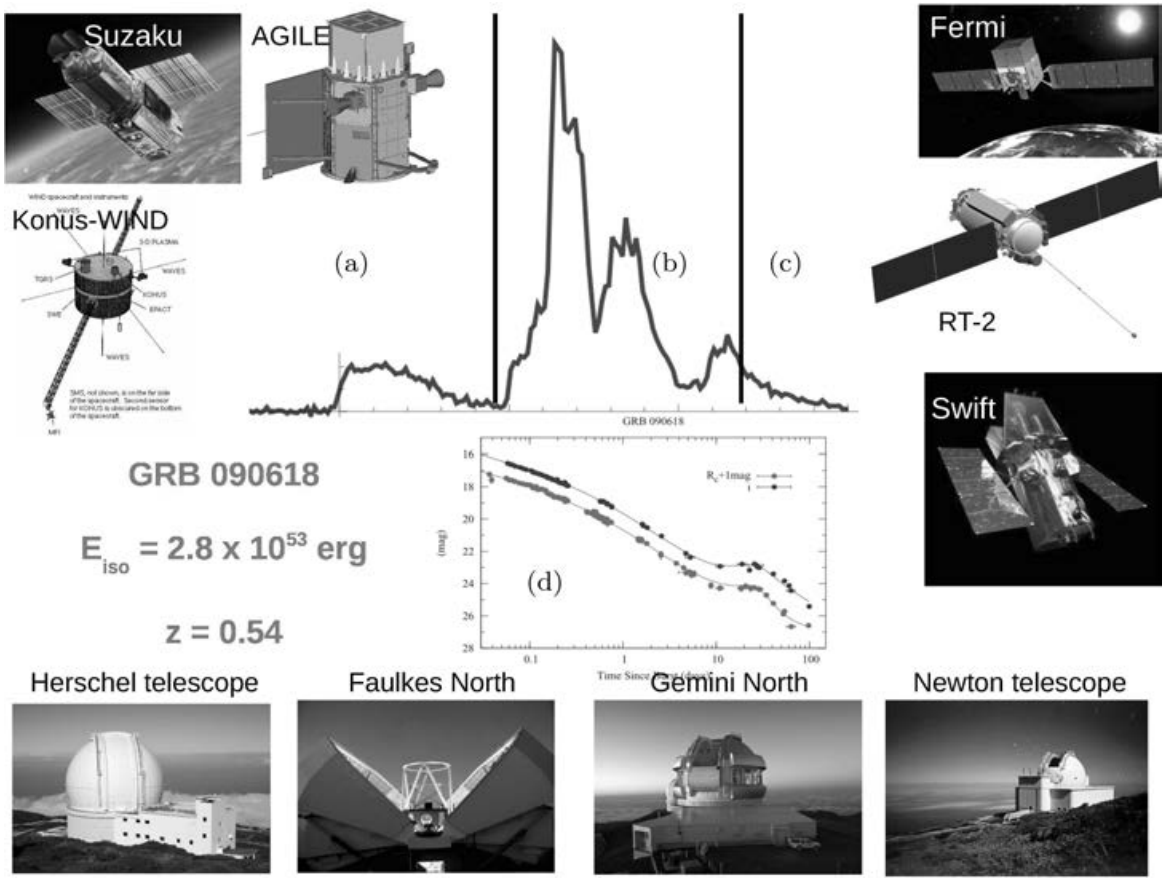

Fig. 15. GRB 090618 observations as the four different episodes implied by the IGC paradigm: (a) Episode 1, (b) Episode 2, (c) Episode 3 and (d) Episode 4 (i.e. the optical observations of the associted SN). Above are the satellites that participated in the observations: (in clockwise order) Fermi/GBM (8–1000 keV), Coronas-Photon/RT-2 (15–1000 keV), Swift/BAT (15–150 keV), Swift/XRT (0.3–10 keV), Swift/UVOT (optical band), AGILE/Super-AGILE (18–60 keV), AGILE/MCAL (350–10^5 keV), Suzaku/WAM (50–5000 keV), Konus/WIND (20–2000 keV). Below are the ground based observatories that participated in the optical observations. Details in Refs. 35, 36 and 97.

fast-rise-exponential-decay (FRED) pulse.[100] The XRT observations started 125 s after the BAT trigger time and lasted ∼25.6 ks[101] and reported an initially bright uncatalogued source, identified as the afterglow of GRB 090618. Its early decay is very steep, ending at 310 s after the trigger time, when it starts a shallower phase, the plateau. Then the light curve breaks into a steeper late phase.

The GRB 090618 was also observed by the gamma ray burst (GBM) monitor on board the Fermi satellite.[102] From an initial analysis, the time-integrated spectrum, $(t_0, t_0 + 140)$ s in the (8–1000) keV range, was fit by a band spectral model[103] with a peak energy $E_{\rm peak} = 155.5$ keV, $\alpha = -1.26$ and $\beta = -2.50$,[104] but with strong spectral variations within that time interval. The redshift of the source $z = 0.54$ was determined thanks to the identification of the MgII, MgI and FeII absorption lines using the KAST spectrograph mounted at the 3 m Shane telescope at the Lick observatory.[105] Given the redshift and the distance of the source, we computed the emitted isotropic energy in the 8–10,000 keV energy range with the Schaefer

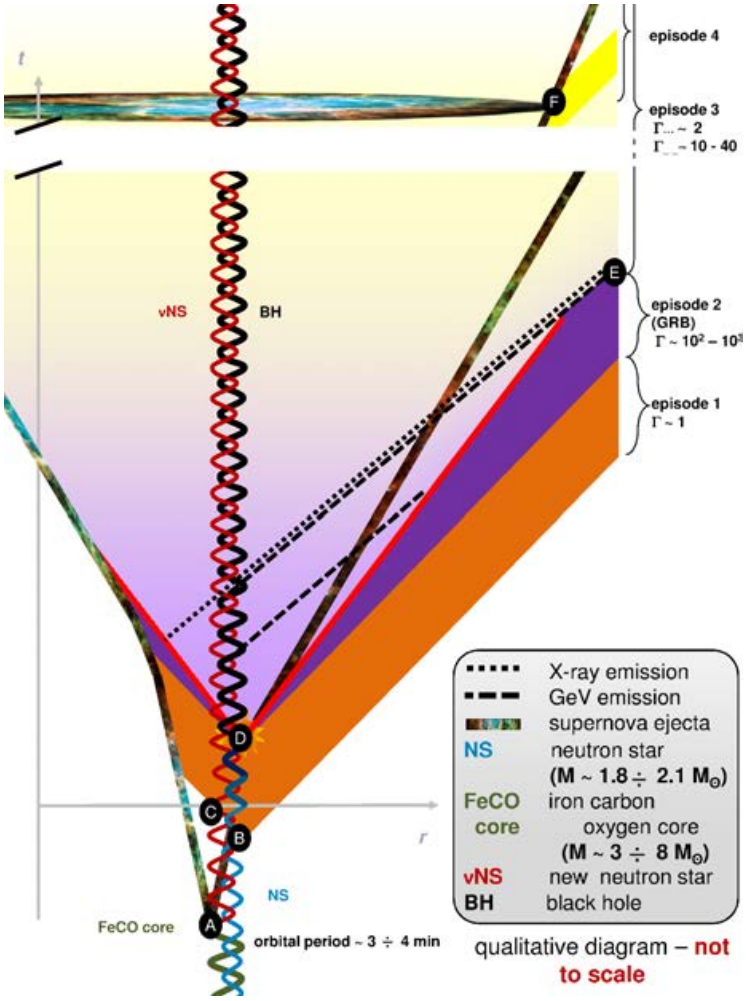

Fig. 16. (Color online) The further evolution of the IGC spacetime diagram (not to scale) illustrates 4 episodes of IGC paradigm: the nonrelativistic *Episode* 1 ($\Gamma \simeq 1$), the relativistic motion of *Episode* 2 ($\Gamma \simeq 10^2 \sim 10^3$), the mildly relativistic *Episode* 3 ($\Gamma \simeq 2$), and nonrelativistic *Episode* 4 ($\Gamma \simeq 1$). Initially there is a binary system composed of a massive star (yellow thick line) and a NS (blue line). The massive star evolves and explodes as a SN at point A, forms a νNS (red line). The companion NS accretes the supernova ejecta starting from point B, interacts with the νNS starting from point C, and collapses into a black hole (black line) at point D, this period from point B to point D we define as *Episode* 1. Point D is the starting of *Episode* 2, with two different components: one impacting on the SN filaments and one due to the collision of GRB outflow and interstellar filaments. At point E, *Episode* 2 ends and *Episode* 3 starts, *Episode* 3 lasts till the optical signal of supernova emerges at point F, where the *Episode* 4 starts. (*Credit to M. Enderli for drawing this visualized spacetime diagram.*)

formula[106]: using the fluence in the range (8–1000 keV) as observed by the Fermi GBM, $S_{obs} = 2.7 \times 10^{-4}$,[104] and the ΛCDM (Λ cold dark matter) cosmological standard model $H_0 = 70\,\mathrm{km/s/Mpc}$, $\Omega_m = 0.27$, $\Omega_\Lambda = 0.73$, we obtain the value $E_{iso} = 2.90 \times 10^{53}$ erg for the emitted isotropic energy.

This GRB was observed also by Konus-WIND,[107] Suzaku-WAM[108] and by the AGILE satellite,[109] which detected emission in the (18–60) keV range and in the MCAL instrument, operating at energies greater than 350 keV, but it did not observe high-energy photons above 30 MeV. GRB 090618 was the first GRB

observed by the Indian payloads RT-2 on board the Russian satellite CORONAS-PHOTON.[110–112] Thanks to the complete data coverage of the optical afterglow of GRB 090618, the presence of a supernova underlying the emission of its optical afterglow was reported.[113] The evidence of a supernova emission came from the presence of several bumps in the light curve and by the change in R_c-i color index over time: in the early phases, the blue color is dominant, typical of the GRB afterglow, but then the color index increases, suggesting a core-collapse SN. At late times, the contribution from the host galaxy was dominant. We have analyzed the GRB 090618 with L. Izzo and other ICRANet researchers and Ph.D. students considering the BAT and XRT data of the Swift satellite together with the Fermi GBM and RT2 data of the Coronas-PHOTON satellite (see Fig. 15). The data reduction was made with the Heasoft v6.10 packages[a] for BAT and XRT, and the Fermi-Science tools for GBM. The details of the data reduction and analysis are given in Ref. 35.

2.3. *The emission process in Episode* 1

2.3.1. *The time-resolved spectra and temperature variation*

A significant outcome of the multi-year work of Felix Ryde and his collaborators[114] has been the identification of thermal plus power-law features observed in time-limited intervals in selected BATSE GRBs. Similar features have also been observed in the data acquired by the Fermi satellite.[114,115] These emissions have been shown to present a thermal plus power-law(s) feature, with a temperature changing in time following a precise power-law behavior. Our aim has been to see if the first 50 s of emission of GRB 090618 conform to this feature. We made a detailed time-resolved analysis, considering different time bin durations to obtain good statistics in the spectra and to take into account the sub-structures in the light curve. We then used two different spectral models to fit the observed data, a classic band spectrum,[103] and a blackbody with a power-law component. To obtain more accurate constraints on the spectral parameters, we made a joint fit considering the observations from both the n4 NaI and the b0 BGO detectors, covering a wider energy range in this way, from 8 keV to 40 MeV. To avoid some bias from low-photon statistics, we considered an energy upper limit of the value of 10 MeV. Our analysis is summarized in Figs. 17–19.

2.3.2. *The power-law decay of the black body temperature*

Particularly interesting is the clear evolution in the time-resolved spectra, which corresponds to the blackbody and power-law component, see Fig. 17. In particular the kT parameter of the blackbody shows a strong decay, with a temporal behavior well described by a double broken power-law function, see the upper panel in Fig. 18.

[a]http://heasarc.gsfc.nasa.gov/lheasoft/.

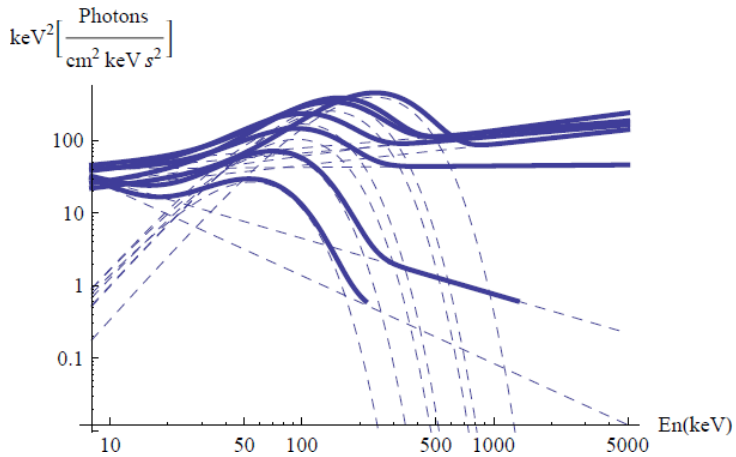

Fig. 17. Evolution of the BB+power-law spectral model in the $\nu F(\nu)$ spectrum of the first emission of GRB 090618. It shows the cooling of the blackbody and associated nonthermal components in time. We only plot the fitting functions for clarity. From Ref. 35.

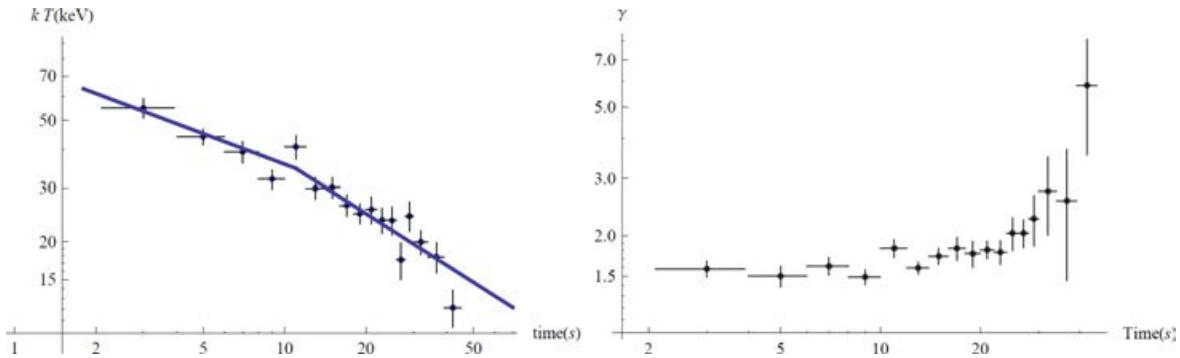

Fig. 18. (Color online) Evolution of the observed temperature kT of the blackbody component and the corresponding evolution of the power-law photon index. The blue line in the upper panel corresponds to the fit of the time evolution of the temperature with a broken power-law function. It shows a break time t_b around 11 s after the trigger time, as obtained from the fitting procedure. From Ref. 35.

From a fitting procedure we find that the best fit (R^2-statistic $= 0.992$) for the two decay indexes for the temperature variation are $a_{kT} = -0.33 \pm 0.07$ and $b_{kT} = -0.57 \pm 0.11$. In Ref. 75, an average value for these parameters is given for a set of 49 GRBs: $\langle a_{kT} \rangle = -0.07 \pm 0.19$ and $\langle b_{kT} \rangle = -0.68 \pm 0.24$. The results presented in Figs. 17 and 18 point to a rapid cooling of the thermal emission with time of the first episode. The evolution of the corresponding power-law spectral component also appears to be strictly related to the change of the temperature kT. The power-law γ index falls, or softens, with temperature, see Fig. 17. An interesting feature appears to occur at the transition of the two power-laws describing the observed decrease of the temperature.

2.3.3. *The radius of the emitting region*

We turn now to estimate an additional crucial parameter for identifying the nature of the blackbody component: the radius $r_{\rm em}$ of the emitter. We proved

that the first episode is not part of a GRB. We can therefore provide the estimate of the emitter radius from nonrelativistic considerations, just corrected for the cosmological redshift z. In fact we find that the temperature $T_{\rm em} = T_{\rm obs}(1+z)$ of the emitter and that the luminosity of the emitter due to blackbody emission is

$$L = 4\pi r_{\rm em}^2 \sigma T_{\rm em}^4 = 4\pi r_{\rm em}^2 \sigma T_{\rm obs}^4 (1+z)^4, \tag{2}$$

where $r_{\rm em}$ is the emitter radius and σ is the Stefan–Boltzmann constant. From the luminosity distance definition, we also have that the observed flux $\phi_{\rm obs}$ given by

$$\phi_{\rm obs} = \frac{L}{4\pi D^2} = \frac{r_{\rm em}^2 \sigma T_{\rm obs}^4 (1+z)^4}{D^2}. \tag{3}$$

We then obtain

$$r_{\rm em} = \left(\frac{\phi_{\rm obs}}{\sigma T_{ob}^4}\right)^{1/2} \frac{D}{(1+z)^2}. \tag{4}$$

The above radius differs from the radius r_{ph} given in Eq. (1) of Ref. 75, which was also clearly obtained by interpreting the early evolution of GRB 970828 as belonging to the photospheric emission of a GRB and assuming a relativistic expansion with a Lorentz gamma factor Γ satisfying

$$r_{ph} = \hat{\mathcal{R}} D \left(\frac{\Gamma}{(1.06)(1+z)^2}\right), \tag{5}$$

where $\hat{\mathcal{R}} = (\phi_{\rm obs}/(\sigma T_{ob}^4))^{1/2}$ and the prefactor 1.06 arises from the dependence of r_{ph} on the angle of the line of sight.[116] Typical values of r_{ph} are at least two orders of magnitude higher than our radius $r_{\rm em}$. Assuming a standard cosmological model ($H_0 = 70$ km/s/Mpc, $\Omega_m = 0.27$ and $\Omega_\Lambda = 0.73$) for estimating the luminosity distance D, and using the values for the observed flux $\phi_{\rm obs}$ and the temperature $kT_{\rm obs}$, we give in Fig. 19 the evolution of the surface radius that emits the blackbody $r_{\rm em}$ as a function of time. Assuming an exponential evolution with time t^δ of the radius in the comoving frame, we obtain the value $\delta = 0.59 \pm 0.11$ from a fitting procedure, which is well compatible with $\delta = 0.5$. We also notice a steeper behavior for the variation of the radius with time corresponding to the first 10 s, which corresponds to the emission before the break of the double power-law behavior of the temperature. We estimate an average velocity of $\bar{v} = 4067 \pm 918$ km/s, $R^2 = 0.91$ in these first 10 s of emission. In episode 1, the observations lead to a core of an initial radius of ∼12,000 km expanding in the early phase with a higher initial velocity of ∼4000 km/s. The effective Lorentz Γ factor is very low, $\Gamma - 1 \sim 10^{-5}$. I proposed to identify this first episode as the early phases of the accretion onto the companion NS which the SN ejects in the IGC scenario, later confirmed by the simulation.[96]

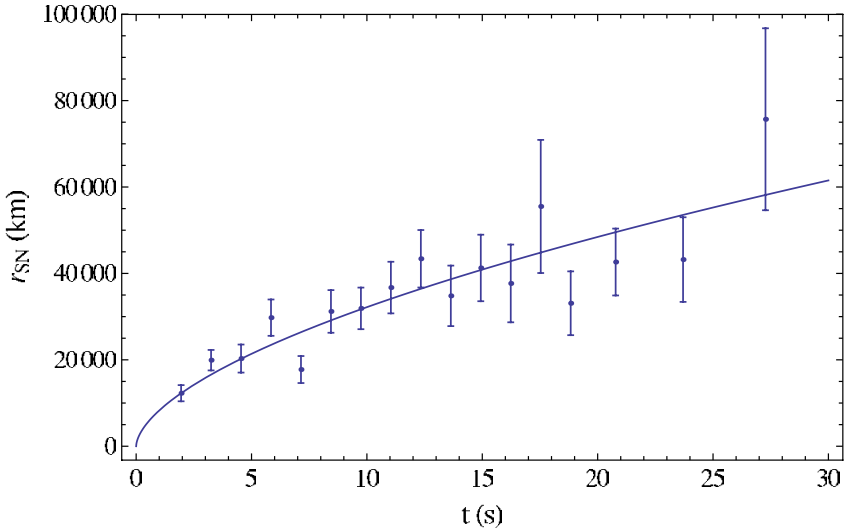

Fig. 19. Evolution of the Episode 1 emitter radius given by Eq. (4). From Ref. 35.

2.4. *The emission process in Episode 2*

2.4.1. *The identification of the P-GRB*

We have proceeded to the analysis of the data between 50 and 150 s after the trigger time as a canonical GRB in the fireshell scenario, namely Episode 2.[97] We proceed to identify the P-GRB within the emission between 50 s and 59 s, since we find a blackbody signature in this early second-episode emission. Considerations based on the time variability of the thermal component bring us to conclude that the first 4 s of this time interval due to the P-GRB emission. The corresponding spectrum (8–440 keV) is well fit ($\tilde{\chi}^2 = d1.15$) with a blackbody of temperature $kT = 29.22 \pm 2.21$ keV (norm $= 3.51 \pm 0.49$), and an extra power-law component with photon index $\gamma = 1.85 \pm 0.06$, (norm $= 46.25 \pm 10.21$). The fit with the band model is also acceptable ($\tilde{\chi}^2 = 1.25$), which gives a low-energy power-law index $\alpha = -1.22 \pm 0.08$, a high-energy index $\beta = -2.32 \pm 0.21$ and a break energy $E_0 = 193.2 \pm 50.8$. In view of the theoretical understanding of the thermal component in the P-GRB (see Sec. 3.2), we focus below on the blackbody+power-law spectral model. The isotropic energy of the second episode is $E_{\rm iso} = (2.49 \pm 0.02) \times 10^{53}$ ergs. The simulation within the fireshell scenario is made assuming $E_{\rm tot}^{e^+e^-} \equiv E_{\rm iso}$. From the observed temperature, we can then derive the corresponding value of the baryon load. The observed temperature of the blackbody component is $kT = 29.22 \pm 2.21$, so that we can determine a value of the baryon load of $B = 1.98 \pm 0.15 \times 10^{-3}$, and deduce the energy of the P-GRB as a fraction of the total $E_{\rm tot}^{e^+e^-}$. We therefore obtain a value of the P-GRB energy of $4.33^{+0.25}_{-0.28} \times 10^{51}$ erg. Next we can derive the radius of the transparency condition, to occur at $r_{\rm tr} = 1.46 \times 10^{14}$ cm. We derive the bulk Lorentz factor of $\Gamma_{\rm th} = 495$ and compare this value with the energy measured only in the blackbody component of $E_{\rm BB} = 9.24^{+0.50}_{-0.58} \times 10^{50}$ erg, and with the energy in the blackbody plus the power-law component of $E_{{\rm BB}+po} = 5.43^{+0.07}_{-0.11} \times 10^{51}$ erg,

and verify that the theoretical value is in between these observed energies. We have found this result to be quite satisfactory: it represents the first attempt to relate the GRB properties to the details of the BH responsible for the overall GRB energetics. The above theoretical estimates were based on a nonrotating BH of $10\,M_\odot$, a total energy of $E_{\rm tot}^{e^+e^-} = 2.49 \times 10^{53}$ erg and a mean temperature of the initial e^+e^- plasma of 2.4 MeV, derived from the expression for the dyadosphere radius, Eq. (1).

2.4.2. *The refinement of the P-GRB nature*

Standing the excellent results obtained in the e^+e^- spectra and the dynamics of the refinement and the direct comparison between theory and observations will have to address a variety of fundamental problems such as (1) the possible effect of rotation of the BH, leading to a more complex dyadotorus structure,[22] (2) an analysis of the general relativistic, electrodynamical and strong interaction descriptions of the gravitational core collapse leading to BH formation,[77,117,118] (3) a possible role of hypercritical accretion process in creating the electron–positron plasma out of neutrino–antineutrino annihilalation.[96,119,120] All these processes could alternatively lead to a dyadosphere near the Kerr–Newmann black hole with an efficiency (42%) similar to the electrodynamical case (50%).

2.4.3. *The prompt emission and the CBM cloud structure*

The prompt emission starts at the above given radius of the transparency, with an initial value of the Lorentz Γ factor of $\Gamma_0 = 495$. To simulate the extended-afterglow emission, we need to determine the radial distribution of the CBM around the burst site, which we assume for simplicity to be spherically symmetric, from which we infer a characteristic size of $\Delta R = 10^{15}$–10^{16} cm. We already described above how the simulation of the spectra and of the observed multi-band light curves have to be performed together and need to be jointly optimized, leading to the determination of the fundamental parameters characterizing the CBM medium.[121] This radial distribution is shown in Fig. 20 and is characterized by a mean value of $\langle n \rangle = 0.6\,\text{part/cm}^3$ and an average density contrast with a $\langle \delta n/n \rangle \approx 2$, see Fig. 20 and Tables 1 and 2. The data up to 8.5×10^{16} cm are simulated with a value for the filling factor $\mathcal{R} = 3 \times 10^{-9}$, while the data from this value on with $\mathcal{R} = 9 \times 10^{-9}$. From the radial distribution of the CBM density, and considering the $1/\Gamma$ effect on the fireshell visible area, we found that the CBM clumps causing the spikes in the extended afterglow emission have masses on the order of 10^{22}–10^{24} g. The value of the α parameter was found to be -1.8 along the total duration of the GRB. In Fig. 21, we show the simulated light curve (8–1000 keV) of the GRB and the corresponding spectrum, using the spectral model described in Refs. 79 and 122. The Episode 2, lasting from 50 s to 151 s, agrees with a canonical GRB in the fireshell scenario.

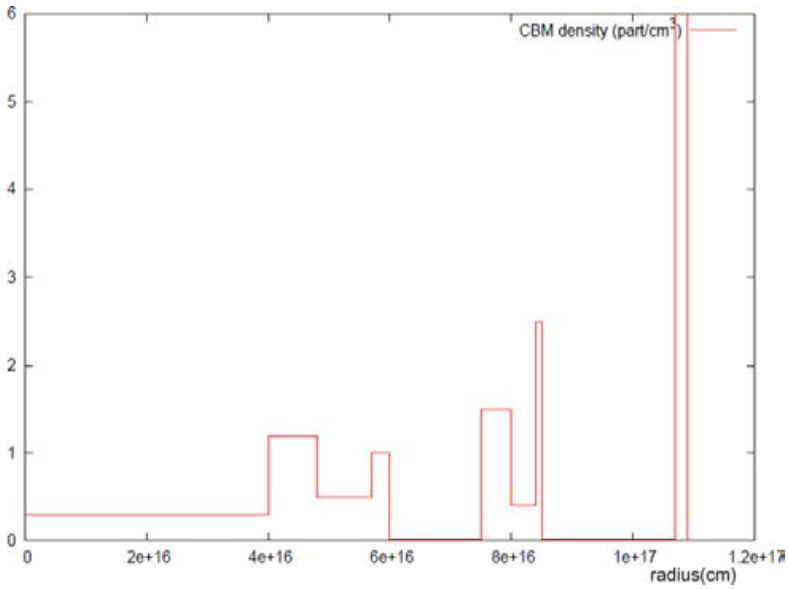

Fig. 20. Radial CBM density distribution for GRB 090618. The characteristic masses of each cloud are on the order of $\sim 10^{22-24}$ g and 10^{16} cm in radii. From Ref. 35.

Table 1. Final results of the simulation of GRB 090618 in the fireshell scenario. From Ref. 35.

Parameter	Value
$E_{\rm tot}^{e^+e^-}$	$2.49 \pm 0.02 \times 10^{53}$ ergs
B	$1.98 \pm 0.15 \times 10^{-3}$
Γ_0	495 ± 40
$kT_{\rm th}$	29.22 ± 2.21 keV
$E_{P\text{-GRB},th}$	$4.33 \pm 0.28 \times 10^{51}$ ergs
$\langle n \rangle$	0.6 part/cm^3
$\langle \delta n/n \rangle$	2 part/cm^3

Table 2. Physical properties of the three clouds surrounding the burst site: the distance from the burst site (column 2), the radius r of the cloud (column 3), the particle density ρ (column 4), and the mass M (the last column). From Ref. 35.

Cloud	Distance (cm)	r (cm)	ρ (#/cm^3)	M (g)
First	4.0×10^{16}	1×10^{16}	1	2.5×10^{24}
Second	7.4×10^{16}	5×10^{15}	1	3.1×10^{23}
Third	1.1×10^{17}	2×10^{15}	4	2.0×10^{22}

2.5. *The emission process of Episode 3*

2.5.1. *The late X-ray emission observed by swift/XRT*

We now turn to the most important feature which has appeared in the analysis of Episode 3 of GRB 090618: the presence of a steep decay, followed by a plateau and a power law steep decay, see Fig. 22. This feature has unexpectedly become a common feature of all GRBs with energy larger than 10^{52} erg and even more striking, all the X-ray emissions at late times, when computed in the rest frame of the source

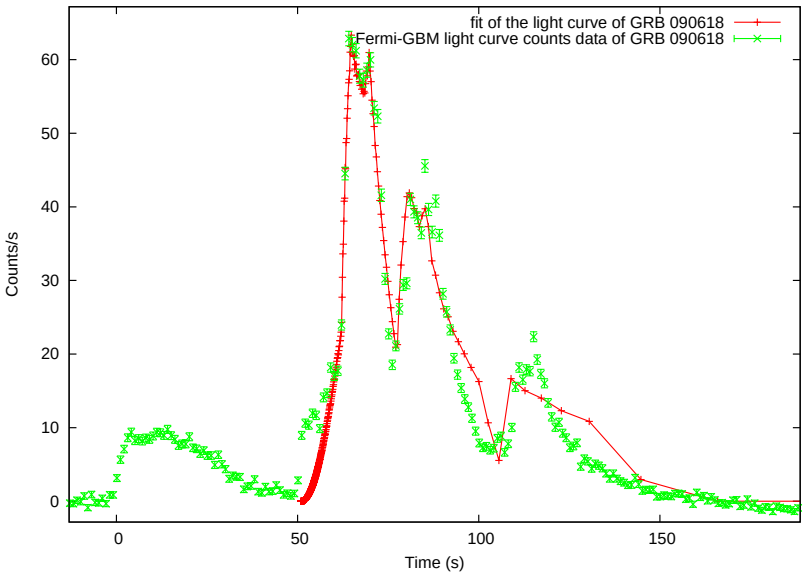

Fig. 21. Simulated light curve of the extended-afterglow of GRB 090618. From Ref. 35.

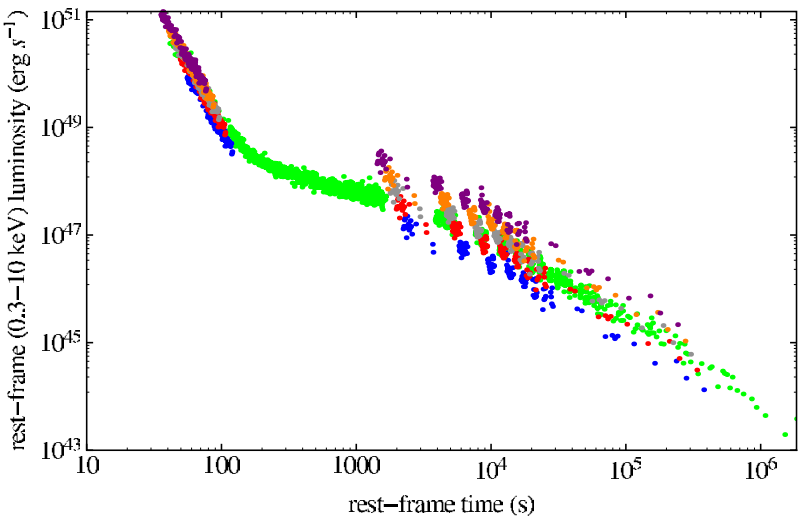

Fig. 22. (Color online) In green we show the rest frame X-ray luminosity light curve of GRB 090618 in the 0.3–10 keV energy range in comparison with the one of GRB 101023, computed for different hypothetical redshifts: respectively, from blue to purple: $z = 0.6, 0.8, 1.0, 1.2, 1.5$. The overlapping at late time of the two X-ray luminosity light curves is obtained for a redshift of $z = 0.9$. For further details see Refs. 95 and 123.

they overlap, see Fig. 23. This feature has become a most powerful method to estimate the cosmological redshift of the source, when not directly observed. We have focused our attention on the analysis of all the available XRT data of these sources.[37] Characteristically, XRT follow-up starts only about 100 s after the BAT trigger (typical repointing time of Swift after the BAT trigger). Since the behavior was similar in all the sources, we have performed an analysis to compare the XRT luminosity light curve $L_{\rm rf}$, where "rf" stands for rest frame, for the six GRBs with measured redshift z in the common rest frame energy range 0.3–10 KeV. To perform this computation, the first step is to convert the observed XRT flux $f_{\rm obs}$ to the one

in the 0.3–10 KeV rest frame energy range. In the detector frame, the 0.3–10 KeV rest frame energy range becomes $[0.3/(1+z)] - [10/(1+z)]$ KeV where z is the redshift of the GRB. We assume a simple power-law function as the best-fit for the spectral energy distribution of the XRT data[b]:

$$\frac{dN}{dA\,dt\,dE} \propto E^{-\gamma}. \tag{6}$$

We can then write the flux light curve $f_{\rm rf}$ in the 0.3–10 KeV rest frame energy range as:

$$f_{\rm rf} = f_{\rm obs} \frac{\displaystyle\int_{\frac{0.3\,\rm keV}{1+z}}^{\frac{10\,\rm keV}{1+z}} E^{-\gamma} dE}{\displaystyle\int_{0.3\,\rm keV}^{10\,\rm keV} E^{-\gamma} dE} = f_{\rm obs}(1+z)^{\gamma-1}. \tag{7}$$

Then we have to multiply $f_{\rm rf}$ by the luminosity distance to get $L_{\rm rf}$:

$$L_{\rm rf} = 4\pi d_l^2(z) f_{\rm rf}, \tag{8}$$

where we assume a standard cosmological model ΛCDM with $\Omega_m = 0.27$ and $\Omega_\Lambda = 0.73$. Clearly, this luminosity must be plotted as a function of the rest frame time $t_{\rm rf}$, namely:

$$t_{\rm rf} = \frac{t_{\rm obs}}{1+z}. \tag{9}$$

2.5.2. "*The golden sample*"

The X-ray luminosity light curves of the six GRBs with measured redshift in the 0.3–10 KeV rest frame energy band are plotted together in Fig. 23 and Table 3.

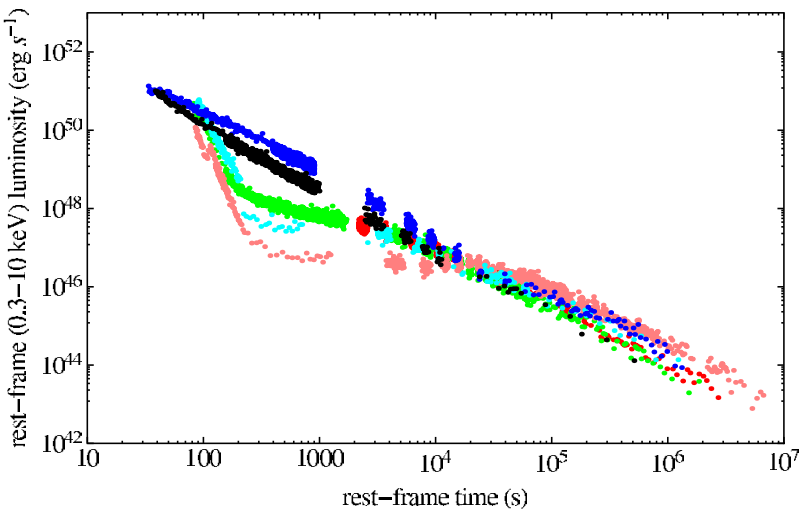

Fig. 23. (Color online) The X-ray luminosity light curves of the six GRBs with measured redshift in the 0.3–10 keV rest frame energy range: in pink GRB 060729, $z = 0.54$; in black GRB 061007, $z = 1.261$; in blue GRB 080319B, $z = 0.937$; in green GRB 090618, $z = 0.54$, in red GRB 091127, $z = 0.49$, in cyan GRB 111228, $z = 0.713$. From Ref. 37.

[b]http://www.swift.ac.uk/.

Table 3. The GRB sample considered in this work. The redshifts of GRB 101023 and GRB 110709B, which are marked by an asterisk, were deduced theoretically by using the method outlined in Ref. 95 and the corresponding isotropic energy computed by assuming these redshifts. From Ref. 37.

GRB	z	$E_{\rm iso}$ (erg)
GRB 060729	0.54	1.6×10^{52}
GRB 061007	1.261	1.2×10^{54}
GRB 080319B	0.937	1.4×10^{54}
GRB 090618	0.54	2.7×10^{53}
GRB 091127	0.49	1.4×10^{52}
GRB 111228	0.713	2.3×10^{52}
GRB 101023	0.9^*	1.3×10^{53}
GRB 110709B	0.75^*	2.72×10^{53}

What is most striking is that these six GRBs, with redshift in the range 0.49–1.261, show a remarkably common behavior of the late X-ray afterglow luminosity light curves (Episode 3) despite that their prompt emissions (Episodes 1 and 2) are very different and that their energetics spans more than two orders of magnitude, see Table 3. Such a common behavior starts between 10^4 and 10^5 s after the trigger and continues up to when the emission falls below the XRT threshold. This universal behavior of Episode 3 represents strong evidence of very low or even the absence of beaming in this particular phase of the X-ray afterglow emission process. I proposed in the presentation that this late time X-ray emission in Episode 3 is related to the process of the SN explosion within the IGC scenario, possibly emitted by the newly born NS and BH and by the supernovae ejecta shocked by the GRB, and not by the GRB itself, see Fig. 16.

2.5.3. *Episode* 3 *as a standard candle*

As an example, we present in Fig. 22 the rest frame X-ray luminosity (0.3–10 KeV) light curve of GRB 090618 (considered as a prototype for the common behavior shown in Fig. 23) with the rest frame X-ray luminosity light curves of GRB 110709B estimated for selected values of its redshifts, $z = 0.4, 0.6, 0.8, 1.0, 1.2$ and similarly the correspondent analysis for GRB 101023 for selected values of the redshift, $z = 0.6, 0.8, 1.0, 1.2, 1.5$. We then find, with A.V. Penacchioni and other ICRANet researchers and Ph.D. students, that GRB 101023 should have been located at $z \sim 0.9$ and GRB 110709B at $z \sim 0.75$. These redshift estimations are within the range expected using the Amati relation as shown in Refs. 95 and 123. This is an important independent confirmation of validity for this new redshift estimator we propose for the family of IGC GRB-SN systems. It should be stressed, however, that the determination of the redshift is done assuming the validity of the standard ΛCDM cosmological model for sources with redshift in the range $z = 0.49$–1.216. We are currently testing the validity of this assumption for sources at larger cosmological redshifts.

3. The GRB-SN and the IGC: The Second Paradigm

3.1. *IGC of a NS to a blackhole by a type Ib/c SN*

The systematic and spectroscopic analysis of GRB-SN events, following the pioneering discovery of the temporal coincidence of GRB 980425[19] and SN 1998bw,[21] has revealed evidence for the association of other nearby GRBs with Type Ib/c SNe (see Ref. 124 for a recent review of all the GRB-SN systems). It has also been clearly understood that SN Ib/c lack Hydrogen (H) and Helium (He) in their spectra, and the most likely explanation is that the SN progenitor star is in a binary system with a compact companion, a NS (see e.g. Refs. 125–127, for details). In the current literature there has been an attempt to explain both the SN and the GRB as two aspects of the same astrophysical phenomenon: the collapsar model. Hence, GRBs have been assumed to originate from a specially violent SN process, a hypernova or a collapsar (see e.g. Ref. 128 and references therein). Both of these possibilities imply a very dense and strong wind-like CBM structure. Such a dense medium appears to be in contrast with the CBM density found in most GRBs within our fireshell model (see e.g. Fig. 10 in Ref. 36). In fact, the average CBM density, inferred from the analysis of the afterglow, has been shown to be in most of the cases of the order of 1 particle cm^{-3} (see e.g. Ref. 44). The only significant contribution to the baryonic matter component in the GRB process is the one represented by the baryon load.[31] In a GRB, the electron–positron plasma, loaded with a certain amount of baryonic matter, is expected to expand at ultra-relativistic velocities with Lorentz factors $\Gamma \gtrsim 100$.[81,129,130] Such an ultra-relativistic expansion can actually occur if the amount of baryonic matter, quantifiable through the baryon load parameter, does not exceed the critical value $B \sim 10^{-2}$ (see Ref. 31, for details). For $B > 10^{-2}$ the electron–positron plasma looses its laminar motion and the turbulence occurs, see Fig. 11.

In our approach, following the first paradigm, we have consistently assumed that the GRB has to originate from the gravitational collapse to a BH. The SN follows, instead, the complicated pattern of the final evolution of a massive star, possibly leading to a NS or to a complete explosion but never to a BH. There is a further general argument in favor of our explanation, namely the extremely different energetics of SNe and GRBs. While the SN energy range is 10^{49}–10^{51} erg, the GRBs are in a larger and wider range of energies 10^{49}–10^{54} erg. It is clear that in no way a GRB, being energetically dominant, can originate from the SN. We explain the temporal coincidence of the two phenomena, the SN explosion and the GRB, using the concept of *IGC*.[91,131]

In recent years, we have outlined two different possible scenarios for the GRB-SN connection. In the first version,[91] we have considered the possibility that GRBs may have caused the trigger of the SN event. For this scenario to occur, the companion star has to be in a very special phase of its thermonuclear evolution (see Ref. 91 for details). More recently in Refs. 121, 131 and 132 I have proposed a different possibility occurring at the final stages of the evolution of a close binary system: the explosion in such a system of a Ib/c SN leads to an accretion process onto

the NS companion. The full spacetime diagram is represented in Fig. 14. Again, in order for this process to occur, a very fine tuning must exist in the thermonuclear evolution of the SN core and in the circular orbit of the companion NS. The NS will reach the critical mass value, undergoing gravitational collapse to a BH. The process of gravitational collapse to a BH leads to the emission of the GRB (see Figs. 24 and 25). Here we evaluate the accretion rate onto the NS and give the explicit expression of the accreted mass as a function of the nature of the components and the binary parameters following Ref. 94. The full spacetime diagram is represented in Fig. 14.

3.2. *The accretion process of the SN ejecta onto the companion NS*

We turn now to the details of the recent work with Jorge Rueda[94] and collaborators, of the accretion process of the SN material onto the NS. In a spherically symmetric accretion process, the magnetospheric radius is[133]

$$R_m = \left(\frac{B^2 R^6}{\dot{M}\sqrt{2GM_{\rm NS}}} \right)^{2/7}, \tag{10}$$

where B, $M_{\rm NS}$, R are the NS magnetic field, mass, radius, and $\dot{M} \equiv dM/dt$ is the mass-accretion rate onto the NS. It can be seen that for high accretion rates the influence of the magnetosphere will be negligible. The NS captures the material ejected from the core collapse of the companion star in a region delimited by the

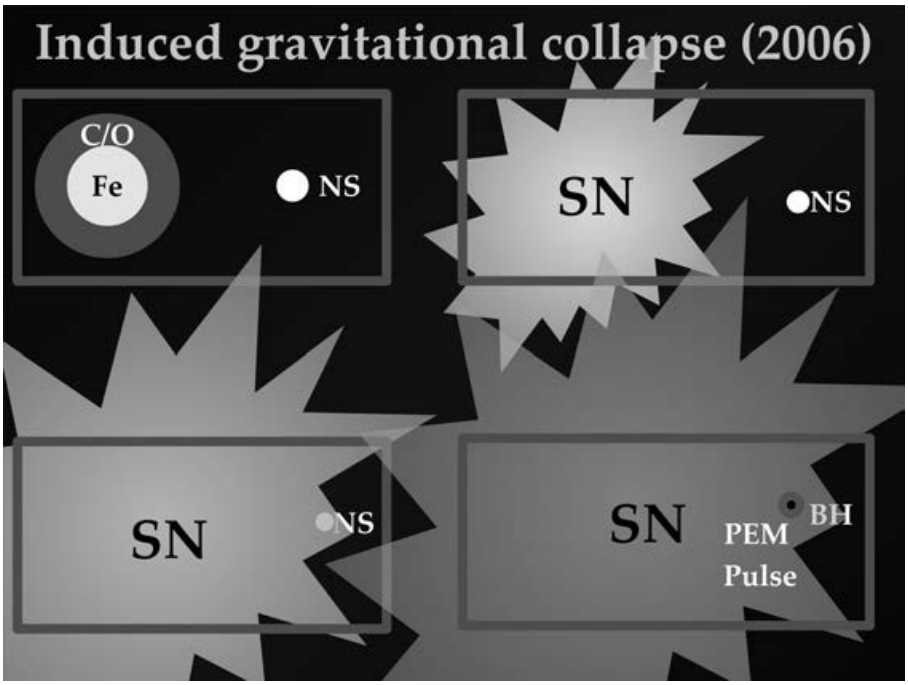

Fig. 24. Process of gravitational collapse to a BH induced by the type Ib/c SN on a companion NS in a close binary system. Figure reproduced from Ref. 131.

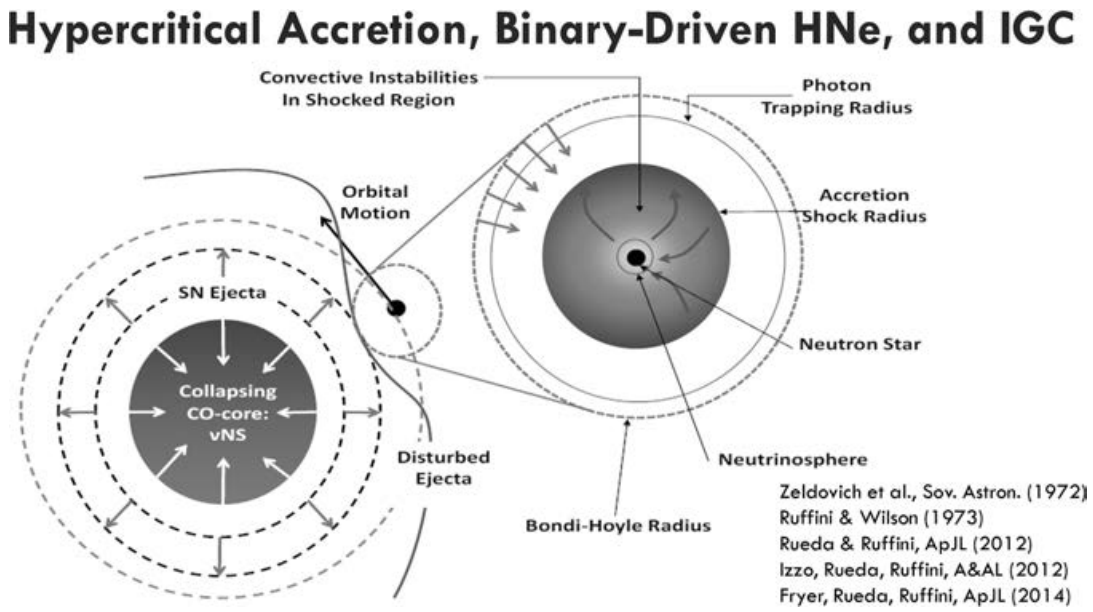

Fig. 25. Hypercritical accretion, binary-driven HNe and IGC.

radius $R_{\rm cap}$ from the NS center

$$R_{\rm cap} = \frac{2GM_{\rm NS}}{v_{\rm rel,ej}^2}, \tag{11}$$

where $M_{\rm NS}$ is the initial NS mass and $v_{\rm rel,ej}$ is the velocity of the ejecta relative to the orbital motion of the NS around the supernova progenitor star

$$v_{\rm rel,ej} = \sqrt{v_{\rm orb}^2 + v_{\rm ej}^2}, \tag{12}$$

with $v_{\rm ej}$ the ejecta velocity in the frame of the supernova progenitor star with mass $M_{\rm SN\text{-}prog}$ and $v_{\rm orb}$ is the orbital velocity of the NS, given by

$$v_{\rm orb} = \sqrt{\frac{G(M_{\rm SN\text{-}prog} + M_{\rm NS})}{a}}, \tag{13}$$

where a is the binary separation, and thus the orbital period of the binary system is

$$P = \sqrt{\frac{4\pi^2 a^3}{G(M_{\rm SN\text{-}prog} + M_{\rm NS})}}. \tag{14}$$

The NS accretes the material that enters into its capture region defined by Eq. (11). The mass-accretion rate is given by[134]

$$\dot{M} = \xi\pi\rho_{\rm ej} R_{\rm cap}^2 v_{\rm ej} = \xi\pi\rho_{\rm ej}\frac{(2GM_{\rm NS})^2}{(v_{\rm orb}^2 + v_{\rm ej}^2)^{3/2}}, \tag{15}$$

where the parameter ξ is lies in the range $1/2 \le \xi \le 1$, $\rho_{\rm ej}$ is the density of the accreted material, and in the last equality we have used Eqs. (11) and (12). The upper value $\xi = 1$ corresponds to the Hoyle–Lyttleton accretion rate.[135] The actual value of ξ depends on the properties of the medium in which the accretion process

occurs, e.g. vacuum or wind. The velocity of the SN ejecta $v_{\rm ej}$ will be much larger than the sound speed c_s of the already existing material between the C+O star and the NS due to the prior mass transfer, namely the Mach number of the SN ejecta will certainly satisfy $\mathcal{M} = v_{\rm ej}/c_s \gg 1$. Thus, in practical calculations we can assume the value $\xi = 1$ in Eq. (15) and the relative velocity $v_{\rm rel,ej}$ of the SN ejecta with respect to the NS companion is given only by the NS orbital velocity and the ejecta velocity as given by Eq. (12). In Fig. 25, we have sketched the accreting process of the supernova ejected material onto the NS. The density of the ejected material can be assumed to decrease in time following the simple power-law[136]

$$\rho_{\rm ej} = \frac{3M_{\rm ej}}{4\pi r^3} = \frac{3M_{\rm ej}}{4\pi\sigma^3 t^{3n}}, \tag{16}$$

where without loss of generality we have assumed that the radius of the SN ejecta expands as $r_{\rm ej} = \sigma t^n$, with σ and n constants. Therefore, the velocity of the ejecta obeys $v_{\rm ej} = n r_{\rm ej}/t$. Equation (15) can be integrated analytically and the accreted mass in a given time interval is given by[94]

$$\Delta M(t) = \int \dot{M} dt = \pi (2GM_{\rm NS})^2 \frac{3M_{\rm ej}}{4\pi n^3 \sigma^6} \mathcal{F} + \text{const.}, \tag{17}$$

where

$$\begin{aligned}\mathcal{F} = t^{-3(n+1)} \Bigg[& -4n(2n-1)t^{4n}\sqrt{kt^{2-2n}+1}\,{}_2F_1\left(\frac{1}{2}, \frac{1}{n-1}; \frac{n}{n-1}; -kt^{2-2n}\right) \\ & - k^2(n^2-1)t^4 + 2k(n-1)(2n-1)t^{2n+2} + 4n(2n-1)t^{4n}\Bigg] \\ & \times [k^3(n-1)(n+1)(3n-1)\sqrt{k+t^{2n-2}}]^{-1},\end{aligned} \tag{18}$$

with $k = v_{\rm orb}^2/(n\,\sigma)^2$ and ${}_2F_1(a,b;c;z)$ is the hypergeometric function. The integration constant is computed with the condition $\Delta M(t) = 0$ for $t \le t_0^{\rm acc}$, where $t_0^{\rm acc}$ is the time at which the accretion process starts, namely the time at which the SN ejecta reaches the NS capture region (see Fig. 25).

3.3. *Reaching the critical mass of the accreting companion NS*

We discuss now the problem of the maximum stable mass of a NS. Nonrotating NS equilibrium configurations have been recently constructed by M. Rotondo, J. Rueda, myself and many students, taking into proper account the strong, weak, electromagnetic and gravitational interactions within general relativity. The equilibrium equations are given by the general relativistic Thomas–Fermi equations coupled with the Einstein–Maxwell equations to form the Einstein–Maxwell–Thomas–Fermi system of equations, which must be solved under the condition of global charge neutrality.[137] These equations supersede the traditional Tolman–Oppenheimer–Volkoff ones that impose the condition of local charge neutrality throughout the configuration. The maximum stable mass $M_{\rm crit} = 2.67\,M_\odot$ of nonrotating NSs has been obtained in Ref. 137.

The high and rapid accretion rate of the SN material can lead the NS mass to reach the critical value $M_{\rm crit} = 2.67\,M_\odot$. This system will undergo gravitational collapse to a BH, producing a GRB. The initial NS mass is likely to be rather high due to the highly nonconservative mass transfer during the previous history of the evolution of the binary system (see e.g. Refs. 125–127, for details). Thus, the NS could reach the critical mass in just a few seconds. Indeed we can see from Eq. (15) that for an ejecta density $10^6\,{\rm g\ cm^{-3}}$ and velocity $10^9\,{\rm cm\ s^{-1}}$, the accretion rate might be as large as $\dot{M} \sim 0.1\,M_\odot s^{-1}$. The occurrence of a GRB-SN event in the scenario depends on some specific conditions satisfied by the binary progenitor system, such as a short binary separation and an orbital period <1 h. This is indeed the case with GRB 090618 and 110709B that we have already analyzed within the context of this scenario in Refs. 36 and 123, respectively (see below in the next subsections). In addition to offering an explanation for the GRB-SN temporal coincidence, the considerations presented here lead to an astrophysical implementation of the concept of proto-BH, generically introduced in our previous works on GRBs 090618, 970828 and 101023 (see Refs. 36, 95 and 138). The proto-BH represents the first stage $20 \lesssim t \lesssim 200$ s of the SN evolution.

It is appropriate now to discuss the possible progenitors of such binary systems. A viable progenitor is represented by X-ray binaries such as Cen X-3 and Her X-1.[6,9,139–143] The binary system is expected to follow an evolutionary track[125–127]: the initial binary system is composed of main-sequence stars 1 and 2 with a mass ratio $M_2/M_1 \gtrsim 0.4$. The initial mass of the star 1 is likely $M_1 \gtrsim 11\,M_\odot$, leaving a NS through a core-collapse event. The star 2, now with $M_2 \gtrsim 11\,M_\odot$ after some almost conservative mass transfer, evolves filling its Roche lobe. It then starts a spiraling in of the NS into the envelope of the star 2. If the binary system does not merge, it will be composed of a helium star and a NS in close orbit. The helium star expands filling its Roche lobe and a nonconservative mass transfer to the NS takes place. This scenario naturally leads to a binary system composed of a C+O star and a massive NS, as the one considered here, see Fig. 25. It is clear that after the occurrence of the SN and the GRB emission, the outcome is represented, respectively, by a NS and a BH. If the NS and the BH are gravitationally bound they give rise to a new kind of binary system, which can lead itself to the merging of the NS and the BH and consequently to a new process of gravitational collapse of the NS into the BH. In this case the system could originate yet another process of GRB emission and possibly a predominant emission in gravitational waves.

4. The Application of the IGC Scenario to GRB 090618

4.1. *The SN ejecta accretion onto the companion NS*

We recall that the blackbody-emitting surface in Episode 1 evolves during the first ∼32 s, as observed in the rest frame, following a power-law behavior

$$r_{\rm em} = \sigma t^n, \quad v_{\rm em} = n\frac{r_{\rm em}}{t} = n\sigma t^{n-1}, \tag{19}$$

where $\sigma = 8.048 \times 10^8\,\mathrm{cm\ s^{-n}}$, $n \approx 3/5$ as shown in Fig. 19, and $v_{\rm em} = dr_{\rm em}/dt \sim 4 \times 10^8\,\mathrm{cm\ s^{-1}}$ at the beginning of the expansion.

When the mass accreted onto the NS triggers the gravitational collapse of the NS into a BH, the authentic GRB emission is observed in the subsequent episode at $t - t_0 \gtrsim 50\,\mathrm{s}$ (observer frame). The characteristics of GRB 090618 are shown in Table 3 of Ref. 35 and we refer to that reference for more details on the GRB light curve and spectrum simulation. We now turn to the details of the accretion process of the SN material onto the NS. We have initially assumed, as an order of magnitude estimate,[36] $r_{\rm SN} = r_{\rm em}$ and $v_{\rm SN} = v_{\rm em}$. The NS of initial mass $M_{\rm NS}$ accretes mass from the SN ejecta at a rate given by[94]

$$\dot{M}_{\rm acc}(t) = \pi \rho_{\rm ej}(t) \frac{(2GM_{\rm NS})^2}{v_{\rm rel,ej}^3}, \quad \rho_{\rm ej}(t) = \frac{3M_{\rm ej}(t)}{4\pi r_{\rm SN}^3(t)}, \tag{20}$$

where $r_{\rm SN}^3(t)$ given by Eq. (19) and $M_{\rm ej}(t) = M_{\rm ej,0} - M_{\rm acc}(t)$ is the available mass to be accreted by the NS as a function of time, with $M_{\rm ej,0}$ the mass ejected in the SN. $v_{\rm rel,ej} = \sqrt{v_{\rm orb}^2 + v_{\rm SN}^2}$ is the velocity of the ejecta relative to the NS, where $v_{\rm SN}$ is the SN ejecta velocity given by Eq. (19) and $v_{\rm orb} = \sqrt{G(M_{\rm core} + M_{\rm NS})/a}$ is the orbital velocity of the NS. Here $M_{\rm core}$ is the mass of the SN core progenitor and a the binary separation. Hereafter we assume $a = 9 \times 10^9\,\mathrm{cm}$, a value higher than the maximum distance traveled by the SN material during the total time interval of Episode 1, $\Delta t \simeq 32\,\mathrm{s}$, $\Delta r \sim 7 \times 10^9\,\mathrm{cm}$ (see Fig. 19). If the accreted mass onto the NS is much smaller than the initial mass of the ejecta, i.e. $M_{\rm acc}/M_{\rm ej,0} \ll 1$, the total accreted mass can be obtained from the formula given by Eq. (8) of Ref. 94, which for GRB 090618 leads to

$$M_{\rm acc}(t) = \int_{t_0^{\rm acc}}^{t} \dot{M}_{\rm acc}(t)dt \approx (2GM_{\rm NS})^2 \frac{15M_{\rm ej,0}t^{2/5}}{8n^3\sigma^6\sqrt{1+kt^{4/5}}}\Bigg|_{t_0^{\rm acc}}^{t}, \tag{21}$$

where $k = v_{\rm orb}^2/(n\sigma)^2$ and $t_0^{\rm acc}$ is the time at which the accretion process starts, namely the time at which the SN ejecta reaches the NS capture region, $R_{\rm cap} = 2GM_{\rm NS}/v_{\rm rel,ej}^2$, so for $t \le t_0^{\rm acc}$ we have $M_{\rm acc}(t) = 0$. The accretion process leads to the gravitational collapse of the NS onto a BH when it reaches the critical mass value. Here we adopt the critical mass $M_{\rm crit} = 2.67\,M_\odot$ computed recently in Ref. 137. Equation (21) is more accurate for massive NSs since the amount of mass needed to reach the critical mass by accretion is much smaller than $M_{\rm ej,0}$. In general, the total accreted mass must be computed from the numerical integration of Eq. (20), which we present below for GRB 090618.

4.2. *Inferences on the binary period*

The occurrence of a GRB-SN event in the accretion induced collapse scenario is subject to some specific conditions of the binary progenitor system such as a short binary separation and orbital period. The orbital period in the present

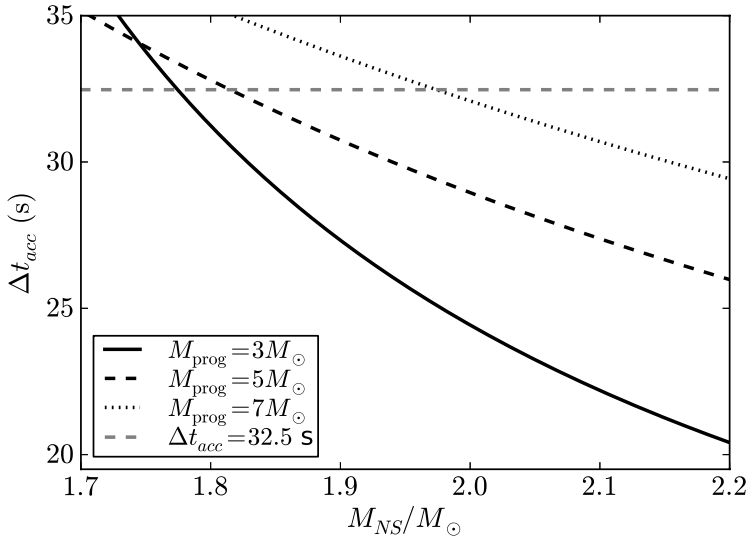

Fig. 26. Time interval $\Delta t_{\rm acc}$ of the accretion process onto the NS as a function of initial NS mass $M_{\rm NS}$ for selected values of the SN core progenitor mass $M_{\rm core}$. The horizontal dashed line is the duration $\Delta t = 32.5$ s of the first episode of GRB 090618, which constrains the duration of the time needed by the NS to reach the critical mass. The crossing points between the dashed horizontal line and the solid curves give the NSs with $M_{\rm NS}$ that reach the critical mass in the time Δt. From Ref. 36.

case is

$$P = \sqrt{\frac{4\pi^2 a^3}{G(M_{\rm core} + M_{\rm NS})}} = 9.1 \left(\frac{M_{\rm core} + M_{\rm NS}}{M_\odot}\right)^{-1/2} \text{min.} \tag{22}$$

We denote by $\Delta t_{\rm acc}$ the total time interval since the beginning of the SN ejecta expansion all the way up to the instant where the NS reaches the critical mass. In Fig. 26, we plot $\Delta t_{\rm acc}$ as a function of the initial NS mass and for different masses of the SN core progenitor mass. The mass of the SN ejecta is assumed to be $M_{\rm ej,0} = M_{\rm core} - M_{\rm rem}$, where $M_{\rm rem}$ is the mass of the central compact remnant (NS) left by the SN explosion. Here we assumed $M_{\rm core} = (3\text{–}8)M_\odot$ at the epoch of the SN explosion, and $M_{\rm rem} = 1.3\,M_\odot$, following some of the type Ic SN progenitors studied in Refs. 125–127.

We can see from Fig. 26 that, for GRB 090618, the mass of the NS companion that collapses onto a BH should be in the range $1.8 \lesssim M_{\rm NS}/M_\odot \lesssim 2.1$ corresponding to the SN Ic progenitors $3 \leq M_{\rm core}/M_\odot \leq 8$. The massive NS companion of the evolved star is in line with the binary scenario proposed in Ref. 131. These results also agree with the well-understood Ib/c nature of the SN associated with GRBs. The most likely explanation for SN Ib/c, which lack H and He in their spectra, is that the SN progenitor star is in a binary system with an NS; see also Refs. 125, 126, 127 and also 144 and 145.

It is also interesting to compare the results on the IGC of an NS to a BH by a type Ib/c SN[94] with the results of Chevalier[136] on the accretion of supernova material by the central NS generated by the supernova. A total accreted mass of up to $0.1\,M_\odot$ in a time of a few hours was obtained there for a normal type II SN.

Thus, a similar amount of mass can be accreted in the two cases, but in the latter the accretion occurs over a longer time. To reach a high accretion rate of the inner SN material onto the central NS, a mechanism is needed that helps to increase the density of the NS surrounding layers, which is decreasing due to the expansion after being unbound by the SN explosion. Reference 136 analyzed the possibility of having a reverse shock wave as this mechanism while it moves back through the SN core. The reverse shock is formed in the interaction of the mantle gas with the low-density envelope. The time scale of the accretion process is thus determined by the time it takes the reverse shock to reach the vicinity of the central newly born NS, which is a few hours in the case of SN II progenitors. However, the existence of a low-density outer envelope, e.g. H and He outer layers, is essential for the strength of the reverse shock. Fall-back accretion onto the central NS is expected to be relevant only in SN II but not in SN Ic like those associated to GRBs, where H and He are absent.

4.3. *The collapse time and the role of neutrinos*

The argument presented in Ref. 94 naturally explains the sequence of events: SN explosion — IGC-BH formation — GRB emission. Correspondingly, the accretion of the material ejected by the SN into the nearby NS of the IGC model presented here occurs almost instantaneously. Indeed for the SN expansion parameters obtained from the observations of Episode 1 in GRB 090618 (see Eq. (19), the accretion of the SN material onto the nearby NS occurs in a few seconds (see Fig. 26). The binary parameters are such that the ejecta density does not decrease too much (from 10^6 g cm^{-3} to $\sim 10^4$ g cm^{-3}) before reaching the capture region of the NS, leading to a high accretion rate. As pointed out in Ref. 136, radiative diffusion will lower the accretion rate up to the Eddington limit (and then to even lower rates) when the trapping radius of the radiation in the flow $r_{\rm tr} = \kappa \dot{M}_{\rm acc}/(4\pi c)$,[136] where κ is the opacity, is equal to the Bondi radius $r_B = GM_{\rm NS}/v^2_{\rm rel,ej}$, the gravitational capture radius. The radius $r_{\rm tr}$ is located where the outward diffusion luminosity is equal to the inward convective luminosity. It can be checked that for the parameters of our system given by Eqs. (19)–(21), the equality $r_{\rm tr} = r_B$ occurs in a characteristic time $\sim$200 days, where we used $\kappa = 0.2$ cm^2 g^{-1}. Thus, this regime is not reached in the present case since the NS is brought to its critical mass just in a few seconds. In the case analyzed by Ref. 136, it happens in a time $\sim$8 days. Only recently we have returned to the previously mentioned papers of Zel'dovich and collaborators[119] and Ruffini and Wilson,[120] since it is clear that the role of neutrino emission is essential in the understanding of the accretion process of the SN ejecta into the companion of NS binary.

It is also a pleasure to show here in Fig. 27 the closest collaborators working at ICRANet headquarters in Pescara and at ICRA at the University of Rome "la Sapienza".

Fig. 27. Group picture. Standing: Carlo Luciano Bianco, Marco Muccino, Wang Yu. Sitting: Remo Ruffini, Giovani Pisani, Jorge Rueda, Milos Kovacevic, Luca Izzo.

5. Recent Highlights and the "Third Paradigm"

Some most recent results have appeared in Refs. 23, 38, 92, 96 and 147 and are summarized in a "third paradigm", see Figs. 28 and 29.

Third paradigm

- *Long GRBs occur in a "**cosmic matrix**" composed of up to 4 different **Episodes**, each one characterized by specific astrophysical processes and Lorentz Γ factors (from $\Gamma \sim 1$ up to $\Gamma \sim 10^3$).*
- *Both short and long GRBs with $E_{\rm iso} > 10^{52}$ erg originate from a gravitational collapse to a BH ($M > M_{\rm crit} \sim 2.6\, M_\odot$) and can have GeV emission:*
  - — Long GRBs → BdHNe → BH + NS binaries → "the" long GRBs.
  - — Short GRBs → massive BNS mergers → BH → "the" short GRBs.
- *Both short and long GRBs with $E_{\rm iso} < 10^{52}$ erg do not form BH and have no GeV emission.*
  - — Long GRBs → binary NSs → X-ray flashes → XRFs.
  - — Short GRBs → short gamma ray flashes → massive NS → S-GRFs.

The progenitor systems of short bursts are traditionally identified with (NS) binary mergers, see, e.g. Refs. 148–157. This theoretical prediction

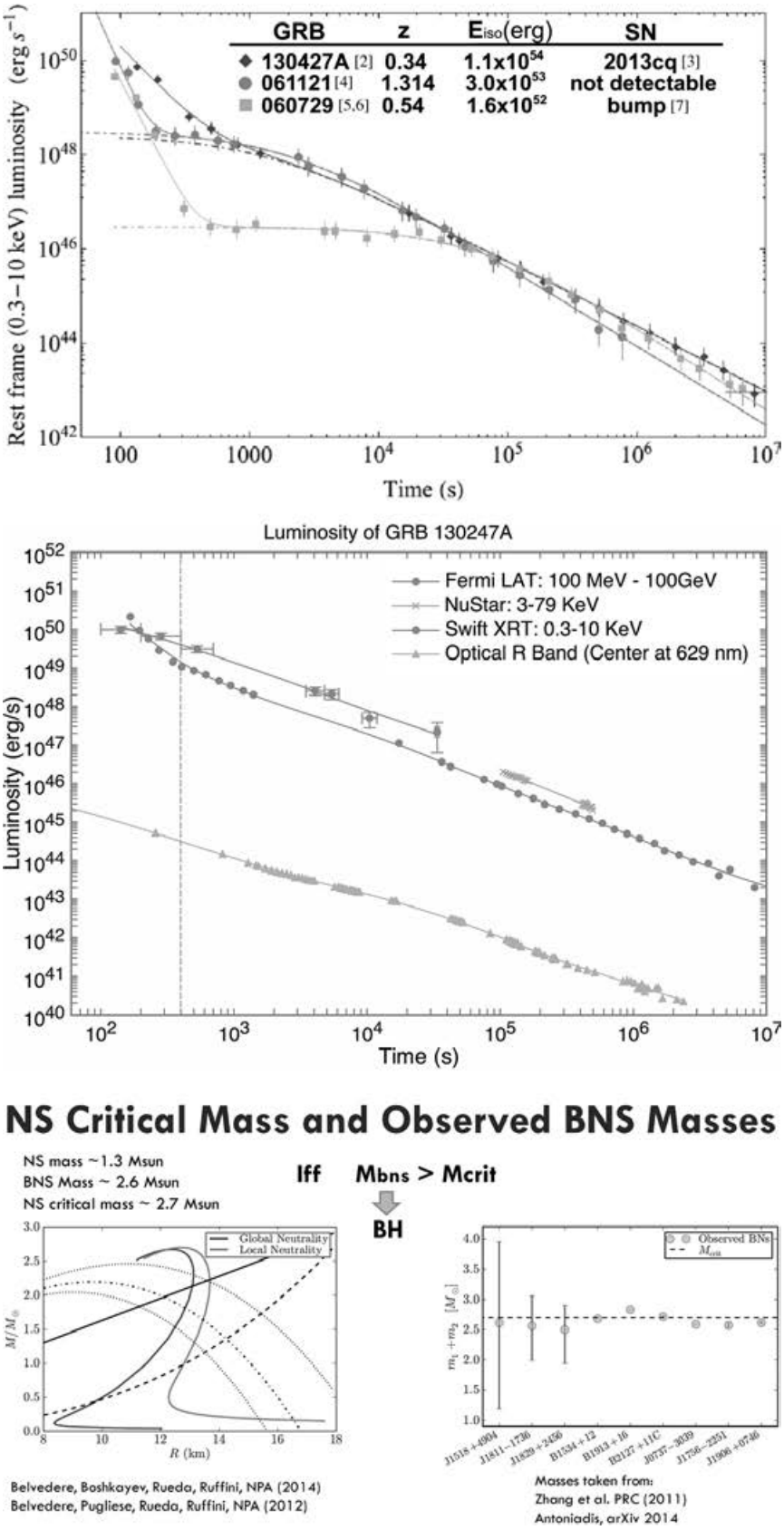

Fig. 28. Top: Episode 3 nesting.[92] Middle: Episode 3 of GRB 130427A, see Ref. 93. Bottom: NS critical mass and observed BNS masses.

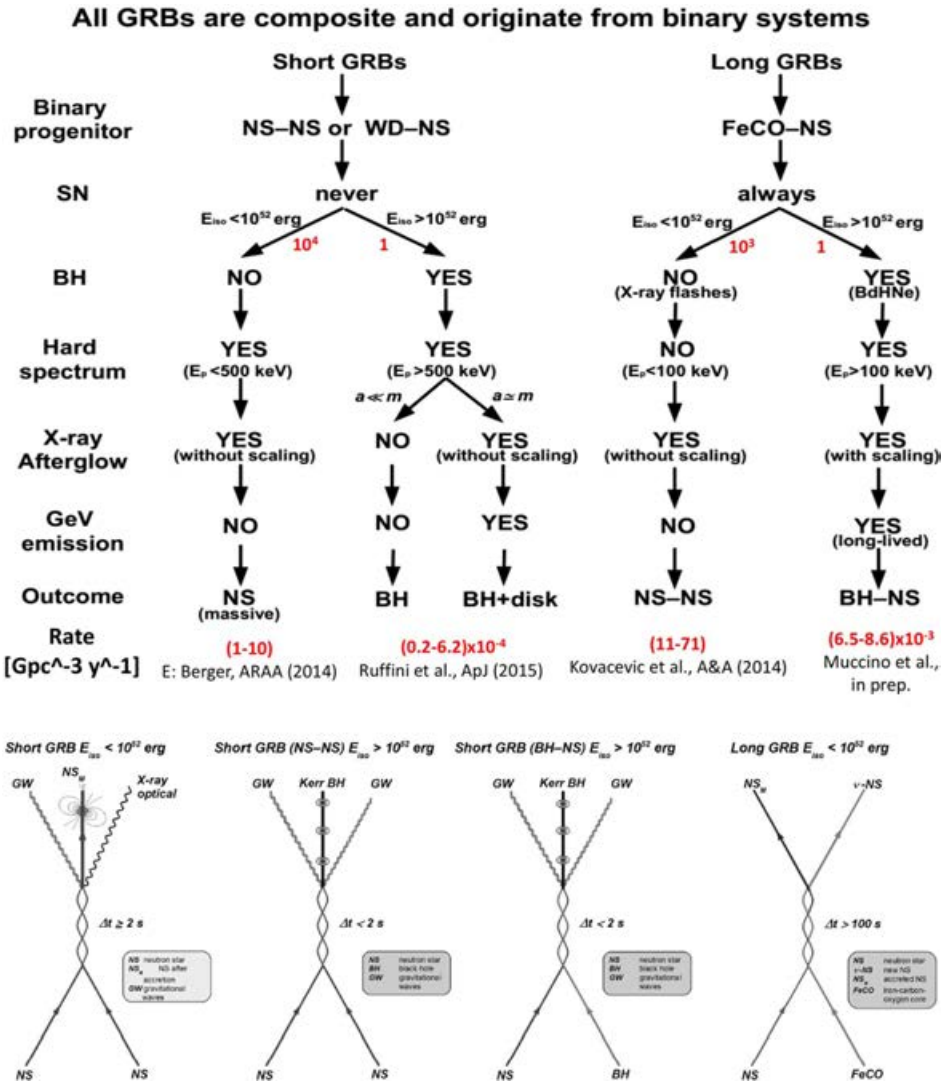

Fig. 29. Top: All GRBs are composite and originate from binary systems, see Refs. 93 and 146. Bottom: the five independent "cosmic matrix" relating SN and GRBs to their constituent NS and BH.

received further observational supports by the successful localization of some short burst afterglows with large off-sets from their hosts galaxies, both late and early type galaxies with no apparent association with star formation, see, e.g. Refs. 157–159.

Reference 148 proposed that the short bursts must be further sub-divided into two different sub-classes, depending on whether or not the NS–NS merger leads to a core with mass larger than the NS critical mass $M_{\rm crit}^{\rm NS}$[167] which gravitationally collapses to a BH. The first class of short bursts is characterized by isotropic energies $E_{\rm iso} \lesssim 10^{52}$ erg and rest-frame spectral peak energies $E_{p,i} \lesssim 2\,{\rm MeV}$[148,168,169] and have as outcome a massive NS (MNS) with additional orbiting material, or even a binary companion (NS or white dwarf, WD), to conserve energy and momentum. We dubbed these moderately hard short bursts as short gamma-ray flashes (S-GRFs). The second class of authentic short GRBs (S-GRBs) has $E_{\rm iso} \gtrsim 10^{52}$ erg

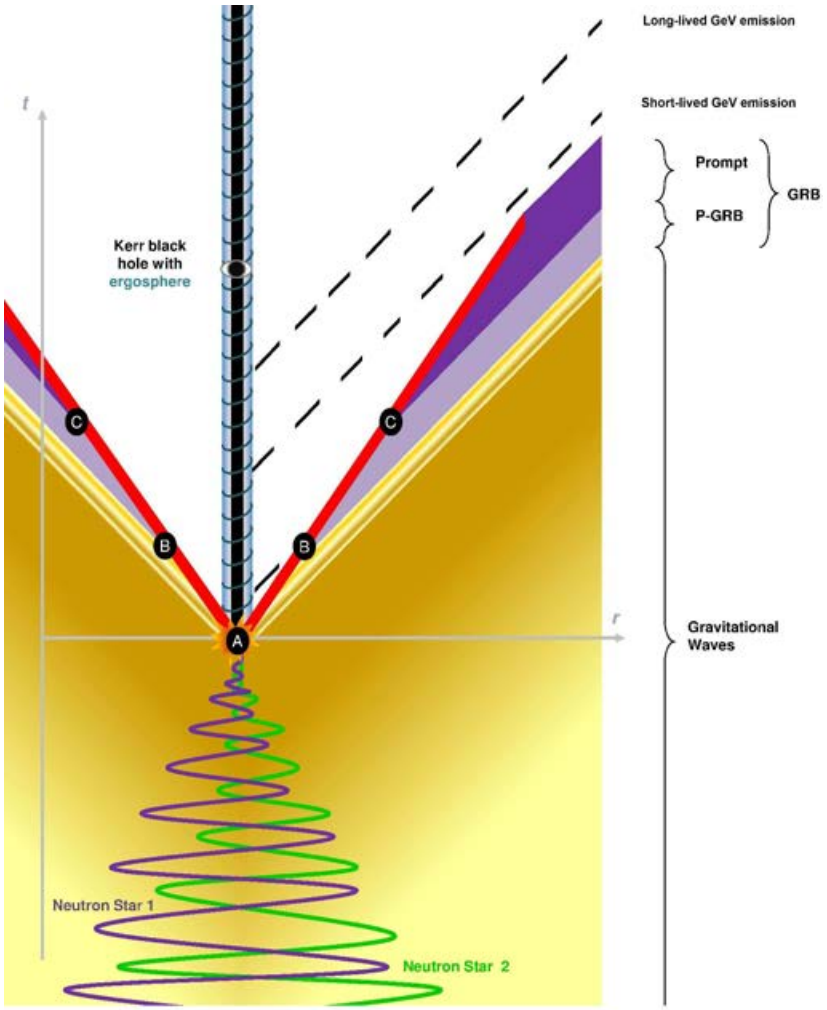

Fig. 30. The spacetime diagram of "the" short GRBs. The orbital separation between the two NSs decreases due to the emission of GWs, until the merging occurs and a family-2 short GRB is emitted. Following the fireshell model: (A) vacuum polarization occurs while the event horizon is formed and a fireshell of e^+e^- plasma self-accelerates radially outward; (B) the fireshell, after engulfing the baryons, keeps self-accelerating and reaches the transparency when the P-GRB is emitted; (C) the accelerated baryons interact with the local CBM giving rise to the prompt emission. The remnant of the merger is a Kerr BH. The accretion of a small (large) amount of orbiting matter onto the BH can lead to the short lived but very energetic 0.1–100 GeV emission observed in GRB 081024B, GRB 090510 and GRB 140619B. The absence of such an emission in GRB 090227B is due to the absence of observations of *Fermi*-LAT. From Ref. 148.

and $E_{p,i} \gtrsim 2\,\mathrm{MeV}$[148,168,169] and lead to the formation of a Kerr BH with additional orbiting material, see Fig. 30. Differently from the case of S-GRFs, they exhibit the systematical presence of the 0.1–100 GeV emission, which is related to the activity of the newly-born BH. The relative rate of these two classes of short bursts has been discussed and presented in Ref. 148. There, it has been proved that the S-GRFs are the more frequent events among the short bursts, see also Ref. 170, as also pointed out from the analogy with NS–NS binaries within our Galaxy, for which only in a subset of them the total mass of the components is larger than M_{crit}^{NS} and can lead to a BH in their merging process. Similar conclusions have been also independently reached in Refs. 171 and 172.

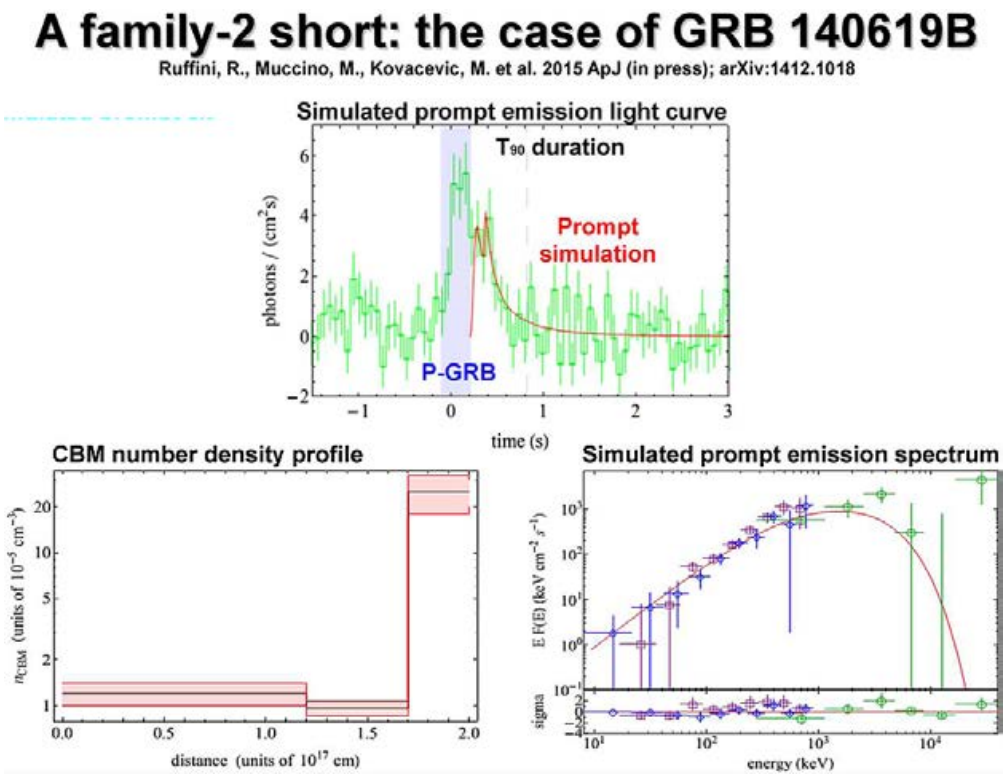

Fig. 31. (Color online) Top: The BGO-b1 (260 keV–40 MeV) simulated light curve of the prompt emission of GRB 140619B (solid red line). Each spike corresponds to the CBM number density profile shown in the figure below. The blue dot-dashed vertical line marks the end of the P-GRB emission. The purple long-dashed and the black dashed vertical lines indicate, respectively, the starting and the ending times of the T_{90} time interval. Clearly visible outside of this time interval is the background noise level. The continuation of the simulation after T_{90} is due to the residual large angle emission of the EQTS due to the density profile. Bottom left: The radial CBM number density distribution of GRB 140619B (black line) and its range of validity (red shaded region). Bottom right: Top panel: comparison between the 8–900 keV data from the NaI-n6 (purple squares) and n9 (blue diamonds) detectors, and the 260 keV–40 MeV data from the BGO-b1 detector (green circles), and the simulation within the firshell model (solid red curve) in the time interval ΔT_2. Bottom panel: the residuals of the above-mentioned data with the simulation. From Ref. 148.

Recently, within the fireshell model for GRBs, see, e.g. for a review Ref. 22, we have identified three examples of such authentic S-GRBs: 090227B,[173] 090510,[174] and 140619B,[148] see Fig. 31. All of them populate the high energy part of the $E_{p,i} - E_{\rm iso}$ relation for short bursts[168,169,174] and consistently exhibit, when they fall within the Fermi-LAT field of view (FoV), $a \lesssim 10^2$ s (in the observer frame) and very energetic GeV emission, starting soon after the transparency emission of the e^+e^- plasma. The apparent absence of the GeV emission in GRB 090227B has already been discussed in Ref. 148 and can be explained simply by the fact that this source was outside the nominal LAT FoV, though significant detection in the LAT low energy (LLE) channel and only one transient-class event with energy above 100 MeV were associated with this GRB.[160]

Much of the current work has been dedicated to extract the maximum amount of information for the building of theoretical model of GRB 130427A, see Figs. 32 and 33, which in the meantime have appeared in the literature.[93]

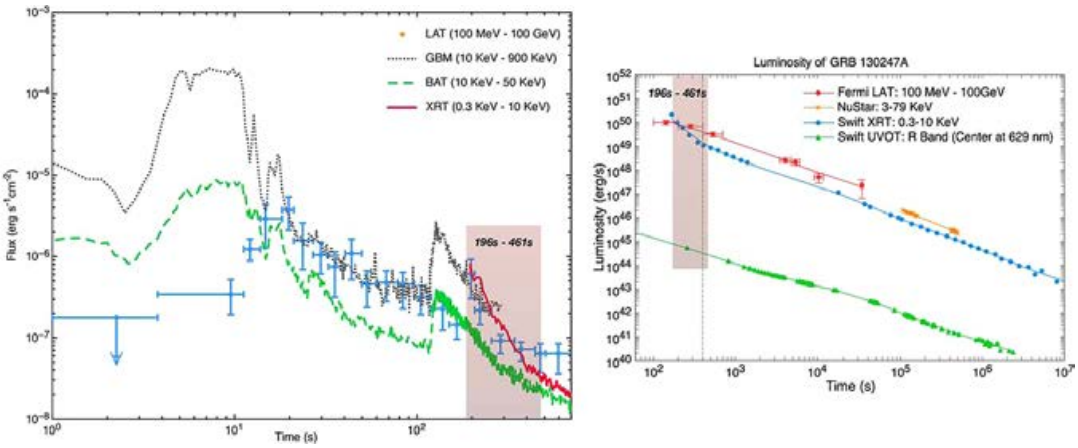

Fig. 32. (Color online) Left: Flux of first 700 s. Blue points are the Fermi-LAT high energy emission from 100 MeV till 100 GeV,[160] gray dotted line represents the Fermi-GBM, from 10 keV to 900 keV, green dashed line represents the photons detected by Swift BAT from 10 keV to 50 keV, and red solid line is the soft X-ray Swift-XRT detection, in the range of 0.3 KeV to 10 KeV. From this figure, clearly the Fermi-LAT emission reaches highest fluence at about 20 s while the gamma-ray detected by Fermi-GBM releases most of the energy within the first 10 s. Right: The multi-wavelength light curve of GRB 130427A. The high energy (100 MeV–100 GeV) emission detected by Fermi-LAT marked with red and soft X-ray (0.3–10 keV) data from Swift-XRT marked with blue are deduced from the original data. NuStar data (3–79 keV) marked with orange comes from Ref. 161. The optical (R band, center at 629 nm) data marked with green comes from ground based satellites.[162] The error bars are too small with respect to the data points except for Fermi-LAT data. The horizontal error bars of Fermi-LAT represent the time bin in which the flux is calculated and vertical bars are statistical $1-\sigma$ errors on the flux (the systematic error of 10% is ignored). The details in the first tens of seconds are ignored as we are interested in the behavior of the high energy light curve on a longer time scale. The vertical gray dashed line at ($\sim$400 s) indicates when the constant decaying slope starts. It is clear that all the energy bands have almost the same slope after 400 s in Episode 3. From Ref. 93.

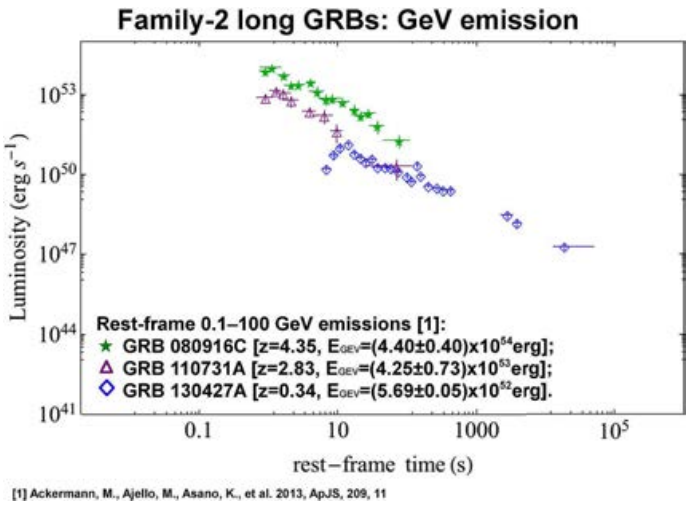

Fig. 33. (Color online) The common power-law behavior of the rest-frame 0.1–100 GeV isotropic luminosity light curves of selected BdHNe: GRB 080916C with green stars,[163,164] GRB 110731A with purple triangles[165] and Primorac D. *et al.* in preparation, and GRB 130427A with blue diamonds.[93,166] For each source the redshift and the total isotropic GeV emitted energy are also indicated. The GeV emission onset occurs soon after the P-GRB emission and during the prompt emission. Within the fireshell model, the GeV emission represents clear signature for a Kerr–Newman BH formation.

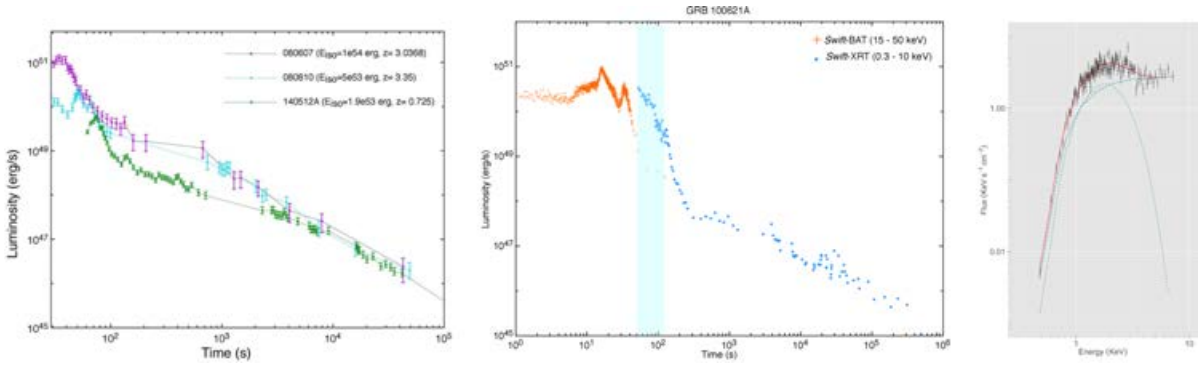

Fig. 34. (Color online) Left: Demonstration of X-ray flares in BdHN: the soft X-ray light-curves (0.3–10 keV) of GRB 080607, 080810, 140512 are transferred to their cosmological rest frame, clearly flares occur before 100 s, and the GBB with lower isotropic energy has a later and less luminous flare. Then comes the plateau, lower isotropic energy GRB has a longer duration plateau. At time later than 10^4 s, three light-curves overlap and decay following a similar power-law behavior. Middle: luminosity light-curve of GRB 100621A. The red crosses and the blue points are the data deduced from Swift-BAT in the energy band 15–50 keV and Swift-XRT in the energy band 0.3–10 keV respectively. The blue shadow indicates a time interval during which thermal component is determined. Light-curve is presented in its cosmological rest frame. Right: the spectrum from 51 s to 130 s and model fitting. Black crosses are the data with uncertainties. Short-dashed line presents the blackbody component with temperature 0.39 keV emitted from a radius of 5.13×10^{12} cm. Long-dashed line corresponds to the nonthermal power-law component. Solid line is the combination of the total two components. Spectrum is shown and fitted in the observers frame.

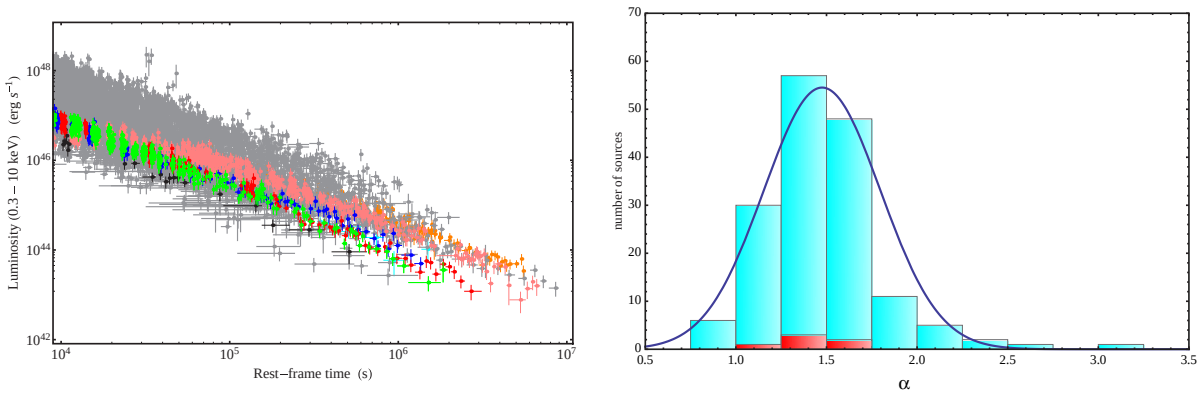

(a) (b)

Fig. 35. (Color online) Panel (a): Late X-Ray Emission (LXRE) luminosity light curves of all 161 sources of the ES (gray) compared with the ones of the GS: GRB 060729 (pink), GRB 061007 (black), GRB 080913B (blue), GRB 090618 (green), GRB 091127 (red), and GRB 111228 (cyan), plus GRB 130427A.[93,175] Panel (b): Distribution of the LXRE power law indexes α within the ES (cyan) compared to the one of the GS (red). Such a distribution follows a Gaussian behavior (blue line) with a mean value of $\mu_\alpha = 1.48$ and a standard deviation of $\sigma_\alpha = 0.32$.

In addition, the main current interest in our group is to probe the impact of the newly formed GRB, originating in the BH formation, on the SN ejecta. There are data on the flares and on the thermal emission in BdHN, which we are currently examining, see Fig. 34. Concurrently, we are considering the LXRE all the way to the afterglow and evidence for asymmetric emission, see Fig. 35.

6. Conclusions

This celebration of the 50th Anniversary of Relativistic Astrophysics comes after 17 years of research addressing the temporal and spatial coincidence of two of the most powerful events in the cosmos: the explosion of a supernova and the emission of a GBM. The first example of such a coincidence occurred with the GRB 980425 and the SN 1998bw. The pioneering results of BeppoSAX were soon followed by many observations from X-ray and gamma ray space observatories (the AGILE, FERMI, KONUS WIND and SWIFT satellites), as well as from ground-based optical telescopes. This has given clear evidence that far from being an exception such a coincidence is quite common: it pervades the occurrence of all most powerful hypernovae and long GRBs. We have followed in this presentation a historical approach explaining how the solution of this enigma has also lead to the unveiling of the basic astrophysical process occurring in long and short GRBs as well as in the occurrence of hypernovae.

The concept of GRB initially envisaged as a single-ultrarelativistic-jetted emission occurring in a "collapsar-fireball" has been superseded by a far reaching scenario (see Fig. 36). Progress has been slow but steady: it has required the introduction of new paradigms, the extension of known relativistic field theories to unexplored regimes, and strong observational support from space and ground observatories. We have outlined in this presentation some crucial moments of these developments. Our new outlook indicates the existence of seven subclasses of GRBs,

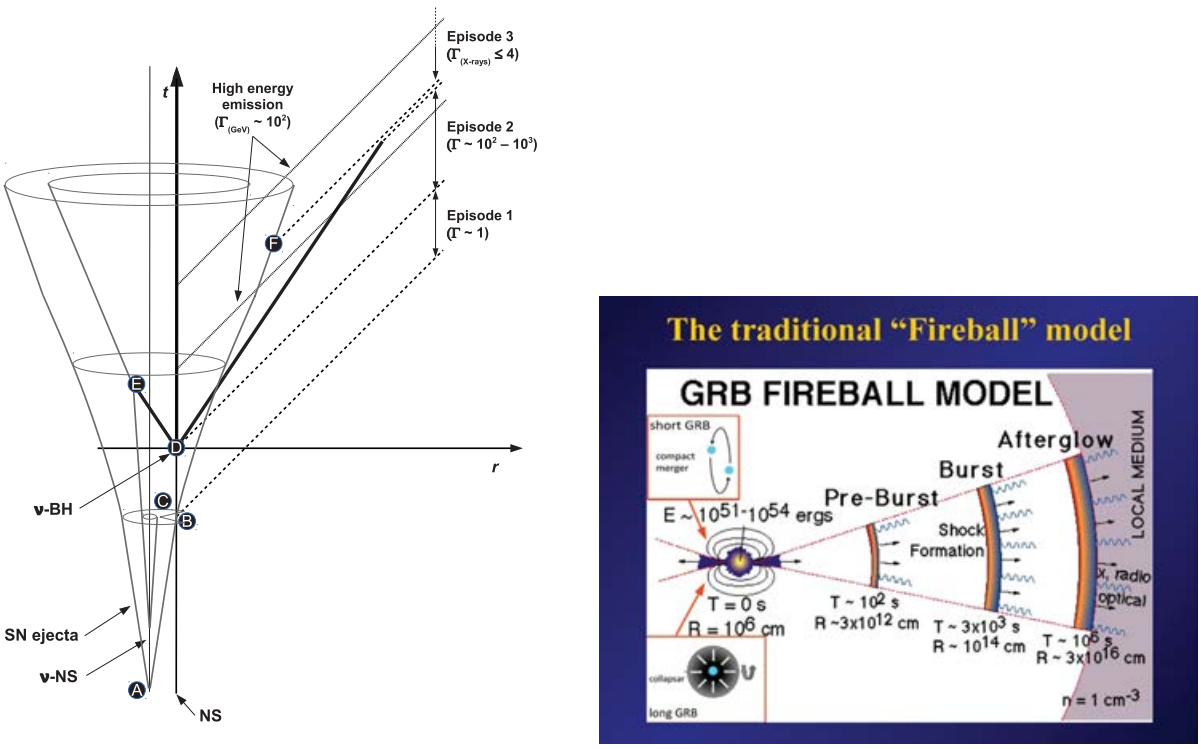

(a) (b)

Fig. 36. Panel (a): Fireshell model. Panel (b): Fireball model.

many more than the initial division into short and long GRBs. The fireball model has been superseded by a more detailed "fireshell" model modulated on the IGC paradigm. The concept of a "cosmic matrix" brings to the attention of the astronomical community a new approach necessary to rationalize a sequence of astrophysical events occurring over a 3 h time scale, when measured in the cosmological rest frame of the GRB. It is as far from describing a single process as it can possibly be. The sequence of events instead encompasses (1) the matter accretion in a tight binary system composed of an Fe-CO core undergoing a SN explosion onto a tight companion NS, (2) the creation of a black hole by the gravitational collapse of the NS, following the accretion process and the emission of the GRB, (3) the concurrent emission of the jetted GeV emission, (4) the interaction of the GRB emission with the SN ejected (first presented here), (5) the final appearance of the optical SN emission after 10 days. It is expected that this celebration of the 50th Anniversary coincides with the opening of new era in relativistic astrophysics.

References

1. W. Baade and F. Zwicky, *Proc. US Nat. Acad. Sci.* **20** (1934) 254.
2. W. Baade and F. Zwicky, *Proc. Nat. Acad. Sci.* **20** (1934) 259.
3. R. Giacconi, H. Gursky, F. R. Paolini and B. B. Rossi, *Phys. Rev. Lett.* **9** (1962) 439.
4. I. S. Shklovsky, *Astrophys. J.* **148** (1967) 1.
5. R. Giacconi and R. Ruffini (eds.), *Physics and Astrophysics of Neutron Stars and Black Holes* (Amsterdam, North Holland Publishing Co., 1978).
6. R. W. Leach and R. Ruffini, *Astrophys. J.* **180** (1973) L15.
7. C. E. Rhoades and R. Ruffini, *Phys. Rev. Lett.* **32** (1974) 324.
8. R. Ruffini, Astrophysics and gravitation, in *Proc. Sixteenth Solvay Conf. Physics*, University of Brussels (September 1973).
9. H. Gursky and R. Ruffini (eds.), Neutron Stars, Black Holes and Binary X-Ray Sources, in *Proc. Annual Meeting*, San Francisco, Calif., 28 February 1974, Vol. 48 (Astrophysics and Space Science Library, 1975).
10. E. Costa, F. Frontera, J. Heise *et al.*, *Nature* **387** (1997) 783.
11. T. Damour and R. Ruffini, *Phys. Rev. Lett.* **35** (1975) 463.
12. R. Ruffini, Fundamental physics from black holes, neutron stars and gamma ray bursts, in *The Twelfth Marcel Grossmann Meeting*, eds. T. Damour, R. Jantzen and R. Ruffini (2012), pp. 286–367.
13. R. Ruffini, Black holes, supernovae and gamma ray bursts, in *The Thirteenth Marcel Grossmann Meeting*, eds. K. Rosquist, R. T. Jantzen and R. Ruffini (World Scientific Publishing Co. Pte. Ltd., 2015), pp. 242–314.
14. R. Ruffini, A. G. Aksenov, M. G. Bernardini *et al.*, *Am. Inst. Phys. Conf. Ser.* **1132** (2009).
15. A. Heger, C. L. Fryer, S. E. Woosley *et al.*, *Astrophys. J.* **591** (2003) 288.
16. E. Verner, F. Bruhweiler and T. Gull, *Astrophys. J.* **624** (2005) 973.
17. A. Damineli, A. Kaufer, B. Wolf *et al.*, *Astrophys. J.* **528** (2000) L101.
18. R. C. Iping, G. Sonneborn, T. R. Gull *et al.*, *Astrophys. J.* **633** (2005) L37.
19. E. Pian, L. Amati, L. A. Antonelli *et al.*, *Astrophys. J.* **536** (2000) 778.
20. S. R. Kulkarni, D. A. Frail, M. H. Wieringa *et al.*, *Nature* **395** (1998) 663.
21. T. J. Galama, P. M. Vreeswijk, J. van Paradijs *et al.*, *Nature* **395** (1998) 670.

22. R. Ruffini, G. Vereshchagin and S. Xue, *Phys. Rep.* **487** (2010) 1.
23. R. Ruffini, Y. Wang, M. Kovacevic *et al.*, GRB 130427A and SN 2013cq: A multi-wavelength analysis of an induced gravitational collapse event, arXiv:1405.5723 (2014).
24. A. Hewish, S. J. Bell, J. D. H. Pilkington *et al.*, *Nature* **217** (1968) 709.
25. W. Arnett, in *From Nuclei to White Dwarfs and Neutron Stars*, eds. A. Mezzacappa and R. Ruffini (World Scientific, Singapore), in press.
26. M. Rees, R. Ruffini and J. A. Wheeler, *Black Holes*, *Gravitational Waves and Cosmology*: *An Introduction to Current Research*, Topics in Astrophysics and Space Physics, Vol. 10 (Gordon and Breach, Science Publishers, Inc., New York, 1974).
27. A. Finzi and R. A. Wolf, *Astrophys. J.* **153** (1968) 865.
28. D. Christodoulou and R. Ruffini, *Phys. Rev. D* **4** (1971) 3552.
29. R. Ruffini, The ergosphere and dyadosphere of black holes, in *The Kerr Spacetime*, eds. D. L. Wiltshire, M. Visser and S. Scott (eds.) (Cambridge University Press, 2009).
30. R. Ruffini, J. D. Salmonson, J. R. Wilson and S.-S. Xue, *Astron. Astrophys.* **350** (1999) 334.
31. R. Ruffini, J. D. Salmonson, J. R. Wilson and S.-S. Xue, *Astron. Astrophys.* **359** (2000) 855.
32. R. Ruffini, Analogies, new paradigms and observational data as growing factors of relativistic astrophysics, in *Fluctuating Paths and Fields*, eds. W. Janke, A. Pelster, H. J. Schmidt and M. Bachmann (World Scientific, Singapore, 2001).
33. W. S. Paciesas, C. A. Meegan, G. N. Pendleton *et al.*, *Astrophys. J. SS* **122** (1999) 465.
34. F. Frontera, GRB Afterglow Discovery with Bepposax: Its Story 15 Years Later, in *The Thirteenth Marcel Grossmann Meeting*, eds. K. Rosquist, R. T. Jantzen and R. Ruffini (World Scientific Publishing Co. Pte. Ltd., 2015), pp. 33–53.
35. L. Izzo, R. Ruffini, A. V. Penacchioni *et al.*, *Astron. Astrophys.* **543** (2012) A10.
36. L. Izzo, J. A. Rueda and R. Ruffini, *Astron. Astrophys.* **548** (2012) L5.
37. G. B. Pisani, L. Izzo, R. Ruffini *et al.*, *Astron. Astrophys.* **552** (2013) L5.
38. M. Muccino, R. Ruffini, C. L. Bianco *et al.*, *Astrophys. J.* **763** (2013) 125.
39. T. Piran, *Rev. Mod. Phys.* **76** (2004) 1143.
40. G. Cavallo and M. J. Rees, *Mon. Not. R. Astron. Soc.* **183** (1978) 359.
41. J. Goodman, Are gamma-ray bursts optically thick?, *Astrophys. J.* **308** (1986) L47.
42. B. Paczynski, *Astrophys. J.* **308** (1986) L43.
43. P. Meszaros, *Rep. Prog. Phys.* **69** (2006) 2259.
44. R. Ruffini, *Int. J. Mod. Phys. D* **20** (2011) 1797.
45. R. Ruffini, Beyond the critical mass: The dyadosphere of black holes, in *Frontiers Science Series 23*: *Black Holes and High Energy Astrophysics*, eds. H. Sato and N. Sugiyama (Universal Academic Press, 1998).
46. G. Preparata, R. Ruffini and S.-S. Xue, *Astron. Astrophys.* **338** (1998) L87.
47. A. Aksenov, R. Ruffini and G. Vereshchagin, *Phys. Rev. Lett.* **99** (2007) 125003.
48. E. Ramirez-Ruiz and E. E. Fenimore, *Astrophys. J.* **539** (2000) 712.
49. M. J. Rees and P. Meszaros, *Astrophys. J.* **430** (1994) L93.
50. M. J. Rees and P. Meszaros, *Mon. Not. R. Astron. Soc.* **258** (1992) 41P.
51. M. Tavani, *Astrophys. J.* **466** (1996) 768.
52. F. Frontera, L. Amati, E. Costa *et al.*, *Astrophys. J. Suppl.* **127** (2000) 59.
53. A. Crider, E. P. Liang, I. A. Smith *et al.*, *Astrophys. J.* **479** (1997) L39.
54. R. D. Preece, M. S. Briggs, T. W. Giblin *et al.*, *Astrophys. J.* **581** (2002) 1248.
55. G. Ghirlanda, A. Celotti and G. Ghisellini, *Astron. Astrophys.* **393** (2002) 409.

56. G. Ghirlanda, A. Celotti and G. Ghisellini, *Astron. Astrophys.* **406** (2003) 879.
57. P. Kumar and E. McMahon, *Mon. Not. R. Astron. Soc.* **384** (2008) 33.
58. T. Piran, R. Sari and Y. Zou, *Mon. Not. R. Astron. Soc.* **393** (2009) 1107.
59. R. D. Blandford and C. F. McKee, *Phys. Fluids* **19** (1976) 1130.
60. E. Molinari, S. D. Vergani, D. Malesani *et al.*, *Astron. Astrophys.* **469** (2007) L13.
61. E. S. Rykoff, F. Aharonian, C. W. Akerlof *et al.*, *Astrophys. J.* **702** (2009) 489.
62. R. Sari and T. Piran, *Astrophys. J.* **520** (1999) 641.
63. G. Ghisellini and A. Celotti, *Astron. Astrophys. Suppl.* **138** (1999) 527.
64. A. A. Zdziarski, R. Svensson and B. Paczynski, *Astrophys. J.* **366** (1991) 343.
65. A. Shemi, *Mon. Not. R. Astron. Soc.* **269** (1994) 1112.
66. A. Pe'er and B. Zhang, *Astrophys. J.* **653** (2006) 454.
67. M. V. Medvedev, *Astrophys. J.* **540** (2000) 704.
68. A. Panaitescu and P. Mészáros, *Astrophys. J.* **544** (2000) L17.
69. B. E. Stern and J. Poutanen, *Mon. Not. R. Astron. Soc.* **352** (2004) L35.
70. D. Eichler and A. Levinson, *Astrophys. J.* **529** (2000) 146.
71. P. Mészáros and M. J. Rees, *Astrophys. J.* **530** (2000) 292.
72. P. Mészáros, *Annu. Rev. Astron. Astrophys.* **40** (2002) 137.
73. F. Daigne and R. Mochkovitch, *Mon. Not. R. Astron. Soc.* **336** (2002) 1271.
74. D. Giannios, *Astron. Astrophys.* **457** (2006) 763.
75. F. Ryde and A. Pe'er, *Astrophys. J.* **702** (2009) 1211.
76. D. Lazzati and M. C. Begelman, *Astrophys. J.* **725** (2010) 1137.
77. R. Ruffini, *Astron. Astrophys. Suppl.* **138** (1999) 513.
78. R. Ruffini, C. L. Bianco, P. Chardonnet *et al.*, *Astrophys. J.* **555** (2001) L113.
79. C. L. Bianco and R. Ruffini, *Astrophys. J.* **605** (2004) L1.
80. C. L. Bianco and R. Ruffini, *Astrophys. J.* **620** (2005) L23.
81. P. Meszaros, P. Laguna and M. J. Rees, *Astrophys. J.* **415** (1993) 181.
82. R. Sari, *Astrophys. J.* **489** (1997) L37.
83. R. Sari, *Astrophys. J.* **494** (1998) L49.
84. E. Waxman, *Astrophys. J.* **491** (1997) L19.
85. M. J. Rees and P. Meszaros, *Astrophys. J.* **496** (1998) L1.
86. J. Granot, T. Piran and R. Sari, *Astrophys. J.* **513** (1999) 679.
87. A. Panaitescu and P. Meszaros, *Astrophys. J.* **493** (1998) L31.
88. A. Gruzinov and E. Waxman, *Astrophys. J.* **511** (1999) 852.
89. J. van Paradijs, C. Kouveliotou and R. A. M. J. Wijers, *Annu. Rev. Astron. Astrophys.* **38** (2000) 379.
90. C. L. Bianco and R. Ruffini, *Astrophys. J.* **633** (2005) L13.
91. R. Ruffini, C. L. Bianco, P. Chardonnet *et al.*, *Astrophys. J.* **555** (2001) L117.
92. R. Ruffini, M. Muccino, C. L. Bianco *et al.*, *Astron. Astrophys.* **565** (2014) L10.
93. R. Ruffini, Y. Wang, M. Enderli *et al.*, *Astrophys. J.* **798** (2015) 10.
94. J. A. Rueda and R. Ruffini, *Astrophys. J.* **758** (2012) L7.
95. A. V. Penacchioni, R. Ruffini, L. Izzo *et al.*, *Astron. Astrophys.* **538** (2012) A58.
96. C. L. Fryer, J. A. Rueda and R. Ruffini, *Astrophys. J.* **793** (2014) L36.
97. R. Ruffini, L. Izzo, A. V. Penacchioni *et al.*, *PoS* (*Texas2010*) (2011) 101.
98. P. Schady, W. H. Baumgartner, A. P. Beardmore *et al.*, *GCN Circ.* **9512** (2009).
99. W. H. Baumgartner, S. D. Barthelmy, J. R. Cummings *et al.*, *GCN Circ.* **9530** (2009) 1.
100. G. J. Fishman, C. A. Meegan, R. B. Wilson *et al.*, *Astrophys. J. Suppl.* **92** (1994) 229.
101. A. P. Beardmore and P. Schady, *GCN Circ.* **9528** (2009) 1.
102. C. Meegan, G. Lichti, P. N. Bhat *et al.*, *Astrophys. J.* **702** (2009) 791.
103. D. Band, J. Matteson, L. Ford *et al.*, *Astrophys. J.* **413** (1993) 281.

104. S. McBreen, *GCN Circ.* **9535** (2009).
105. S. B. Cenko, D. A. Perley, V. Junkkarinen *et al.*, *GCN Circ.* **9518** (2009).
106. B. E. Schaefer, *Astrophys. J.* **660** (2007) 16.
107. S. Golenetskii, R. Aptekar, E. Mazets *et al.*, *GCN Circ.* **9553** (2009) 1.
108. K. Kono, A. Daikyuji, E. Sonoda *et al.*, *GCN Circ.* **9568** (2009) 1.
109. F. Longo, E. Moretti, G. Barbiellini *et al.*, *GCN Circ.* **9524** (2009).
110. Y. Kotov, A. Kochemasov, S. Kuzin *et al.*, in *37th COSPAR Scientific Assembly* (Montréal, Canada, 13–20 July 2008), p. 1596.
111. A. Nandi, A. R. Rao, S. K. Chakrabarti *et al.*, Indian Payloads (RT-2 Experiment) Onboard CORONAS-PHOTON Mission, arXiv:0912.4126 (December 2009).
112. A. R. Rao, J. P. Malkar, M. K. Hingar *et al.*, *Astrophys. J.* **728** (2011) 42.
113. Z. Cano, D. Bersier, C. Guidorzi *et al.*, *Mon. Not. R. Astron. Soc.* **413** (2011) 669.
114. F. Ryde, M. Axelsson, B. B. Zhang *et al.*, *Astrophys. J.* **709** (2010) L172.
115. S. Guiriec, V. Connaughton, M. S. Briggs *et al.*, *Astrophys. J.* **727** (2011) L33.
116. A. Pe'er, *Astrophys. J.* **682** (2008) 463.
117. C. Cherubini, A. Geralico, H. J. A. Rueda and R. Ruffini, *Phys. Rev. D* **79** (2009) 124002.
118. R. Ruffini, C. L. Bianco, P. Chardonnet *et al.*, New perspectives in physics and astrophysics from the theoretical understanding of gamma-ray bursts, in *Cosmology and Gravitation*, eds. M. Novello and S. E. Perez Bergliaffa, American Institute of Physics Conference Series, Vol. 668 (American Institute of Physics, 2003).
119. Y. B. Zel'dovich, L. N. Ivanova and D. K. Nadezhin, *Soviet Astron.* **16** (1972) 209.
120. R. Ruffini and J. Wilson, *Phys. Rev. Lett.* **31** (1973) 1362.
121. R. Ruffini, M. G. Bernardini, C. L. Bianco *et al.*, The role of grb 031203 in clarifying the astrophysical grb scenario, in *The 6th Integral Workshop — The Obscured Universe*, eds. S. Grebenev, R. Sunyaev, C. Winkler, A. Parmar and L. Ouwehand, Vol. SP-622 (ESA Special Publication, 2007), p. 561.
122. B. Patricelli, M. G. Bernardini, C. L. Bianco *et al.*, *Int. J. Mod. Phys. D* **20** (2011) 1983.
123. A. V. Penacchioni, R. Ruffini, C. L. Bianco *et al.*, *Astron. Astrophys.* **551** (2013) A133.
124. J. Hjorth and J. S. Bloom, *The Gamma-Ray Burst — Supernova Connection*, in *Gamma-Ray Bursts*, eds. C. Kouveliotou, R. A. M. J. Wijers and S. Woosley, Cambridge Astrophysics Series, Vol. 51 (Cambridge University Press, Cambridge, 2012), pp. 169–190.
125. K. Nomoto and M. Hashimoto, *Phys. Rep.* **163** (1988) 13.
126. K. Nomoto, H. Yamaoka, O. R. Pols *et al.*, *Nature* **371** (1994) 227.
127. K. Iwamoto, K. Nomoto, P. Höflich *et al.*, *Astrophys. J.* **437** (1994) L115.
128. S. E. Woosley and J. S. Bloom, *Annu. Rev. Astron. Astrophys.* **44** (2006) 507.
129. A. Shemi and T. Piran, *Astrophys. J.* **365** (1990) L55.
130. T. Piran, A. Shemi and R. Narayan, *Mon. Not. R. Astron. Soc.* **263** (1993) 861.
131. R. Ruffini, M. G. Bernardini, C. L. Bianco *et al.*, On gamma-ray bursts, in *The Eleventh Marcel Grossmann Meeting*, eds. H. Kleinert, R. T. Jantzen and R. Ruffini (World Scientific, Singapore, 2008).
132. R. Ruffini, M. G. Bernardini, C. L. Bianco *et al.*, Black hole physics and astrophysics: The grb-supernova connection and urca-1 — urca-2, in *The Tenth Marcel Grossmann Meeting*, eds. M. Novello, S. Perez Bergliaffa and R. Ruffini (World Scientific, Singapore, 2006).
133. O. D. Toropina, M. M. Romanova and R. V. E. Lovelace, *Mon. Not. R. Astron. Soc.* **420** (2012) 810.
134. H. Bondi and F. Hoyle, *Mon. Not. R. Astron. Soc.* **104** (1944) 273.

135. F. Hoyle and R. A. Lyttleton, *Proc. Cambridge Philos. Soc.* **35** (1939) 405.
136. R. A. Chevalier, *Astrophys. J.* **346** (1989) 847.
137. R. Belvedere, D. Pugliese, J. A. Rueda *et al.*, *Nucl. Phys. A* **883** (2012) 1.
138. L. Izzo, R. Ruffini, C. L. Bianco *et al.*, On the thermal and double episode emissions in GRB 970828, arXiv:1205.6651 (2012).
139. E. Schreier, R. Levinson, H. Gursky *et al.*, *Astrophys. J.* **172** (1972) L79.
140. R. E. Wilson, *Astrophys. J.* **174** (1972) L27.
141. H. Tananbaum, H. Gursky, E. M. Kellogg *et al.*, *Astrophys. J.* **174** (1972) L143.
142. K. Davidson and J. P. Ostriker, *Astrophys. J.* **179** (1973) 585.
143. M. L. Rawls, J. A. Orosz, J. E. McClintock *et al.*, *Astrophys. J.* **730** (2011) 25.
144. A. V. Tutukov and A. V. Fedorova, *Astron. Rep.* **51** (2007) 291.
145. R. A. Chevalier, *Astrophys. J.* **752** (2012) L2.
146. M. Muccino, R. Ruffini, M. Kovacevic *et al.*, GRB 140619B: A short GRB from a binary neutron stars merger leading to the black hole formation, (2014) arXiv e-prints.
147. R. Ruffini, L. Izzo, M. Muccino *et al.*, *Astron. Astrophys.* **569** (2014) A39.
148. R. Ruffini, M. Muccino, M. Kovacevic *et al.*, *Astrophys. J.* **808** (2015) 190.
149. J. Goodman, *Astrophys. J.* **308** (1986) L47.
150. B. Paczynski, *Astrophys. J.* **308** (1986) L43.
151. D. Eichler, M. Livio, T. Piran and D. N. Schramm, *Nature* **340** (1989) 126.
152. R. Narayan, T. Piran and A. Shemi, *Astrophys. J.* **379** (1991) L17.
153. P. Meszaros and M. J. Rees, *Astrophys. J.* **482** (1997) L29.
154. S. Rosswog, E. Ramirez-Ruiz and M. B. Davies, *Mon. Not. R. Astron. Soc.* **345** (2003) 1077.
155. W. H. Lee, E. Ramirez-Ruiz and D. Page, *Astrophys. J.* **608** (2004) L5.
156. K. Belczynski, R. Perna, T. Bulik *et al.*, *Astrophys. J.* **648** (2006) 1110.
157. E. Berger, *Annu. Rev. Astron. Astrophys.* **52** (2014) 43.
158. D. B. Fox, D. A. Frail, P. A. Price *et al.*, *Nature* **437** (2005) 845.
159. N. Gehrels, C. L. Sarazin, P. T. O'Brien *et al.*, *Nature* **437** (2005) 851.
160. M. Ackermann, M. Ajello, K. Asano *et al.*, *Astrophys. J. Suppl.* **209** (2013) 11.
161. C. Kouveliotou, J. Granot, J. L. Racusin *et al.*, *Astrophys. J.* **779** (2013) L1.
162. D. A. Perley, S. B. Cenko, A. Corsi *et al.*, *Astrophys. J.* **781** (2014) 37.
163. A. A. Abdo, M. Ackermann, M. Arimoto *et al.*, *Science* **323** (2009) 1688.
164. L. Izzo, M. G. Bernardini, C. L. Bianco *et al.*, *Int. J. Mod. Phys. D* **20** (2011) 1949.
165. M. Ackermann, M. Ajello, K. Asano *et al.*, *Astrophys. J.* **763** (2013) 71.
166. M. Ackermann, M. Ajello, K. Asano *et al.*, *Science* **343** (2014) 42.
167. R. Belvedere, D. Pugliese, J. A. Rueda *et al.*, *Nucl. Phys. A* **883** (2012) 1.
168. F.-W. Zhang, L. Shao, J.-Z. Yan and D.-M. Wei, *Astrophys. J.* **750** (2012) 88.
169. G. Calderone, G. Ghirlanda, G. Ghisellini *et al.*, *Mon. Not. R. Astron. Soc.* **448** (2015) 403.
170. R. Ruffini, J. A. Rueda, M. Muccino *et al.*, *Astrophys. J.* **832** (2016) 136.
171. C. L. Fryer, K. Belczynski, E. Ramirez-Ruiz *et al.*, The Fate of the Compact Remnant in Neutron Star Mergers, arXiv e-prints (2015).
172. S. Lawrence, J. G. Tervala, P. F. Bedaque and M. C. Miller, *Astrophys. J.* **808** (2015) 186.
173. M. Muccino, R. Ruffini, C. L. Bianco *et al.*, *Astrophys. J.* **763** (2013) 125.
174. R. Ruffini, M. Muccino, Y. Aimuratov *et al.*, *Astrophys. J.* **831** (2016) 178.
175. G. B. Pisani, L. Izzo, R. Ruffini *et al.*, *Astron. Astrophys.* **552** (2013) L5.

The Astrophysical Journal, 852:53 (27pp), 2018 January 1 https://doi.org/10.3847/1538-4357/aa9e8b

Early X-Ray Flares in GRBs

R. Ruffini[1,2,3,4], Y. Wang[1,2], Y. Aimuratov[3,1,2], U. Barres de Almeida[4], L. Becerra[1,2], C. L. Bianco[1,2], Y. C. Chen[1,2], M. Karlica[1,2,3], M. Kovacevic[1,2,3], L. Li[2,5], J. D. Melon Fuksman[1,2], R. Moradi[1,2], M. Muccino[1,2], A. V. Penacchioni[2,6,7], G. B. Pisani[1,2], D. Primorac[1,2], J. A. Rueda[1,2,4], S. Shakeri[2,8], G. V. Vereshchagin[1,2], and S.-S. Xue[1,2]

[1] ICRA and Dipartimento di Fisica, Sapienza Università di Roma, Piazzale Aldo Moro 5, I-00185 Rome, Italy
[2] ICRANet, Piazza della Repubblica 10, I-65122 Pescara, Italy; yu.wang@icranet.org
[3] Université de Nice Sophia Antipolis, CEDEX 2, Grand Château Parc Valrose, Nice, France
[4] ICRANet-Rio, Centro Brasileiro de Pesquisas Físicas, Rua Dr. Xavier Sigaud 150, 22290-180 Rio de Janeiro, Brazil
[5] Department of Physics, Stockholm University, SE-106 91 Stockholm, Sweden
[6] ASI Science Data Center, Via del Politecnico s.n.c., I-00133 Rome, Italy
[7] Dept. of Physical Sciences, Earth and Environment, University of Siena, Via Roma 56, I-53100 Siena, Italy
[8] Department of Physics, Isfahan University of Technology, 84156-83111, Iran
Received 2017 April 8; revised 2017 November 8; accepted 2017 November 23; published 2018 January 5

Abstract

We analyze the early X-ray flares in the GRB "flare–plateau–afterglow" (FPA) phase observed by *Swift*-XRT. The FPA occurs only in one of the seven GRB subclasses: the binary-driven hypernovae (BdHNe). This subclass consists of long GRBs with a carbon–oxygen core and a neutron star (NS) binary companion as progenitors. The hypercritical accretion of the supernova (SN) ejecta onto the NS can lead to the gravitational collapse of the NS into a black hole. Consequently, one can observe a GRB emission with isotropic energy $E_{\rm iso} \gtrsim 10^{52}$ erg, as well as the associated GeV emission and the FPA phase. Previous work had shown that gamma-ray spikes in the prompt emission occur at $\sim 10^{15}$–10^{17} cm with Lorentz Gamma factors $\Gamma \sim 10^2$–10^3. Using a novel data analysis, we show that the time of occurrence, duration, luminosity, and total energy of the X-ray flares correlate with $E_{\rm iso}$. A crucial feature is the observation of thermal emission in the X-ray flares that we show occurs at radii $\sim 10^{12}$ cm with $\Gamma \lesssim 4$. These model-independent observations cannot be explained by the "fireball" model, which postulates synchrotron and inverse-Compton radiation from a single ultrarelativistic jetted emission extending from the prompt to the late afterglow and GeV emission phases. We show that in BdHNe a collision between the GRB and the SN ejecta occurs at $\simeq 10^{10}$ cm, reaching transparency at $\sim 10^{12}$ cm with $\Gamma \lesssim 4$. The agreement between the thermal emission observations and these theoretically derived values validates our model and opens the possibility of testing each BdHN episode with the corresponding Lorentz Gamma factor.

Key words: binaries: general – black hole physics – gamma-ray burst: general – hydrodynamics – stars: neutron – supernovae: general

Supporting material: machine-readable table

1. Introduction

Following the discovery of the gamma-ray bursts (GRBs) by the *Vela* satellites (Klebesadel et al. 1973) and the observations by the BATSE detectors on board the *Compton Gamma-Ray Observatory* (*CGRO*; Gehrels et al. 1993), a theoretical framework for the interpretation of GRBs was established. This materialized into the "traditional" model of GRBs developed in a large number of papers by various groups. They all agree in their general aspects: short GRBs are assumed to originate from the merging of binary neutron stars (NSs; see, e.g., Goodman 1986; Paczynski 1986; Eichler et al. 1989; Narayan et al. 1991, 1992; Mészáros & Rees 1997), and long GRBs are assumed to originate from a "collapsar" (Woosley 1993; Paczyński 1998; MacFadyen & Woosley 1999; Bromberg et al. 2013), which, in turn, originates from the collapse of the core of a single massive star to a black hole (BH) surrounded by a thick massive accretion disk (Piran 2004). In this traditional picture, the GRB dynamics follows the "fireball" model, which assumes the existence of an ultrarelativistic collimated jet (see, e.g., Shemi & Piran 1990; Meszaros et al. 1993; Piran et al. 1993; Mao & Yi 1994). The structures of long GRBs were described by either internal or external shocks (see Rees & Meszaros 1992, 1994). The emission processes were linked to the occurrence of synchrotron and/or inverse-Compton radiation coming from the jetted structure, characterized by Lorentz factors $\Gamma \sim 10^2$–10^3, in what later will become known as the "prompt emission" phase (see Section 3).

The joint X-ray, gamma-ray, and optical observations heralded by *BeppoSAX* and later extended by *Swift* discovered the X-ray "afterglow," which allowed the optical identification and the determination of the GRBs' cosmological distance. The first evidence for the coincidence of a GRB and a supernova (SN; GRB 980425/SN 1998bw) was also announced as well as the first observation of an early X-ray flare (XRT), later greatly extended in number and spectral data by the *Swift* satellite, the subjects of this paper. The launch of the *Fermi* and *AGILE* satellites led to the equally fundamental discovery of GeV emission both in long and short GRBs (see Section 2).

The traditional model was modified in light of these new basic information by extending the description of the "collapsar" model, adopted for the prompt emission, to both the afterglow and GeV emission. This approach, based on the gravitational collapse of a single massive star, which was initially inspired by analogies with the astrophysics of active galactic nuclei, has been adopted with the aim to identify a "standard model" for all long GRBs and vastly accepted by concordance (see, e.g., Piran 1999, 2004; Mészáros 2002, 2006; Gehrels et al. 2009; Berger 2014; Kumar & Zhang 2015).

Attempts to incorporate the occurrence of an SN in the collapsar by considering nickel production in the accretion process around the BH were also proposed (MacFadyen & Woosley 1999). In 1999, a pioneering work by Fryer et al. (1999b) introduced considerations based on population synthesis computations and emphasized the possible relevance of binary progenitors in GRBs.

Since 2001, we have been developing an alternative GRB model based on the concept of induced gravitational collapse (IGC) paradigm, which involves, as progenitors, a binary system with standard components: an evolved carbon–oxygen core (CO_{core}) and a binary companion NS. The CO_{core} undergoes a traditional SN Ic explosion, which produces a new NS (νNS) and a large amount of ejecta. There is a multitude of new physical processes, occurring in selected episodes, associated with this process. The "first episode" (see Section 3) of the binary-driven hypernova (BdHN) is dominated by the hypercritical accretion process of the SN ejecta onto the companion NS. This topic has been developed in, e.g., Ruffini et al. (2001c), Rueda & Ruffini (2012), Fryer et al. (2014), and Becerra et al. (2015, 2016). These processes are not considered in the collapsar model. Our SN is a traditional Type Ic, the creation of the νNS follows standard procedure occurring in pulsar physics (see, e.g., Negreiros et al. 2012), the companion NS is a standard one regularly observed in binaries (see e.g., Rueda & Ruffini 2012; Rueda et al. 2017), and the physics of hypercritical accretion has been developed by us in a series of recent articles (see Section 3.4).

In a BdHN, the BH and a vast amount of e^+e^- plasma are formed only after the accreting NS reaches the critical mass and the "second episode" starts (see Section 3.5). The main new aspect of our model addresses the interaction of the e^+e^- plasma with the SN ejecta. We apply the fireshell model, which makes use of a general relativistic correct spacetime parametrization of the GRBs as well as a new set of relativistic hydrodynamics equation for the dynamics of the e^+e^- plasma. Selected values of the baryon loads are adopted in correspondence with the different time-varying density distributions of the SN ejecta.

In the "third episode" (see Section 3.6), we also mention the perspectives, utilizing the experience gained from both data analysis and theory for the specific understanding of X-ray flares, to further address in forthcoming publications the more comprehensive case of gamma-ray flares, the consistent treatment of the afterglow, and finally the implication of the GeV radiation.

As the model evolved, we soon realized that the discovery of new sources was not leading to a "standard model" of long GRBs but, on the contrary, they were revealing a number of new GRB subclasses with distinct properties characterizing their light curves, spectra, and energetics (see Ruffini et al. 2016b). Moreover, these seven subclasses did not necessarily contain a BH. We soon came to the conclusion that only in the subclass of BdHNe, with an E_{iso} larger than 10^{52} erg, does the hypercritical accretion from the SN onto the NS lead to the creation of a newly born BH with the associated signatures in the long GRB emission (see, e.g., Becerra et al. 2015, 2016).

While our alternative model was progressing, we were supported by new astrophysical observations: the great majority of GRBs are related to SNe Ic, which have no trace of hydrogen and helium in their optical spectra and are spatially correlated with bright star-forming regions in their host galaxies (Fruchter et al. 2006; Svensson et al. 2010). Most massive stars are found in binary systems (Smith 2014) where most SNe Ic occur and which favor the deployment of hydrogen and helium from the SN progenitors (Smith et al. 2011), and the SNe associated with long GRBs are indeed of Type Ic (Della Valle 2011). In addition, these SNe associated with long bursts are broad-lined Ic SNe (hypernovae) showing the occurrence of some energy injection leading to a kinetic energy larger than that of traditional SNe Ic (Lyman et al. 2016).

The present paper addresses the fundamental role of X-ray flares as a separatrix between the two alternative GRB models and leads to the following main results, two obtained by data analysis and one obtained from the comparison of the alternative models:

(1) The discovery of precise correlations between the X-ray flares and the GRB E_{iso}.
(2) The radius of the occurrence of X-ray flares ($\sim 10^{12}$ cm) and the Lorentz Gamma factor ~ 2.
(3) The occurrence of a sharp break between the prompt emission phase and the flare–plateau–afterglow (FPA) phase, not envisaged in the current GRB literature. This transition is evidence of a contradiction in using the ultrarelativistic jetted emission to explain the X-ray flares, the plateau, and the afterglow.

In Section 2, we recall, following the gamma-ray observations by the *Vela* satellites and the *CGRO*, the essential role of *BeppoSAX* and the *Swift* satellite. These satellites provided X-ray observations specifically of the X-ray flares, to which our new data analysis techniques and paradigms have been applied. We also recall that the *Fermi* and *AGILE* satellites announced the existence of GeV emission, which has become essential for establishing the division of GRBs into different subclasses.

In Section 3, we update our classification of GRBs with known redshift into seven different subclasses (see Table 2). For each subclass, we indicate the progenitor "in-states" and the corresponding "out-states." We update the list of BdHNe (see Appendix A): long GRBs with $E_{iso} \gtrsim 10^{52}$ erg, with an associated GeV emission and with the occurrence of the FPA phase. We also recall the role of appropriate time parametrization for GRBs, which properly distinguishes the four time variables that enter into their analysis. Finally, we recall the essential theoretical background needed for the description of the dynamics of BdHNe, the role of neutrino emission in the process of hypercritical accretion of the SN ejecta onto the binary companion NS, the description of the dynamics of the e^+e^-–baryon plasma, and the prompt emission phase endowed with gamma-ray spikes. We then briefly address the new perspectives opened up by the present work, to be further extended to the analysis of gamma-ray flares, to the afterglow, and the essential role of each BdHN component, including the νNS. Having established the essential observational and theoretical backgrounds in Sections 2 and 3, we proceed to the data analysis of the X-ray flares.

In Section 4, we address the procedure used to compare and contrast GRBs at different redshifts, including the description in their cosmological rest frame as well as the consequent K corrections. This procedure has been ignored in the current GRB literature (see, e.g., Chincarini et al. 2010 and references therein

as well as Section 11 of this paper). We then identify BdHNe as the only sources where early-time X-ray flares are identifiable. We recall that X-ray flares have neither been found in X-ray flashes nor in short GRBs. We also show that a claim of the existence of X-ray flares in short bursts has been superseded. We recall our 345 classified BdHNe (through the end of 2016). Their T_{90},[9] properly evaluated in the source rest frame, corresponds to the duration of their prompt emission phase, mostly shorter than 100 s. Particular attention has been given to distinguishing X-ray flares from gamma-ray flares and spikes, each characterized by distinct spectral distributions and specific Lorentz Gamma factors. The gamma-ray flares are generally more energetic and with specific spectral signatures (see, e.g., the significant example of GRB 140206A in Section 5 below). In this article we focus on the methodology of studying X-ray flares: we plan to apply this knowledge to the case of the early gamma-ray flares. Out of the 345 BdHNe, there are 211 that have complete *Swift-XRT* observations, and among them, there are 16 BdHNe with a well-determined early X-ray flare structure. They cover a wide range of redshifts as well as the typical range of BdHN isotropic energies ($\sim 10^{52}$–10^{54} erg). The sample includes all identifiable X-ray flares.

In Section 5, we give the X-ray luminosity light curves of the 16 BdHNe in our sample and, when available, the corresponding optical observations. As usual, these quantities have been K-corrected to their rest frame (see Figures 9–24 and Section 4). In order to estimate the global properties of these sources, we also examine data from the *Swift*, Konus-*Wind*, and *Fermi* satellites. The global results of this large statistical analysis are given in Table 3, where the cosmological redshift z, the GRB isotropic energy $E_{\rm iso}$, the flare peak time t_p, peak luminosity L_p, duration Δt, and the corresponding E_f are reproduced. This lengthy analysis has been carried out over the past years, and only the final results are summarized in Table 3.

In Section 6, we present the correlations between t_p, L_p, Δt, E_f, and $E_{\rm iso}$ and give the corresponding parameters in Table 4. In this analysis, we applied the Markov Chain Monte Carlo (MCMC) method, and we also have made public the corresponding numerical codes in https://github.com/YWangScience/AstroNeuron and https://github.com/YWangScience/MCCC.

In Section 7, we discuss the correlations between the energy of the prompt emission, the energy of the FPA phase, and $E_{\rm iso}$ (see Tables 5–6 and Figures 29–31).

In Section 8, we analyze the thermal emission observed during the X-ray flares (see Table 7). We derive, in an appropriate relativistic formalism, the relations between the observed temperature and flux and the corresponding temperature and radius of the thermal emitter in its comoving frame.

In Section 9, we use the results of Section 8 to infer the expansion speed of the thermal emitter associated with the thermal components observed during the flares (see Figure 32 and Table 8). We find that the observational data imply a Lorentz factor $\Gamma \lesssim 4$ and a radius of $\approx 10^{12}$ cm for such a thermal emitter.

In Section 10, we present a theoretical treatment using a new relativistic hydrodynamical code to simulate the interaction of the e^+e^-–baryon plasma with the high-density regions of the SN ejecta. We first test the code in the same low-density domain of validity describing the prompt emission phase, and then we apply it in the high-density regime of the propagation of the plasma inside the SN ejecta, which we use for the theoretical interpretation of the X-ray flares. Most remarkably, the theoretical code leads to a thermal emitter with a Lorentz factor $\Gamma \lesssim 4$ and a radius of $\approx 10^{12}$ cm at transparency. The agreement between these theoretically derived values and the ones obtained from the observed thermal emission validates the model and the binary nature of the BdHN progenitors, in clear contrast with the traditional ultrarelativistic jetted models.

In Section 11, we present our conclusions. We first show how the traditional model, describing GRBs as a single system with ultrarelativistic jetted emission extending from the prompt emission all the way to the final phases of the afterglow and of the GeV emission, is in conflict with the X-ray flare observations. We also present three new main results that illustrate the new perspectives opened up by our alternative approach based on BdHNe.

A standard flat ΛCDM cosmological model with $\Omega_M = 0.27$, $\Omega_\Lambda = 0.73$, and $H_0 = 71$ km s^{-1} Mpc^{-1} is adopted throughout the paper, while Table 1 summarizes the acronyms we have used.

Table 1
Alphabetic Ordered List of the Acronyms Used in this Work

Extended Wording	Acronym
Binary-driven hypernova	BdHN
Black hole	BH
Carbon–oxygen core	CO_{core}
Circumburst medium	CBM
Flare–Plateau–Afterglow	FPA
Gamma-ray burst	GRB
Gamma-ray flash	GRF
Induced gravitational collapse	IGC
Massive neutron star	MNS
Neutron star	NS
New neutron star	νNS
Proper gamma-ray burst	P-GRB
Short gamma-ray burst	S-GRB
Short gamma-ray flash	S-GRF
Supernova	SN
Ultrashort gamma-ray burst	U-GRB
White dwarf	WD
X-ray flash	XRF

2. Background for the Observational Identification of the X-Ray Flares

The discovery of GRBs by the *Vela* satellites (Klebesadel et al. 1973) was presented at the AAAS meeting in February 1974 in San Francisco (Gursky & Ruffini 1975). The *Vela* satellites were operating in gamma-rays in the 150–750 keV energy range and only marginally in X-rays (3–12 keV; Cline et al. 1979). Soon after it was hypothesized from first principles that GRBs may originate from an e^+e^- plasma in the gravitational collapse to a Kerr–Newman BH, implying an energy $\sim 10^{54}\, M_{\rm BH}/M_\odot$ erg (Damour & Ruffini 1975; see also Ruffini 1998).

Since 1991, the BATSE detectors on the *CGRO* (see Gehrels et al. 1993) have been leading to the classification of GRBs on the basis of their spectral hardness and of their observed T_{90} duration in the 50–300 keV energy band into short/hard bursts ($T_{90} < 2$ s) and long/soft bursts ($T_{90} > 2$ s (Mazets et al. 1981; Dezalay et al. 1992; Klebesadel 1992; Kouveliotou et al. 1993; Tavani 1998). Such an emission was later called the GRB

[9] T_{90} is the duration of the interval starting (ending) when 5% (95%) of the total energy of the event in gamma-rays has been emitted.

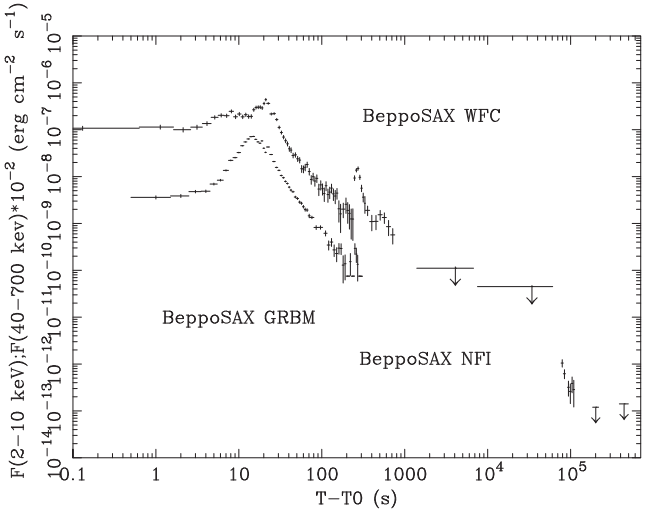

Figure 1. First X-ray flare observed by *BeppoSAX* in GRB 011121. Reproduced from Piro et al. (2005).

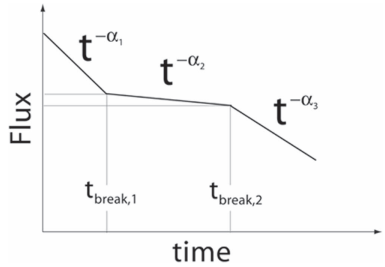

Figure 2. Schematic diagram of the X-ray light- curve composed of three power-law segments with different slopes ($3 \lesssim \alpha_1 \lesssim 5$, $0.5 \lesssim \alpha_2 \lesssim 1.0$, $1 \lesssim \alpha_3 \lesssim 1.5$). Figure taken from Nousek et al. (2006).

"prompt emission." In a first attempt, it was proposed that short GRBs originate from merging binary NSs (see, e.g., Goodman 1986; Paczynski 1986; Eichler et al. 1989; Narayan et al. 1991, 1992; Mészáros & Rees 1997) and long GRBs originate from a single source with ultrarelativistic jetted emission (Woosley 1993; Paczyński 1998; MacFadyen & Woosley 1999; Bromberg et al. 2013).

The *BeppoSAX* satellite, operating since 1996, joined the expertise of the X-ray and gamma-ray communities. Its gamma-ray burst monitor (GRBM) operating in the 40–700 keV energy band determined the trigger of the GRB, and two wide-field cameras operating in the 2–30 keV X-ray energy band allowed the localization of the source within an arcminute resolution. This enabled a follow-up with the narrow-field instruments (NFI) in the 2–10 keV energy band. *BeppoSAX* discovered the X-ray afterglow (Costa et al. 1997), characterized by an X-ray luminosity decreasing with a constant index of ~ -1.3 (see de Pasquale et al. 2006 as well as Pisani et al. 2016). This emission was detected after an "8 hr gap" following the prompt emission identified by BATSE. The consequent determination of the accurate positions by the NFI, transmitted to the optical (van Paradijs et al. 1997) and radio telescopes (Frail et al. 1997), allowed the determination of the GRB cosmological redshifts (Metzger et al. 1997). The derived distances of $\approx$5–10 Gpc confirmed their cosmological origin and their unprecedented energetics, $\approx 10^{50}$–10^{54} erg, thus validating our hypothesis derived from first principles (Damour & Ruffini 1975; Ruffini 1998).

To *BeppoSAX* goes the credit of the discovery of the temporal and spatial coincidence of GRB 980425 with SN 1998bw (Galama et al. 1998), which suggested the connection between GRBs and SNe, soon supported by many additional events (see, e.g., Woosley & Bloom 2006; Della Valle 2011; Hjorth & Bloom 2012). *BeppoSAX* also discovered the first "X-ray flare" in GRB 011121 closely following the prompt emission (Piro et al. 2005); see Figure 1. Our goal in this paper is to show how the X-ray flares, thanks to the observational campaign of the *Swift* satellite, have become the crucial test for understanding the astrophysical nature of the GRB–SN connection.

The *Swift* Burst Alert Telescope (BAT), operating in the 15–150 keV energy band, can detect GRB prompt emissions and accurately determine their position in the sky within 3 arcmin. Within 90 s, *Swift* can re-point the narrow-field X-ray telescope (XRT), operating in the 0.3–10 keV energy range, and relay the burst position to the ground. This overcomes the "8 hr gap" in the *BeppoSAX* data.

Thanks to the *Swift* satellite, the number of detected GRBs increased rapidly to 480 sources with known redshifts. By analyzing the light curve of some long GRBs, including the data in the "8 hr gap" of *BeppoSAX*, Nousek et al. (2006) and Zhang et al. (2006) discovered three power-law segments in the XRT flux light curves of some long GRBs. We refer to these as the "Nousek–Zhang power laws" (see Figure 2). The nature of this feature has been the subject of a long debates, still ongoing, and is finally resolved in this article.

We have used *Swift*-XRT data in differentiating two distinct subclasses of long GRBs: XRFs with $E_{\rm iso} \lesssim 10^{52}$ erg and BdHNe with $E_{\rm iso} \gtrsim 10^{52}$ erg (see Section 3). An additional striking difference appears between the XRT luminosities of these two subclasses when measured in their cosmological rest frames: in the case of BdHNe, the light curves follow a specific behavior that conforms to the Nousek–Zhang power law (see, e.g., Penacchioni et al. 2012, 2013; Pisani et al. 2013, 2016; Ruffini et al. 2014). None of these features are present in the case of XRFs (see Figure 3).

Finally, the *Fermi* satellite (Atwood et al. 2009), launched in 2008, detects ultrahigh energy photons from 20 MeV to 300 GeV with the Large Area Telescope (LAT) and detects photons from 8 keV to 30 MeV with the Gamma-ray Burst Monitor (GBM). For the purposes of this article addressing long GRBs, the *Fermi* observations have been prominent in further distinguishing between XRFs and BdHNe: the *Fermi*-LAT GeV emission has been observed only in BdHNe and never in XRFs.

3. Background for the Theoretical Interpretation of X-Ray Flares and Their Dynamics

3.1. The Classification of GRBs

The very extensive set of observations carried out by the above satellites in coordination with the largest optical and radio telescopes over a period of almost 40 years has led to an impressive set of data on 480 GRBs, all characterized by spectral, luminosity, and time variability information, and each one with a well-established cosmological redshift. By

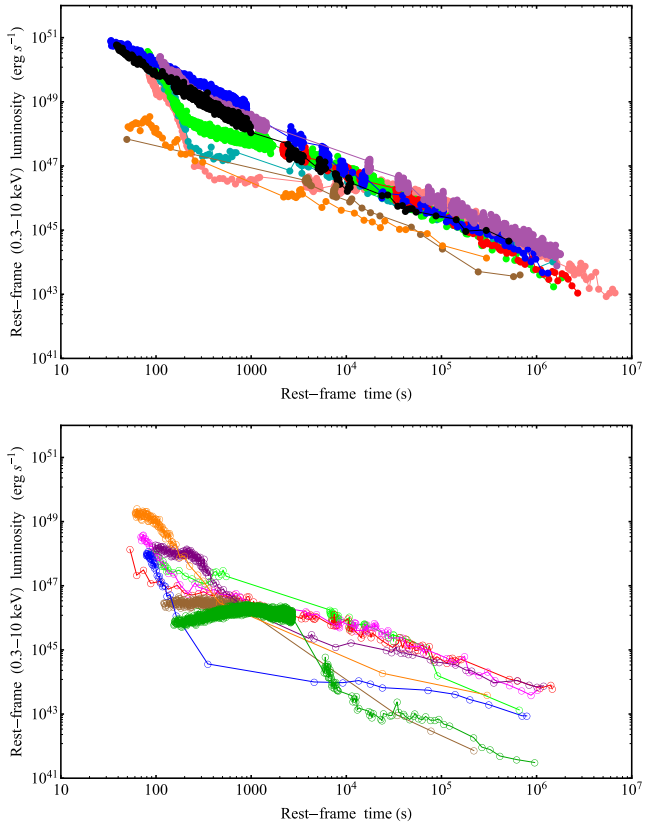

Figure 3. X-ray light curves of long GRBs observed by *Swift*. Top panel: BdHNe 050525 (brown), 060729 (pink), 061007 (black), 080319B (blue), 090618 (green), 091127 (red), 100816A (orange), 111228A (light blue), and 130427A (purple). Bottom panel: XRFs 050416A (red), 060218 (dark green), 070419A (orange), 081007 (magenta), 100316D (brown), 101219B (purple), and 130831A (green). XRFs have generally lower and more scattered light curves. All of these GRBs have known redshifts, and the light curves have been transformed to their cosmological rest frames.

classifying both the commonalities and the differences among all GRBs, it has been possible to create "equivalence relations" and divide GRBs into a number of subclasses, each one identified by a necessary and sufficient number of observables. We recall in Table 2 and Figure 4 the binary nature of all GRB progenitors and their classification into seven different subclasses (see, e.g., Ruffini et al. 2016b). In Table 2, we indicate the number of sources in each subclass, the nature of their progenitors and final outcomes of their evolution, their rest-frame T_{90}, their rest-frame spectral peak energy $E_{\rm p,i}$ and $E_{\rm iso}$ as well as the isotropic energy in X-rays $E_{\rm iso,X}$ and in GeV emission $E_{\rm iso,GeV}$, and finally their local observed number density rate. In Figure 4, we mention the $E_{\rm p,i}$–$E_{\rm iso}$ relations for these sources, including the Amati one for BdHNe and the MuRuWaZha one for the short bursts (see Ruffini et al. 2016a, 2016b), comprising short gamma-ray flashes (S-GRFs) with $E_{\rm iso} \lesssim 10^{52}$ erg, authentic short GRBs (S-GRBs) with $E_{\rm iso} \gtrsim 10^{52}$ erg, and gamma-ray flashes (GRFs), sources with hybrid short/long burst properties in their gamma-ray light curves, i.e., an initial spike-like harder emission followed by a prolonged softer emission observed up to $\sim$100 s, originating from NS–white dwarf binaries (Caito et al. 2009, 2010; Ruffini et al. 2016b). We have no evidence for an $E_{\rm p,i}$ and $E_{\rm iso}$ relation in the XRFs (see Figure 4). The Amati and the MuRuWaZha relations have not yet been theoretically understood, and as such they have no predictive power.

3.2. The Role of Time Parametrization in GRBs

Precise general relativistic rules in the spacetime parameterization of GBRs are needed (Ruffini et al. 2001a). Indeed, there are four time variables entering this discussion, which have to be properly distinguished one from another: (1) the comoving time $t_{\rm com}$, which is the time used to compute the evolution of the thermodynamical quantities (density, pressure, temperature); (2) the laboratory time $t = \Gamma t_{\rm com}$, where as usual the Lorentz Gamma factor is $\Gamma = (1 - \beta^2)^{-1/2}$ and $\beta = v/c$ is the expansion velocity of the source; (3) the arrival time t_a at which each photon emitted by the source reaches an observer in the cosmological rest frame of the source, given by (see also Bianco et al. 2001; Ruffini et al. 2002; Bianco & Ruffini 2005a)

$$t_a = t - \frac{r(t)}{c}\cos\vartheta, \tag{1}$$

where $r(t)$ is the radius of the expanding source in the laboratory frame and ϑ is the displacement angle of the normal to the emission surface from the line of sight; and (4) the arrival time at the detector on the Earth, $t_a^d = t_a(1 + z)$, corrected for cosmological effects, where z is the source redshift needed in order to compare GRBs at different redshifts z. As emphasized in Ruffini et al. (2001a, p. L108), "the bookkeeping of these four different times and the corresponding space variables must be done carefully in order to keep the correct causal relation in the time sequence of the events involved." The chain of relations between these four times is given by (see e.g., Bianco et al. 2001; Ruffini et al. 2001a, 2002; Bianco & Ruffini 2005a, and see also Sections 8 and 9 for the dynamics of the flares)

$$\begin{aligned} t_a^d &= (1 + z)t_a = (1 + z)\left(t - \frac{r(t)}{c}\cos\vartheta\right) \\ &= (1 + z)\left(\Gamma t_{\rm com} - \frac{r(\Gamma t_{\rm com})}{c}\cos\vartheta\right). \end{aligned} \tag{2}$$

The proper use of these four time variables is mandatory in modeling GRB sources, especially when we are dealing with a model not based on a single component but on multiple components, each characterized by a different world line and a different Lorentz Gamma factor, as is the case for BdHNe (see Sections 4 and 5).

3.3. The Role of the GRBs' Cosmological Rest Frame

In addition to all of the above, in order to compare the luminosities of different GRBs at different, redshifts we need to express the observational data in the cosmological rest frames of each source (where the arrival time is t_a), and correspondingly apply the K correction to luminosities and spectra (see Section 4). This formalism is at the very foundation of the treatment presented in this paper and has been systematically neglected in the great majority of current GRB models.

3.4. Episode 1: The Hypercritical Accretion Process

In order to describe the dynamics of BdHNe, a number of different episodes involving different physical conditions have

Table 2
Summary of the Seven GRB Subclasses (XRFs, BdHNe, BH–SN, Short Gamma-ray Flashes (S-GRFs), Authentic Short GRBs (S-GRBs), Ultrashort GRBs (U-GRB), and GRFs) and Their Observational Properties

	Subclass	Number	In-state (Progenitor)	Out-state (Final outcome)	T_{90} (s)	$E_{p,i}$ (MeV)	E_{iso} (erg)	$E_{iso,X}$ (erg)	$E_{iso,Gev}$ (erg)	ρ_{GRB} ($Gpc^{-3}yr^{-1}$)
I	XRFs	82	CO_{core}–NS	νNS–NS	~ 2–10^3	$\lesssim 0.2$	$\sim 10^{48}$–10^{52}	$\sim 10^{48}$–10^{51}	⋯	100^{+45}_{-34}
II	BdHNe	345	CO_{core}–NS	νNS–BH	~ 2–10^2	~ 0.2–2	$\sim 10^{52}$–10^{54}	$\sim 10^{51}$–10^{52}	$\lesssim 10^{53}$	$0.77^{+0.09}_{-0.08}$
III	BH–SN	⋯	CO_{core}–BH	νNS–BH	~ 2–10^2	$\gtrsim 2$	$> 10^{54}$	$\sim 10^{51}$–10^{52}	$\gtrsim 10^{53}$	$\lesssim 0.77^{+0.09}_{-0.08}$
IV	S-GRFs	33	NS–NS	MNS	$\lesssim 2$	$\lesssim 2$	$\sim 10^{49}$–10^{52}	$\sim 10^{49}$–10^{51}	⋯	$3.6^{+1.4}_{-1.0}$
V	S-GRBs	7	NS–NS	BH	$\lesssim 2$	$\gtrsim 2$	$\sim 10^{52}$–10^{53}	$\lesssim 10^{51}$	$\sim 10^{52}$–10^{53}	$(1.9^{+1.8}_{-1.1}) \times 10^{-3}$
VI	U-GRBs	⋯	νNS–BH	BH	$\ll 2$	$\gtrsim 2$	$> 10^{52}$	⋯	⋯	$\gtrsim 0.77^{+0.09}_{-0.08}$
VII	GRFs	13	NS–WD	MNS	~ 2–10^2	~ 0.2–2	$\sim 10^{51}$–10^{52}	$\sim 10^{49}$–10^{50}	⋯	$1.02^{+0.71}_{-0.46}$

Note. In the first five columns, we indicate the GRB subclasses and their corresponding number of sources with measured z, in-states, and out-states. In the following columns, we list the ranges of T_{90} in the rest frame, the rest-frame spectral peak energies $E_{p,i}$ and E_{iso} (rest frame 1–10^4 keV), the isotropic energy of the X-ray data $E_{iso,X}$ (rest frame 0.3–10 keV), and the isotropic energy of the GeV emission $E_{iso,GeV}$ (rest frame 0.1–100 GeV). In the last column, we list, for each GRB subclass, the local observed number density rate ρ_{GRB} obtained in Ruffini et al. (2016b). For details, see Ruffini et al. (2014, 2015b, 2015c), Fryer et al. (2015), Ruffini et al. (2016a, 2016b), and Becerra et al. (2016).

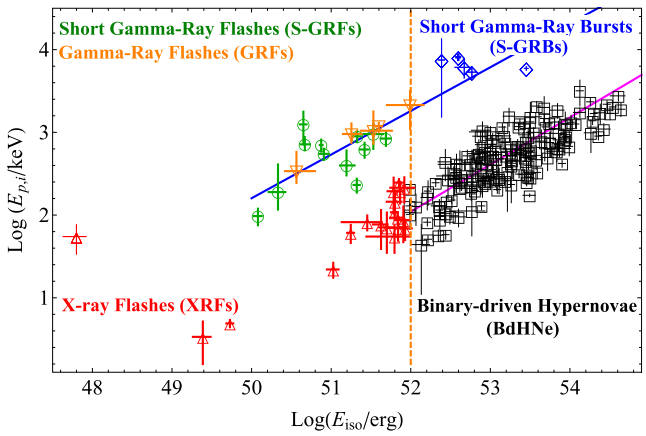

Figure 4. Updated $E_{p,i}$–E_{iso} plane for the subclasses defined in Ruffini et al. (2016b): XRF (red triangles) cluster in the region defined by $E_{p,i} \lesssim 200$ keV and $E_{iso} \lesssim 10^{52}$ erg. BdHN (black squares) cluster in the region defined by $E_{p,i} \gtrsim 200$ keV and $E_{iso} \gtrsim 10^{52}$ erg and fulfilling the Amati relation (solid magenta line with slope $\alpha = 0.57 \pm 0.06$ and extra scatter $\sigma = 0.25$; see, e.g., Amati & Della Valle 2013; Calderone et al. 2015). S-GRFs (green circles) and the initial spike-like emission of the GRFs (orange reverse triangles) are concentrated in the region defined by $E_{p,i} \lesssim 2$ MeV and $E_{iso} \lesssim 10^{52}$ erg, while S-GRBs (blue diamonds) are concentrated in the region defined by $E_{p,i} \gtrsim 2$ MeV and $E_{iso} \gtrsim 10^{52}$ erg. Short bursts and GRFs fulfill the MuRuWaZha relation (blue solid line with slope $\alpha = 0.53 \pm 0.07$ and extra scatter $\sigma = 0.24$; see, e.g., Zhang et al. 2012; Calderone et al. 2015; Ruffini et al. 2015b, 2016a). The BH–SN and U-GRB subclasses (see Table 2 in Ruffini et al. 2016b for details) are not in the plot since their observational identifications are still pending. The crucial difference between BdHNe and XRFs, and S-GRBs and S-GRFs, is that BdHNe and S-GRBs form a BH, their energy is $\gtrsim 10^{52}$ erg, and they exhibit GeV emission.

to be described. Episode 1 is dominated by the IGC paradigm: the hypercritical accretion of an SN ejecta onto the companion binary NS (see, e.g., Fryer et al. 2014, 2015; Becerra et al. 2015, 2016). Weak interactions and neutrinos (see, e.g., Fermi 1934), which play a fundamental role in SNe through the URCA process (Gamow & Schoenberg 1940, 1941), are also needed in the case of hypercritical accretion processes onto an NS in an SN fallback (Colgate 1971; Zel'dovich et al. 1972; Ruffini & Wilson 1973). They are especially relevant in the case of BdHNe where the accretion rate onto the NS companion from CO_{core} can reach up to $\dot{M} = 0.1\, M_\odot\ s^{-1}$ (Rueda & Ruffini 2012; Fryer et al. 2014; Becerra et al. 2015, 2016). Due to weak interactions, e^+e^- pairs annihilate to $\nu\bar{\nu}$ pairs with a cross-section $\sigma \sim G_F \langle E_e \rangle^2$ (Munakata et al. 1985; Itoh et al. 1989). In the thermal system of e^+e^- pairs at large temperature $kT > m_e c^2$ and density $n_e \sim T^3$, the neutrino emissivity of the e^+e^- annihilation is $\epsilon_{e^+e^-} \sim n_e^2 \langle \sigma v_e \rangle \langle E_e \rangle \sim 10^{25} (kT/\mathrm{MeV})^9$ erg s^{-1} cm^{-3}, leading to neutrino luminosities $L_\nu \sim R_{NS}^3 \epsilon_{e^+e^-} \sim 10^{52}$ erg s^{-1}, which dominate over other microscopic processes for cooling (Becerra et al. 2016). Thus, e^+e^- pair annihilation to $\nu\bar{\nu}$ is the main process for cooling, allowing the process of hypercritical accretion to convert gravitational energy into thermal energy, to build up high temperature, and consequently to form an e^+e^- plasma. Only at the end of Episode 1, as the critical mass of the companion NS is reached, is a BH is formed with the additional e^+e^- pairs linked to the BH electrodynamical process (Damour & Ruffini 1975; Cherubini et al. 2009).

3.5. Episode 2: e^+e^- Pairs Colliding with the SN Ejecta

Episode 2 is dominated by the new phenomenon of the impact of e^+e^- pairs generated in the GRB on the SN ejecta. We describe this process within the fireshell model. Two main differences exist between the fireshell and the fireball models. In the fireshell model, the e^+e^- plasma is initially in thermal equilibrium and undergoes ultrarelativistic expansion, keeping this condition of thermal equilibrium all the way to reaching transparency (Ruffini 1998; see also Aksenov et al. 2007; Ruffini et al. 2010 and references therein), while in the fireball model (Cavallo & Rees 1978), the e^+e^- pairs undergo an initial annihilation process that produces the photons driving the fireball. An additional basic difference is that the evolution of the e^+e^- plasma is not imposed by a given asymptotic solution but integrated following the relativistic fluid dynamics equations. The plasma, with energy $E_{e^+e^-}$, first goes through an initial acceleration phase (Ruffini et al. 1999). After colliding with the baryons (of total mass M_B), characterized by the baryon load parameter $B = M_B c^2 / E_{e^+e^-}$, the optically thick plasma keeps accelerating until it reaches transparency and emits a proper gamma-ray burst (P-GRB; see Ruffini et al. 2000). The accelerated baryons then interact with the circumburst medium (CBM) clouds (Ruffini et al. 2001b); the equation of motion of the plasma has been integrated, leading to results that differ from

the ones in Blandford & McKee's (1976) self-similar solution (see Bianco & Ruffini 2004, 2005a, 2005b, 2006). By using Equation (2), which defines "equitemporal surfaces" (see Bianco et al. 2001; Bianco & Ruffini 2004, 2005a, 2005b, 2006), it has been possible to infer the structure of the gamma-ray spikes in the prompt emission, which for the most part has been applied to the case of BdHNe (see, e.g., Ruffini et al. 2002, 2016a; Bernardini et al. 2005; Izzo et al. 2012; Patricelli et al. 2012; Penacchioni et al. 2012, 2013). For typical baryon loads of $10^{-4} \lesssim B \lesssim 10^{-2}$ leading to Lorentz Gamma factors $\Gamma \approx 10^2$–10^3 at transparency for the e^+e^-–baryon plasma, characteristic distances from the BH of $\approx 10^{15}$–10^{17} cm have been derived (see, e.g., Ruffini et al. 2016b and references therein). Those procedures are further generalized in this paper to compute the propagation of e^+e^- through the SN ejecta (see Section 10), after computing their density profiles (see Figure 35) and the corresponding baryon load (see Figure 34). The equations have been integrated all the way up to the condition of transparency (see Figures 36 and 37).

3.6. Episode 3: Ongoing Research on the Gamma-Ray Flares, Afterglow, and GeV Emission

We have exemplified the necessary steps in the analysis of each episode, which include determining the physical nature of each episode and the corresponding world line with the specific time-dependent Lorentz Gamma factor and so determining, using Equation (2), the arrival time at the detector, which has to agree, for consistency, with the one obtained from the observations. This program is applied in this article specifically for the analysis of early X-ray flares (see Sections 8 and 9). We will follow the same procedures for (1) the more complex analysis of gamma-ray flares, (2) the analysis of the afterglow consistent with the constraints on the X-ray flares observations, and (3) the properties of the GeV emission, common to BdHNe and S-GRBs (Ruffini et al. 2015c, 2016a). Having established the essential observational and theoretical background in Sections 2 and 3, we proceed to the data analysis of the early X-ray flares (see Sections 4–10).

4. The Early Flares and Sample Selection

With the increase in the number of observed GRBs, an attempt was made to analyze the X-ray flares and other processes considered to be similar in the observer reference frame, independent of the nature of the GRB type and of the value of their cosmological redshift or the absence of such a value. The goal of this attempt was to identify their "standard" properties, following a statistical analysis methodology often applied in classical astronomy (see Chincarini et al. 2007; Falcone et al. 2007; Margutti et al. 2010 as well as the review articles by Piran 1999, 2004; Mészáros 2002, 2006; Berger 2014; Kumar & Zhang 2015). We now summarize our alternative approach, having already given in the introduction and in Sections 2 and 3 the background for the observational identification and the theoretical interpretation of the X-ray flares.

As a first step, we only consider GRBs with an observed cosmological redshift. Having ourselves proposed the classification of all GRBs into seven different subclasses (see Section 3), we have given preliminary attention to verifying whether X-ray flares actually occur preferentially in some of these subclasses and if so, identifying the physical reasons determining such a correlation. We have analyzed all X-ray flares and found, a posteriori, that X-ray flares only occur in BdHNe. No X-ray flare has been identified in any other GRB subclass, either long or short. A claim of their existence in short bursts (Barthelmy et al. 2005; Fan et al. 2005; Dai et al. 2006) has been superseded: GRB 050724 with $T_{90} \sim 100$ s is not a short GRB, but actually a GRF, expected to originate in the merging of an NS and a white dwarf (see Figure 4); the X-ray data for this source from XRT are sufficient to assert that there is no evidence of an X-ray flare as defined in this section. GRB 050709 is indeed a short burst. It has been classified as an S-GRF (Aimuratov et al. 2017) and has been observed by *HETE* with very sparse X-ray data (Butler et al. 2005), and no presence of an X-ray flare can be inferred; the *Swift* satellite pointed at this source too late, 38.5 hr after the *HETE* trigger (Morgan et al. 2005).

As a second step, since all GRBs have a different redshift z, in order to compare them we need a description of each of them in its own cosmological rest frame. The luminosities have to be estimated after doing the necessary K corrections and the time coordinate in the observer frame has to be corrected by the cosmological redshift $t_a^d = (1+z)t_a$. This also affects the determination of the T_{90} of each source (see, e.g., Figure 38 in Section 11 where the traditional approach by Kouveliotou et al. 1993 and Bromberg et al. 2013 has been superseded by ours).

As a third step, we recall an equally important distinction from the traditional fireball approach with a single ultrarelativistic jetted emission. Our GRB analysis envisages the existence of different episodes within each GRB, each one characterized by a different physical process and needing the definition of its own world line and corresponding Gamma factors, essential for estimating the time parametrization in the rest frame of the observer (see Section 2).

These three steps are applied in the present article, which specifically addresses the study of early X-ray flares and their fundamental role in establishing the physical and astrophysical nature of BdHNe and in distinguishing our binary model from the traditional one.

Before proceeding, let us recall the basic point of the K correction. All of the observed GRBs have a different redshift. In order to compare them, it is necessary to refer to each of them in its cosmological rest frame. This step has often been ignored in the current literature (Chincarini et al. 2007; Falcone et al. 2007; Margutti et al. 2010). Similarly, for the flux observed by the above satellites in Section 2, each instrument is characterized by its fixed energy window $[\epsilon_{\rm obs,1}; \epsilon_{\rm obs,2}]$. The observed flux $f_{\rm obs}$, defined as the energy per unit area and time in a fixed instrumental energy window $[\epsilon_{\rm obs,1}; \epsilon_{\rm obs,2}]$, is expressed in terms of the observed photon number spectrum $n_{\rm obs}$ (i.e., the number of observed photons per unit energy, area, and time) as

$$f_{{\rm obs},[\epsilon_{\rm obs,1};\epsilon_{\rm obs,2}]} = \int_{\epsilon_{\rm obs,1}}^{\epsilon_{\rm obs,2}} \epsilon\, n_{\rm obs}(\epsilon) d\epsilon. \quad (3)$$

It then follows that the luminosity L of the source (i.e., the total emitted energy per unit time in a given bandwidth), expressed by definition in the source cosmological rest frame, is related to $f_{\rm obs}$ through the luminosity distance $D_L(z)$:

$$L_{[\epsilon_{\rm obs,1}(1+z);\epsilon_{\rm obs,2}(1+z)]} = 4\pi D_L^2(z) f_{{\rm obs},[\epsilon_{\rm obs,1};\epsilon_{\rm obs,2}]}. \quad (4)$$

The above Equation (4) gives the luminosities in different cosmological rest-frame energy bands, depending on the source

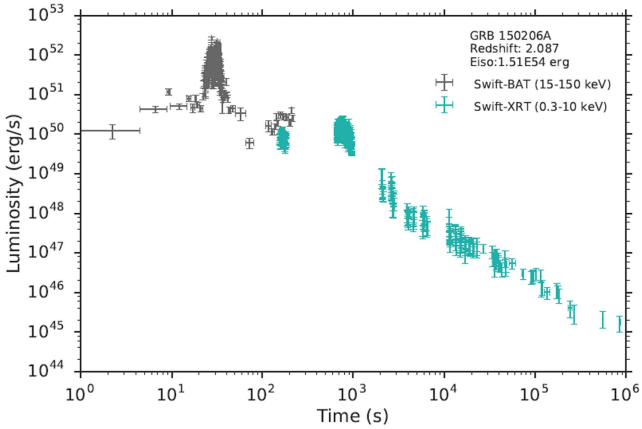

Figure 5. GRB 150206A is an example of a GRB with incomplete data, which therefore must be excluded. It only has 30 s *Swift-XRT* observations in the early 300 s. Flare determination is not possible under these conditions.

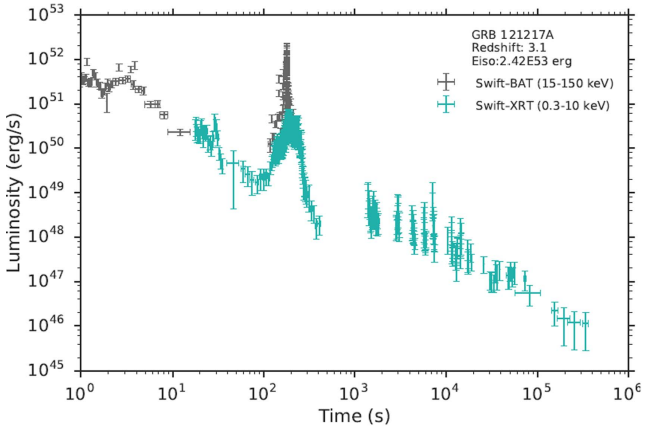

Figure 6. GRB 121217A clearly shows a gamma-ray flare observed by *Swift*-BAT, which coincides with a soft X-ray component observed by *Swift*-XRT. From the spectral analysis, it has a soft power-law photon index, and most of the energy is deposited in high-energy gamma-rays. This is an indication that the soft X-ray component is likely the low-energy part of a gamma-ray flare. For these reasons, we exclude it from our sample.

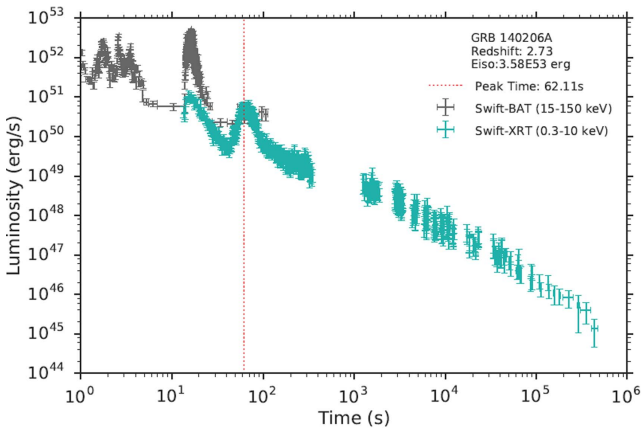

Figure 7. GRB 140206A has two flares. A gamma-ray flare coincides with the first flare while it is dim in the second one. The spectral analysis, using both *Swift*-XRT and *Swift*-BAT data, indicates a power-law index -0.88 ± 0.03 for the first flare. While the second flare requires an additional blackbody component; its power-law index is -1.73 ± 0.06 and its blackbody temperature is 0.54 ± 0.07 keV. Clearly, the energy of the first flare is contributed mainly by gamma-ray photons—it is a gamma-ray flare, and the second flare is an X-ray flare that we consider in this article.

redshift. To express the luminosity L in a fixed cosmological rest-frame energy band, e.g., $[E_1; E_2]$, common to all sources, we can rewrite Equation (4) as

$$L_{[E_1;E_2]} = 4\pi D_L^2 f_{\mathrm{obs},\left[\frac{E_1}{1+z};\frac{E_2}{1+z}\right]} = 4\pi D_L^2 k[\epsilon_{\mathrm{obs},1};\ \epsilon_{\mathrm{obs},2};\ E_1;\ E_2;\ z] f_{\mathrm{obs},[\epsilon_{\mathrm{obs},1};\epsilon_{\mathrm{obs},2}]}, \quad (5)$$

where we have defined the K-correction factor:

$$k[\epsilon_{\mathrm{obs},1};\ \epsilon_{\mathrm{obs},2};\ E_1;\ E_2;\ z] = \frac{f_{\mathrm{obs},\left[\frac{E_1}{1+z};\frac{E_2}{1+z}\right]}}{f_{\mathrm{obs},[\epsilon_{\mathrm{obs},1};\epsilon_{\mathrm{obs},2}]}} = \frac{\int_{E_1/(1+z)}^{E_2/(1+z)} \epsilon\ n_{\mathrm{obs}}(\epsilon) d\epsilon}{\int_{\epsilon_{\mathrm{obs},1}}^{\epsilon_{\mathrm{obs},2}} \epsilon\ n_{\mathrm{obs}}(\epsilon) d\epsilon}. \quad (6)$$

If the energy range $[\frac{E_1}{1+z}; \frac{E_2}{1+z}]$ is not fully inside the instrumental energy band $[\epsilon_{\mathrm{obs},1}; \epsilon_{\mathrm{obs},2}]$, it may well happen that we will need to extrapolate n_{obs} within the integration boundaries $[\frac{E_1}{1+z}; \frac{E_2}{1+z}]$.

Finally, we express each luminosity in a rest-frame energy band that coincides with the energy window of each specific instrument.

We turn now to the selection procedure for early X-ray flares. We take the soft X-ray flux light curves of each source with known redshift from the *Swift-XRT* repository (Evans et al. 2007, 2009). We then apply the above K correction to obtain the corresponding luminosity light curves in the rest frame 0.3–10 keV energy band. Starting from 421 *Swift*-XRT light curves, we found in 50 sources X-ray flare structures in the early 200 s. Remarkably, all of them are in BdHNe. We further filter our sample by applying the following criteria:

1. We exclude GRBs with flares having a low (<20) signal-to-noise ratio or with an incomplete data coverage of the early X-ray light curve—14 GRBs are excluded (see e.g., Figure 5).
2. We consider only X-ray flares and do not address here the gamma-ray flares, which will be studied in a forthcoming article—eight GRBs having only gamma-ray flares are temporarily excluded (see, e.g., Figure 6). In Figure 7, we show an illustrative example of the possible co-existence of an X-ray flare and a gamma-ray flare, and a way to distinguish them.
3. We also ignore here the late X-ray flare, including the ultralong GRB, which will be discussed in a forthcoming paper—six GRBs are consequently excluded.
4. We ignore the GRBs for which the soft X-ray energy observed by *Swift*-XRT (0.3–10 keV) before the plateau phase is higher than the gamma-ray energy observed by *Swift*-BAT (15–150 keV) during the entire valid *Swift*-BAT observation. This *Swift*-BAT anomaly points to an incomplete coverage of the prompt emission—six GRBs are excluded (see, e.g., Figure 8).

Finally, we have found 16 BdHNe satisfying all of the criteria to be included in our sample. Among them, seven

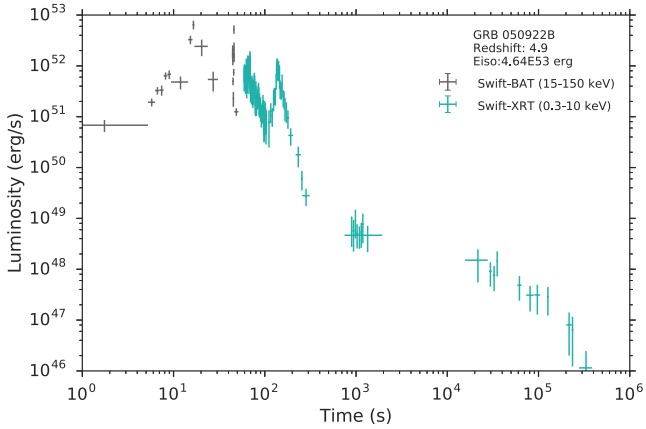

Figure 8. The *Swift*-BAT data of GRB 050922B has poor resolution—it cannot provide valid information after 50 s. The energy observed in its energy band, 15–150 keV, during this 50 s duration is 1.19×10^{53} erg. The energy observed by *Swift*-XRT is higher; the energy of the flares (60–200 s) in the *Swift*-XRT band 0.3–10 keV is 3.90×10^{53} erg. These results imply that the *Swift*-BAT observations may not cover the entire prompt emission phase; the isotropic energy computed from the *Swift*-BAT data is not reliable, and consequently the *Swift*-XRT observed partial prompt emission, which brings complexity to the X-ray light curve, makes the identification of the authentic X-ray flare more difficult.

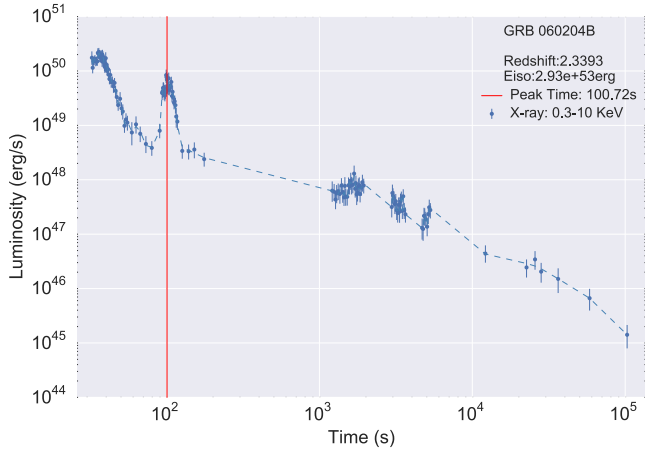

Figure 9. 060204B: this GRB triggered *Swift*-BAT (Falcone et al. 2006); *Swift*-XRT began observing 28.29 s after the BAT trigger. There is no observation from the *Fermi* satellite. X-shooter found its redshift at 2.3393 based on the host galaxy (Perley et al. 2016). The isotropic energy of this GRB reaches 2.93×10^{53} erg, computed from *Swift*-BAT data.

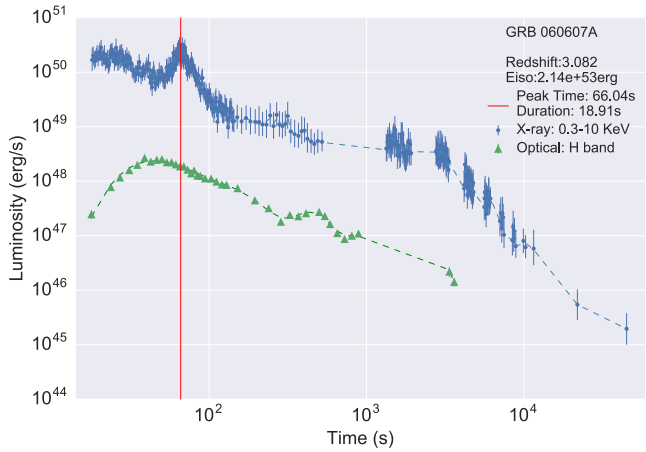

Figure 10. 060607A: this source was detected by the *Swift* satellite (Ziaeepour et al. 2006). It has a bright optical counterpart (Ziaeepour et al. 2006). It is located at a redshift $z = 3.082$ (Ledoux et al. 2006). The prompt light curve presents a doubled-peaked emission that lasts around 10 s, plus a second emission at ∼25 s of 2.5 s duration. The isotropic energy is $E_{\rm iso} = 2.14 \times 10^{53}$ erg. Optical data are from Nysewander et al. (2009).

BdHNe show a single flare. The other nine BdHNe contain two flares: generally, we exclude the first one, which appears to be a component from the gamma-ray spike or gamma-ray flare, and therefore select the second one for analysis (see, e.g., Figure 7).

These 16 selected BdHNe cover a wide range of redshifts. The closest one is GRB 070318 with redshift $z = 0.84$, and the farthest one is GRB 090516A with redshift $z = 4.11$. Their isotropic energy is also distributed over a large range: five GRBs have energies of the order of 10^{52} erg, nine GRBs of the order of 10^{53} erg, and two GRBs have extremely high isotropic energies $E_{\rm iso} > 10^{54}$ erg. Therefore, this sample is well-constructed although the total number is limited.

5. The XRT Luminosity Light Curves of the 16 BdHN Sample

We now turn to the light curves of each of these 16 GRBs composing our sample (see Figures 9–24). The blue curves represent the X-rays observed by *Swift*-XRT, and the green curves are the corresponding optical observations when available. All of the values are in the rest frame and the X-ray luminosities have been *K*-corrected. The red vertical lines indicate the peak time of the X-ray flares. The rest-frame luminosity light curves of some GRBs show different flare structures compared to the observed count flux light curves. An obvious example is GRB 090516A, which follows from comparing Figure 18 in this paper with Figure 1 in Troja et al. (2015). The details of the FPA, as well as their correlations or the absence of correlation with $E_{\rm iso}$, are given in the next section.

We then conclude that in our sample, there are *Swift* data for all GRBs: Konus-*Wind* observed GRBs 080607, 080810, 090516A, 131030A, 140419A, 141221A, and 151027A, while *Fermi* detected GRBs 090516A, 140206, 141221A, and 151027A. The energy coverage of the available satellites is limited, as mentioned in Section 2: *Fermi* detects the widest photon energy band, from 8 keV to 300 GeV, Konus-*Wind* observes from 20 keV to 15 MeV, and *Swift*-BAT has a narrow coverage from 15 keV to 150 keV. No GeV photons were observed, though GRB 090516A and 151027 were in the *Fermi*-LAT field of view. This contrasts with the observations of S-GRBs for which, in all of the sources so far identified and within the *Fermi*-LAT field of view, GeV photons were always observed (Ruffini et al. 2016a, 2016b) and can always freely reach a distant observer. These observational facts suggest that NS–NS (or NS–BH) mergers leading to the formation of a BH leave the surrounding environment poorly contaminated with the material ejected in the merging process ($\lesssim 10^{-2}$–$10^{-3}\,M_\odot$) and therefore the GeV emission, originating from the accretion on the BH formed in the merger process (Ruffini et al. 2016a) can be observed. On the other hand, BdHNe originate in $\rm CO_{core}$–NS binaries in which the material ejected from the $\rm CO_{core}$ explosion ($\approx M_\odot$) greatly pollutes the environment where the GeV emission has to propagate to reach the observer (see Section 3). This, together with the asymmetries of the SN

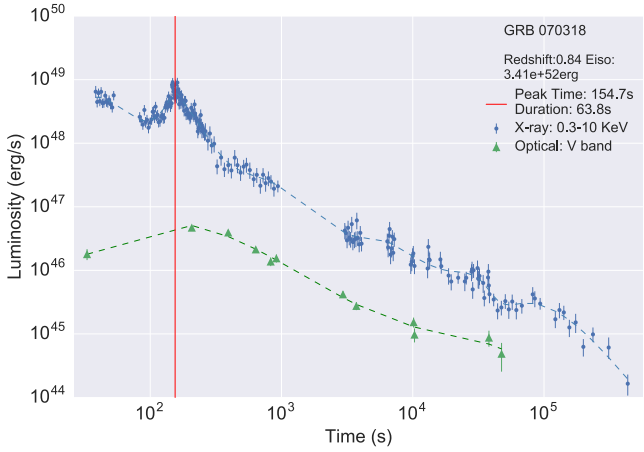

Figure 11. 070318: this source was detected by the *Swift* satellite (Cummings et al. 2007). It has a spectroscopic redshift of $z = 0.836$ (Jaunsen et al. 2007). The prompt light curve shows a peak with a typical fast-rise exponential-decay (FRED) behavior lasting about 55 s. XRT began observing the field 35 s after the BAT trigger. The isotropic energy is $E_{\rm iso} = 3.64 \times 10^{52}$ erg. From the optical observation at ∼20 days, no source or host galaxy is detected at the position of the optical afterglow, indicating that the decay rate of the afterglow must have steepened after some hours (Cobb 2007). Its optical data are from Chester et al. (2008).

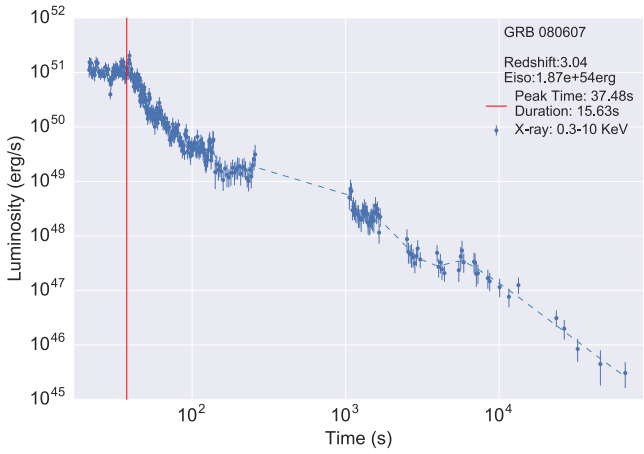

Figure 12. 080607: this source has been observed by *AGILE* (Marisaldi et al. 2008), Konus-*Wind* (Golenetskii et al. 2008), and *Swift* (Mangano et al. 2008). UVOT detected only a faint afterglow, since the source is located at a redshift $z = 3.04$. The isotropic energy is $E_{\rm iso} = 1.87 \times 10^{54}$ erg. The BAT prompt light curve shows a very pronounced peak that lasts ∼10 s, followed by several shallow peaks until 25 s. The *Swift* localization is at about 113° off-axis with respect to the *AGILE* pointing, so well out of the field of view of the *AGILE* gamma-ray imaging detector (GRID), which does not show any detection. The Konus-*Wind* light curve in the 50–200 keV range shows a multiple-peak emission lasting 15 s.

ejecta (see Section 3 and Becerra et al. 2016), lead to the possibility that the GeV emission in BdHNe can be "obscured" by the material of the SN ejecta, explaining the absence of GeV photons in the above cases of GRBs 090516A and 151027.

We derive the isotropic energy $E_{\rm iso}$ by assuming the prompt emission to be isotropic and by integrating the prompt photons in the rest-frame energy range from 1 keV to 10 MeV (Bloom et al. 2001). None of the satellites is able to cover the entire energy band of $E_{\rm iso}$, so we need to fit the spectrum and find the best-fit function, then extrapolate the integration of energy by using this function. This method is relatively safe for GRBs observed by *Fermi* and Konus-*Wind*, but six GRBs in our

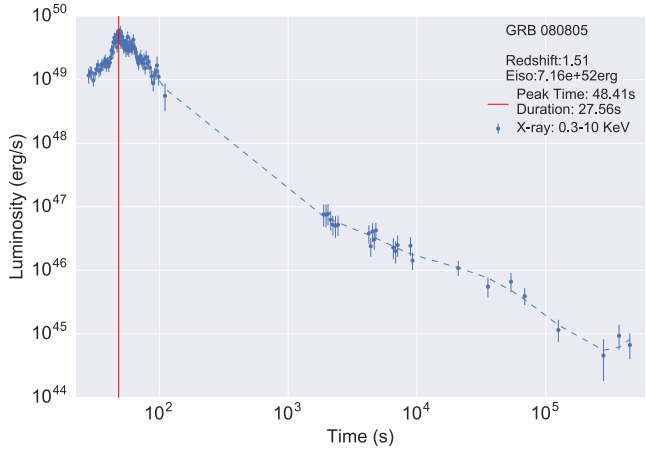

Figure 13. 080805: this source was detected by *Swift* (Pagani et al. 2008). The prompt light curve shows a peak with a FRED behavior lasting about 32 s. The redshift is $z = 1.51$, as reported by VLT (Jakobsson et al. 2008), and the isotropic energy is $E_{\rm iso} = 7.16 \times 10^{52}$ erg.

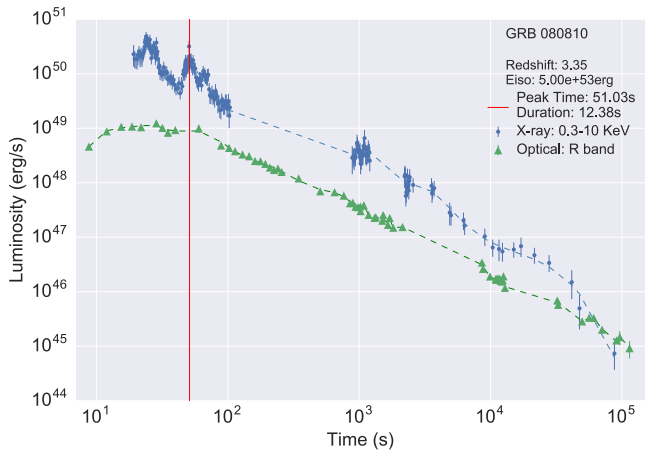

Figure 14. 080810: this source was detected by *Swift* (Golenetskii et al. 2008). The BAT light curve shows a multiple-peaked structure lasting about 23 s. XRT began observing the field 76 s after the BAT trigger. The source is located at a redshift of $z = 3.35$ and has an isotropic energy $E_{\rm iso} = 3.55 \times 10^{53}$ erg. Optical data are taken from Page et al. (2009).

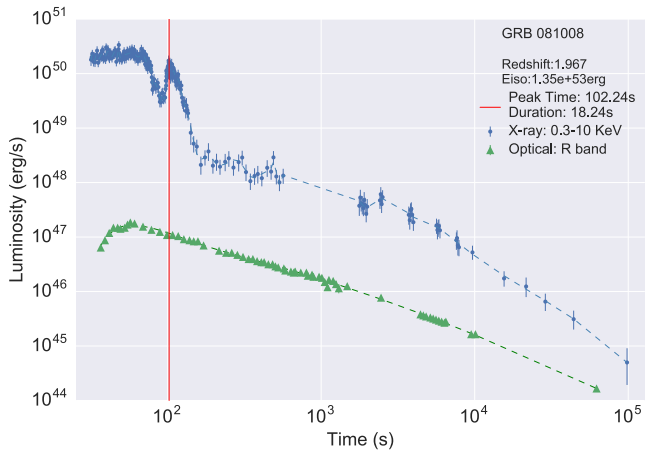

Figure 15. 081008: this source was detected by *Swift* (Racusin et al. 2008). The prompt emission lasts about 60 s and shows two peaks separated by 13 s. It is located at $z = 1.967$, as reported by VLT (D'Avanzo et al. 2008), and has an isotropic energy $E_{\rm iso} = 1.07 \times 10^{53}$ erg. Optical data are from Yuan et al. (2010).

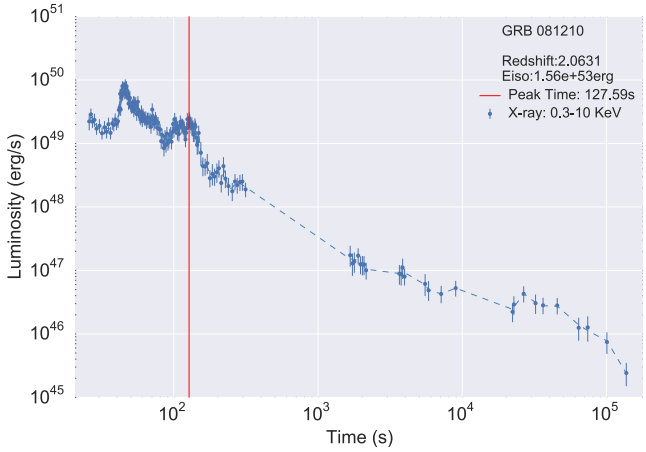

Figure 16. 081210: this GRB was detected by *Swift*-BAT (Krimm et al. 2008), *Swift*-XRT began observing 23.49 s after the BAT trigger. The BAT light curve begins with two spikes with a total duration of about 10 s and an additional spike at 45.75 s. There is no observation from the *Fermi* satellite. X-shooter found its redshift to be 2.0631 (Perley et al. 2016). The isotropic energy of this GRB is 1.56×10^{53} erg.

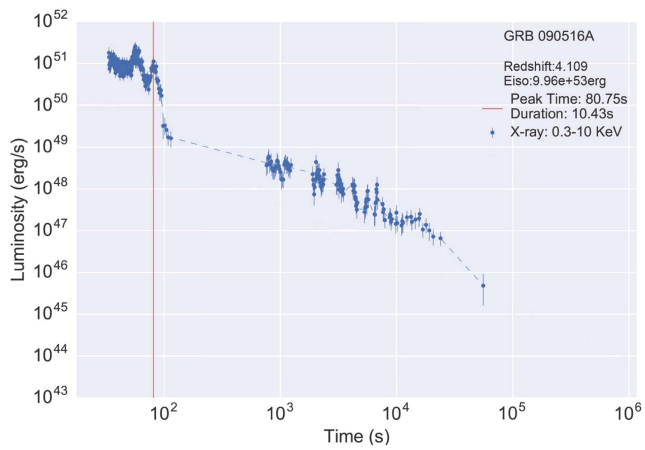

Figure 17. 090516A: this source was detected by *Swift* (Rowlinson et al. 2009), Konus-*Wind*, and *Fermi*/GBM (McBreen 2009). The BAT prompt light curve is composed of two episodes, the first starting 2 s before the trigger and lasting up to 10 s after the trigger, while the second episode starts at 17 s and lasts approximately 2 s. The GBM light curve consists of about five overlapping pulses from $T_{F,0} - 10$ s to $T_{F,0} + 21$ s (where $T_{F,0}$ is the trigger time of the *Fermi*/GBM). Konus-*Wind* observed this GRB in the waiting mode. VLT identified the redshift of the afterglow as $z = 4.109$ (de Ugarte Postigo et al. 2012), in agreement with the photometric redshift obtained with GROND (Rossi et al. 2009). *Fermi*-LAT was inside the field of view, following the standard *Fermi*-LAT likelihood analysis in https://fermi.gsfc.nasa.gov/ssc/data/analysis/scitools/likelihood_tutorial.html, the upper limit of the observed count flux is 4.76×10^{-6} photons cm^{-2} s^{-1}, and no GeV photon was found for this high redshift and low observed fluence GRB. The isotropic energy is $E_{iso} = 6.5 \times 10^{53}$ erg.

sample have been observed only by *Swift*, so we uniformly fit and extrapolate these six GRBs by power laws and cutoff power laws; we then take the average value as E_{iso}. In general, our priority in computing E_{iso} is *Fermi*, Konus-*Wind*, then *Swift*. In order to take into account the expansion of the universe, all of our computations consider the K correction. The formula of K correction for E_{iso} varies depending on the best-fit function. The energy in the X-ray afterglow is computed in the cosmological rest-frame energy band from 0.3 to 10 keV. We smoothly fit the luminosity light curve using an algorithm named locally weighted regression (Cleveland & Devlin 1988),

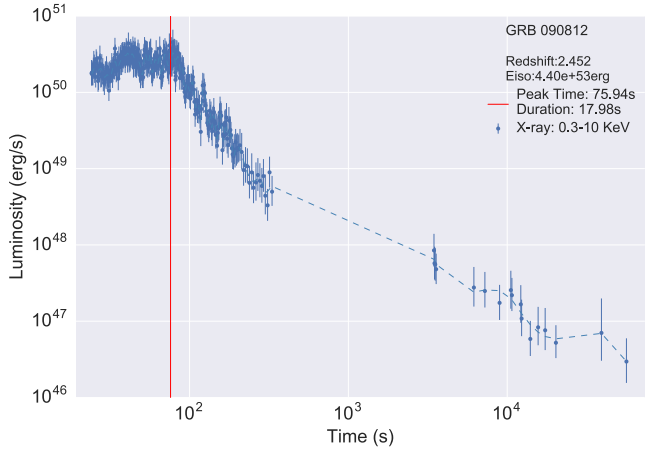

Figure 18. 090812: this source was detected by *Swift* (Stamatikos et al. 2009). It has a redshift $z = 2.452$ as confirmed by VLT (de Ugarte Postigo et al. 2012) and an isotropic energy $E_{iso} = 4.75 \times 10^{53}$ erg. The BAT light curve shows three successive bumps lasting ~20 s in total. XRT began observing the field 22 s after the BAT trigger (Stamatikos et al. 2009). The BAT light curve shows a simple power-law behavior.

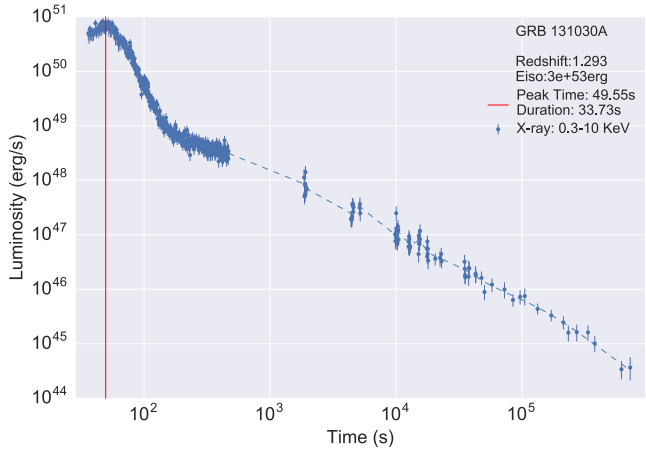

Figure 19. 131030A: this source was observed by *Swift* (Troja et al. 2013) and Konus-*Wind* (Golenetskii et al. 2013). The BAT light curve shows two overlapping peaks starting, with respect to the *Swift*-BAT trigger $T_{B,0}$, at $\sim T_{B,0} - 3.5$ s and peaking at $\sim T_{B,0} + 4.4$ s (Barthelmy et al. 2013). The duration is 18 s in the 15–350 keV band. The Konus-*Wind* light curve shows a multipeaked pulse from $\sim T_{KW,0} - 1.3$ s until $\sim T_{KW,0} + 11$ s (where $T_{KW,0}$ is the Konus-*Wind* trigger time). The redshift of this source is $z = 1.293$, as determined by NOT (Xu et al. 2013). The isotropic energy is $E_{iso} = 3 \times 10^{53}$ erg.

which provides a sequence of power-law functions. The corresponding energy in a fixed time interval is obtained by summing up all of the integrals of the power laws within it. This method is applied to estimate the energy of the flare E_f as well as the energy of the FPA phase up to 10^9 s, E_{FPA}. An interesting alternative procedure was used in Swenson & Roming (2014) to fit the light curve and determine the flaring structure with a Bayesian Information method. On this specific aspect, the two treatments are equally valid and give compatible results.

Table 3 contains the relevant energy and time information of the 16 BdHNe of the sample: the cosmological redshift z, E_{iso}, the flare peak time t_p, the corresponding peak luminosity L_p, the flare duration Δt, and the energy of the flare E_f. To determine t_p, we apply a locally weighted regression, which results in a

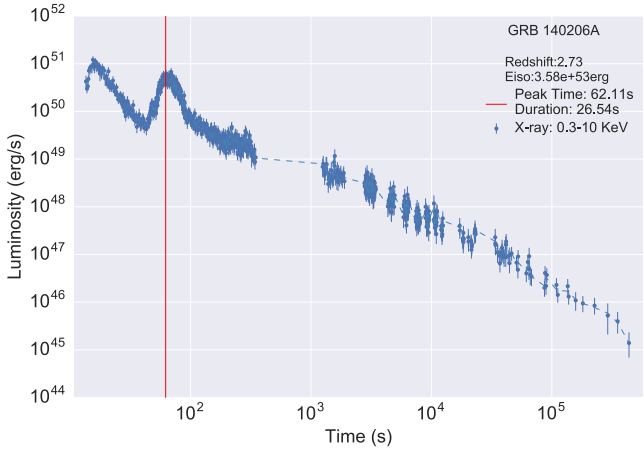

Figure 20. 140206A: this source was detected by all instruments on board *Swift* (Lien et al. 2014) and by *Fermi*/GBM (von Kienlin & Bhat 2014). The GBM light curve shows a single pulse with a duration of ∼7 s (50–300 keV). The source was outside the field of view, 123° from the LAT boresight at the time of the trigger. The BAT light curve shows a multipeaked structure with roughly three main pulses (Sakamoto et al. 2014). The source duration in the 15–350 keV band is 25 s. The redshift, as observed by NOT (Malesani et al. 2014), is $z = 2.73$, and the isotropic energy is $E_{\rm iso} = 4.3 \times 10^{53}$ erg.

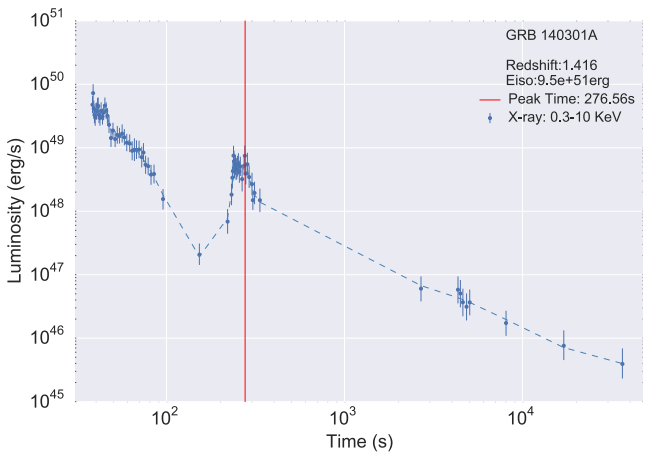

Figure 21. 140301A: this GRB triggered *Swift*-BAT (Page et al. 2014); the BAT light curve has a single spike with a duration of about 4 s. XRT started to observe 35.63 s after the BAT trigger. There is no observation from the *Fermi* satellite. From the X-shooter spectrum analysis, the redshift was revealed at 1.416 (Kruehler et al. 2014). The isotropic energy of this GRB is 9.5×10^{51} erg.

smoothed light curve composed of power-law functions: the flare peak is localized where the power-law index is zero. Therefore, t_p is defined as the time interval between the flare peak and the trigger time of *Swift*-BAT.[10] Correspondingly, we find the peak luminosity L_p at t_p and its duration Δt, which is defined as the time interval between a start time and an end time where the luminosity is half of L_p. We have made public the entire details including the codes online.[11]

[10] In reality, the GRB occurs earlier than the trigger time, since there is a short period when the flux intensity is lower than the satellite trigger threshold (Fenimore et al. 2003).

[11] https://github.com/YWangScience/AstroNeuron

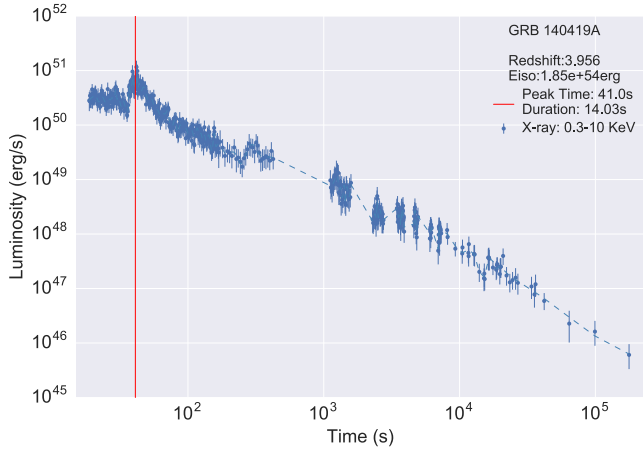

Figure 22. 140419A: this source was detected by Konus-*Wind* (Golenetskii et al. 2014) and *Swift* (Marshall et al. 2014). The Konus-*Wind* light curve shows a broad pulse from $\sim T_{\rm KW,0} - 2$ s to $\sim T_{\rm KW,0} + 8$ s, followed by softer pulses around $\sim T_{\rm KW,0} + 10$ s. The total duration of the burst is ∼16 s. The BAT light curve shows two slightly overlapping clusters of peaks, starting at $\sim T_{\rm B,0} - 2$ s, peaking at $\sim T_{\rm B,0} + 2$ s and $\sim T_{\rm B,0} + 10$ s, and ending at $\sim T_{\rm B,0} + 44$ s (Baumgartner et al. 2014). The total duration (in 15–350 keV) is 19 s. The redshift of this source, as determined by Gemini, is $z = 3.956$ (Tanvir et al. 2014), and its isotropic energy is $E_{\rm iso} = 1.85 \times 10^{54}$ erg.

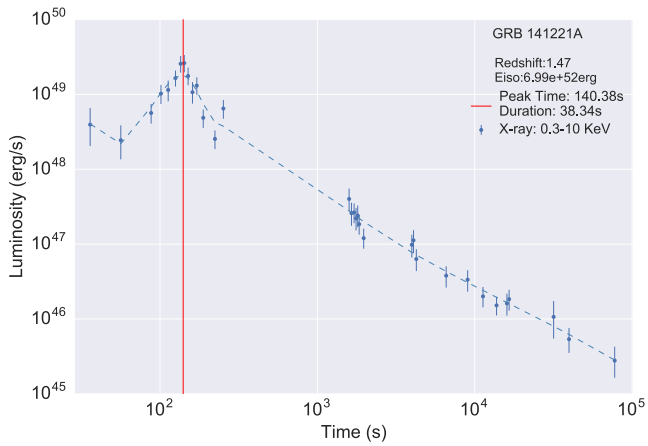

Figure 23. 141221A: this source is located at a spectroscopic redshift $z = 1.47$, as determined by Keck (Perley et al. 2014). Its isotropic energy is $E_{\rm iso} = 1.91 \times 10^{52}$ erg. The emission was detected by all of the instruments on board *Swift* (Sonbas et al. 2014) and by *Fermi*/GBM (Yu 2014). The GBM light curve consists of two pulses with a duration of about 10 s (50–300 keV). The source was 76° from the LAT boresight at the time of the trigger, out of the field of view. The BAT light curve showed a double-peaked structure with a duration of about 8 s. XRT began observing the field 32 s after the BAT trigger.

6. Statistical Correlation

We then establish correlations between the above quantities characterizing each luminosity light curve of the sample with the $E_{\rm iso}$ of the corresponding BdHN. We have relied heavily on the MCMC method and iterated 10^5 times to obtain the best fit of the power law and their correlation coefficient. The main results are summarized in Figures 25–28. All of the codes are publicly available online.[12] We conclude that the peak time and

[12] https://github.com/YWangScience/MCCC

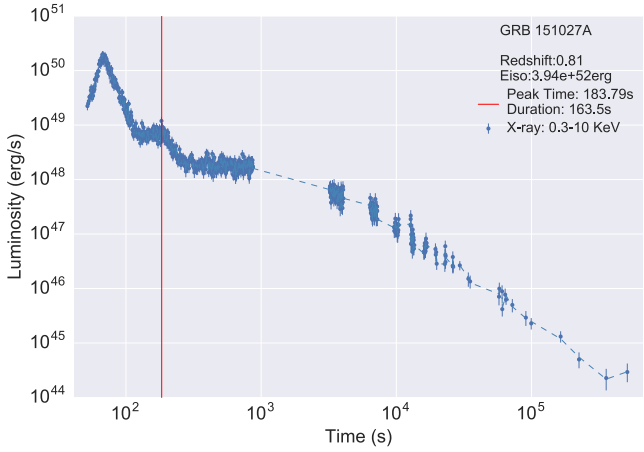

Figure 24. 151027A: this source was detected by MAXI (Masumitsu et al. 2015), Konus-*Wind* (Golenetskii et al. 2015), *Swift* (Maselli et al. 2015), and *Fermi*/GBM (Toelge et al. 2015). It is located at a redshift $z = 0.81$, as determined by Keck/HIRES (Perley et al. 2015), and the isotropic energy is $E_{\rm iso} = 3.94 \times 10^{52}$ erg. The LAT boresight of the source was $10^{\rm o}$ at the time of the trigger, and there are no clear associated high-energy photons; an upper limit of the observed count flux is computed to be 9.24×10^{-6} photons cm^{-2} s^{-1} following the standard *Fermi*-LAT likelihood analysis. The BAT light curve showed a complex peaked structure lasting at least 83 s. XRT began observing the field 48 s after the BAT trigger. The GBM light curve consists of three pulses with a duration of about 68 s in the 50–300 keV band. The Konus-*Wind* light curve consists of at least three pulses with a total duration of ∼66 s. The MAXI detection is not significant, but the flux is consistent with the interpolation from the *Swift*/XRT light curve.

the duration of the flare, as well as the peak luminosity and the total energy of flare, are highly correlated with $E_{\rm iso}$, with correlation coefficients larger than 0.6 (or smaller than −0.6). The average values and the 1σ uncertainties are shown in Table 4.

7. The Partition of the Electron–Positron Plasma Energy Between the Prompt Emission and the FPA

The energy of the prompt emission is proportional to $E_{\rm iso}$ if and only if spherical symmetry is assumed: this clearly follows from the prompt emission time-integrated luminosity. We are now confronted with a new situation: the total energy of the FPA emission up to 10^9 s ($E_{\rm FPA}$) is also proportional to $E_{\rm iso}$, following the correlation given in Tables 5 and 6, and Figure 29. What is clear is that there are two very different components where the energy of the dyadosphere $E_{e^+e^-}$ is utilized: the energy $E_{\rm prompt}$ of the prompt emission and the energy $E_{\rm FPA}$ of the FPA, i.e., $E_{e^+e^-} = E_{\rm iso} = E_{\rm prompt} + E_{\rm FPA}$. Figures 30 and 31 show the distribution of $E_{e^+e^-} = E_{\rm iso}$ between these two components.

As a consequence of the above, in view of the presence of the companion SN remnant ejecta (see Becerra et al. 2016 for more details), we assume here that the spherical symmetry of the prompt emission is broken. Part of the energy due to the impact of the e^+e^- plasma on the SN is captured by the SN ejecta, and gives rise to the FPA emission as originally proposed by Ruffini (2015). We shall return to the study of the impact between the plasma and the SN ejecta in Section 10 after studying the motion of the matter composing the FPA in the next few sections.

It can also be seen that the relative partition between $E_{\rm prompt}$ and $E_{\rm FPA}$ strongly depends on the value of $E_{e^+e^-}$: the lower the GRB energy, the higher the FPA energy percentage, and consequently the lower the prompt energy percentage (see Figure 31).

In Becerra et al. (2016), we indicate that both the value of $E_{e^+e^-}$ and the relative ratio of the above two components can in principle be explained in terms of the geometry of the binary nature of the system: the smaller the distance is between the $CO_{\rm core}$ and the companion NS, the shorter the binary period of the system, and the larger the value of $E_{e^+e^-}$.

8. On the Flare Thermal Emission, Its Temperature, and Dynamics

We discuss now the profound difference between the prompt emission, which we recall is emitted at distances of the order of 10^{16} cm away from the newly born BH with $\Gamma \approx 10^2$–10^3, and the FPA phase. We focus on a further fundamental set of data, which originates from a thermal emission associated with the flares.[13] Only in some cases is this emission so clear and prominent that it allows the estimation of the flare expansion speed and the determination of its mildly relativistic Lorentz factor $\Gamma \lesssim 4$, which creates a drastic separatrix both in the energy and in the Gamma factor between the astrophysical nature of the prompt emission and of the flares.

Following the standard data reduction procedure of *Swift*-XRT (Romano et al. 2006; Evans et al. 2007, 2009), X-ray data within the duration of flare are retrieved from the United Kingdom *Swift* Science Data Centre (UKSSDC)[14] and analyzed by Heasoft.[15] Table 7 shows the fit of the spectrum within the duration Δt of the flare for each BdHN of the sample. As a first approximation, in computing the radius, we have assumed a constant expansion velocity of $0.8c$ indicated for some BdHNe, such as GRB 090618 (Ruffini et al. 2014) and GRB 130427A (Ruffini et al. 2015c). Out of 16 sources, seven BdHNe have highly confident thermal components (significance >0.95; see boldfaced entries in Table 7), which means that the addition of a blackbody spectrum improves a single power-law fit (which is, conversely, excluded at the 2σ confidence level). These blackbodies have fluxes in a range from 1% to 30% of the total flux and share a similar order of magnitude radii, i.e., $\sim 10^{11}$–10^{12} cm. In order to have a highly significant thermal component, the blackbody radiation itself should be prominent as well as its ratio to the nonthermal part. Another critical reason is that the observable temperature must be compatible with the satellite bandpass. For example, *Swift*-XRT observes in the 0.3–10 keV photon energy band, but the hydrogen absorption affects the lower energy part (∼0.5 keV), and data are not always adequate beyond 5 keV, due to the low effective area of satellite for high-energy photons. The reliable temperature only ranges from 0.15 keV to 1.5 keV (since the peak photon energy is equal to the temperature times 2.82), so the remaining nine GRBs may contain a thermal component in the flare but outside the satellite bandpass.

We now attempt to perform a more refined analysis to infer the value of β from the observations. We assume that during the flare, the blackbody emitter has spherical symmetry and expands with a constant Lorentz Gamma factor. Therefore, the expansion velocity β is also constant during the flare. The relations between the comoving time $t_{\rm com}$, the laboratory time t,

[13] The late afterglow phases have been already discussed in Pisani et al. (2013, 2016).
[14] http://www.swift.ac.uk
[15] http://heasarc.gsfc.nasa.gov/lheasoft/

Table 3
GRB Sample Properties of the Prompt and Flare Phases

GRB	z	T_{90} (s)	$E_{\rm iso}$ (erg)	t_p (s)	L_p (erg s^{-1})	Δt (s)	E_f (erg)	α_f
060204B	2.3393	40.12	$2.93(\pm0.60) \times 10^{53}$	100.72 ± 6.31	$7.35(\pm2.05) \times 10^{49}$	17.34 ± 6.83	$8.56(\pm0.82) \times 10^{50}$	2.73
060607A	3.082	24.49	$2.14(\pm1.19) \times 10^{53}$	66.04 ± 4.98	$2.28(\pm0.48) \times 10^{50}$	18.91 ± 3.84	$3.33(\pm0.32) \times 10^{51}$	1.72
070318	0.84	28.80	$3.41(\pm2.14) \times 10^{52}$	154.7 ± 12.80	$6.28(\pm1.30) \times 10^{48}$	63.80 ± 19.82	$3.17(\pm0.37) \times 10^{50}$	1.84
080607	3.04	21.04	$1.87(\pm0.11) \times 10^{54}$	37.48 ± 3.60	$1.14(\pm0.27) \times 10^{51}$	15.63 ± 4.32	$1.54(\pm0.24) \times 10^{52}$	2.08
080805	1.51	31.08	$7.16(\pm1.90) \times 10^{52}$	48.41 ± 5.46	$4.66(\pm0.59) \times 10^{49}$	27.56 ± 9.33	$9.68(\pm1.24) \times 10^{50}$	1.25
080810	3.35	18.25	$5.00(\pm0.44) \times 10^{53}$	51.03 ± 6.49	$1.85(\pm0.53) \times 10^{50}$	12.38 ± 4.00	$1.80(\pm0.17) \times 10^{51}$	2.37
081008	1.967	62.52	$1.35(\pm0.66) \times 10^{53}$	102.24 ± 5.66	$1.36(\pm0.33) \times 10^{50}$	18.24 ± 3.63	$1.93(\pm0.16) \times 10^{51}$	2.46
081210	2.0631	47.66	$1.56(\pm0.54) \times 10^{53}$	127.59 ± 13.68	$2.23(\pm0.21) \times 10^{49}$	49.05 ± 6.49	$8.86(\pm0.54) \times 10^{50}$	2.28
090516A	4.109	68.51	$9.96(\pm1.67) \times 10^{53}$	80.75 ± 2.20	$9.10(\pm2.26) \times 10^{50}$	10.43 ± 2.44	$7.74(\pm0.63) \times 10^{51}$	3.66
090812	2.452	18.77	$4.40(\pm0.65) \times 10^{53}$	77.43 ± 16.6	$3.13(\pm1.38) \times 10^{50}$	17.98 ± 4.51	$5.18(\pm0.61) \times 10^{51}$	2.20
131030A	1.293	12.21	$3.00(\pm0.20) \times 10^{53}$	49.55 ± 7.88	$6.63(\pm1.12) \times 10^{50}$	33.73 ± 6.55	$3.15(\pm0.57) \times 10^{52}$	2.22
140206A	2.73	7.24	$3.58(\pm0.79) \times 10^{53}$	62.11 ± 12.26	$4.62(\pm0.99) \times 10^{50}$	26.54 ± 4.31	$1.04(\pm0.59) \times 10^{51}$	1.73
140301A	1.416	12.83	$9.50(\pm1.75) \times 10^{51}$	276.56 ± 15.50	$5.14(\pm1.84) \times 10^{48}$	64.52 ± 10.94	$3.08(\pm0.22) \times 10^{50}$	2.30
140419A	3.956	16.14	$1.85(\pm0.77) \times 10^{54}$	41.00 ± 4.68	$6.23(\pm1.45) \times 10^{50}$	14.03 ± 5.74	$7.22(\pm0.88) \times 10^{51}$	2.32
141221A	1.47	9.64	$6.99(\pm1.98) \times 10^{52}$	140.38 ± 5.64	$2.60(\pm0.64) \times 10^{49}$	38.34 ± 9.26	$7.70(\pm0.78) \times 10^{50}$	1.79
151027A	0.81	68.51	$3.94(\pm1.33) \times 10^{52}$	183.79 ± 16.43	$7.10(\pm1.75) \times 10^{48}$	163.5 ± 30.39	$4.39(\pm2.91) \times 10^{51}$	2.26

Note. This table contains the redshift z, the T_{90} in the rest frame, the isotropic energy $E_{\rm iso}$, the flare peak time t_p in the rest frame, the flare peak luminosity L_p, the flare duration where the starting and ending time correspond to half of the peak luminosity Δt, the flare energy E_f within the time interval Δt, and α_f the power-law index from the fitting of the flare's spectrum.

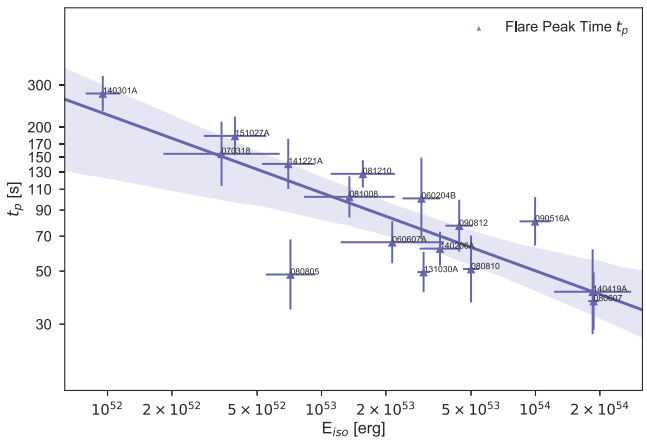

Figure 25. Relation between $E_{\rm iso}$ and t_p fit by a power law. The shaded area indicates the 95% confidence level.

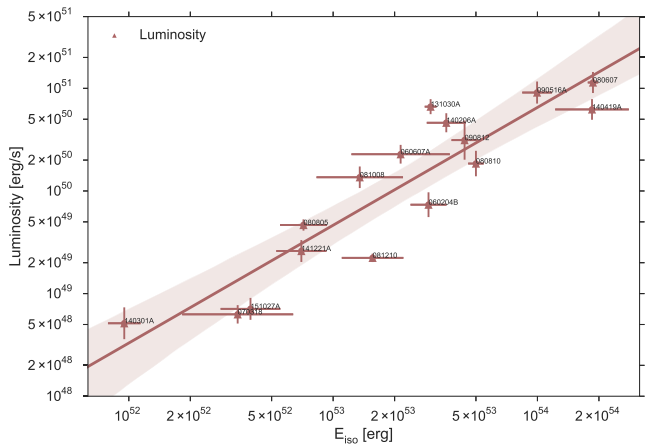

Figure 27. Relation between $E_{\rm iso}$ and L_p fit by a power law. The shaded area indicates the 95% confidence level.

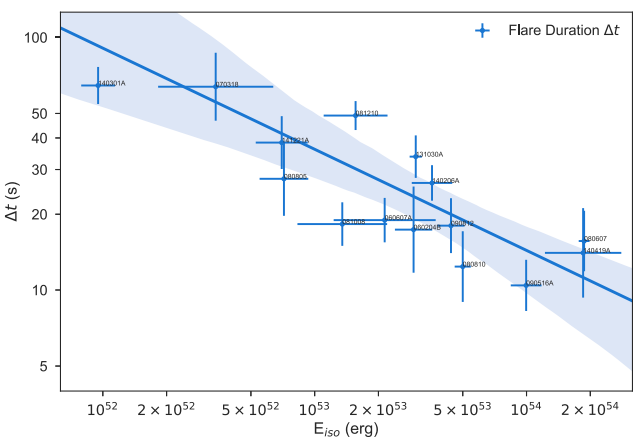

Figure 26. Relation between $E_{\rm iso}$ and Δt fit by a power law. The shaded area indicates the 95% confidence level.

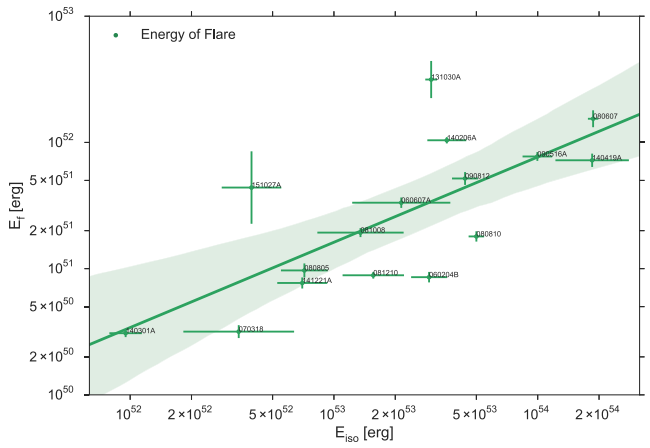

Figure 28. Relation between $E_{\rm iso}$ and E_f fit by a power law. The shaded area indicates the 95% confidence level.

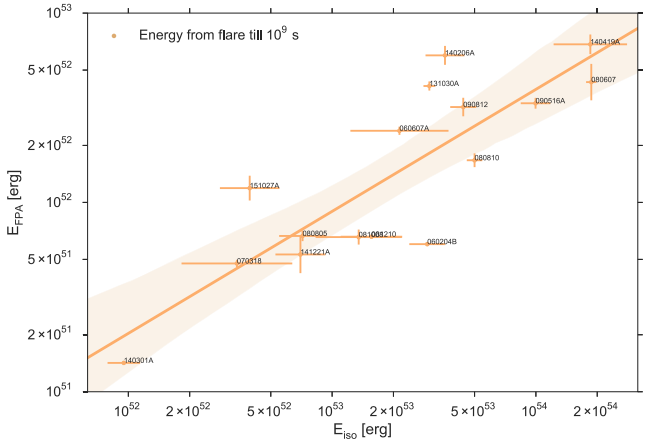

Figure 29. Relation between $E_{\rm iso}$ and $E_{\rm FPA}$ fit by a power law. The shaded area indicates the 95% confidence level.

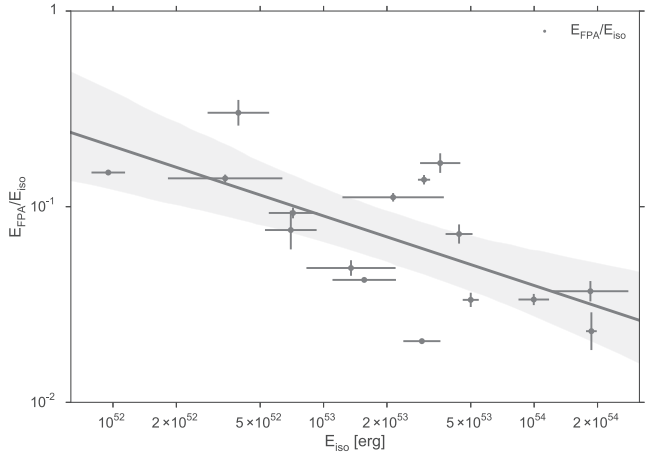

Figure 30. Relation between the percentage of $E_{e^+e^-}$ going to the SN ejecta and accounting for the energy in FPA, i.e., $E_{\rm FPA}/E_{\rm iso} \times 100\%$, and $E_{\rm iso}$ fit by a power law. The shaded area indicates the 95% confidence level.

Table 4
Power-law Correlations Among the Quantities in Table 3

Correlation	Power-law Index	Coefficient
$E_{\rm iso} - t_p$	$-0.290(\pm 0.010)$	$-0.764(\pm 0.123)$
$E_{\rm iso} - \Delta t$	$-0.461(\pm 0.042)$	$-0.760(\pm 0.138)$
$E_{\rm iso} - L_p$	$1.186(\pm 0.037)$	$0.883(\pm 0.070)$
$E_{\rm iso} - E_f$	$0.631(\pm 0.117)$	$0.699(\pm 0.145)$

Note. The values and uncertainties (at the 1σ confidence level) of the power-law index and of the correlation coefficient are obtained from 10^5 MCMC iterations. All relations are highly correlated.

Table 5
GRB Sample Properties of the Prompt and FPA Phases

GRB	z	$E_{\rm iso}$ (erg)	$E_{\rm FPA}$ (erg)
060204B	2.3393	$2.93(\pm 0.60) \times 10^{53}$	$6.02(\pm 0.20) \times 10^{51}$
060607A	3.082	$2.14(\pm 1.19) \times 10^{53}$	$2.39(\pm 0.12) \times 10^{52}$
070318	0.84	$3.41(\pm 2.14) \times 10^{52}$	$4.76(\pm 0.21) \times 10^{51}$
080607	3.04	$1.87(\pm 0.11) \times 10^{54}$	$4.32(\pm 0.96) \times 10^{52}$
080805	1.51	$7.16(\pm 1.90) \times 10^{52}$	$6.65(\pm 0.42) \times 10^{51}$
080810	3.35	$5.00(\pm 0.44) \times 10^{53}$	$1.67(\pm 0.14) \times 10^{52}$
081008	1.967	$1.35(\pm 0.66) \times 10^{53}$	$6.56(\pm 0.60) \times 10^{51}$
081210	2.0631	$1.56(\pm 0.54) \times 10^{53}$	$6.59(\pm 0.60) \times 10^{51}$
090516A	4.109	$9.96(\pm 1.67) \times 10^{53}$	$3.34(\pm 0.22) \times 10^{52}$
090812	2.452	$4.40(\pm 0.65) \times 10^{53}$	$3.19(\pm 0.36) \times 10^{52}$
131030A	1.293	$3.00(\pm 0.20) \times 10^{53}$	$4.12(\pm 0.23) \times 10^{52}$
140206A	2.73	$3.58(\pm 0.79) \times 10^{53}$	$5.98(\pm 0.69) \times 10^{52}$
140301A	1.416	$9.50(\pm 1.75) \times 10^{51}$	$1.42(\pm 0.14) \times 10^{50}$
140419A	3.956	$1.85(\pm 0.77) \times 10^{54}$	$6.84(\pm 0.82) \times 10^{52}$
141221A	1.47	$6.99(\pm 1.98) \times 10^{52}$	$5.31(\pm 1.21) \times 10^{51}$
151027A	0.81	$3.94(\pm 1.33) \times 10^{52}$	$1.19(\pm 0.18) \times 10^{52}$

Note. This table lists z, $E_{\rm iso}$, and the FPA energy $E_{\rm FPA}$ from the flare until 10^9 s.

the arrival time t_a, and the arrival time t_a^d at the detector, given in Equation (2), in this case become

$$\begin{aligned} t_a^d &= t_a(1+z) = t(1-\beta\cos\vartheta)(1+z) \\ &= \Gamma t_{\rm com}(1-\beta\cos\vartheta)(1+z). \end{aligned} \tag{7}$$

We can infer an effective radius R of the blackbody emitter from (1) the observed blackbody temperature $T_{\rm obs}$, which

Table 6
Power-law Correlations Among the Quantities in Table 5

Correlation	Power-law Index	Coefficient
$E_{\rm iso}$–$E_{\rm FPA}$	$0.613(\pm 0.041)$	$0.791(\pm 0.103)$
$E_{\rm iso}$–$E_{\rm FPA}/E_{\rm iso}$	$-0.005(\pm 0.002)$	$0.572(\pm 0.178)$

Note. The statistical considerations of Table 4 are valid here as well.

comes from the spectral fit of the data during the flare; (2) the observed bolometric blackbody flux $F_{\rm bb,obs}$, computed from $T_{\rm obs}$ and the normalization of the blackbody spectral fit; and (3) the cosmological redshift z of the source (see also Izzo et al. 2012). We recall that $F_{\rm bb,obs}$ by definition is given by

$$F_{\rm bb,obs} = \frac{L}{4\pi D_L(z)^2}, \tag{8}$$

where $D_L(z)$ is the luminosity distance of the source, which in turn is a function of the cosmological redshift z, and L is the source bolometric luminosity (i.e., the total emitted energy per unit time). L is Lorentz invariant, so we can compute it in the comoving frame of the emitter using the usual blackbody expression,

$$L = 4\pi {R_{\rm com}}^2 \sigma {T_{\rm com}}^4, \tag{9}$$

where $R_{\rm com}$ and $T_{\rm com}$ are the comoving radius and the comoving temperature of the emitter, respectively, and σ is the Stefan–Boltzmann constant. We recall that $T_{\rm com}$ is constant over the entire shell due to our assumption of spherical symmetry. From Equations (8) and (9), we then have

$$F_{\rm bb,obs} = \frac{{R_{\rm com}}^2 \sigma {T_{\rm com}}^4}{D_L(z)^2}. \tag{10}$$

We now need the relation between $T_{\rm com}$ and the observed blackbody temperature $T_{\rm obs}$. Considering both the cosmological redshift and the Doppler effect due to the velocity of the

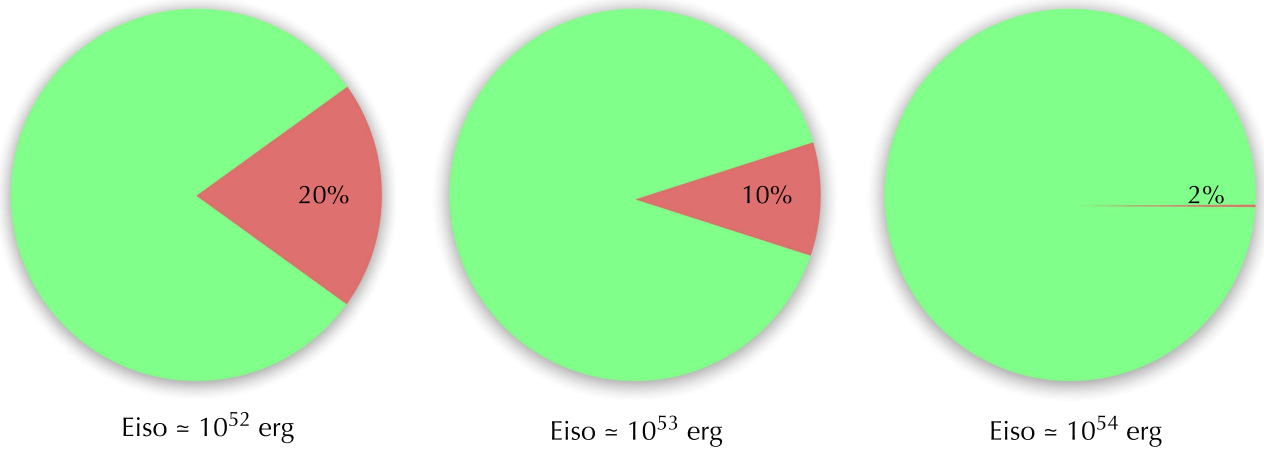

Figure 31. Distribution of the GRB total energy $E_{e^+e^-} = E_{\rm iso}$ into prompt and FPA energies. The percentage of $E_{e^+e^-}$ going to the SN ejecta accounting for the energy in the FPA phase appears in red, i.e., $E_{\rm FPA}/E_{\rm iso} \times 100\%$. The green part is therefore the percentage of $E_{e^+e^-}$ used in the prompt emission, i.e., $E_{\rm prompt}/E_{\rm iso} \times 100\%$. It can be seen that the lower the GRB energy $E_{e^+e^-} = E_{\rm iso}$, the higher the FPA energy percentage, and consequently the lower the prompt energy percentage.

emitting surface, we have

$$T_{\rm obs}(T_{\rm com}, z, \Gamma, \cos\vartheta) = \frac{T_{\rm com}}{(1+z)\Gamma(1-\beta\cos\vartheta)} = \frac{T_{\rm com}\mathcal{D}(\cos\vartheta)}{1+z}, \quad (11)$$

where we have defined the Doppler factor $\mathcal{D}(\cos\vartheta)$ as

$$\mathcal{D}(\cos\vartheta) \equiv \frac{1}{\Gamma(1-\beta\cos\vartheta)}. \quad (12)$$

Equation (11) gives us the observed blackbody temperature of the radiation coming from different points of the emitter surface, corresponding to different values of $\cos\vartheta$. However, since the emitter is at a cosmological distance, we are not able to resolve spatially the source with our detectors. Therefore, the temperature that we actually observe corresponds to an average of Equation (11) computed over the emitter surface:[16]

$$T_{\rm obs}(T_{\rm com}, z, \Gamma) = \frac{1}{1+z}\frac{\int_\beta^1 \mathcal{D}(\cos\vartheta)T_{\rm com}\cos\vartheta d\cos\vartheta}{\int_\beta^1 \cos\vartheta d\cos\vartheta} = \frac{2}{1+z}\frac{\beta(\beta-1)+\ln(1+\beta)}{\Gamma\beta^2(1-\beta^2)}T_{\rm com} = \Theta(\beta)\frac{\Gamma}{1+z}T_{\rm com}, \quad (13)$$

where we defined

$$\Theta(\beta) \equiv 2\,\frac{\beta(\beta-1)+\ln(1+\beta)}{\beta^2}. \quad (14)$$

[16] From the point of view of the observer, the spectrum is not a perfect blackbody, coming from a convolution of blackbody spectra at different temperatures. The blackbody component we obtain from the spectral fit of the observed data is an effective blackbody of temperature $T_{\rm obs}$, analogous to other cases of effective temperatures in cosmology (see, e.g., Ruffini et al. 1983).

Table 7
Radii and Temperatures of the Thermal Components Detected Within the Flare Duration Δt

GRB	Radius (cm)	$kT_{\rm obs}$ (keV)	Significance
060204B	**1.80(±1.11) × 10^11**	**0.60(±0.15)**	**0.986**
060607A	**1.67(±1.01) × 10^11**	**0.92(±0.24)**	**0.991**
070318	*unconstrained*	1.79(±1.14)	0.651
080607	**1.52(±0.72) × 10^12**	**0.49(±0.10)**	**0.998**
080805	1.12(±1.34) × 10^11	1.31(±0.59)	0.809
080810	**2.34(±4.84) × 10^11**	**0.61(±0.57)**	**0.999**
081008	**1.84(±0.68) × 10^12**	**0.32(±0.03)**	**0.999**
081210	*unconstrained*	0.80(±0.51)	0.295
090516A	*unconstrained*	1.30(±1.30)	0.663
090812	1.66(±1.84) × 10^12	0.24(±0.12)	0.503
131030A	**3.67(±1.02) × 10^12**	**0.55(±0.06)**	**0.999**
140206A	**9.02(±2.84) × 10^11**	**0.54(±0.07)**	**0.999**
140301A	*unconstrained*	*unconstrained*	0.00
140419A	1.85(±1.17) × 10^12	0.23(±0.05)	0.88
141221A	1.34(±2.82) × 10^12	0.24(±0.24)	0.141
151027A	1.18(±0.67) × 10^12	0.29(±0.06)	0.941

Note. The observed temperatures $kT_{\rm obs}$ are inferred from fitting with a power-law plus blackbody spectral model. The significance of a blackbody is computed by the maximum likelihood ratio for comparing nested models and its addition improves a fit when the significance is >0.95. The radii are calculated assuming mildly relativistic motion ($\beta = 0.8$) and isotropic radiation. The GRBs listed in boldface have prominent blackbodies, with radii of the order of $\sim 10^{11}$–10^{12} cm. Uncertainties are given at the 1σ confidence level.

We have used the fact that due to relativistic beaming, we observe only a portion of the surface of the emitter defined by

$$\beta \leqslant \cos\vartheta \leqslant 1, \quad (15)$$

and we used the definition of Γ given in Section 3. Therefore, inverting Equation (13), the comoving blackbody temperature $T_{\rm com}$ can be computed from the observed blackbody temperature $T_{\rm obs}$, the source cosmological redshift z. and the emitter Lorentz Gamma factor as follows:

$$T_{\rm com}(T_{\rm obs}, z, \Gamma) = \frac{1+z}{\Theta(\beta)\Gamma}T_{\rm obs}. \quad (16)$$

We can now insert Equation (16) into Equation (10) to obtain

$$F_{\rm bb,obs} = \frac{{R_{\rm com}}^2}{D_L(z)^2}\sigma T_{\rm com}^4 = \frac{{R_{\rm com}}^2}{D_L(z)^2}\sigma\left[\frac{1+z}{\Theta(\beta)\Gamma}T_{\rm obs}\right]^4. \quad (17)$$

Since the radius $R_{\rm lab}$ of the emitter in the laboratory frame is related to $R_{\rm com}$ by

$$R_{\rm com} = \Gamma R_{\rm lab}, \quad (18)$$

we can insert Equation (18) into Equation (17) and obtain

$$F_{\rm bb,obs} = \frac{(1+z)^4}{\Gamma^2}\left(\frac{R_{\rm lab}}{D_L(z)}\right)^2\sigma\left[\frac{T_{\rm obs}}{\Theta(\beta)}\right]^4. \quad (19)$$

Solving Equation (19) for $R_{\rm lab}$, we finally obtain the thermal emitter's effective radius in the laboratory frame:

$$R_{\rm lab} = \Theta(\beta)^2\Gamma\frac{D_L(z)}{(1+z)^2}\sqrt{\frac{F_{\rm bb,obs}}{\sigma T_{\rm obs}^4}} = \Theta(\beta)^2\Gamma\phi_0, \quad (20)$$

where we have defined ϕ_0,

$$\phi_0 \equiv \frac{D_L(z)}{(1+z)^2}\sqrt{\frac{F_{\rm bb,obs}}{\sigma T_{\rm obs}^4}}. \quad (21)$$

In astronomy, the quantity ϕ_0 is usually identified with the radius of the emitter. However, in relativistic astrophysics, this identity cannot be straightforwardly applied, because the estimate of the effective emitter radius $R_{\rm lab}$ in Equation (20) crucially depends on the knowledge of its expansion velocity β (and, correspondingly, of Γ).

It must be noted that Equation (20) above gives the correct value of $R_{\rm lab}$ for all values of $0 \leqslant \beta \leqslant 1$ by taking all of the relativistic transformations properly into account. In the non-relativistic limit ($\beta \to 0$, $\Gamma \to 1$), we have, respectively:

$$\Theta \underset{\beta\to 0}{\longrightarrow} 1, \qquad \Theta^2 \underset{\beta\to 0}{\longrightarrow} 1, \quad (22)$$

$$T_{\rm com} \underset{\beta\to 0}{\longrightarrow} T_{\rm obs}(1+z), \qquad R_{\rm lab} \underset{\beta\to 0}{\longrightarrow} \phi_0, \quad (23)$$

as expected.

9. Implications on the Dynamics of the Flares from Their Thermal Emission

An estimate of the expansion velocity β can be deduced from the ratio between the variation of the emitter effective radius $\Delta R_{\rm lab}$ and the emission duration in laboratory frame Δt, i.e.,

$$\beta = \frac{\Delta R_{\rm lab}}{c\Delta t} = \Theta(\beta)^2\Gamma(1-\beta\cos\vartheta)(1+z)\frac{\Delta\phi_0}{c\Delta t_a^d}, \quad (24)$$

where we have used Equation (20) and the relation between Δt and Δt_a^d given in Equation (7). We then have

$$\beta = \Theta(\beta)^2\frac{1-\beta\cos\vartheta}{\sqrt{1-\beta^2}}(1+z)\frac{\Delta\phi_0}{c\Delta t_a^d}, \quad (25)$$

where we used the definition of Γ given in Section 3.

For example, in GRB 081008, we observe a temperature of $T_{\rm obs} = (0.44 \pm 0.12)$ keV between $t_a^d = 280$ s and $t_a^d = 300$ s (i.e., 20 s before the flare peak time), and a temperature of $T_{\rm obs} = (0.31 \pm 0.05)$ keV between $t_a^d = 300$ s and $t_a^d = 320$ s (i.e., 20 s after the flare peak time, see the corresponding spectra in Figure 32). In these two time intervals, we can infer ϕ_0, and by solving Equation (25) and taking the errors of the parameters properly into account, get the value of $\langle\beta\rangle$ corresponding to the average expansion speed of the emitter from the beginning of its expansion up to the upper bound of the time interval considered. The results so obtained are listed in Table 8. Moreover, we can also compute the value of $\langle\beta\rangle$ between the two time intervals considered above. For $\cos\vartheta = 1$, namely along the line of sight, we obtain $\langle\beta\rangle = 0.90^{+0.06}_{-0.31}$ and $\langle\Gamma\rangle = 2.34^{+1.29}_{-1.10}$. In conclusion, no matter what the details of the approximation adopted, the Lorentz Gamma factor is always moderate, i.e., $\Gamma \lesssim 4$.

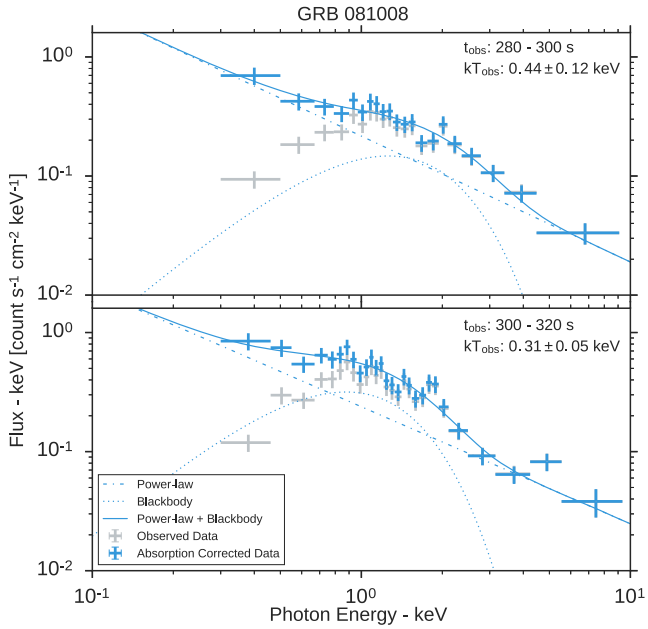

Figure 32. Thermal evolution of GRB 081008 ($z = 1.967$) in the observer frame. The X-ray flare of this GRB peaks at 304(±17) s. Upper panel: *Swift*-XRT spectrum from 280 s to 300 s. Lower panel: *Swift-XRT* spectrum from 300 to 320 s. The gray points are the observed data markedly absorbed at low energies, while the blue points are absorption-corrected ones. The data are fit with a combination of power-law (dotted–dashed lines) and blackbody (dotted lines) spectra. The power-law + blackbody spectra are shown as solid curves. Clearly, the temperature decreases with time from ∼0.44 keV to ∼0.31 keV, but the ratio of the thermal component goes up from ∼20% to ∼30%. This is a remarkably high percentage of our sample.

Table 8
List of the Physical Quantities Inferred from the Thermal Components Observed During the Flare of GRB 081008

Time Interval	$280\ {\rm s} \leqslant t_a^d \leqslant 300\ {\rm s}$	$300\ {\rm s} \leqslant t_a^d \leqslant 320\ {\rm s}$
$T_{\rm obs}$ (keV)	0.44 ± 0.12	0.31 ± 0.05
ϕ_0 (cm)	$(5.6 \pm 3.2) \times 10^{11}$	$(1.44 \pm 0.48) \times 10^{12}$
$\langle\beta\rangle_{(\cos\vartheta=1)}$	$0.19^{+0.10}_{-0.11}$	$0.42^{+0.10}_{-0.12}$
$\langle\Gamma\rangle$	$1.02^{+0.03}_{-0.02}$	$1.10^{+0.07}_{-0.05}$
$R_{\rm lab}$ (cm)	$(7.1 \pm 4.1) \times 10^{11}$	$(2.34 \pm 0.78) \times 10^{12}$

Note. For each time interval, we summarize the observed temperature $T_{\rm obs}$, ϕ_0, the average expansion speed $\langle\beta\rangle$ computed from the beginning up to the upper bound of the considered time interval, and the corresponding average Lorentz factor $\langle\Gamma\rangle$ and laboratory radius $R_{\rm lab}$.

10. The Electron–Positron Plasma as the Common Origin of the Prompt Emission and the X-Ray Flares

10.1. Necessity for a New Hydrodynamic Code for $10 \leqslant B \leqslant 10^2$

As stated above, there are many different components of BdHNe: following episode 1 of the hypercritical accretion of the SN ejecta onto the NS, the prompt emission occurs with $\Gamma \approx 10^2$–10^3, which represents the most energetic component accelerated by the e^+e^- plasma; a third component, which encompasses the X-ray flare with $\Gamma \lesssim 4$ and represents only a fraction of $E_{e^+e^-}$ ranging from 2% to 20% (see Figure 31); finally, there are in addition the gamma-ray flare and the late X-ray flares, which will be addressed in a forthcoming publication, as well as the late afterglow phases, which have been already addressed in Pisani et al. (2013, 2016) but whose dynamics will be discussed elsewhere. As already mentioned, for definiteness, we address here the case of X-ray flares.

In Section 3.5, we showed that our model successfully explains the entire prompt emission as originating from the transparency of an initially optically thick e^+e^- plasma with a baryon load $B < 10^{-2}$ reaching $\Gamma \approx 10^2$–10^3 and the accelerated baryons interacting with the clouds of the CBM. The fundamental equations describing the dynamics of the optically thick plasma, its self-acceleration to ultrarelativistic velocities, and its interaction with the baryon load have been described in Ruffini et al. (1999, 2000). A semi-analytic approximate numerical code was developed, which assumed that the plasma expanded as a shell with a constant thickness in the laboratory frame (the so-called "slab" approximation; see Ruffini et al. 1999). This semi-analytic approximate code was validated by comparing its results with the ones obtained by numerically integrating the complete system of equations for selected values of the initial conditions. It turns out that the semi-analytic code is an excellent approximation to the complete system of equations for $B < 10^{-2}$, which is the relevant regime for the prompt emission, but this approximation is not valid beyond this limit (see Ruffini et al. 1999, 2000 for details).

We examine here the possibility that the energy of the X-ray flare component also originates from a fraction of the e^+e^- plasma energy (see Figure 31) interacting with the much denser medium of the SN ejecta with $10 \lesssim B \lesssim 10^2$. The above-mentioned semi-analytic approximate code cannot be used for this purpose, since it is valid only for $B < 10^{-2}$, and therefore, thanks to the more powerful computers we have at present, we move on here to a new numerical code to integrate the complete system of equations.

We investigate if indeed the dynamics to be expected from an initially pure e^+e^- plasma with a negligible baryon load relativistically expanding in the fireshell model, with an initial Lorentz factor $\Gamma \sim 100$, and then impacting such an SN ejecta can lead, reaching transparency, to the Lorentz factor $\Gamma \lesssim 4$ inferred from the thermal emission observed in the flares (see Tables 7 and 8, and Figure 32).

We have performed hydrodynamical simulations of such a process using the one-dimensional relativistic hydrodynamical (RHD) module included in the freely available PLUTO[17] code (Mignone et al. 2011). In the spherically symmetric case considered here, only the radial coordinate is used and the code integrates partial differential equations with two variables: radius and time. This permits the study of the evolution of the plasma along one selected radial direction at a time. The code integrates the equations of an ideal relativistic fluid in the absence of gravity, which can be written as follows:

$$\frac{\partial(\rho\Gamma)}{\partial t} + \nabla.(\rho\Gamma\boldsymbol{v}) = 0, \tag{26}$$

$$\frac{\partial m_r}{\partial t} + \nabla.(m_r\boldsymbol{v}) + \frac{\partial p}{\partial r} = 0, \tag{27}$$

$$\frac{\partial \mathcal{E}}{\partial t} + \nabla.(\boldsymbol{m} - \rho\Gamma\boldsymbol{v}) = 0, \tag{28}$$

where ρ and p are, respectively, the comoving fluid density and pressure, $\boldsymbol{v}$ is the coordinate velocity in natural units ($c = 1$), $\Gamma = (1 - \boldsymbol{v}^2)^{-\frac{1}{2}}$ is the Lorentz Gamma factor, $\boldsymbol{m} = h\Gamma^2\boldsymbol{v}$ is the fluid momentum, m_r its radial component, $\mathcal{E}$ is the internal energy density, and h is the comoving enthalpy density, which is defined by $h = \rho + \epsilon + p$. In this last definition, ϵ is equal to $\mathcal{E}$ measured in the comoving frame. We define $\mathcal{E}$ as follows:

$$\mathcal{E} = h\Gamma^2 - p - \rho\Gamma. \tag{29}$$

The first two terms on the right-hand side of this equation coincide with the T^{00} component of the fluid energy–momentum tensor $T^{\mu\nu}$, and the last one is the mass density in the laboratory frame.

Under the conditions discussed in Appendix B, the plasma satisfies the equation of state of an ideal relativistic gas, which can be expressed in terms of its enthalpy as

$$h = \rho + \frac{\gamma p}{\gamma - 1}, \tag{30}$$

with $\gamma = 4/3$. Fixing this equation of state completely defines the system, leaving the choice of the boundary conditions as the only remaining freedom. To compute the evolution of these quantities in the chosen setup, the code uses the Harten–Lax–van Leer-contact Riemann solver. Time integration is performed by means of a second-order Runge–Kutta algorithm, and a second-order total variation diminishing scheme is used for spatial reconstruction (Mignone et al. 2011). Before each integration step, the grid is updated according to an adaptive mesh refinement algorithm, provided by the CHOMBO library (Colella et al. 2003).

It must be emphasized that the above equations are equivalent (although written in a different form) to the complete system of equations used in Ruffini et al. (1999, 2000). To validate this new numerical code, we compare its results with the ones obtained with the old semi-analytic "slab" approximate code in the domain of its validity (i.e., for $B < 10^{-2}$), finding excellent agreement. As an example, in Figure 33 we show the comparison between the Lorentz Gamma factors computed with the two codes for one particular value of $E_{e^+e^-}$ and B.

We can then conclude that for $B < 10^{-2}$, the new RHD code is consistent with the old semi-analytic "slab" approximate one, which in turn is consistent with the treatment done in Ruffini et al. (1999, 2000). This is not surprising, since we already stated that the above system of equations is equivalent to the one considered in Ruffini et al. (1999, 2000).

Having validated the new RHD code in the region of parameter space where the old semi-analytic one can also be

[17] http://plutocode.ph.unito.it/

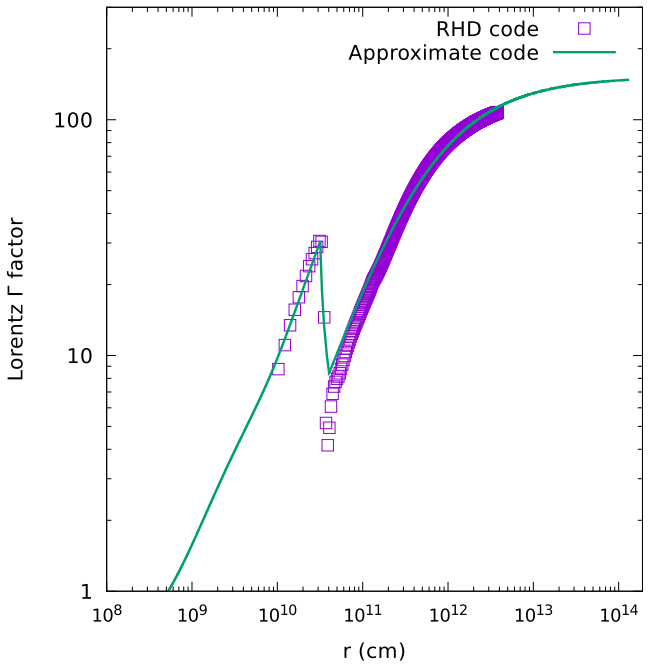

Figure 33. Lorentz Gamma factor computed with the new RHD code compared with the one computed with the old semi-analytic approximate code. This plot is for $E_{e^+e^-} = 1.0 \times 10^{53}$ erg and $B = 6.61 \times 10^{-3}$. Similar agreement is found for other values of $E_{e^+e^-}$ and B as long as $B < 10^{-2}$.

used, we now explore the region of $B > 10^{-2}$, which is relevant for the interaction of the plasma with the SN ejecta.

10.2. Inference from the IGC Scenario for the Ejecta Mass Profile

We start with the shape of the SN ejecta, following the results of the numerical simulations in Becerra et al. (2016).

The first simulations of the IGC process were presented in Fryer et al. (2014) including (1) detailed SN explosions of the CO_{core} obtained from a 1D core-collapse SN code code of Los Alamos (Fryer et al. 1999a); (2) the hydrodynamic details of the hypercritical accretion process; and (3) the evolution of the SN ejecta material entering the Bondi–Hoyle region all the way up to its incorporation into the NS in a spherically symmetric approximation. Then, in Becerra et al. (2015), estimates of the angular momentum carried by the SN ejecta and transferred to the NS via accretion were presented. The effects of such angular momentum transfer on the evolution and fate of the system were examined there. These calculations followed the following procedure: first, the accretion rate onto the NS is computed by adopting a homologous expansion of the SN ejecta and introducing the pre-SN density profile of the CO_{core} envelope from numerical simulations. Then, the angular momentum that the SN material might transfer to the NS is estimated: it turns out that the ejecta have enough angular momentum to circularize for a short time and form a disk-like structure around the NS. Then, the evolution of the NS central density and rotation angular velocity is followed by computing the equilibrium configurations from the numerical solution of the axisymmetric Einstein equations in full rotation, until the critical point of collapse of the NS to a BH is reached, accounting for the stability limits given by mass shedding and the secular axisymmetric instability. In Becerra et al. (2016), an improved simulation of all of the above processes leading to a BdHN was recently presented. In particular:

1. The accretion rate estimate includes the effects of the finite size/thickness of the ejecta density profile.
2. Different CO_{core} progenitors leading to different SN ejecta masses were also considered.
3. The maximum orbital period, P_{max}, up to which the accretion onto the NS companion is high enough to bring it to the critical mass for gravitational collapse to a BH, first estimated in Becerra et al. (2015), was computed for allpossible initial values of the mass of the NS companion. Various values of the angular momentum transfer efficiency parameter were also explored there.
4. It was shown there how the presence of the NS companion gives rise to large asymmetries in the SN ejecta. As we show here, such a density of the SN ejecta modified by the presence of the NS companion plays a crucial role in the physical explanation for the occurrence of X-ray flares.
5. The evolution of the SN material and its consequent accretion onto the NS companion is followed via a smoothed-particle-hydrodynamic-like code in which point-like particles describe the SN ejecta. The trajectory of each particle is computed by solving the Newtonian equations of motion including the effects of the gravitational field of the NS on the SN ejecta, including the orbital motion as well as the changes in the NS gravitational mass owing to the accretion process via the Bondi–Hoyle formalism. The initial conditions of the SN are obtained from the Los Alamos core-collapse SN code (Fryer et al. 1999a). The initial power-law density profile of the CO envelope is simulated by populating the inner layers with more particles. The particles crossing the Bondi–Hoyle radius are captured and accreted by the NS so we remove them from the system. We adopted a total number of 16 million particles in this simulation.

For further details, we refer the reader to Becerra et al. (2016) and references therein.

10.3. The Density Profile of the Ejecta and the Reaching of Transparency

We now use the results of a simulation with the following binary parameters: the NS has an initial mass of 2.0 $M_\odot$; the CO_{core} obtained from a progenitor with a zero-age main-sequence mass $M_{ZAMS} = 30\ M_\odot$ leads to a total ejecta mass of 7.94 $M_\odot$ and follows an approximate power-law profile $\rho^0_{ej} \approx 3.1 \times 10^8 (8.3 \times 10^7/r)^{2.8}$ g cm^{-3}. The orbital period is $P \approx 5$ minutes, i.e., a binary separation $a \approx 1.5 \times 10^{10}$ cm. For these parameters, the NS reaches the critical mass and collapses to form a BH.

Figure 34 shows the SN ejecta mass that is enclosed within a cone of 5° of the semi-aperture angle, whose vertex is at the position of the BH at the moment of its formation (see the lower-left panel of Figure 6 in Becerra et al. 2016), and whose axis is along various directions measured counterclockwise with respect to the line of sight. Figure 35 shows instead the cumulative radial mass profiles within a selected number of the aforementioned cones. We can see from these plots how the e^+e^- plasma engulfs different amounts of baryonic mass

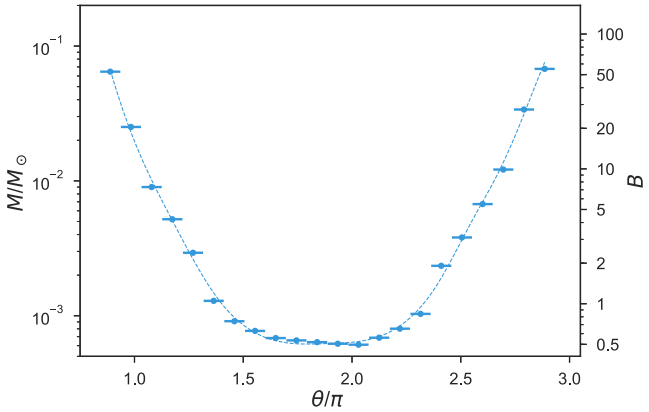

Figure 34. SN ejecta mass enclosed within a cone of 5° of semi-aperture angle, whose vertex is at the position of the BH at the moment of its formation (see the lower-left panel of Figure 6 in Becerra et al. 2016), and whose axis is along various directions measured counterclockwise with respect to the line of sight. The binary parameters of this simulations are the following: the NS has an initial mass of 2.0 $M_\odot$; the CO_{core} obtained from a progenitor with a zero-age -main-sequence mass $M_{ZAMS} = 30\,M_\odot$ leads to a total ejecta mass 7.94 $M_\odot$, and the orbital period is $P \approx 5$ minutes, i.e., a binary separation $a \approx 1.5 \times 10^{10}$ cm. The vertical axis on the right side gives, as an example, the corresponding value of the baryon loading B assuming a plasma energy of $E_{e^+e^-} = 3.16 \times 10^{53}$ erg.

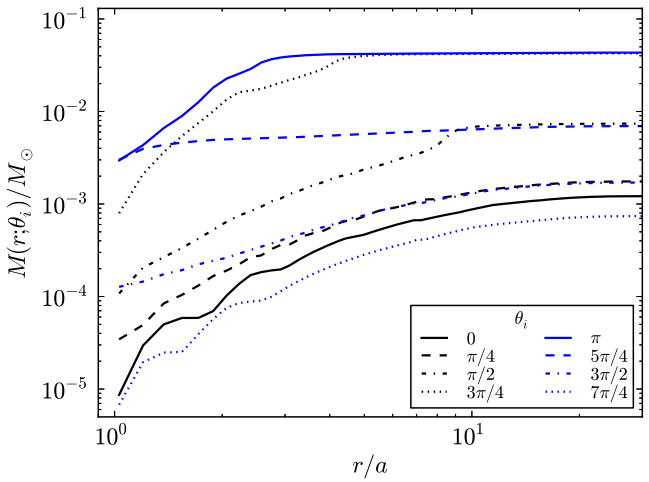

Figure 35. Cumulative radial mass profiles within selected cones among the ones used in Figure 34. We note that the final value for the cumulative mass reached at the end of each direction, namely the value when each curve flattens, is consistent with the total integrated mass value of the corresponding direction shown in Figure 34. The binary parameters of these simulations are the following: the NS has an initial mass of 2.0 $M_\odot$; the CO_{core} obtained from a progenitor with a zero-age main-sequence mass $M_{ZAMS} = 30\,M_\odot$ leads to a total ejecta mass 7.94 $M_\odot$, and the orbital period is $P \approx 5$ minutes, i.e., a binary separation $a \approx 1.5 \times 10^{10}$ cm.

along different directions due to the asymmetry of the SN ejecta created by the presence of the NS binary companion and the accretion process onto it (see Becerra et al. 2016).

In these calculations, we have chosen initial conditions consistent with those of the BdHNe. At the initial time, the e^+e^- plasma has $E_{e^+e^-} = 3.16 \times 10^{53}$ erg, a negligible baryon load, and is distributed homogeneously within a region of radii on the order of 10^8–10^9 cm. The surrounding SN ejecta, whose pressure has been assumed to be negligible, has a mass density

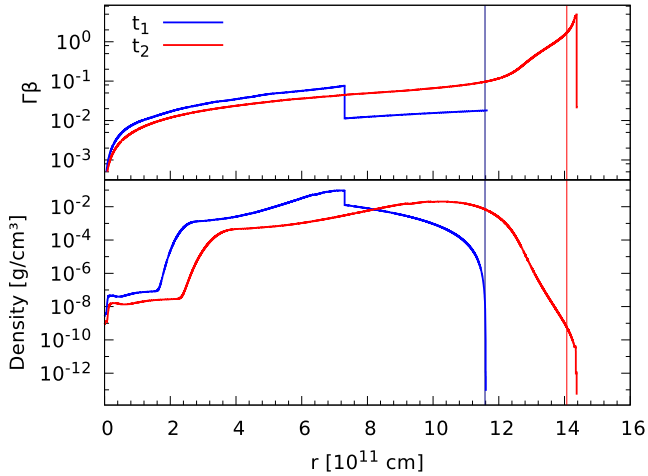

Figure 36. Top panel: distribution of the velocity inside the SN ejecta at the two fixed values of the laboratory times t_1 (before the plasma reaches the external surface of the ejecta) and t_2 (the moment at which the plasma, after having crossed the entire SN ejecta, reaches the external surface). We plotted the quantity $\Gamma\beta$, recalling that we have $\Gamma\beta \sim \beta$ when $\beta < 1$, and $\Gamma\beta \sim \Gamma$ when $\beta \sim 1$. Bottom panel: corresponding distribution of the mass density of the SN ejecta in the laboratory frame ρ_{lab}. These particular profiles are made using a baryon load $B = 200$. The dashed vertical lines corresponds to the two values of the transparency radius R_{ph}; see Figure 37 and Equation (32). In particular, we see that at t_1, the shock front has not yet reached R_{ph} and the system is optically thick.

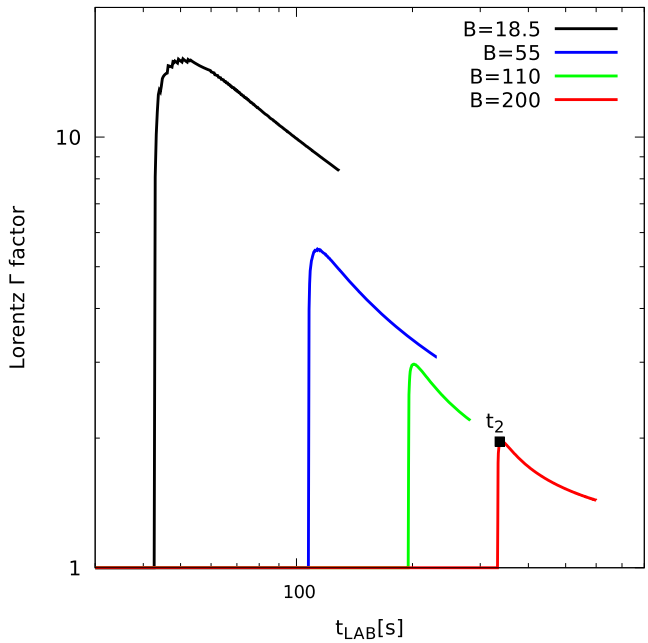

Figure 37. Lorentz Γ factor at the transparency radius R_{ph} as a function of the laboratory time for $E_{e^+e^-} = 3.16 \times 10^{53}$ erg and various selected values of the B parameter. Such B values correspond to the expansion of the e^+e^- plasma along various selected directions inside the remnant (see Figures 34 and 35). Along the red curve, corresponding to $B = 200$, the laboratory time instant t_2 represented in Figure 36 (at t_1 the plasma has not yet reached R_{ph}) is marked. We see that these results are in agreement with the Lorentz Gamma factor $\Gamma \lesssim 4$ inferred from the thermal emission observed in the flare (see Section 9).

radial profile given by

$$\rho \propto (R_0 - r)^\alpha, \tag{31}$$

where the parameters R_0 and α, with $2 < \alpha < 3$, as well as the normalization constant, are chosen to fit the profiles obtained in

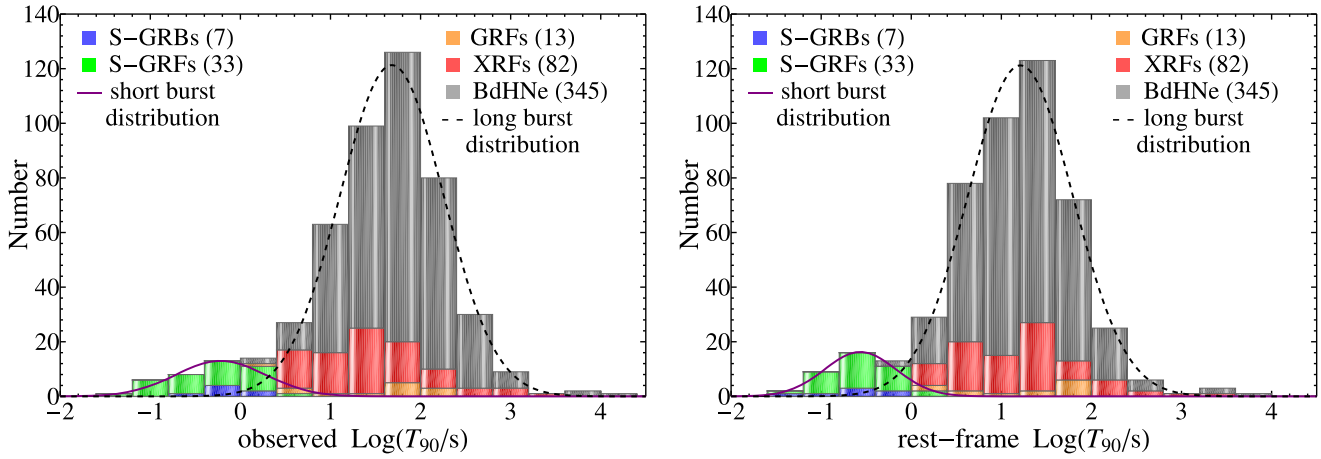

Figure 38. Histograms of T_{90} distributions in the (left panel) observer frame (which is the traditional treatment widely adopted in many previous articles; left panel; see, e.g., Kouveliotou et al. 1993; Bromberg et al. 2013, and references therein) and (right panel) in the cosmological rest frame (which is the approach adopted in the present paper). Both histograms are built using the total number of GRBs with known redshift. The contribution to the total distributions and the number of sources of each subclass are highlighted in the legend (the choice of colors is the same as in Figure 4). The short burst (solid purple curve) and the long burst (dashed black curve) distributions are also shown. In the observer frame, we obtain $T_{90}^{\rm short} = 0.60^{+1.31}_{-0.41}$ s and $T_{90}^{\rm long} = 48^{+133}_{-35}$ s; in the cosmological rest frame, we have $T_{90}^{\rm short} = 0.27^{+0.41}_{-0.16}$ s and $T_{90}^{\rm long} = 16^{+46}_{-12}$ s. The T_{90} value discriminating between short and long bursts shifts from ≈2 s in the observer frame to ≈0.75 s in the cosmological rest frame. The existence of BdHNe with $T_{90} \gtrsim 10^2$ s indicates the origin of the possible contamination between the prompt emission spikes and the X-ray flares, which is indeed observed in some cases (see Section 4 for details).

Becerra et al. (2016) and represented in Figure 35. The initial radial velocity is taken to be $v_r \propto r$ in order to reproduce the homologous expansion of the SN ejecta before its interaction with the plasma. Every choice of these parameters corresponds to studying the evolution along a single given direction.

The evolution from these initial conditions leads to the formation of a shock and to its subsequent expansion until reaching the outermost part of the SN. In Figure 36, we show the radial distribution profiles of the velocity and mass density $\rho_{\rm lab}$ in the laboratory frame inside the SN ejecta as a function of r for $B = 200$ at two selected values of the laboratory time. The velocity distribution peaks at the shock front (with a Lorentz Gamma factor $\Gamma \lesssim 4$), and behind the front it forms a broad tail of accelerated material with $0.1 \lesssim \beta \lesssim 1$.

Figure 37 shows the Lorentz Γ factor at the transparency radius $R_{\rm ph}$, namely the radius at which the optical depth τ, calculated from the observer's line of sight, is equal to 1. If we assume a constant cross-section, τ becomes Lorentz invariant, and therefore we can compute it in laboratory coordinates in the following way:

$$\tau = \int_{R_{\rm ph}}^{\infty} dr\ \sigma_T\ n_{e^-}(r), \tag{32}$$

where $\sigma_T = 6.65 \times 10^{-25}$ cm^2 is the Thomson cross-section, and the electron density is related to the baryon mass density by means of the formula $n_{e^-} = \rho\ \Gamma/m_P$, where m_P is the proton mass, the mass of the electrons and positrons is considered to be negligible with respect to that of the baryons, and we have assumed one electron per nucleon on average. The values of Γ at $r = R_{\rm ph}$ computed in this way are shown in Figure 37, as a function of the time measured in the laboratory frame, for several values of $B > 10^{-2}$ corresponding to the expansion of the e^+e^- plasma along several different directions inside the SN ejecta (see Figures 34 and 35).

We conclude that the relativistic expansion of an initially pure e^+e^- plasma (see Figure 33), interacting with an SN ejecta with the above-described induced asymmetries (see Figures 39–40), leads to the formation of a shock that reaches the outermost part of the ejecta with Lorentz Gamma factors at the transparency radius $\Gamma(R_{\rm ph}) \lesssim 4$. This is in striking agreement with the one inferred from the thermal component observed in the flares (see Section 9). The spacetime diagram of the global scenario is represented in Figure 39. Clearly in this approach neither ultrarelativistic jetted emission nor synchrotron or inverse-Compton processes play any role.

11. Summary, Conclusions and Perspectives

11.1. Summary

In the last 25 years, the number of observed GRBs has exponentially increased, thanks to unprecedented technological developments in all ranges of wavelengths, going from the X-ray to the gamma-ray, to GeV radiation as well as to the radio and the optical. In spite of this progress, the traditional GRB approach has continued to follow the paradigm of a single system (the "collapsar" paradigm; see Woosley 1993), where accretion onto an already formed BH occurs (see, e.g., Piran 2004 and references therein). Following the fireball model, synchrotron and inverse-Compton emission processes, related to an ultrarelativistic jetted emission described by the Blandford & McKee (1976) solution, have been assumed to occur (see, e.g., Troja et al. 2015 for one of the latest example where this approach is further extended to the GeV emission component). The quest for a "standard" GRB model has been pursued even recently (see, e.g., Chincarini et al. 2007; Margutti et al. 2010), ignoring differences among GRB subclasses and/or neglecting all relativistic corrections in the time parameterizations presented in Section 3. Under these conditions, it is not surprising that the correlations we have found here have been missed.

It is appropriate to recall that a "standard" GRB energy of 10^{51} erg (Frail et al. 2001) was considered, assuming the collimation of GRBs and the existence of a light-curve break in

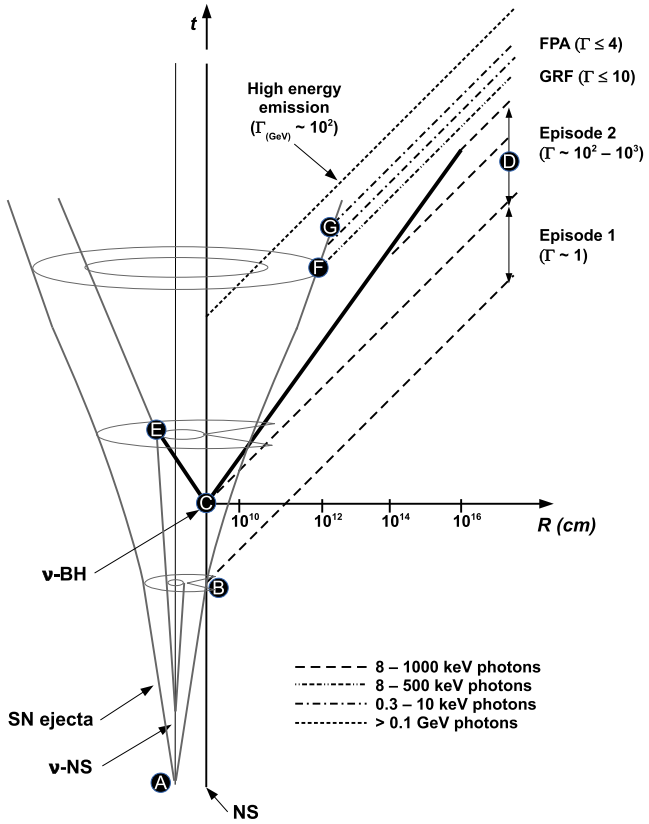

Figure 39. Spacetime diagram (not to scale) of a BdHN. The CO_{core} explodes as an SN at point A and forms a new NS (νNS). The companion NS (bottom-right line) accretes the SN ejecta starting from point B, giving rise to the non-relativistic episode 1 emission (with Lorentz factor $\Gamma \approx 1$). At point C, the NS companion collapses into a BH, and an e^+e^- plasma—the dyadosphere—is formed (Ruffini et al. 1999). The following self-acceleration process occurs in a spherically symmetric manner (thick black lines). A large portion of plasma propagates in the direction of the line of sight, where the environment is cleared by the previous accretion into the NS companion, finding a baryon load $B \lesssim 10^{-2}$ and leading to the GRB prompt gamma-ray spikes (GRSs; episode 2, point D) with $\Gamma \sim 10^2$–10^3. The remaining part of the plasma impacts the high-density portion of the SN ejecta (point E), propagates inside the ejecta encountering a baryon load $B \sim 10^1$–10^2, and finally reaches transparency, leading to the gamma-ray flare emission (point F) in gamma-rays with an effective Lorentz factor $\Gamma \lesssim 10$ and to the FPA emission (point G) corresponding to the X-ray flares with an effective $\Gamma \lesssim 4$ (see Sections 9 and 10). In the meantime, accretion over the newly formed BH produces the high-energy GeV emission with $\Gamma \sim 10^2$. For simplicity, this diagram is 2D and static and does not attempt to show the 3D rotation of the ejecta.

the GRB afterglows. This possibility followed from the traditional approach expecting the ultrarelativistic component to extend all the way from the prompt emission to the last phases of the afterglow (Mao & Yi 1994; Panaitescu & Mészáros 1999; Sari et al. 1999). This "traditional" approach to GRBs has appeared in a large number of papers over recent decades and is well summarized in a series of review papers (see, e.g., Piran 1999, 2004; Mészáros 2002, 2006; Berger 2014; Kumar & Zhang 2015), whichare disproved by the data presented here in which the upper limit for the Lorentz factor $\Gamma \lesssim 4$ is established in the FPA phase.

Since 2001, we have followed an alternative approach, introducing three paradigms: the spacetime parametrization of GRBs (Ruffini et al. 2001a), the field equations of the prompt emission phase (Ruffini et al. 2002), and the IGC paradigm (Rueda & Ruffini 2012; Penacchioni et al. 2013; Ruffini et al. 2015c); see Section 3. Since then,

(a) we have demonstrated that all GRBs originate in binary systems: the short GRBs in binary NSs or in binaries composed of an NS and a BH (Fryer et al. 2015; Ruffini et al. 2016b); the long GRBs in binary systems composed of CO_{core} and a, NS, or alternatively a BH and a CO_{core}, or also a white dwarf and an NS;

(b) we have divided GRBs into seven different subclasses (Ruffini et al. 2016b), each characterized by specific signatures in their spectra and luminosities in the various energy bands;

(c) we have addressed the new physical and astrophysical processes in the ultrarelativistic regimes made possible by the vast amount of gravitational and rotational energies in such binaries.

As we recalled in Sections 1–3, we have confirmed the binary nature of the GRB progenitors (see, e.g., Fryer et al. 2014, 2015; Becerra et al. 2015, 2016; Ruffini et al. 2016a; Aimuratov et al. 2017). We have obtained the first evidence of the formation of a BH in the hypercritical accretion process of the SN ejecta onto the binary NS companion: the BdHN (Ruffini et al. 2014, 2015c, 2016b), which is clearly different from the single-star collapsar model. Finally, in this paper, we have addressed the interaction that occurs in a BdHN of the GRB on the SN ejecta considered as the origin of the X-ray flares. We use this process and the mildly relativistic region in which it occurs as a discriminant between the traditional approach and our binary system approach: we use the X-ray flare properties as a discriminant between our BdHN and the "fireball" GRB models.

11.2. Conclusions

We have reached three major results.

(1) We have searched X-ray flares in all GRBs and identified 16 of them with excellent data. After examining the seven GRB subclasses (Ruffini et al. 2016b), we conclude that they all occur in BdHNe, and no X-ray flares are observed in other GRB sources. This indicates a link between the occurrence of the flare and the formation of a black hole in long GRBs. In Section 4, we have shown how the previously proposed association of X-ray flares with the short GRBs 050724 and 050709 has been superseded.

By a statistical analysis, we correlate the time of occurrence of their peak luminosity in the cosmological rest frame, their duration, their energy, and their X-ray luminosity to the corresponding GRB E_{iso}. We also correlate the energy of the FPA phase, E_{FPA}, as well as the relative ratio E_{FPA}/E_{iso}, to E_{iso}.

(2) Using the data from the associated thermal emission, the relativistic relation between the comoving time, the arrival time at the detector, and the cosmological and Doppler corrections, we determine the thermal emitter effective radii as a function of the rest-frame time. We determine the expansion velocity of the emitter β as the ratio between the variation of the emitter effective radius ΔR_{lab} and the emission duration in laboratory time; see Equation (25). We obtain a radius of 10^{12} cm for the effective radius of the emitter, moving with $\Gamma \lesssim 4$ at a time $\sim$100 s in the rest frame (see Table 8). These results show the clear rupture between the processes in the prompt emission phase, occurring prior to the flares at radii of the order of 10^{16} cm and $\Gamma = 10^2$–10^3, and the ones in the X-ray flares.

(3) We have modeled the X-ray flares by considering the impact of the GRB on the SN ejecta, introducing a new set of

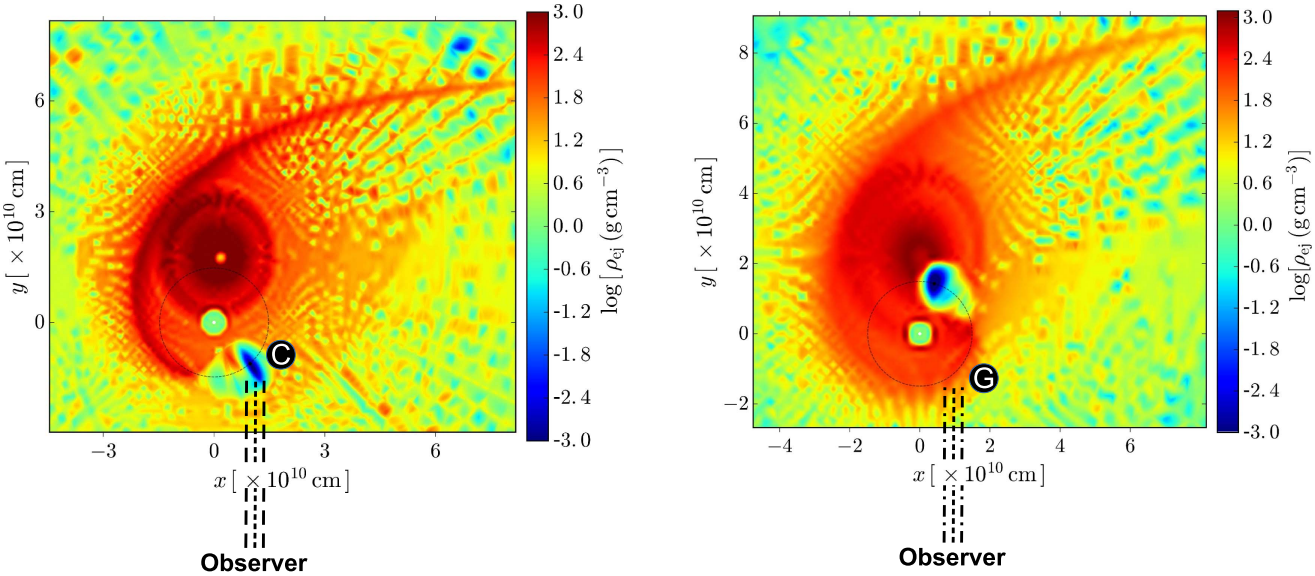

Figure 40. Two snapshots of the distribution of matter in the equatorial plane of the progenitor's binary system. The one on the right side corresponds to point C, when the BH is formed and a large portion of the e^+e^- plasma starts to self-accelerate in a low-density environment ($B \lesssim 10^{-2}$) toward the observer producing the GRB prompt emission. The one on the left side corresponds to point G, when the remaining part of the plasma, after propagating inside the high-density SN ejecta ($B \sim 10^2$–10^3), reaches transparency and produces the FPA emission in the X-rays, which is directed toward the observer due to the rotation of the ejecta in the equatorial plane. The simulations of the matter distributions in the three snapshots are from Becerra et al. (2016).

relativistic hydrodynamic equations for the expansion of the optically thick e^+e^- plasma into a medium with baryon load in the range 10–10^2. The matter density and velocity profiles of the ejecta are obtained from the 1D core-collapse code developed at Los Alamos (Fryer et al. 1999a). With this we generate the initial conditions for our smoothed-particle-hydrodynamics-like simulation (Becerra et al. 2016), which follows the evolution of the ejecta matter and the accretion rate at the position of the Bondi–Hoyle surface of the NS binary companion. In our simulations, we have adopted 16 million particles (see Section 10 for further details). We start the simulation of the interaction of the e^+e^- plasma with such ejecta at 10^{10} cm and continue all the way to 10^{12} cm, where transparency is reached. We found full agreement between the radius of the emitter at transparency and the one derived from the observations, as well as between the time of the peak energy emission and the observed time of arrival of the flare, derived following Equation (2) using the computed Lorentz Γ factor of the world line of the process.

We can now conclude the following.

The existence of such mildly relativistic Lorentz Gamma factors in the FPA phase rules out the traditional GRB model, including the claims of the existence of GRB beaming, collimation, and break in the luminosity (see, e.g., Piran 1999, 2004; Frail et al. 2001; Mészáros 2002, 2006; Berger 2014; Kumar & Zhang 2015). In these models, the common underlying assumption is the existence of a single ultrarelativistic component extending from the prompt radiation, through the FPA phase, all the way to the late afterglow and to the GeV emission, assuming a common dynamics solely described by the Blandford & McKee (1976) solution; see, however, Bianco & Ruffini (2005b, 2006). These assumptions were made without ever looking for observational support. It is not surprising that all GRB models in the current literature purport the existence of an ultrarelativistic Lorentz Gamma factor extending into the afterglow, among many others; see, e.g., Jin et al. (2010) and Yi et al. (2015). All these claims have been disproven by the present article, where a drastic break from ultrarelativistic physics with $\Gamma \sim 10^2$–10^3, occurring in the prompt emission, is already indicated at times $\sim$100 s, when the Lorentz Gamma factor is limited to $\Gamma \leqslant 4$.

In our approach, a multi-episode structure for each GRB is necessary. Each episode, being characterized by a different physical process, leads to a different world line with a specific Lorentz Gamma factor at each event. The knowledge of the world line is essential, following Equation (2) in Section 3, to compute the arrival time of the signals in the observer frame and to compare it with the observations. This procedure, previously routinely adopted in the prompt emission phase of a BdHN, has for the first time been introduced here for X-ray flares. As a byproduct, we have confirmed both the binarity and the nature of the progenitors of the BdHNe, composed of a CO_{core} undergoing an SN explosion and accreting onto a close-by binary NS, and the impact of the GRB on the hypernova ejecta.

11.3. Perspectives

Far from representing solely a criticism of the traditional approach, in this paper, (1) we exemplify new procedures in data analysis—see Sections 4 to 7, (2) we open up the topic to an alternative style of conceptual analysis which adopts procedures well-tested in high-energy physics and not yet appreciated in the astrophysical community—see Sections 8–10, and (3) we introduce new tools for simulation techniques affordable with present-day large computer facilities—see figures in Section 11, which, if properly guided by a correct theoretical understanding, can be particularly helpful in the visualization of these phenomena.

We give three specific examples of our new approach and indicate as well, when necessary, some disagreements with current approaches:

(A) The first step in any research on GRBs is to represent the histogram of T_{90} for the GRB subclasses. We report in

Figure 38 the T_{90} values for all of the GRB subclasses we have introduced (see Ruffini et al. 2016b). The values reported are both in the observer frame (left panel; see, e.g., Kouveliotou et al. 1993; Bromberg et al. 2013) and properly converted to the cosmological rest frame of the sources (right panel). The large majority of papers on GRBs have been neglecting the cosmological corrections and subdivision in the subclasses, making impossible the comparison of T_{90} among different GRBs (see, e.g., Falcone et al. 2007; Chincarini et al. 2010).

(B) For the first time, we present a simplified spacetime diagram of BdHNe (see Figure 39). This spacetime diagram emphasizes the many different emission episodes, each one with distinct corresponding Lorentz Gamma factors and consequently leading through Equation (2) to a specific value of their distinct times of occurrence in the cosmological rest frame of the GRB (see Figure 39). In all episodes we analyzed for the X-ray flares, and more generally for the entire FPA phase, there is no need for collapsar-related concepts. Nevertheless, in view of the richness of the new scenario in Figure 39, we have been examining the possibility that such concepts can play a role in additional episodes, either in BdHNe or in any of the additional six GRB subclasses, e.g., in S-GRBs. These results are being submitted for publication. The use of spacetime diagrams in the description of GRBs is indeed essential in order to illustrate the causal relation between the source in each episode, the place of occurrence, and the time at detection. Those procedures have been introduced long ago in the study of high-energy particle physics processes and codified in textbooks. Our group, since the basic papers (Ruffini et al. 2001a, 2001b, 2001c), has widely shared these spacetime formulations (see, e.g., in Taylor & Wheeler 1992) and also extended the concept of the quantum S-Matrix (Wheeler 1937; Heisenberg 1943) to the classic astrophysical regime of the many components of a BdHN, introducing the concept of the cosmic matrix (Ruffini et al. 2015c). The majority of astrophysicists today make wide use of the results of nuclear physics in the study of stellar evolution (Bethe 1991) and also of Fermi statistics in general relativity (Oppenheimer & Volkoff 1939). They have not yet been ready, however, to approach these additional concepts more typical of relativistic astrophysics and relativistic field theories, which are necessary for the study of GRBs and active galactic nuclei.

(C) The visual representation of our result (see Figure 40) has been made possible thanks to the simulations of SN explosions with the core-collapse SN code developed at Los Alamos (see, e.g., Fryer et al. 1999a, 2014; Frey et al. 2013), the smoothed-particle-hydrodynamics-like simulations of the evolution of the SN ejecta accounting for the presence of an NS companion (Ruffini et al. 2016b), and the possibility of varying the parameters of the NS, of the SN, and of the distance between the two to explore all possibilities (Becerra et al. 2015; Ruffini et al. 2016b). We recall that these signals occur in each galaxy every ~hundred million years, but with their luminosity of $\sim 10^{54}$ erg, they can be detected in all 10^9 galaxies. The product of these two factors gives the "once per day" rate. They are not visualizable in any other way, but analyzing the spectra and time of arrival of the photons now, and simulating these data on the computer, we see that they indeed already occurred billions of years ago in our past light cone, and they are revived by scientific procedures today.

We are happy to acknowledge fruitful discussions with Fulvio Melia, Tsvi Piran, and Bing Zhang in our attempt to make these new results clearer for a broader audience, and with Roy Kerr on the implication of the GRB GeV emission for the Kerr–Newman solution. We also thank the second referee for important suggestions. We acknowledge the continuous support of the MAECI. This work made use of data supplied by the UK *Swift* Science Data Center at the University of Leicester. M.Ka. and Y.A. are supported by the Erasmus Mundus Joint Doctorate Program Grant N. 2014–0707 from EACEA of the European Commission. M.M. and J.A.R. acknowledge the partial support of the project N 3101/GF4 IPC-11 and the target program F.0679 0073-6/PTsF of the Ministry of Education and Science of the Republic of Kazakhstan.

Appendix A
The Complete List of BdHNe

We present here in Table 9 the complete list of the 345 BdHNe observed through the end of 2016, which includes the 161 BdHNe already presented in Pisani et al. (2016).

Appendix B
Parameters of the Equation of State

We give here details concerning the determination of the value of the index γ and verify the accuracy of our assumption $\gamma = 4/3$ adopted in the equation of state of the plasma (30). This index is defined as

$$\gamma \equiv 1 + \frac{p}{\epsilon}. \tag{33}$$

The total internal energy density and pressure are computed as

$$\epsilon = \epsilon_{e^-} + \epsilon_{e^+} + \epsilon_\gamma + \epsilon_B \tag{34}$$

$$p = p_{e^-} + p_{e^+} + p_\gamma + p_B, \tag{35}$$

where the subscript B indicates the contributions of the baryons in the fluid. The number and energy densities, as well as the pressure of the different particles, can be computed in natural units ($c = \hbar = k_B = 1$) using the following expressions (see, e.g., Landau & Lifshitz 1980):

$$n_{e^-} = A\,T^3 \int_0^\infty f(z, T, m_e, \mu_{e^-}) z^2\, dz \tag{36}$$

$$n_{e^+} = A\,T^3 \int_0^\infty f(z, T, m_e, \mu_{e^+}) z^2\, dz \tag{37}$$

$$\epsilon_{e^-} = A\,T^4 \int_0^\infty f(z, T, m_e, \mu_{e^-}) \times \sqrt{z^2 + (m_e/T)^2}\, z^2\, dz - m_e\, n_{e^-} \tag{38}$$

$$\epsilon_{e^+} = A\,T^4 \int_0^\infty f(z, T, m_e, \mu_{e^+}) \times \sqrt{z^2 + (m_e/T)^2}\, z^2\, dz - m_e\, n_{e^+} \tag{39}$$

Table 9
List of the BdHNe Considered in This Work

GRB	z	$E_{\rm iso}$[a]	LX[b]	Early Flare[c]	UL[d]	T_{90}[e]	Instrument[f]	Reference[g]
970228	0.695	1.65 ± 0.16				80	B-SAX	(1)
970828	0.958	30.4 ± 3.6				90	BATSE	(2)
971214	3.42	22.1 ± 2.7				40	BATSE	IAUC 6789
980329	3.5	267 ± 53				54	B-SAX	(3)
980703	0.966	7.42 ± 0.74				400	BATSE	GCN 143
990123	1.6	241 ± 39				63.3	BATSE	GCN 224
990506	1.3	98.1 ± 9.9				131.33	BATSE	GCN 306
990510	1.619	18.1 ± 2.7				75	BATSE	GCN 322
990705	0.842	18.7 ± 2.7				42	B-SAX	(4)
991208	0.706	23.0 ± 2.3				68	Ulysses	(5)

Notes. It is composed of 345 sources spanning 12 years of *Swift*/XRT observation activity. In the table, we report important observational features: the redshift z, the isotropic energy $E_{\rm iso}$, the observing instrument in the gamma-ray band, and the corresponding reference from which we take the gamma-ray spectral parameters in order to estimate $E_{\rm iso}$.
[a] In units of 10^{52} erg.
[b] "LX" marks the sources with *Swift*/XRT data observed up to times larger than 10^4 s in the rest frame after the initial explosion.
[c] "C" and "E" mark the sources showing an early flare in *Swift*/XRT, and they stand for "confirmed" and "excluded," respectively. The 16 "C" sources compose the sample considered in the present paper.
[d] "UL" stands for ultralong, indicating sources with $T_{90} \gtrsim 1000$ s.
[e] Observed T_{90} (s).
[f] "B-SAX" stands for *BeppoSAX*/GRBM; "BATSE" stands for *Compton-GRO*/BATSE; "Ulysses" stands for *Ulysses*/GRB; "KW" stands for Konus/*WIND*; "HETE" stands for *HETE*-2/FREGATE; "*Swift*" standss for *Swift*/BAT; "*Fermi*" stands for *Fermi*/GBM.
[g] (1) Frontera et al. (1998), (2) Ruffini et al. (2015a), (3) in 't Zand et al. (1998), (4) Amati et al. (2000), (5) Hurley et al. (2000), (6) in't Zand et al. (2001), (7) Barraud et al. (2003), (8) Shirasaki et al. (2008), (9) Cenko et al. (2006).

(This table is available in its entirety in machine-readable form.)

$$p_{e^-} = A\,\frac{T^4}{3}\int_0^\infty f(z, T, m_e, \mu_{e^-})\frac{z^4}{\sqrt{z^2 + (m_e/T)^2}}\,dz \quad (40)$$

$$p_{e^+} = A\,\frac{T^4}{3}\int_0^\infty f(z, T, m_e, \mu_{e^+})\frac{z^4}{\sqrt{z^2 + (m_e/T)^2}}\,dz \quad (41)$$

$$\epsilon_\gamma = a\,T^4 \quad (42)$$

$$p_\gamma = \frac{a\,T^4}{3} \quad (43)$$

$$\epsilon_B = \frac{3}{2} n_N\,T \quad (44)$$

$$p_B = n_N\,T, \quad (45)$$

where

$$f(z, T, m, \mu) = \frac{1}{e^{\sqrt{z^2+(m/T)^2} - \mu/T} + 1} \quad (46)$$

is the Fermi–Dirac distribution, m_e is the electron mass, n_N the nuclei number density, $a = 8\pi^5 k_B^4/15h^3c^3 = 7.5657 \times 10^{-15}$ erg cm^{-3} K^{-4} the radiation constant, and $A = 15a/\pi^4$. If the pair annihilation rate is zero, i.e., if the reaction $e^- + e^+ \leftrightarrows 2\gamma$ is in equilibrium, then the equality $\mu_{e^-} = -\mu_{e^+} \equiv \mu$ holds, since the equilibrium photons have zero chemical potential. Besides, charge neutrality implies that the difference in the number of electrons and positrons is equal to the number of protons in the baryonic matter, which can be expressed as

$$n_{e^-}(\mu, T) - n_{e^+}(\mu, T) = Z\,n_B, \quad (47)$$

where n_B is the baryon number density and $1/2 < Z < 1$ is the average number of electrons per nucleon. The number density n_B is related to the other quantities as

$$\rho = m_p\,n_B + m_e(n_{e^-} + n_{e^+}), \quad (48)$$

where m_p is the proton mass. If the baryons are only protons, then $Z = 1$ and $n_N = n_B$. Together with Equation (47), this completely defines the mass density as a function of (μ, T). The equation of state that relates the pressure with the mass and internal energy densities is thus defined implicitly as the parametric surface

$$\{(\rho(\mu, T), \epsilon(\mu, T), p(\mu, T)):\ T > 0,\ \mu \geqslant 0\} \quad (49)$$

that satisfies all of the above relations.

In the cases relevant for the simulations performed in Section 10, we indeed have that the index γ in the equation of state of the plasma, Equation (30), satisfies $\gamma = 4/3$ with a maximum error of 0.2%.

ORCID iDs

R. Ruffini https://orcid.org/0000-0003-0829-8318
Y. Wang https://orcid.org/0000-0001-7959-3387
Y. Aimuratov https://orcid.org/0000-0001-5717-6523
U. Barres de Almeida https://orcid.org/0000-0001-7909-588X
C. L. Bianco https://orcid.org/0000-0001-7749-4078
Y. C. Chen https://orcid.org/0000-0002-7543-2727
M. Kovacevic https://orcid.org/0000-0003-4928-4510
R. Moradi https://orcid.org/0000-0002-2516-5894
M. Muccino https://orcid.org/0000-0002-2234-9225
A. V. Penacchioni https://orcid.org/0000-0001-7816-3668
G. B. Pisani https://orcid.org/0000-0003-3452-2491
J. A. Rueda https://orcid.org/0000-0003-4904-0014
G. V. Vereshchagin https://orcid.org/0000-0002-1623-3576

References

Aimuratov, Y., Ruffini, R., Muccino, M., et al. 2017, ApJ, 844, 83
Aksenov, A. G., Ruffini, R., & Vereshchagin, G. V. 2007, PhRvL, 99, 125003

Amati, L., & Della Valle, M. 2013, IJMPD, 22, 30028
Amati, L., Frontera, F., Vietri, M., et al. 2000, Sci, 290, 953
Atwood, W. B., Abdo, A. A., Ackermann, M., et al. 2009, ApJ, 697, 1071
Barraud, C., Olive, J.-F., Lestrade, J. P., et al. 2003, A&A, 400, 1021
Barthelmy, S. D., Baumgartner, W. H., Cummings, J. R., et al. 2013, GCN, 15456, 1
Barthelmy, S. D., Chincarini, G., Burrows, D. N., et al. 2005, Natur, 438, 994
Baumgartner, W. H., Barthelmy, S. D., Cummings, J. R., et al. 2014, GCN, 16127, 1
Becerra, L., Bianco, C. L., Fryer, C. L., Rueda, J. A., & Ruffini, R. 2016, ApJ, 833, 107
Becerra, L., Cipolletta, F., Fryer, C. L., Rueda, J. A., & Ruffini, R. 2015, ApJ, 812, 100
Berger, E. 2014, ARA&A, 52, 43
Bernardini, M. G., Bianco, C. L., Chardonnet, P., et al. 2005, ApJL, 634, L29
Bethe, H. A. 1991, The Road from LOS Alamos (Melville, NY: AIP)
Bianco, C. L., & Ruffini, R. 2004, ApJL, 605, L1
Bianco, C. L., & Ruffini, R. 2005a, ApJL, 620, L23
Bianco, C. L., & Ruffini, R. 2005b, ApJL, 633, L13
Bianco, C. L., & Ruffini, R. 2006, ApJL, 644, L105
Bianco, C. L., Ruffini, R., & Xue, S.-S. 2001, A&A, 368, 377
Blandford, R. D., & McKee, C. F. 1976, PhFl, 19, 1130
Bloom, J. S., Frail, D. A., & Sari, R. 2001, AJ, 121, 2879
Bromberg, O., Nakar, E., Piran, T., & Sari, R. 2013, ApJ, 764, 179
Butler, N., Ricker, G., Atteia, J.-L., et al. 2005, GCN, 3570, 1
Caito, L., Amati, L., Bernardini, M. G., et al. 2010, A&A, 521, A80
Caito, L., Bernardini, M. G., Bianco, C. L., et al. 2009, A&A, 498, 501
Calderone, G., Ghirlanda, G., Ghisellini, G., et al. 2015, MNRAS, 448, 403
Cavallo, G., & Rees, M. J. 1978, MNRAS, 183, 359
Cenko, S. B., Kasliwal, M., Harrison, F. A., et al. 2006, ApJ, 652, 490
Cherubini, C., Geralico, A., Rueda, H. J. A., & Ruffini, R. 2009, PhRvD, 79, 124002
Chester, M. M., Wang, X. Y., Cummings, J. R., et al. 2008, in AIP Conf. Ser. 1000, Gamma-Ray Bursts 2007, ed. M. Galassi, D. Palmer, & E. Fenimore (Melville, NY: AIP), 421
Chincarini, G., Mao, J., Margutti, R., et al. 2010, MNRAS, 406, 2113
Chincarini, G., Moretti, A., Romano, P., et al. 2007, ApJ, 671, 1903
Cleveland, W., & Devlin, S. 1988, J. Am. Stat. Assoc., 83, 596
Cline, T. L., Desai, U. D., Trainor, J., et al. 1979, ApJL, 229, L47
Cobb, B. E. 2007, GCN, 6296, 1
Colella, P., Graves, D. T., Johnson, J. N., et al. 2003, Chombo Software Package for AMR Applications Design Document, Tech. Rep. LBNL-6615E
Colgate, S. A. 1971, ApJ, 163, 221
Costa, E., Frontera, F., Heise, J., et al. 1997, Natur, 387, 783
Cummings, J. R., Barthelmy, S. D., Burrows, D. N., et al. 2007, GCN, 6210, 1
Dai, Z. G., Wang, X. Y., Wu, X. F., & Zhang, B. 2006, Sci, 311, 1127
Damour, T., & Ruffini, R. 1975, PhRvL, 35, 463
D'Avanzo, P., D'Elia, V., & Covino, S. 2008, GCN, 8350, 1
de Pasquale, M., Piro, L., Gendre, B., et al. 2006, A&A, 455, 813
de Ugarte Postigo, A., Fynbo, J. P. U., Thöne, C. C., et al. 2012, A&A, 548, A11
Della Valle, M. 2011, IJMPD, 20, 1745
Dezalay, J.-P., Barat, C., Talon, R., et al. 1992, in AIP Conf. Ser. 265, Gamma-Ray Bursts, ed. W. S. Paciesas & G. J. Fishman (Melville, NY: AIP), 304
Eichler, D., Livio, M., Piran, T., & Schramm, D. N. 1989, Natur, 340, 126
Evans, P. A., Beardmore, A. P., Page, K. L., et al. 2007, A&A, 469, 379
Evans, P. A., Beardmore, A. P., Page, K. L., et al. 2009, MNRAS, 397, 1177
Falcone, A., Barbier, L., Barthelmy, S., et al. 2006, GCN, 4655, 1
Falcone, A. D., Morris, D., Racusin, J., et al. 2007, ApJ, 671, 1921
Fan, Y. Z., Zhang, B., & Proga, D. 2005, ApJL, 635, L129
Fenimore, E. E., Palmer, D., Galassi, M., et al. 2003, in AIP Conf. Ser. 662, Gamma-Ray Burst and Afterglow Astronomy 2001: A Workshop Celebrating the First Year of the HETE Mission, ed. G. R. Ricker & R. K. Vanderspek (Melville, NY: AIP), 491
Fermi, E. 1934, NCim, 11, 1
Frail, D. A., Kulkarni, S. R., Nicastro, L., Feroci, M., & Taylor, G. B. 1997, Natur, 389, 261
Frail, D. A., Kulkarni, S. R., Sari, R., et al. 2001, ApJL, 562, L55
Frey, L. H., Fryer, C. L., & Young, P. A. 2013, ApJL, 773, L7
Frontera, F., Costa, E., Piro, L., et al. 1998, ApJL, 493, L67
Fruchter, A. S., Levan, A. J., Strolger, L., et al. 2006, Natur, 441, 463
Fryer, C., Benz, W., Herant, M., & Colgate, S. A. 1999a, ApJ, 516, 892
Fryer, C. L., Oliveira, F. G., Rueda, J. A., & Ruffini, R. 2015, PhRvL, 115, 231102
Fryer, C. L., Rueda, J. A., & Ruffini, R. 2014, ApJL, 793, L36
Fryer, C. L., Woosley, S. E., & Hartmann, D. H. 1999b, ApJ, 526, 152
Galama, T. J., Vreeswijk, P. M., van Paradijs, J., et al. 1998, Natur, 395 670
Gamow, G., & Schoenberg, M. 1940, PhRv, 58, 1117
Gamow, G., & Schoenberg, M. 1941, PhRv, 59, 539
Gehrels, N., Chipman, E., & Kniffen, D. A. 1993, A&AS, 97, 5
Gehrels, N., Ramirez-Ruiz, E., & Fox, D. B. 2009, ARA&A, 47, 567
Golenetskii, S., Aptekar, R., Frederiks, D., et al. 2013, GCN, 15413, 1
Golenetskii, S., Aptekar, R., Frederiks, D., et al. 2014, GCN, 16134, 1
Golenetskii, S., Aptekar, R., Frederiks, D., et al. 2015, GCN, 18516, 1
Golenetskii, S., Aptekar, R., Mazets, E., et al. 2008, GCN, 7862, 1
Goodman, J. 1986, ApJL, 308, L47
Gursky, H., & Ruffini, R. (ed.) 1975, in Proc. Annual Meeting, Astrophysics and Space Science Library, Vol. 48, Neutron Stars, Black Holes and Binary X-ray Sources (Dordrecht: Reidel), 454
Heisenberg, W. 1943, ZPhy, 120, 513
Hjorth, J., & Bloom, J. S. 2012, in Gamma-Ray Bursts, ed. C. Kouveliotou, R. A. M. J. Wijers, & S. Woosley (Cambridge: Cambridge Univ. Press), 169
Hurley, K., Cline, T., Mazets, E., et al. 2000, ApJL, 534, L23
in 't Zand, J. J. M., Amati, L., Antonelli, L. A., et al. 1998, ApJL, 505, L119
in't Zand, J. J. M., Kuiper, L., Amati, L., et al. 2001, ApJ, 559, 710
Itoh, N., Adachi, T., Nakagawa, M., Kohyama, Y., & Munakata, H. 1989, ApJ, 339, 354
Izzo, L., Ruffini, R., Penacchioni, A. V., et al. 2012, A&A, 543, A10
Jakobsson, P., Fynbo, J. P. U., Vreeswijk, P. M., & de Ugarte Postigo, A. 2008, GCN, 8077, 1
Jaunsen, A. O., Fynbo, J. P. U., Andersen, M. I., & Vreeswijk, P. 2007, GCN, 6216, 1
Jin, Z.-P., Fan, Y.-Z., & Wei, D.-M. 2010, ApJ, 724, 861
Klebesadel, R. W. 1992, in Gamma-Ray Bursts—Observations, Analyses and Theories, ed. C. Ho, R. I. Epstein, & E. E. Fenimore (Cambridge: Cambridge Univ. Press), 161
Klebesadel, R. W., Strong, I. B., & Olson, R. A. 1973, ApJL, 182, L85
Kouveliotou, C., Meegan, C. A., Fishman, G. J., et al. 1993, ApJL, 413, L101
Krimm, H. A., Beardmore, A. P., Brown, P. J., et al. 2008, GCN, 8648, 1
Kruehler, T., Tanvir, N. R., Malesani, D., Xu, D., & Fynbo, J. P. U. 2014, GCN, 15900, 1
Kumar, P., & Zhang, B. 2015, PhR, 561, 1
Landau, L. D., & Lifshitz, E. M. 1980, Statistical Physics. Pt.1 (3rd ed.; Portsmouth, NH: Butterworth-Heinemann)
Ledoux, C., Vreeswijk, P., Smette, A., Jaunsen, A., & Kaufer, A. 2006, GCN, 5237, 1
Lien, A. Y., Barthelmy, S. D., Chester, M. M., et al. 2014, GCN, 15784, 1
Lyman, J. D., Bersier, D., James, P. A., et al. 2016, MNRAS, 457, 328
MacFadyen, A., & Woosley, S. E. 1999, ApJ, 524, 262
Malesani, D., Xu, D., Fynbo, J. P. U., et al. 2014, GCN, 15800, 1
Mangano, V., Cummings, J. R., Cusumano, G., et al. 2008, GCN, 7847, 1
Mao, S., & Yi, I. 1994, ApJL, 424, L131
Margutti, R., Guidorzi, C., Chincarini, G., et al. 2010, MNRAS, 406, 2149
Marisaldi, M., Fuschino, F., Galli, M., et al. 2008, GCN, 7866, 1
Marshall, F. E., Cummings, J. R., Gronwall, C., et al. 2014, GCN, 16118, 1
Maselli, A., D'Ai, A., Lien, A. Y., et al. 2015, GCN, 18478, 1
Masumitsu, T., Negoro, H., Kawai, N., et al. 2015, GCN, 18525, 1
Mazets, E. P., Golenetskii, S. V., Ilinskii, V. N., et al. 1981, Ap&SS, 80, 3
McBreen, S. 2009, GCN, 9415, 1
Mészáros, P. 2002, ARA&A, 40, 137
Mészáros, P. 2006, RPPh, 69, 2259
Meszaros, P., Laguna, P., & Rees, M. J. 1993, ApJ, 415, 181
Mészáros, P., & Rees, M. J. 1997, ApJL, 482, L29
Metzger, M. R., Djorgovski, S. G., Kulkarni, S. R., et al. 1997, Natur, 387, 878
Mignone, A., Zanni, C., Tzeferacos, P., et al. 2011, ApJS, 198, 7
Morgan, A., Grupe, D., Gronwall, C., et al. 2005, GCN, 3577, 1
Munakata, H., Kohyama, Y., & Itoh, N. 1985, ApJ, 296, 197
Narayan, R., Paczynski, B., & Piran, T. 1992, ApJL, 395, L83
Narayan, R., Piran, T., & Shemi, A. 1991, ApJL, 379, L17
Negreiros, R., Ruffini, R., Bianco, C. L., & Rueda, J. A. 2012, A&A, 540, A12
Nousek, J. A., Kouveliotou, C., Grupe, D., et al. 2006, ApJ, 642, 389
Nysewander, M., Reichart, D. E., Crain, J. A., et al. 2009, ApJ, 693, 1417
Oppenheimer, J. R., & Volkoff, G. M. 1939, PhRv, 55, 374
Paczynski, B. 1986, ApJL, 308, L43
Paczyński, B. 1998, ApJL, 494, L45
Pagani, C., Baumgartner, W. H., Chester, M. M., et al. 2008, GCN, 8059, 1
Page, K. L., Barthelmy, S. D., Baumgartner, W. H., et al. 2014, GCNR, 460, 1
Page, K. L., Willingale, R., Bissaldi, E., et al. 2009, MNRAS, 400, 134
Panaitescu, A., & Mészáros, P. 1999, ApJ, 526, 707
Patricelli, B., Bernardini, M. G., Bianco, C. L., et al. 2012, ApJ, 756, 16

Penacchioni, A. V., Ruffini, R., Bianco, C. L., et al. 2013, A&A, 551, A133
Penacchioni, A. V., Ruffini, R., Izzo, L., et al. 2012, A&A, 538, A58
Perley, D. A., Cao, Y., & Cenko, S. B. 2014, GCN, 17228, 1
Perley, D. A., Hillenbrand, L., & Prochaska, J. X. 2015, GCN, 18487, 1
Perley, D. A., Krühler, T., Schulze, S., et al. 2016, ApJ, 817, 7
Piran, T. 1999, PhR, 314, 575
Piran, T. 2004, RvMP, 76, 1143
Piran, T., Shemi, A., & Narayan, R. 1993, MNRAS, 263, 861
Piro, L., De Pasquale, M., Soffitta, P., et al. 2005, ApJ, 623, 314
Pisani, G. B., Izzo, L., Ruffini, R., et al. 2013, A&A, 552, L5
Pisani, G. B., Ruffini, R., Aimuratov, Y., et al. 2016, ApJ, 833, 159
Racusin, J. L., Baumgartner, W. H., Brown, P. J., et al. 2008, GCN, 8344, 1
Rees, M. J., & Meszaros, P. 1992, MNRAS, 258, 41P
Rees, M. J., & Meszaros, P. 1994, ApJL, 430, L93
Romano, P., Campana, S., Chincarini, G., et al. 2006, A&A, 456, 917
Rossi, A., Afonso, P., & Greiner, J. 2009, GCN, 9382, 1
Rowlinson, B. A., Beardmore, A. P., Evans, P. A., et al. 2009, GCN, 9374, 1
Rueda, J. A., Aimuratov, Y., de Almeida, U. B., et al. 2017, IJMPD, 26, 1730016
Rueda, J. A., & Ruffini, R. 2012, ApJL, 758, L7
Ruffini, R. 1998, in Frontiers Science Series 23, Black Holes and High Energy Astrophysics, ed. H. Sato & N. Sugiyama (Tokyo: Universal Academic Press), 167
Ruffini, R. 2015, in Thirteenth Marcel Grossmann Meeting: On Recent Developments in Theoretical and Experimental General Relativity, Astrophysics and Relativistic Field Theories, ed. K. Rosquist (Singapore: World Scientific), 242
Ruffini, R., Bianco, C. L., Chardonnet, P., Fraschetti, F., & Xue, S.-S. 2002, ApJL, 581, L19
Ruffini, R., Bianco, C. L., Fraschetti, F., Xue, S.-S., & Chardonnet, P. 2001a, ApJL, 555, L107
Ruffini, R., Bianco, C. L., Fraschetti, F., Xue, S.-S., & Chardonnet, P. 2001b, ApJL, 555, L113
Ruffini, R., Bianco, C. L., Fraschetti, F., Xue, S.-S., & Chardonnet, P. 2001c, ApJL, 555, L117
Ruffini, R., Izzo, L., Bianco, C. L., et al. 2015a, ARep, 59, 626
Ruffini, R., Muccino, M., Aimuratov, Y., et al. 2016a, ApJ, 831, 178
Ruffini, R., Muccino, M., Bianco, C. L., et al. 2014, A&A, 565, L10
Ruffini, R., Muccino, M., Kovacevic, M., et al. 2015b, ApJ, 808, 190
Ruffini, R., Rueda, J. A., Muccino, M., et al. 2016b, ApJ, 832, 136
Ruffini, R., Salmonson, J. D., Wilson, J. R., & Xue, S. 2000, A&A, 359, 855
Ruffini, R., Salmonson, J. D., Wilson, J. R., & Xue, S.-S. 1999, A&A, 350, 334
Ruffini, R., Song, D. J., & Stella, L. 1983, A&A, 125, 265
Ruffini, R., Vereshchagin, G., & Xue, S. 2010, PhR, 487, 1
Ruffini, R., Wang, Y., Enderli, M., et al. 2015c, ApJ, 798, 10
Ruffini, R., & Wilson, J. 1973, PhRvL, 31, 1362
Sakamoto, T., Barthelmy, S. D., Baumgartner, W. H., et al. 2014, GCN, 15805, 1
Sari, R., Piran, T., & Halpern, J. P. 1999, ApJL, 519, L17
Shemi, A., & Piran, T. 1990, ApJL, 365, L55
Shirasaki, Y., Yoshida, A., Kawai, N., et al. 2008, PASJ, 60, 919
Smith, N. 2014, ARA&A, 52, 487
Smith, N., Li, W., Filippenko, A. V., & Chornock, R. 2011, MNRAS, 412, 1522
Sonbas, E., Cummings, J. R., D'Elia, V., et al. 2014, GCN, 17206, 1
Stamatikos, M., Cummings, J. R., Evans, P. A., et al. 2009, GCN, 9768, 1
Svensson, K. M., Levan, A. J., Tanvir, N. R., Fruchter, A. S., & Strolger, L.-G. 2010, MNRAS, 405, 57
Swenson, C. A., & Roming, P. W. A. 2014, ApJ, 788, 30
Tanvir, N. R., Levan, A. J., Cucchiarra, A., Perley, D., & Cenko, S. B. 2014, GCN, 16125, 1
Tavani, M. 1998, ApJL, 497, L21
Taylor, E. F., & Wheeler, J. A. 1992, Spacetime Physics—Introduction to Special Relativity (2nd ed.; New York: W. H. Freeman & Co.)
Toelge, K., Yu, H. F., & Meegan, C. A. 2015, GCN, 18492, 1
Troja, E., Barthelmy, S. D., Baumgartner, W. H., et al. 2013, GCN, 15402, 1
Troja, E., Piro, L., Vasileiou, V., et al. 2015, ApJ, 803, 10
van Paradijs, J., Groot, P. J., Galama, T., et al. 1997, Natur, 386, 686
von Kienlin, A., & Bhat, P. N. 2014, GCN, 15796, 1
Wheeler, J. A. 1937, PhRv, 52, 1107
Woosley, S. E. 1993, ApJ, 405, 273
Woosley, S. E., & Bloom, J. S. 2006, ARA&A, 44, 507
Xu, D., Fynbo, J. P. U., Jakobsson, P., et al. 2013, GCN, 15407, 1
Yi, S.-X., Wu, X.-F., Wang, F.-Y., & Dai, Z.-G. 2015, ApJ, 807, 92
Yu, H.-F. 2014, GCN, 17216, 1
Yuan, F., Schady, P., Racusin, J. L., et al. 2010, ApJ, 711, 870
Zel'dovich, Y. B., Ivanova, L. N., & Nadezhin, D. K. 1972, SvA, 16 209
Zhang, B., Fan, Y. Z., Dyks, J., et al. 2006, ApJ, 642, 354
Zhang, F.-W., Shao, L., Yan, J.-Z., & Wei, D.-M. 2012, ApJ, 750, 88
Ziaeepour, H. Z., Barthelmy, S. D., Gehrels, N., et al. 2006, GCN, 5233, 1